Improving the Earthquake Resilience of Existing Multi-Storey Concentrically Braced Frames Office Buildings in Moderate to High Seismic Zones

Ovidiu Mircea Serban

A Thesis

in

The Department

of

Building, Civil and Environmental Engineering

Presented in Partial Fulfillment of the Requirements

for the Degree of Master of Applied Science (Civil Engineering) at

Concordia University

Montreal, Quebec, Canada

March 2015

CONCORDIA UNIVERSITY
School of Graduate Studies

This is to certify that the thesis prepared

By: _____

Entitled: _____

and submitted in partial fulfillment of the requirements for the degree of

_____

complies with the regulations of the University and meets the accepted standards with respect to originality and quality.

Signed by the final examining committee:

Dr. Ashutosh Bagchi _____ Chair

Dr. Ramin Sedaghati _____ Examiner

Dr. Khaled Galal _____ Examiner

Dr. Lucia Tirca _____ Supervisor

Approved by _____
Chair of Department or Graduate Program Director

_____
Dean of Faculty

Date _____

ABSTRACT

Improving the Earthquake Resilience of Existing Multi-Storey Concentrically Braced Frames Office Buildings in Moderate to High Seismic Zones

Ovidiu Mircea Serban

In the past decades, concentrically braced frames (CBF) have been frequently employed as earthquake resistant systems for low- and middle-rise buildings. Their configuration and straightforward design made them appealing for engineers. It is noted that building structures designed and built in Canada prior to 1970 were not proportioned to carry seismic loads, while those constructed between 1970 and 1985 were designed to withstand lower seismic forces than those required by the current code. As a consequence, these buildings are characterized by lack of seismic resilience and therefore are vulnerable to earthquakes. Herein, the building's resilience is defined as the capability of a system to maintain a level of functionality in the aftermath of an earthquake event and is characterized by the performance metrics such as fragility, loss, and recovery functions.

To quantify the seismic resilience of existing office buildings, a methodology was proposed and exemplified in a case study comprising of 3- and 6-storey fictitious CBF office buildings located in Quebec City and Vancouver. These buildings were designed in accordance with the requirements of the 1980 edition of the National Building Code and CSA/S16.1-M78 standard. It is noted that before 1985, Quebec City and Vancouver were located in the same seismic zone (the seismic demand was identical) and the Vancouver buildings were selected for comparison purpose.

The proposed seismic resilience methodology consists in selecting the Rehabilitation Objective Class and the associated performance levels corresponding to earthquake hazard levels (e.g. 2%/50 yrs., 10%/50 yrs. and 50%/50 yrs.). To achieve this step, nonlinear dynamic time-history analyses are required and fragility curves computed for different hazard levels for both existing and retrofitted 3- and 6-storey fictitious buildings were generated from the Incremental Dynamic Analysis curves (IDA). Both aleatoric and epistemic uncertainties were considered. The loss estimation model is a function of system's components deficiency determined by the use of performance limit thresholds for different damage states. In addition, functionality curves computed for different hazard levels using an exponential recovery model are also shown.

The seismic assessment process was done according to performance based design principles and nonlinear time-history analysis by means of IDA using the OpenSees framework (Open System for Earthquake Engineering Simulation). Herein, all studied buildings were assessed against the current code demand. Based on the results, the buildings located in Quebec City and Vancouver show deficiencies at the level of structural members, especially the buildings located in Vancouver. Moreover, all brace-to-frame connections had insufficient strength and showed failure due to shearing of the welds. As reported from IDA curves, all existing buildings experienced collapse when subjected to ground motion intensities in agreement with the current code demand and a retrofit action was required.

To respond to the Rehabilitation Objective Class defined as Basic Safety by the ASCE/SEI 41-13 provisions, the selected rehabilitation strategy consisted in local strengthening of system's components (e.g. cover plating steel columns or beams and gusset plate replacement). According to the results, when the 3- and 6-storey retrofitted buildings located in Quebec City were subjected to ground motions scaled to the current code demand, their functionality was higher than 86.67% and 75.7%, respectively. Conversely, for the Vancouver buildings, besides the retrofit action, it is suggested to double the number of CBFs in order to pass the current code requirements. In conclusion, the proposed retrofit scheme for Quebec City buildings was able to improve the building performance and implicitly its earthquake resilience

AKNOWLEDGEMENTS

First, I would like to start expressing my gratitude to my advisor Dr. Lucia Tirca. An endeavor of this sort would not be possible without her support, encouragement and expert guidance. In the last years the door to Dr. Tirca's office was always open whenever I needed a good advice or I found myself into a dead end with the research. Her passion, patience and dedication towards research have inspired me along this entire path and incented me to strive towards perfection.

I am fortunate to have attended a university that supports its graduate students very well through teaching assistantships and fellowships. Special thanks to Concordia University and its wonderful team of valuable professors, who have provided a network of knowledge and support helping me to grow, and learn to become a successful graduate student. In addition I would like to express my appreciation to my committee members: Dr. Ashutosh Bagchi, Dr. Khaled Galal, and Dr. Ramin Sedaghati for taking the time to read my research and for their valuable input to this Master Thesis.

I will never forget my multicultural friends: Mingzheng Wang, Nenghui Lin, Suliman Abdalla, Masaaki Ohira, Qianli Xu, Yan Jiang, Leon Chen and all the people from the office: Omer Yagob, Sameh Y., Hamid A., Arash R., Farzad G.. It was a pleasure to meet you guys! I wish you best of luck in your careers/research and I hope our paths will cross again in the future. There are so many others whom I may inadvertently left out and I sincerely thank all of them for their help.

I extend my respect to my family back home, especially to my parents, who gave me the freedom to take my own path, for their endless love and encouragement throughout this journey. Mom, Dad, Milu, Cristina you will always be in my heart although you are miles away!

Words cannot express how grateful I am to my mother-in-law Vicky, to my father-in-law George; their support and encouragement was in the end what made this thesis possible. Thank you from my heart for your patience, good thoughts and kindness. I'm glad I had a chance to learn from you!

At the end, and most importantly, I would like to express appreciation to my beloved wife Oana, who spent sleepless nights with me and was always my support in the moments when I felt down and discouraged. I consider myself the luckiest in the world to have such a supportive wife. Thank you and I love you!

So what else is there to say? I did it –finally!!!

To the one that has always gave me strength to never give up, Oana.

To my grandmother, Viorica.

TABLE OF CONTENTS

LIST OF FIGURES

LIST OF TABLES

LIST OF SYMBOLS

A	horizontal design ground acceleration ratio; Area
A_g	gross area
A_{gv}	gross area in shear
A_m	interface area of the weld
A_n	net area
A_w	shear area of the weld
B_x	ratio at level x used to determine torsional sensitivity
B	maximum value of B_x
b	flange width
C	construction type factor
C_a	shape factor
C_b	basic roof snow load factor
C_e	Euler buckling load
C_f	compressive force in a member or component under factored load; factored axial load
C_r	factored compressive resistance of a member or component
C_s	snow load coefficient, roof slope factor for snow calculation
C_u	probable compressive resistance of bracing members
C'_u	post-buckling probable compressive resistance of bracing members
C_w	wind exposure factor
D	dimension of the building in the direction parallel to the applied lateral force
D_s	dimension of the lateral force - resisting system in the direction parallel to the applied lateral force

D_n	plan dimension of the building in the direction of computed eccentricity
D_w	weld leg width
E	elastic modulus of steel (200000 MPa assumed)
e	computed eccentricity between the centre of mass and center of rigidity at the considered level
e_x	design eccentricity
F	foundation factor
F_a	acceleration-based site coefficient
F_t	portion of V to be concentrated at the top of the structure
F_u	specified minimum tensile strength
F_v	velocity-based site coefficient
F_i ,F_x	lateral force applied to level i or x, respectively
F_y	specified minimum yield stress, yield point or yield strength
f	live load reduction factor
f_{rec}	recovery function used to calculate the resilience
G	shear modulus for steel taken as 77000 *MPa*
$H(t)$	Heaviside step function returning zero values for negative argument and one for positive argument
h	clear depth of web between flanges
h_n	total height of the building
h_i,h_x	the height above the base to level i, or x respectively, where the base of the structure is the level at which horizontal earthquake motions are considered to be imparted to the structure
h_{typ}	typical storey height

h_{gf} ground floor height

I, I_a importance factor

I_E earthquake importance factor of the structure

I_x, I_y moment of inertia about x-x, y-y

J torsion constant

K numerical coefficient that reflects the type of construction, damping, ductility & energy absorption capacity; effective length factor

KL effective length

l, L length

L_w welding length

M_f bending moment in a member or component under factored loads

M_{max} maximum bending moment

M_p plastic moment = ZF_y

M_r factored moment resistance of a member or component

m_R median capacity of the fragility function (the IM level with 50% probability of collapse)

M_{tx} torsional moments in the horizontal plan of the building

M_v factor to account for higher mode effect on the base shear

M_y yield moment = SF_y

P_i total gravity load causing the P-Δ shear which is carried by the columns of the SFRS under consideration at level i

$Q(t)$ functionality of a system (%)

R_d ductility related force modification factor reflecting the capability of a structure to dissipate energy through reversed cyclic inelastic behaviour

R_o overstrength-related force modification factor

r_x, r_y radius of gyration about x-x ,y-y axis

$S_a(T)$ design spectral response acceleration at the fundamental period of vibration

$S_a(T_1,5\%)$ 5% damped spectral acceleration at the structure's first mode period

S seismic response factor; structural flexibility factor, roof snow load

S_{MT} maximum design ground motion intensity to calculate the collapse margin ratio (CMR)

S_r associated rain load in kPa with a 1-in-50 probability of exceedance per year

S_s ground snow load in kPa with a 1-in-50 probability of exceedance per year

S_0 snow load on the ground

S_x elastic section modulus with respect to axis x-x

S_y elastic section modulus with respect to axis y-y

$\hat{S}_{CT}$ spectral intensity when half of the ground motions cause the structure to collapse in order to calculate the CMR

T_{emp} empirical expression for the fundamental vibration period of the structure

T_f tensile force in a member or component under factored loads

T_{RE} recovery time from an extreme event

T_r factored tensile resistance of a member or component

T_u probable tensile resistance of bracing members

T_x floor torque at level x

$T_{1,dyn}$ fundamental lateral period of vibration of the building, in the direction under consideration , based on dynamic analysis

t_f flange thickness

t_{gp} gusset plate thickness

t_{0E}	initial time when the extreme event happen , for resilience calculation
U_t	factor to account for efficiency of the tensile area
U_2	amplification factor for P-Δ effects
V	lateral seismic design force at the base of the structure
V_{dyn}	dynamic base shear
V'_i	additional shear force from P-Δ effects at level i
V_r	factored shear resistance of the fillet weld
W	seismic weight
W_i, W_x	portion of W that is located at or is assigned to level i, or x respectively
W_w	Whitmore width of the gusset plate
w	web thickness; load per unit of length
$w_{sec\text{-}beam}$	uniform distributed load on the secondary beam
X_u	ultimate strength of the electrode used for welded connections
Z	plastic section modulus of a steel section
β_C	uncertainty in capacity
$\beta_{D\mid Sa}$	seismic demand uncertainty
β_R	logarithmic standard deviation used to develop fragility curves
β_{RR}	aleatoric uncertainty
β_{RU}	modeling (epistemic) uncertainty
ε_o	the strain at which one cycle cause failure
φ, ϕ	performance factor
λ	non-dimensional slenderness ratio in column formula

θ_x stability factor at level x to account for P-Δ effects

ξ damping coefficient

ω coefficient used to determine equivalent uniform bending effect in beam-columns

Δ_i deflection at storey *i*

CHAPTER 1. INTRODUCTION AND RESEARCH OBJECTIVES

1.1. Introduction

In the aftermath of a hazard event, community needs to assure security for all citizens and to provide emergency shelters and maintain operational all its public facilities. Recent studies had shown that the risk of economic losses is a consequence of building stock performance under the effect of unpredictable natural hazards like: earthquakes, floods, hurricanes, etc. Both system vulnerability and hazard are conditioning parameters. In an extended approach, other causes of disaster risk are demographic and socio-political like the urbanization process which implies changes in buildings density and population growth which in turn may contribute to increase the number of casualties during an urban earthquake. Studies showed that there is no systematic program for hazard vulnerability assessment implemented on a large scale in Canada, although the Western and Eastern Cost are at high and moderate-to-high seismic risk, respectively.

In order to reduce the losses, mitigations and preventive measures should be taken before the extreme event happens. Mitigation actions can reduce the vulnerability of these facilities. However, in case of insufficient mitigation actions, or in case that the events exceed expectations, damage occurs and a recovery process is necessary in order to maintain a functional system/community. In this study, it is intended to propose a methodology with emphasis on quantification of seismic resilience of existing office buildings designed and built in Eastern Canada according to NBCC 1980 and CSA/S16.1-M78. In addition, it is proposed a costly effective retrofit scheme in order to improve buildings performance and enhance their resilience. Resilience is defined as the capacity of systems to recover after severe disasters of any type. However, the main focus of this study is only on seismic events, with the possibility of extension for other natural hazards. This is a new research field that embraces engineering with organizational, economical, and social aspects.

1.2. Research overview and methodology

In Canada, the general seismic loading and analysis requirements for building structures are given in the National Building Code of Canada (NBCC), whereas special seismic design and detailing provisions for steel structures are described in CSA S-16 standard. In the last decades, substantial efforts have been made to upgrade the existing NBCC code and CSA/S16 standard, while lower interest was allocated to edit guidelines regarding the seismic assessment and retrofit of existing urban buildings located in areas characterized by moderate to high seismic hazard.

In addition, the existing building stock designed and built prior to the 1970 was proportioned to carry gravity and wind load only, while that constructed between 1970 and 1985 was designed to withstand lower seismic forces in comparison with those required by the current code. For this reason, in the event of an earthquake that may occur close to urban areas, the existing building stock is vulnerable to damage. In general, eastern Canadian earthquakes occurred at a depth less than 30 km and could be considered catastrophic for a magnitude larger than six. On the other hand, the buildings located on the western coast are subjected to crustal (M7-7.5) and subduction ground motions (M9). It is important to note that, Concentrically Braced Frames (CBF) were among the most popular structural systems used for low- and middle-rise buildings, in eastern Canada. Regarding the evolution of Building Code, the first probabilistic seismic map of Canada (0.01 probability of exceedance per annum) was included in the 1970 edition of NBCC, while in the 1980 edition it was considered the same seismic map as in 1970 with an increased plateau in short period range. The limit state design was introduced in the 1978 edition of the Canadian structural steel design standard, CSA/S16. In this light, the existing CBF building structures designed and built either on the eastern or western coast are at high seismic risk.

In this context, to manage the earthquake risk of existing office buildings, one must understand the earthquake hazard and reduce building vulnerability. Thus, in order to predict the vulnerability, the year of building construction and knowledge of changes in code and regulations are essential parameters. Moreover, depending on the hazard level and building vulnerability, the decision maker's choices are: i) accept the risk and keep the building "as is", ii) apply reasonable mitigation measures to reduce partially the seismic risk and iii) apply mitigation measures to minimize, the risk. Therefore, the purpose of this study is two-fold: i) to assess the vulnerability of low- and middle-rise CBF office buildings located in high and high to moderate seismic zones that were

designed and constructed during the time span 1980-1989 and ii) to quantify the seismic resilience of these buildings pre- and post-retrofit.

1.3. Thesis organization

This research work is grouped into six chapters as follows:

- Chapter 1 covers a brief introduction including a general overview of the research conducted for this thesis, a well-defined objective and a proposed methodology. The description and steps to follow in order to complete this study are also provided.
- Chapter 2 reports on a systematic literature review conducted in order to identify the potential seismic hazard in Canada and what type of buildings are prone to seismic risk. In addition, some guidelines regarding the seismic performance assessment of existing buildings are reviewed and several possible retrofit techniques are discussed. Finally, the concept of seismic resilience including its attributes and characteristics is described at the end of the chapter.
- Chapter 3 presents the design of fictitious 3- and 6-storey office buildings located in representative Canadian locations i.e. Quebec City, QC (3Q, 6Q), was selected for eastern Canada and Vancouver, B.C, (3V, 6V) for western Canada. It is noted that, the design of the low- and middle- rise buildings was based on the 1980 NBCC in conjunction with CSA/S16.1-M78 standard.
- In Chapter 4, the existing low- and middle-rise CBF office buildings designed using NBCC 1980 and CSA/S16.1-M78 standard are evaluated in order to identify possible seismic deficiencies. Herein, the collapse safety of the studied buildings was evaluated for each performance group in terms of demand-to-capacity ratios according to the current code provisions (NBCC 2010 and CSA/S16-09 standard). In addition, the assessment process was based on the equivalent static force procedure and Incremental Dynamic Analysis (IDA) by means of nonlinear time-history analysis. It is noted that for buildings located in Vancouver only the equivalent static force procedure was considered.
- Chapter 5 covers the selection of the rehabilitation objective class and the retrofit scheme together with the seismic assessment of post-retrofit buildings using non-linear time history analysis as explained in Chapter 4. Furthermore, using collapse data obtained from IDA results, a collapse fragility function was defined through a cumulative distribution function

(CDF) for both cases: before and after retrofit. In addition, Chapter 5 provides a suggested procedure to assess the performance of office buildings when subjected to probable earthquake shakings, in order to quantify their seismic resilience. Thus, the functionality was computed using an exponential recovery function showing the dependence on the performance measures expressed through damage states and seismic input.

- Chapter 6 concludes this research also provides some recommendations for possible future studies.

CHAPTER 2. LITERATURE REVIEW

This Chapter reports on a literature review conducted in order to identify the potential seismic risk of Concentrically Braced steel Frames (CBFs) designed and detailed according to the 1980 edition of National Building Code of Canada (NBCC) and CSA/ S16.1-M78 steel design standard. Next, some guidelines regarding the seismic performance assessment of existing buildings are reviewed and several possible retrofit techniques are discussed. Then, the concept of seismic resilience including its attributes and characteristics are described.

2.1. Seismic hazard in Canada

In Canada, each year, approximately 4000 earthquakes are detected by seismologists. According to Natural Resources of Canada (NRC), the seismic map was divided in four earthquake zones: western, eastern, northern and central (**Figure 2.1)**. Adams and Atkinson (2003) summarized that about 25% of earthquakes have been recorded in the western region of Canada, 14% in the eastern region while the difference was recorded in the northern zone.

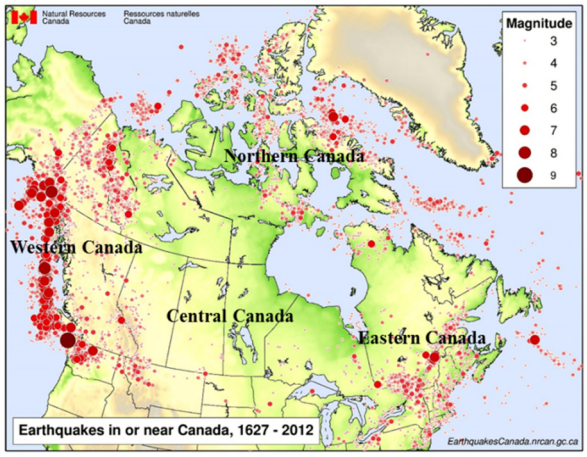

Figure 2.1 Map of significant Canadian earthquakes, 1627-2012 (NRC)

Moreover, among the significant Canadian earthquakes recorded in the interval 1600-2007, Lamontagne et al. (2008) has shown that the distribution of earthquakes with magnitude 6 or greater as well as some smaller ones felt by many Canadians is as follows: 25% of significant earthquakes have been recorded in eastern Canada, 60% in western Canada (British Columbia) and 15 % in the northern Canada.

2.1.1. Seismic hazard in Eastern Canada

Eastern Canada is located in a relatively stable continental region within the North American Plate and as a consequence, has a relatively low rate of earthquake activity. However, large and damaging earthquakes have occurred here in the past and could occur in the future. According to NRC, each year approximately 450 earthquakes occur in eastern Canada. Of this number, around four exceed magnitude 4, thirty will exceed magnitude 3, and about twenty-five events are reported felt. Statistically, about three seismic events above magnitude 5 are recorded over a ten-year period. Although earthquakes can occur throughout the region, researchers have identified certain clusters of earthquake activity given as follows: Eastern Northern Ontario, Southern Great Lakes, West Quebec, Charlevoix-Kamouraska, Lower St. Lawrence, Northern Appalachians and Laurentian Slope.

The pattern of earthquake events recorded in these clusters shows concentrations along the Maniwaki – Montreal axis (West Quebec zone) and along St- Laurent River (Charlevoix zone) as illustrated in **Figure 2.2(a)** and (**b)**. Located 100 km from Quebec City, the Charlevoix seismic zone is the most seismically active region of eastern Canada. Historically, the zone has been subjected to five earthquakes of magnitude 6 or larger in: 1663 (M7), 1791 (M6), 1860 (M6), 1870 (M6.5) and 1925 (M6.2). Furthermore, from data collected by Lamontagne et al. (2008), ten earthquakes (9 recorded in Quebec and 1 in Ontario) can be identified as being significant for eastern Canada having magnitudes between 5 and 7. Among the ten significant earthquakes, only two of them could be considered at high risk: the 1663 and 1870 Charlevoix. If an earthquake of similar magnitude would occur nowadays in vicinity of densely populated cities such as Quebec City, Montreal or Ottawa, the risk of losses could be high (Tirca et al. 2013).

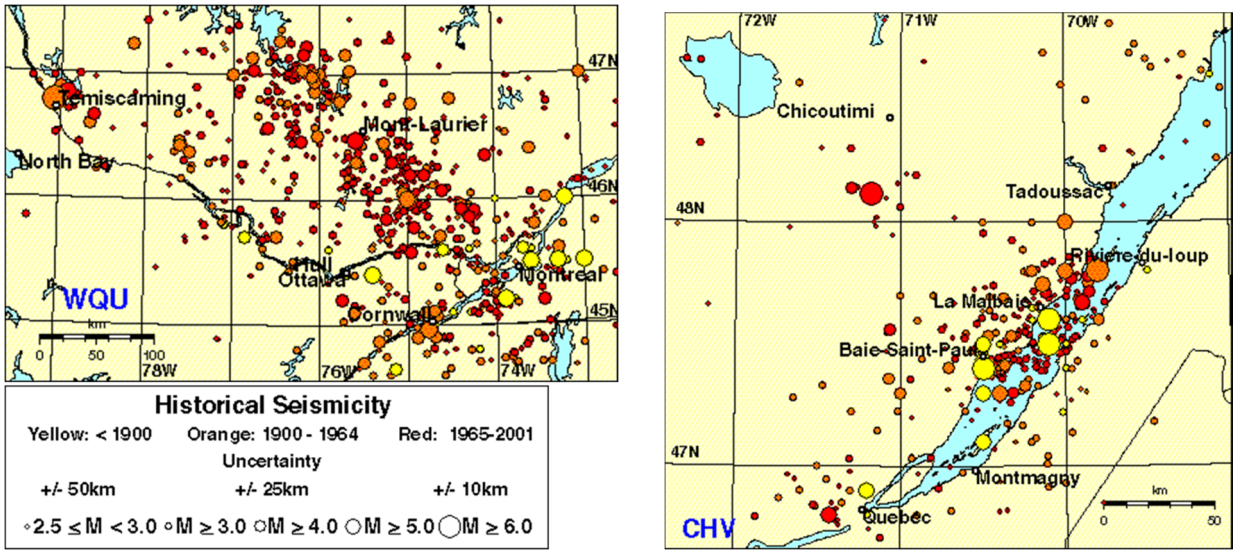

(a) (b)

Figure 2.2 Distribution of earthquake events in Eastern Canada : (a) West Quebec seismic zone (NRC); (b) Charlevoix seismic zone (NRC);

2.1.2. Seismic hazard in Western Canada

Each year, more than 1000 earthquakes are recorded in western Canada. Hence, the Pacific Coast is the most earthquake-prone region of Canada, with more than 100 earthquakes of magnitude 5 or greater that have occurred during the past 70 years in the offshore region to the west of Vancouver Island. According to Geological Survey of Canada, the concentration of earthquakes along the west coast is related to the presence of active faults that are constantly moving relative to one another at speeds of about *2-10 cm/year*. The clusters of earthquake activity are: Offshore BC Region, Cascadia Subduction Zone, St. Elias Region and the Southwestern Yukon, Northern and Southern Cordillera and the Interior Platform. According to Cassidy et al., (2010) earthquakes from the western coast occur: i) within the subducting ocean plate typically at 30−60 km depth (e.g., M6.5 earthquake beneath downtown Seattle in 1965); ii) within the continental crust down to 30 km depth (e.g., M7.3 earthquake on central Vancouver Island in 1946) and iii) along the subduction faults in the offshore region causing giant subduction earthquakes (e.g., the M8.1 Queen Charlotte Island earthquake in 1949). Moving inland from the coast, the frequency and magnitude of earthquakes decrease.

2.2. Evolution of National Building Code of Canada (NBCC)

In Canada, the evolution of seismic design of structures can be summarized by studying the 11 editions of the NBCC edited nearly every five years since 1941. To better understand the changes that affect the design of structures to withstand earthquake loads, a historical background of NBCC editions (Mitchell et al., 2010) dating back to 1970 is described below.

2.2.1. The 1970-1980 NBCC versus the 2010 NBCC

The first truly probabilistic seismic zoning map was developed by Milne and Davenport (1969) using expected accelerations having a probability of exceedance of 0.01 per annum (100 years return period) was introduced in the 1970 edition of NBCC (NRCC, 1970). As in the previous editions, there were kept the same four seismic zones, but the boundary lines from one zone to the other were based on acceleration values considered as a percentage of *g*. In this seismic map, illustrated in **Figure 2.3**, Montreal and Ottawa changed from Zone 3 to Zone 2, while Quebec City remains in Zone 3.

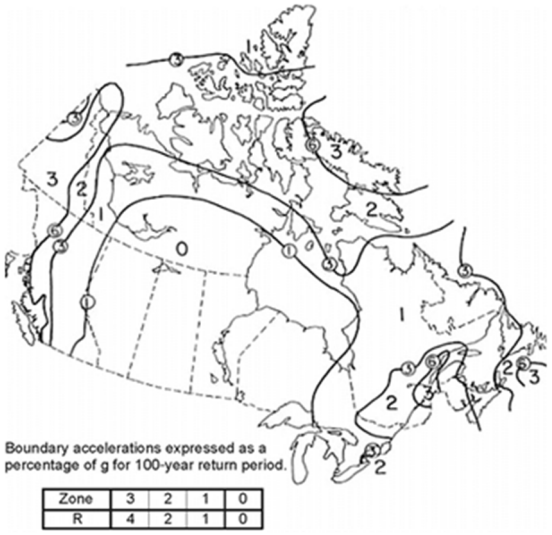

Figure 2.3 First seismic zoning map based on acceleration having a probability of exceedance 0.01 per annum (NBCC 1970)

Another key observation is made regarding the evaluation of the base shear. Hence, in the 1970 edition, the base shear was computed based on the fundamental period of vibration of the building. The minimum lateral seismic force, V is given as:

$$V = \frac{1}{4} R\ (KCIFW) \tag{2.1}$$

where R is the seismic regionalization factor (**Figure 2.3**); K represents the construction type factor ; F is the foundation factor with values of 1.5 for highly compressible soils and 1.0 for other soil conditions, I is the importance factor and W is the total seismic weight (dead load plus 25% snow plus live load for storage areas). For buildings with large assemblies of people, (i.e. hospitals and power stations) the importance factor is $I = 1.3$, otherwise $I=1.0$. On the other hand, C represents the structural flexibility factor where: $C = 0.1$ for 1- and 2-storey buildings and $C = 0.05/T^{1/3} < 0.1$ for other buildings. In the previous expression, T represents the fundamental period of the building, where $T = 0.1N$ for moment resisting frames and $T = 0.05h_n/D^{1/2}$ for other types of structural systems, while D and h_n are measured in feet and are the dimension of the building parallel with the direction of applied seismic force and height of the building, respectively.

Furthermore, the 1975 edition of NBCC (NRCC, 1975) permitted the use of the dynamic analysis to assess the seismic forces. In addition, it has introduced the limit states design with load and material resistance factors as an alternative approach to working stress design. A response spectrum with 5% damping was adopted for the dynamic analysis and was scaled to the design ground acceleration A, having the values of 0.0g, 0.02g 0.04g and 0.08g for zones 0, 1, 2, and 3, respectively. Similarly, the seismic zoning map developed in 1970 was used in the 1975 NBCC edition. The minimum seismic base shear, V, was given as:

$$V = ASKIFW \tag{2.2}$$

where A is the horizontal design ground acceleration with the values given above, while S is the seismic response factor defined in **Eq.(2.3)**. Frames with tension-compression diagonal bracing or chevron require $K=1.0$ while for tension only braces $K=1.3$. In addition, an intermediate foundation factor $F = 1.3$ was introduced to account for soft soils or for compact coarse-grained or stiff fine-grained soils with a depth greater than 50 ft.

$$S = \frac{0.5}{T^{1/3}} \leq 1.0 \tag{2.3}$$

In the above equation the expression for the fundamental period of the structure, T, is the same as per 1970 NBCC. It is noted that the term AS in **Eq. (2.2)** was calibrated to be 20% less than the term $RC/4$ given in **Eq. (2.1)**.Torsional moments in the horizontal plan of the building are computed for each storey using **Eq. (2.4).** Design eccentricity e_x, is calculated by one of **Eqs. (2.5)** or (**2.6)**, whichever provides the greater stresses. The 0.5 factor of e, was aimed at increasing the

design force levels of the "stiff side" of the structure. On the other hand, if e_x, exceeds $D_n/4$ then, dynamic analysis is required or the torsional moment computed with **Eq. (2.4)** needs to be doubled. The term D_n represents the plan dimension of the building in the direction of computed eccentricity.

$$M_{tx} = (V - \sum_{i=1}^{x} F_i)e_x \tag{2.4}$$

In the above equation, V represents the design base shear; F_i is the lateral force applied at level i, and e_x is the design eccentricity as calculated bellow:

$$e_x = 1.5e + 0.05Dn \tag{2.5}$$

$$e_x = 0.5e - 0.05Dn \tag{2.6}$$

The 1980 edition of NBCC (NRCC, 1980) uses the same seismic zoning map as in 1970 with an increased plateau in short period range. In addition, this edition introduced for the first time the SI units. However, the consideration of such a low acceleration magnitude provides an inadequate seismic protection (Mitchell et al., 2010) especially for buildings located in high-density urban areas. The minimum design lateral seismic force equation remained the same as in 1975 NBCC (**Eq. (2.2)**), except for the seismic response factor S, and for the fundamental period of the structure, calculated with the following expression: $T = 0.09h_n/D^{1/2}$; where, h_n is the total building height and D represents the dimension of the building in the direction parallel to the applied seismic force. The seismic response factor S, is given bellow:

$$S = \frac{0.5}{T^{1/2}} \leq 1.0 \tag{2.7}$$

It is noted that for regular structures, NBCC 1980 allows to determine the earthquake induced forces using the equivalent static force procedure (ESFP). According to this procedure, a concentrated load F_t given in **Eq. (2.8)** is applied at the roof level**.** The F_t value from **Eq. (2.8)** cannot exceed $0.15V$ if $h_n/D_s > 3$ (otherwise $F_t=0$). Herein, h_n is the total building height and D_s represents the dimension of the lateral force resisting system parallel to the direction of the applied lateral forces. The remaining seismic load, V-F_t, is distributed along the building height as a function of the relative product of the seismic weight and the elevation from the ground at the level under consideration in accordance with **Eq. (2.9)**.

$$F_t = 0.004V\left(\frac{h_n}{D_s}\right)^2 \leq 0.15V, if\ \frac{h_n}{D_s} > 3 \tag{2.8}$$

$$F_x = (V - F_t)\frac{W_x h_x}{\sum_{i=1}^{n} W_i h_i} \tag{2.9}$$

According to Part 4 of NBCC 1980, in designing buildings and their structural members the following load combinations are considered (whichever combination produces the most unfavorable effects):

(i) 1.25DL + 1.5LL

(ii) 1.25DL + 1.5Q (2.10)

(iii) 1.25DL + 0.7(1.5LL + 1.5Q) (where Q is either the wind or earthquake load)

Major changes were incorporated in the 2005 and 2010 editions of NBCC (NRCC, 2005; 2010). One key change is the Uniform Hazard Spectrum (UHS) approach (NEHRP, 1997) that was adopted, giving site specific response spectral accelerations for numerous locations across Canada. Herein, these spectral accelerations have a probability of exceedance of 2% in 50 years with a return period of 2475 years. This lower probability provides a more uniform margin of collapse, one that is much closer to the probability of structural failure (Heidebrecht, 2003). Another key note is that the dynamic analysis became the preferred method for structures with certain irregularities.

Based on the equivalent static force procedure (ESFP) the minimum lateral design base shear, V is calculated as per **Eq. (2.11)**. However, V shall not be taken less than the base shear calculated according to **Eq. (2.12)**.

$$V = S(T_a)\, M_v I_E\, W/R_d R_o \tag{2.11}$$

$$V = S(2.0)\, M_v I_E\, W/R_d R_o \tag{2.12}$$

where $S(T_a)$ is the design spectral acceleration given at specified periods of *0.2*, *0.5*, *1.0* and *2.0 s* for each city in Canada. The $S(T_a)$ term replaces the seismic zone factor A given in NBCC 1980. In **Eq. (2.11)** M_v is a factor that accounts for higher mode effects on the base shear, while I_E represents the importance factor which is taken as *1.0* for *normal* structures, *1.3* for *High Importance* structures (e.g. schools, community centres) and *1.5* for *Post-disaster* structures (e.g.

hospitals). Since 2005, the ductility-related force modification factor R_d and the overstrength-related factor R_o accounting for the reserve strength in a structure were introduced. Typical values for R_d, and R_o for different seismic force resisting systems (SFRS) are given in CSA S16 standard and are discussed in the next section. In addition, for SFRS with $R_d \geq 1.5$, V need not to be taken greater than $2/3[S(0.2)I_E W/R_d R_o]$.

The design spectral acceleration values are modified by the acceleration and velocity based-site coefficients F_a and F_v to obtain the design spectrum. For site class C, $F_a = F_v = 1.00$. Thus, the design spectrum $S(T_a)$, is determined at the fundamental vibration period of the structure using linear interpolation between the values given in **Eq. (2.13)**.

$$
\begin{aligned}
S(T) &= F_a S_a(0.2)\ for\ T \leq 0.2\ s \\
S(T) &= min[F_V S_a(0.5), F_a S_a(0.2)]\ \ for\ T \leq 0.5\ s \\
S(T) &= F_V S_a(1.0)\ for\ T = 1.0\ s \\
S(T) &= F_V S_a(2.0)\ for\ T = 2.0\ s \\
S(T) &= F_V S_a(2.0)/2\ for\ T \geq 4.0\ s
\end{aligned}
\tag{2.13}
$$

According to NBCC 2010 (NRCC, 2010), the empirical equation for the fundamental period of the structure T_{emp} for braced frames is given in **Eq. (2.14)**. Alternatively, a dynamic analysis can be used to determine the fundamental period of vibration however such computed period cannot exceed $2T_{emp}$.

$$T_{emp} = 0.025 h_n \tag{2.14}$$

Torsional effects are considered by applying torsional moments T_x about a vertical axis at each level, from the combination whichever provides the greater stresses:

$$T_x = F_x(e_x \pm 0.1 D_{nx}) \tag{2.15}$$

Herein, F_x is the lateral storey force at level x obtained from **Eq. (2.9)** and D_{nx} is the dimension of the building at level x, perpendicular to the direction of seismic loading. It is noted that the concentrated force at the top of the structure F_t is given as $F_t = 0.07\ T_a\ V$ and should be $\leq 0.25\ V$.

Torsional sensitivity is determined by calculating the maximum value B, among floors, where B_x computed at level x is $B_x = \delta_{max}/\delta ave$. In the aforementioned expression, δ_{max} is the maximum storey displacement at the extreme points of the structure at level x induced by the equivalent static forces acting at distances $\pm 0.1 D_{nx}$ from the centre of mass at each floor and δ_{ave} is the average of the displacements at the extreme points of the structure at level x produced by the above forces. When B exceeds 1.7 and $I_E F_a S_a(0.2) > 0.35$ a 3-D dynamic analysis is required. Moreover, the building is considered torsional sensitive and the resulted base shear should be scaled (if required) to reach V, where V is the earthquake design force computed from **Eq. (2.11).** However, if the building is regular, in the design process, V can be replaced by $0.8V$.

According to NBCC 2010, the calculated elastic maximum interstorey drift at any level including that from accidental torsion shall be multiplied by $R_d R_o / I_E$ to get an estimate of the interstorey drift due to nonlinear response. These deflections are limited to $1\% h_s$, $2\% h_s$ and $2.5\% h_s$ for post-disaster buildings, schools, and all other buildings respectively; where h_s is the interstorey height.

The evolution of spectral acceleration for two representative locations in Canada (i.e. Quebec City, Qc. and Vancouver, B.C.) for site class C is shown in **Figure 2.4**. As illustrated, the seismic demand has considerably increased from 1975 until 2010 for both locations especially for low-rise buildings located in Vancouver. The significant increase in demand is attributed to the evolution of seismic hazards. Thus, the first seismic hazard map was released in 1970 and it was based on a probability of exceedance of 50% in 50 years (NRCC, 1970). However, the 1985 (NRCC, 1985) and 2005 (NRCC, 2005) maps were developed for a probability of exceedance of 10% and 2% in 50 years, respectively (475 and 2500 years return period). It is noted that both Quebec and Vancouver were in the same seismic zone 3 according to the first seismic zoning map from 1970 therefore they have the same acceleration spectra in 1975 and 1980.

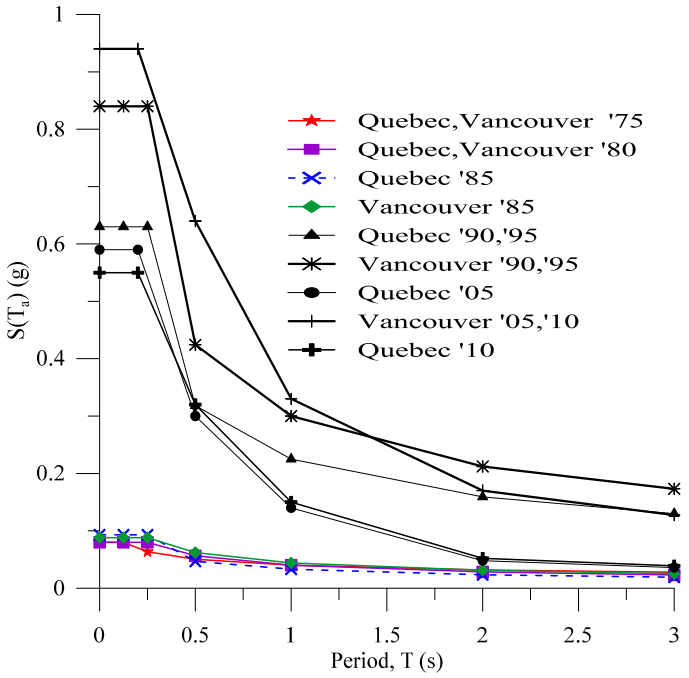

Figure 2.4 Evolution of code acceleration spectra for Quebec City and Vancouver

2.3. Seismic design and provisions in CSA S16

Seismic design provisions of steel framed building structures are given in the editions of CSA/S16 standard (Canadian Standards Association). In this regard, the limit state design was introduced in the 1974 edition of CSA/S16 standard as an alternative to working stress method. The CSA/S16.1-M78 standard was the first based on the SI system. Further on, the CSA/S16 standard was updated in 1984, 1989, 2001 and 2009. Prior to the 1989, only a few requirements were addressed to structural engineers in the field of seismic design. In addition, all members and connections were designed for factored loads, while a brittle failure mode may occur. However, after 1989, the capacity design method was introduced in CSA/S16 in order to establish a strength hierarchy along the load path such that the inelastic response can be accommodated by the ductile elements, while the remaining elements must possess sufficient resistance in order to assure their elastic response. Therefore, special design provisions including ductility and capacity design approach were incorporated in the 1989 edition (Tremblay, 2011).

Two editions of CSA S16: S16.1-M78 (1978) and the current S16-2009 (2009) are further reviewed to better understand the differences between the limit states design approach and the capacity design philosophy which significantly affect the design of structures.

2.3.1. Seismic design provisions according to CSA S16.1-M1978

The safety criterion used by CSA/S16.1-M78 was based on the factored resistance of the members which has to exceed (or equal) the effect of factored loads. In addition, two basic types of constructions are permitted for all or part of a structure in this standard: *continuous construction* – all elements are rigidly framed or continuous over supports and *simple construction*- ends of beams, girders and trusses are free to rotate (pinned connection). Moreover, the CSA/S16.1-M78 standard, limits the slenderness ratio which is taken as the ratio of effective length (*KL*) to the corresponding radius of gyration (*r*) to 200 for compression members while for tension members the maximum value is 300. In addition, the structural sections are divided in 4 classes of section depending on the maximum width-to-thickness ratios of their elements subjected to compression. For elements subjected to axial tension, the factored tensile resistance T_r, is taken as the lesser of:

i) $$T_r = \varphi A_n F_y \qquad \text{When } \frac{A_n}{A_g} \geq F_y/F_u$$

$$= \varphi \left(F_u \frac{A_n}{A_g} \right) A_g \qquad \text{When } \frac{A_n}{A_g} < F_y/F_u \tag{2.16}$$

ii) $$T_r = 0.85\varphi A_n F_u$$

In the above equation, φ is a performance factor taken as *0.9* unless otherwise specified, A_g is the gross area of the section while A_n represents the critical net area taken as $0.85A_g$ when $F_y/F_u \leq 0.75$ or $0.9A_g$ when $0.75 < F_y/F_u \leq 0.8$. On the other hand, for W shapes and hollow structural sections (HSS), Class C (cold formed non-stress relieved), the factored axial compressive resistance C_r is given in **Eq. (2.17).** In the equation, A represents the cross sectional area of the member, F_y is the yield strength of the steel while E is the elastic modulus of steel and the member slenderness λ is given by the expression: $\lambda = \frac{KL}{r}\sqrt{\frac{Fy}{\pi^2 E}}$, while $\varphi = 0.9$.

a) $0.00 \leq \lambda \leq 0.15$ $\quad C_r = \varphi A F_y$

b) $0.15 < \lambda \leq 1.00$ $\quad C_r = \varphi A F_y (\ 1.035 - 0.202\lambda \ - 0.222\lambda^2)$

c) $1.00 < \lambda \leq 2.00$ $\quad C_r = \varphi A F_y (-0.111 + 0.636\lambda^{-1} + 0.087\lambda^{-2})$ (2.17)

d) $2.00 < \lambda \leq 3.60$ $\quad C_r = \varphi A F_y (0.009 + 0.877\lambda^{-2})$

e) $3.60 < \lambda$ $\quad C_r = \varphi A F_y \lambda^{-2}$

2.3.2. Seismic design provisions according to CSA S16-2009

The design provisions are based on the capacity design approach. In this light, the remaining elements (non-ductile) such as: brace connections, columns, beams and other connections along the seismic load path must be designed to resist the probable resistance of braces. Moreover, each seismic force resisting system (SFRS) should possess adequate ductility such that the structure can dissipate energy while preserving a stable response under the designed earthquake loads. Since the 2005 edition of NBCC, two related force modification factors were introduced: R_d and R_0 which are the ductility- and overstrength-related force modification factors, respectively. According to NBCC 2010 the *conventional construction* system (CC) has $R_d=1.5$ and $R_o=1.3$. For this type of system, the CSA/S16-2009 standard requires that the connections along the seismic load path to be either detailed to exhibit a ductile failure mode or be designed for seismic loads corresponding to $R_d=1.0$. Additional requirements apply to CC structures if their height exceeds *15 m* in the case of assembly occupancy. For other occupancies located in areas where $0.35 \leq I_E F_a S_a(0.2) \leq 0.75$ and $I_E F_a S_a(0.2) > 0.75$, the limit height is *60 m* and *40 m*, respectively. For instance, the design seismic forces are linearly increased as a function of the building height by 2% per meter of height above the recommended height limit without exceeding seismic forces determined with $R_d R_o = 1.3$.

Since 1978, the calculation of member resistance did not change too much. For example, in CSA/S16-2009 standard, the factored tensile resistance T_r, developed by a member subjected to axial tension is:

$$T_r = \phi A_g F_y \leq \phi_u A_{ne} F_u \tag{2.18}$$

In **Eq. (2.18)**, the first term refers to the yielding of the gross cross-section, while the second term is related to rupture of the effective net section, A_{ne}. Herein, the latter is smaller than A_n to account for shear lag effect, if required. In the case of net section rupture, $\phi_u=0.75$, and corresponds approximately to the product 0.85φ from **Eq. (2.16 ii)** specified in 1978.

According to CSA/S16-2009 standard, the factored axial compressive resistance C_r, is:

$$C_r = \phi A F_y (1 + \lambda^{2n})^{-1/n} \tag{2.19}$$

where $\lambda = \frac{KL}{r}\sqrt{\frac{Fy}{\pi^2 E}}$ and $n=1.34$ for hot-rolled, fabricated structural sections and HSS manufactured in accordance with CSA G40.20, Class C (cold-formed non-stress relieved).

Another key modification in the 2009 CSA/S16 standard is about connection design philosophy. For example, in CSA/S16.1-M78 the connections had to be designed for 50% of the factored tension (T_r) or compression (C_r) member resistance, depending on which one governs the design. However, this requirement was abandoned in 2001. Moreover, the block shear failure and the shear lag effects were not considered in the 1978 standard. Thus, the factored resistance for a potential failure involving the simultaneous development of tensile and shear component areas are taken as follows:

$$T_{r,BS} = \Phi_u \left[U_t A_n F_u + 0.6 A_{gv} \frac{(F_y + F_u)}{2} \right] \tag{2.20}$$

where Φ_u is a factor taken as *0.75* for steel, U_t represents the efficiency factor taken as *1.0* for symmetrical blocks, while A_n and A_{gv} represent the net area in tension and the gross area along the shear failure plane, respectively.

In addition, the shear lag effect is also required to be considered for the net rupture of the HSS welded connection. For this reason, in CSA/ S16-14 (CSA, 2014), a new clause *12.3.3.4* has been added to specifically address the shear lag factor *U* for all slotted HSS welded connections. This clause was based on the research conducted by Martinez-Saucedo and Packer (2009). Thus, the effective net area A_{ne}, is reduced with the shear lag effect factor as shown in **Eq. (2.21).**

$$T_r = 0.85 \phi (A_{ne} U) F_u \tag{2.21}$$

Moreover, the research conducted by Packer (2014) shows that the welding length L_w has an influence over the net rupture of the brace. Therefore, with a long weld length the full capacity of the HSS can be attained whereas for shorter weld lengths the cross-sectional capacity is reduced by shear lag. As illustrated in **Figure 2.5(a)**, the HSS is usually "over-slotted" in order to accommodate field welding and adjustments, thus there is a hole in the bracing member at the end of the gusset plate which creates a net section smaller than the cross-sectional area of the tube. Hence, this type of connection is liable to fail by fracture which is a brittle failure mode. As shown in the **Figure 2.5(a)**, $\bar{x'}$ represents the vertical distance between upper face of the gusset plate to the center of gravity of top half slotted-end HSS weld connection and is used to calculate the shear lag factor *U*, given by **Eq. (2.22)** and **Eq. (2.23)**, depending on $\bar{x'}/L_w$.

$$U = 1.1 - \frac{\bar{x'}}{L_w}, but \geq 0.8 \; when \; 0.1 < \bar{x'}/L_w \leq 0.3 \tag{2.22}$$

$$U = 1.0 \; when \; \bar{x}'/L_w \leq 0.1 \tag{2.23}$$

The bi-linear approximation given in the above equations, addressed in *Clause 12.3.3.4* of CSA S16-14 standard according to Packer (2014) is shown in **Figure 2.5(b)**. Note that this bi-linear approximation represents a conservative version of the curve suggested by Martinez-Saucedo and Packer (2009) which was calibrated against experimental results and is represented with dashed line in **Figure 2.5(b)**.

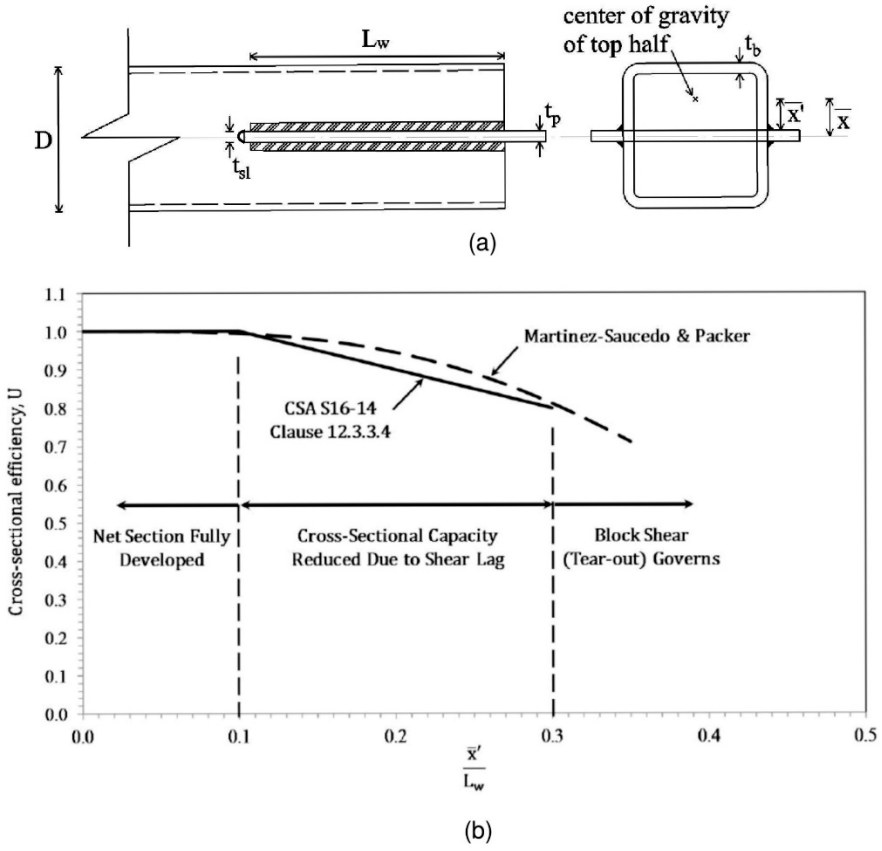

Figure 2.5 Shear lag effect in brace-to-frame connections : (a) Slotted end HSS welded connection; (b) Bi-linear approximation used for U, in CSA S16-14, for all slotted HSS welded connections with single concentric gusset plates (Packer, 2014)

2.4. Building stock distribution across Canada

Based on a survey released by Natural Resources Canada in 2012 (NRC, 2012), in Tirca et al., (2015) is summarized the distribution of non-residential buildings based on region, type of occupancy and year of construction. The building stock distribution is given in **Figure 2.6** for Quebec (QC) and British Columbia (BC). As illustrated, the selected 1980-1989 non-residential building stock has the largest distribution which is *25%* in Qc. and *22%* in B.C. Among the total

building inventory, the vast majority (*90.6%*) are three stories in height or less and *7.9%* are in the range of *4* to *9* storey height. In addition, under the auspices of Canadian Association of Earthquake Engineering (CANCEE), Heidebrecht (1999) conducted a survey at several consulting companies in Vancouver, Montreal and Quebec City, in order to determine the most common structural systems in use.

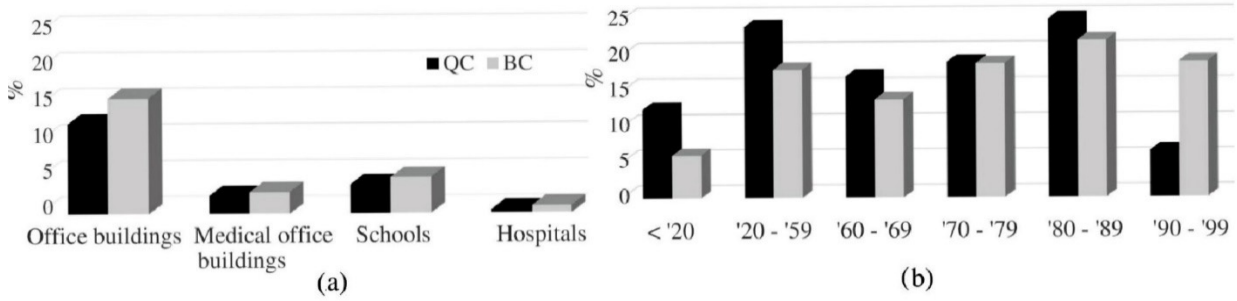

Figure 2.6 Building inventory in Canada: (a) distribution by occupancy, (b) distribution by year of construction (Tirca et al., 2015)

Thus, the respondents in Montreal and Quebec City indicated that over *50%* of the buildings being constructed were low-rise steel concentrically braced frames (CBF) with nominal ductility. Almost all of these were in the one- to three-storey height range. On the other hand, for Vancouver, the survey indicated that the percentage of CBF buildings was lower, instead reinforced concrete shear walls were more popular (Heidebrecht, 2003).

To conclude, the existing building stock designed and built prior to the 1970 was proportioned to carry gravity and wind load only, while that constructed between 1970 and 1985 was designed to withstand lower seismic forces in comparison with those required by the current code; thus the existing building stock is prone to damage and a seismic performance assessment is required. (Jiang et al., 2012)

2.5. Seismic Performance Assessment of existing buildings

In agreement with FEMA 547 standard (2006), seismic deficits are described as classes of structural deficiencies expressed in terms of: global strength, global stiffness, configuration, load path and component detailing. Deficiencies in global strength refer to the strength of SFRS and are common to older buildings, due to lack in seismic design details or because of a design with inadequate strength requirements. In the same way, a deficiency in global stiffness, is identified when interstorey drift is larger than the critical values. Failure to meet evaluation standards is often

the result of a building placing excessive drift demands on existing poorly detailed components. For example, critical drifts most often occur in the lowest levels of frame structures for low-rise buildings. On the other hand, critical drifts levels may occur in the upper floors as well, especially for medium and high-rise buildings.

Although deficiencies in global strength and stiffness have significant effect on seismic performance, a discontinuity in the load path, or inadequate strength in the load path, may be considered overarching because this deficiency will prevent the SFRS from being effective. Several load path deficiencies are difficult to be categorizing because strength deficiency may be considered to be part of another element. Lastly, component detailing in this context refers to design decisions that affect a component's or system's behaviour beyond the strength computed from nominal demand, usually in the nonlinear range. Examples include braced frames with brittle and weak connections that are unable to develop the capacity of the diagonal brace, (e.g. 1980 buildings), or brittle beam-column connections in moment frames that are unable to develop the capacity of the frame elements.

There are several procedures and standards in order to assess the seismic behaviour of existing buildings which are reviewed in the next subsections. In addition, some retrofit techniques are evaluated at the end of this section.

2.5.1. FEMA P695

According to FEMA P695 (2009) standard, the structural system is divided into bins, labelled performance groups which reflect changing in seismic behaviour of an existing structure when comparing it to a similar structure system proportioned to comply with current design. Therefore, the collapse safety of the studied system is evaluated for each performance group in terms of demand-to-capacity ratio. Thus, in the evaluation process of CBFs performance groups are divided into groups of structural members: braces, beams, columns and brace connections.

One primary parameter to characterize the collapse safety of a structure is the Collapse Margin Ratio (CMR). In the methodology given in FEMA P695 the nonlinear static analysis is used to provide statistical data on system overstrength and ductility capacity, while nonlinear dynamic analyses are used to assess the median collapse capacities and the CMR. Herein the nonlinear response is evaluated for a pre-defined ensemble of ground motions that are used for collapse assessment of all systems. In addition, for collapse evaluation, the ground motions are

systematically scaled to increasing earthquake intensities until median collapse is established. According to FEMA P695, the median collapse is the ground motion intensity in which half of the records in the selected set cause collapse of the structure. The ratio between the median collapse intensity and maximum design ground motion intensity is defined as the CMR. It is noted that the maximum design ground motion intensity is obtained from the response spectrum of the design level ground motions (2% in 50 years, for Canada) at the fundamental period, *T* of the building.

The median collapse capacity is obtained through Incremental Dynamic Analysis (IDA), as proposed by Vamvatsikos and Cornell (2002). In **Figure 2.7(a)** is shown an example of IDA results for a single structure subjected to a suite of ground motions of varying intensities. In this illustration, sideway collapse is the governing mechanism, due to excessive lateral displacement. Additionally, using collapse data obtained from IDA results, a collapse fragility function can be defined through a cumulative distribution function (CDF), relating the ground motion intensity to the probability of collapse (Ibarra et al., 2002) . An example of a cumulative distribution plot obtained from the collapse data of IDA curves is shown in **Figure 2.7(b).**

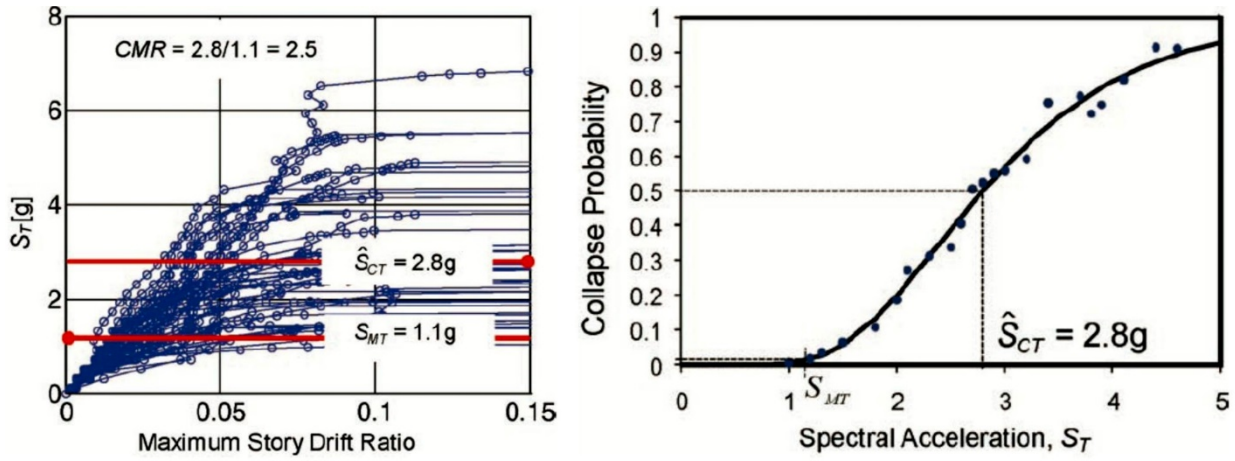

(a) (b)

Figure 2.7 Nonlinear time history analysis response plots for seismic assessment performance procedure: (a) IDA curves; (b) Fragility curve (FEMA P695, 2009)

In the above figure, the median collapse capacity, $\hat{S}_{CT} = 2.8g$ was defined as the spectral intensity when half of the ground motions caused the structure to collapse while $S_{MT} = 1.1g$ represents the maximum considered earthquake (design level) ground motion intensity. The Incremental Dynamic Analysis procedure and the fragility analysis are presented in detail in the next sections.

2.5.2. Incremental Dynamic Analysis

According to Vamvatsikos and Cornell (2002), Incremental Dynamic Analysis (IDA) is a parametric study used to estimate the structural performance under seismic loads. Thus, a structural model is subjected to a suit of ground motions scaled to multiple levels of intensity. The line connecting the successive points that measure on the vertical axis an engineering demand measure parameter (EDM) and on the horizontal axis a given intensity measure parameter (IM), is known as the IDA curve . Common examples of proposed IMs are the Peak Ground Acceleration (PGA), Peak Ground Velocity (PGV), the $\xi=5\%$ damped Spectral Acceleration at the structure's first mode period ($S_a(T_1,5\%)$). In addition, these IMs should be selected to cover a range from elastic to nonlinear and finally to collapse of the structure. On the other hand, an EDM is an observable quantity, which is determined from the output of the corresponding nonlinear dynamic analysis, depending on the application and the structure itself. Hence, possible choices can be: maximum base shear, rotations, peak roof drift, the floor peak interstorey drift angles, or their maximum.

Four patterns of IDA curves shown in **Figure 2.8** have been identified by Vamvatsikos and Cornell (2002). Herein, the response is ranging from a gradual degradation towards collapse to a rapid, back-and-forth twisting behavior. It is noted that the curves exhibit different linear-elastic regions, depending on the ground motion signature; however such a behavior is associated to the first nonlinearity that happen, in this case when the first brace buckling occurs. As illustrated, an IDA curve can "soften" after the initial buckling and accelerates towards large drifts (**Figure 2.8 (a)**), in the same time a bit of hardening can be observed in **Figure 2.8 (b)** while the curves illustrated in **Figure 2.8 (c)** and **(d)** seem to weave around the elastic slope. These twisting patterns of curves c) and d) are successive segments of "softening" and "hardening" in which the slope or stiffness decreases or increases with higher IM. However, it is assumed that the model allows the collapse mechanism formation based on the EDM parameter selection; hence a final softening segment occurs when the structure accumulates damage at increasingly high rates, signalling the onset of dynamic instability. The latter is defined as the point "where deformations increase in an unlimited manner for vanishingly small increments in the IM". In addition, the curve flattens as the damage moves towards infinity. This waving behaviour is defined as "structural resurrection", an extreme case of hardening, where the system is pushed to global collapse at a given IM. However, it appears as non-collapsing at a higher intensity level.

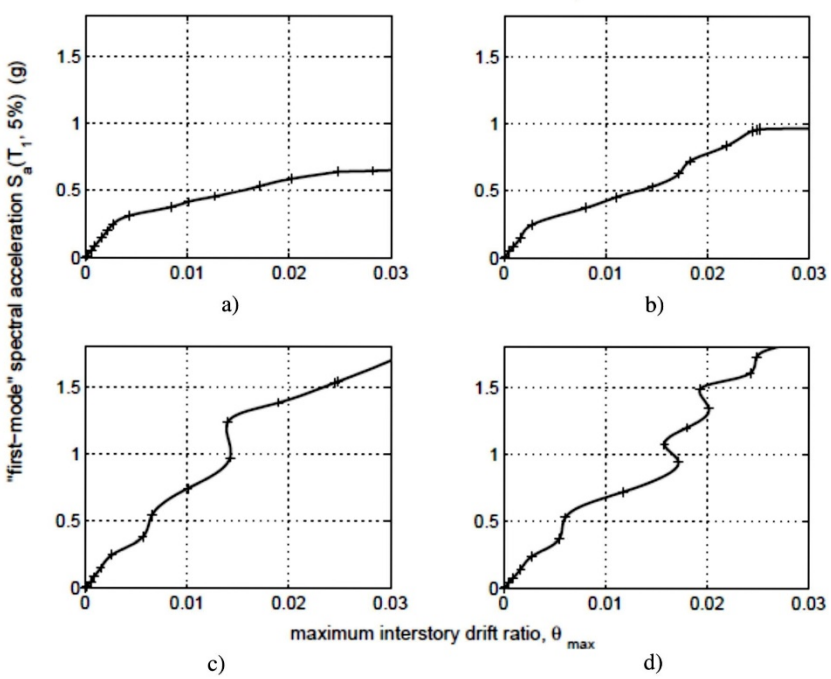

Figure 2.8 Different responses of a 5-storey braced frame under different ground motion records: (a) softening case; (b) hardening case; (c) severe hardening; (d) weaving behavior (Vamvatsikos and Cornell, 2002)

One advantage of IDA approach is that limit-states (performance levels) and capacity points can be defined on such a curve. For instance, Immediate Occupancy is a structural performance level associated with reaching a given EDM value, usually in terms of maximum interstorey drift ratio, θ_{max}, while Global Collapse is related to the IM or EDM value where dynamic instability was observed. While Immediate Occupancy is relatively easy to define (e.g. θ_{max}= 2% for steel SMRFs according to FEMA 350 guidelines) the Global Collapse is very difficult because each structure has dissimilar responses under different ground motions records. Performance level definition is discussed in more detail in *Section 2.5.4*. It is suggested that the non-convergence of the time-integration scheme is the safest numerical equivalent of the actual dynamic collapse, but this in turn can suffer from the quality of the numerical code, stepping or even round-off error of the integration process. However, FEMA 350 (2000) proposes a *20%* tangent slope approach, in which the last point on the curve with a tangent slope equal to *20%* of the elastic slope is defined as the capacity point. Herein, the flattening of the curve is an indicator of dynamic instability. Special attention needs to be given for the "weaving" behaviour of an IDA curve that can provide several such points where the structure head towards collapse, only to recover at higher IM levels; these lower points should be discarded as capacity candidates. It is noted that 20% tangent slope

approach mentioned earlier is more suitable for MRFs; however other rational engineering assumptions can be made in conjunction with this approach (for other structure types) in order to define the Global Collapse.

Conversely, one disadvantage of this method is the concern expressed about the validity of the outputs obtained from records that have been scaled (up or down) because "weaker" records are not necessary representative of "stronger" ones. Also the computation time, the more analyses per record, the better the accuracy and the longer for IDA to complete, can be a disadvantage.

2.5.3. Fragility Analysis

Fragility function describes the probability of failure to meet the performance objectives as a function of demand on the system response. In general, a lognormal cumulative distribution function is often used to derive fragility functions (Ibarra et al., 2002; Baker and Cornell, 2005; Elingwood et al., 2007) given as:

$$P(PL/IM=x) = \Phi(ln(x/m_R)/\beta_R) \tag{2.24}$$

where, $P(PL/IM = x)$ is the probability that a ground motion with $IM = x$ will exceed a given performance level PL; $\Phi(\ )$ is the standard normal cumulative distribution function (CDF), while m_R is the median capacity (expressed in units consistent with the IM, e.g. spectral acceleration) and β_R is the logarithmic standard deviation.

Although, it may be easy to assess a building vulnerability through fragility analysis, the concept of risk involves hazard, consequences and context. As a result, there are uncertainties about ground motion intensity, spectral shape, modelling and others. Although, the level of damage for structural and nonstructural damage can be predicted with the results from structural analyses, being similar with the results from experimental tests conducted in the past, the tested components forces and deformations may not be identical to those predicted by the response analyses.

However, it is possible to assess these performance measures by means of probability distribution performance functions. In his research, Elingwood et al. (2007) incorporates, two types of uncertainties in the fragility calculation i.e. aleatoric and epistemic uncertainty. The first type measures the inherent randomness in the seismic capacity of the structure (β_{RR}) while the second one depends on the quality of the analysis and supporting databases. To include both aleatoric and

epistemic uncertainties, the value of β_R in **Eq. (2.24)** is replaced by the square root of the sum of the squares of β_{RR} and β_{RU}, where β_{RR} is the aleatoric component of uncertainty and β_{RU} is the modeling (epistemic) uncertainty. The expression is given bellow:

$$\beta_R = \sqrt{\beta^2_{\mathrm{RR}} + \beta^2_{RU}} \tag{2.25}$$

In order to calculate the aleatoric uncertainty, the following relationship can be used:

$$\beta_{RR} = \sqrt{\beta^2_{\mathrm{D|Sa}} + \beta^2_C} \tag{2.26}$$

where βc is the uncertainty in capacity and depends on the considered Performance Level and $\beta_{D|Sa}$ represents the seismic demand uncertainty, calculated from the nonlinear time history analysis (IDA). Because of the nonlinear nature and large scatter of the response due to record-to-record variation, a nonlinear regression analysis of the power-law form (Luco and Cornell, 2007) given in **Eq. (2.27)** may be used. In addition, a logarithmic transform of **Eq. (2.27)** reduces it to a linear form given in **Eq. (2.28)**, where *a* and *b* are constants which are determined using a simple linear regression analysis, and *EDP* represents the engineering demand parameter used to build the IDA curve as described in *Section 2.5.2*. Therefore, the "best" fitted linear regression line is the one that passes through the data points with the least total error which can be obtained by minimizing the sum of the squared errors, s^2. The s^2 parameter is also known as the standard error, where *s* is the conditional standard deviation. The expression of seismic demand uncertainty can be computed as: $\beta_{D|Sa}=(ln(1+s^2))^{0.5}$, (Wen et all., 2004).

$$EDP = aS_a{}^b \tag{2.27}$$

$$\ln EDP = ln\, a + b\, ln\, S_a \tag{2.28}$$

In addition, HAZUS (FEMA, 2003) incorporates fragility functions for several seismic force resisting systems and nonstructural components for different damage states.

2.5.4. Retrofit techniques for vulnerable buildings

The ASCE 41-13 (2013) standard provides guidance about the rehabilitation objective classes, the targeted performance levels and rehabilitation strategies. The methodology given in the aforementioned standard is presented herein.

First, the ASCE 41-13 standard requires the selection of a Rehabilitation Objective Class for a building that has been identified previously as deficient and needs to be upgraded. For example a

typical Rehabilitation Objective Class for Office buildings is *Basic Safety*, for critical or essential structures (e.g. hospitals, fire stations, police stations) it is *Enhanced Rehabilitation*, while for other less critical structures is *Limited Rehabilitation Objective*. Thus, each Rehabilitation Objective Class consists of one or more rehabilitation goals. Each goal consists of a target building Performance Level (PL) and an earthquake hazard level. According to the standard, the building PLs are: *Operational (O), Immediate Occupancy (IO), Life Safety (LS) and Collapse Prevention (CP)*. In this light, **Figure 2.9** presents the matrix of Rehabilitation Objectives related to the extent of damage (Performance Level) and the earthquake hazard level.

		Target Building Performance Levels			
		Operational Performance Level (1-A)	Immediate Occupancy Performance Level (1-B)	Life Safety Performance Level (3-C)	Collapse Prevention Performance Level (5-E)
Earthquake Hazard Level	50%/50 year	a	b	c	d
	20%/50 year	e	f	g	h
	BSE-1 (~ 10%/50 year)	i	j	k	l
	BSE-2 (~ 2%/50 year)	m	n	o	p

[1]Each cell in the above matrix represents a discrete Rehabilitation Objective.

[2]The Rehabilitation Objectives in the matrix above may be used to represent the three specific Rehabilitation Objectives defined in Sections 1.4.1, 1.4.2, and 1.4.3, as follows:

Basic Safety Objective (BSO)	k and p
Enhanced Objectives	k and m, n, or o
	p and i or j
	k and p and a, b, c, or f
	m, n, or o alone
Limited Objectives	k alone
	p alone
	c, d, g, h, or l alone

Figure 2.9 Rehabilitation Objective matrix (ASCE 41-13)

As illustrated, the Basic Safety Objective (BSO) is the rehabilitation objective that achieves the dual rehabilitation goals of *LS* for the Basic Service Earthquake 1 (BSE-1) and *CP* for BSE-2. In other words, buildings meeting the BSO are expected to experience little damage from frequent, moderate earthquakes (10% in 50 years probability of exceedance) while for more severe rare events (2% in 50 years probability of exceedance) significantly damage and potential economic

losses are expected. Moreover, each performance level corresponding to a given earthquake hazard level, can be defined on each IDA curve by acceptable ranges of deformation demand on structural and nonstructural components which imply probable levels of damage. Damage levels namely*: Very Light, Light, Moderate* and *Severe* vary as a continuous function of building deformation and are associated to the defined building performance levels. For example, the *Moderate damage state* extends from the threshold of *Moderate damage* to *Severe damage.* It can be summarized that *Damage Measures (DM)* are functions of *Engineering Demand Parameters (EDP),* which are functions of *Intensity Measures (IM).* In addition, ASCE/SEI 41-13 standard provides suggested maximum interstorey drift and maximum residual interstorey drift values for each performance level. These values corresponding to steel braced frames (BF) structures are given in **Figure 2.10** (Tirca et al., 2015).

Performance Levels	**Operational**	**Immediate Occupancy**	**Life Safety**	**Collapse Prevention**
Performance Ranges	No structural damage	Damage Control range	Limited Safety range	Collapse
Degree of Damage	None / Very Light Damage	Light Damage	Moderate Damage	Complete Damage
Damage Levels	**Very Light**	**Light**	**Moderate**	**Severe**
Suggested $\delta_{max.}$		0.5%hs	1.5%hs	2.0%hs
Suggested $\delta_{max.res.}$		-	0.5%hs	2.0%hs

Figure 2.10 Mapping damage control against building performance levels according to ASCE 41-13 (Tirca et al., 2015)

Regarding the rehabilitation strategies, it is beneficial for the rehabilitated SFRS to have an appropriate level of redundancy so that any localized failure of system's components will not result in local collapse or instability. Several rehabilitation strategies such as: i) local modification of components, ii) removal of existing irregularities, iii) global structural stiffening and strengthening, iv) mass reduction, v) seismic isolation or supplemental energy dissipation, are recommended in ASCE 41-13. Out of these retrofit strategies, local modification of components tends to be the most economical rehabilitation approach. Local strengthening allows one or more under-strength components or connections to resist the demands predicted by analysis without affecting the overall response of the structure. This includes measures such as cover plating steel columns or beams and gusset plate replacement. Such measures increase the strength of the components and allow it to resist more earthquake-induced forces, before the onset of damage.

Another technique given in ASCE 41-13 is the cross-section reduction (weakening) of a selected structural component, in order to increase the flexibility and response displacement capacity. This technique is very popular and it was studied by several researchers (Viti et al., 2006; Jiang, 2013) providing good results. Regardless of the rehabilitation measure used, it is important that the retrofitted building shall not develop a reduction of the performance level of the existing building, neither shall create a new structural irregularity making the existing irregularity more severe, nor shall result in an increase in the seismic forces to any deficient component.

2.6. Seismic Resilience

The risk of economic losses as effect of natural disasters (e.g. earthquakes) is correlated with the state of building stock performance. Both system vulnerability and hazard are conditioning parameters. In an extended approach, other causes of disaster risk are demographic and socio-political. In general, vulnerability originates in physical fragility systems designed and built prior to modern codes (Bankoff et al., 2004). These are also characterized by lack of resilience which is defined by the ability of the system "to reduce the chances of a shock, to absorb such a shock if it occurs and to recover quickly after the shock" (Bruneau et al., 2003). In other words, resilience was defined as the capacity of systems to recover after severe disasters of any type.This section describes a general methodology and recommended procedures to assess the seismic resilience of individual buildings based on their performance. Performance measures include potential casualties and expected losses, repair and replacement cost due to unsafe conditions.

In order to reduce the losses, mitigations and preventive measures should be taken before the extreme event happens. Mitigation actions can reduce the vulnerability of buildings. However, in case of insufficient mitigation actions, or in case that the events exceed expectations, damage occurs and a recovery process is necessary in order to maintain a functional level. Past studies (Bruneau et al., 2003; Chang et al., 2004) had shown that the resilience can be conceptualized based on four interrelated dimensions: technical, organizational, social and economic. The first two components are mostly related to the resilience of critical systems (e.g. hospitals) while the last two are more related to the affected community.

Resilience was defined by Bruneau et al., (2004; 2007) using a mathematical function describing the functionality ($Q(t)$) of the system expressed in percentage (%). For example, resilience is 100%

for an un-damaged system, whereas for total loss of the building the resilience is 0%. In addition for a single event, resilience is defined by the following equation:

$$Res_i = \int_{t_{0E}}^{t_{0E}+T_{RE}} Q(t)\, dt \tag{2.29}$$

where t is the time, t_{0E} represents the initial time when the extreme event happen, T_{RE} is the recovery time from the event and $Q(t)$ is the functionality defined as (Cimellaro et al., 2006; 2009):

$$Q(t) = 1 - L(I, T_{RE})\left[H(t - T_{0E}) - H\left(t - (T_{0E} + T_{RE})\right)\right] f_{rec}(t, T_{0E}, T_{RE}) \tag{2.30}$$

In **Eq. (2.30)**, I is the earthquake intensity, $L(I, T_{RE})$ is the loss function, $f_{rec}\ (t, t_{0E}, T_{RE})$ is the recovery function and $H(t)$is the Heaviside step function. As shown, the evaluation of resilience requires a loss estimation model and a recovery function model which are defined in the next sections. Graphically, the resilience is defined as the normalised area under the $Q(t)$ function as illustrated in **Figure 2.11**. In the figure, T_{LC} represents the life span for a given system and includes the building recovery time.

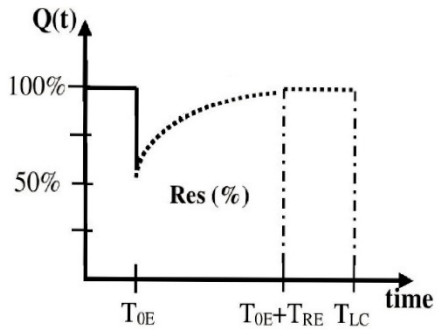

Figure 2.11 Representation of seismic resilience

It is noted that the recovery time T_{RE} is a random variable with high uncertainties, and typically depends on several parameters as: earthquake intensity, resource availability, materials and labor. In consequence is the most difficult quantity to predict in the resilience function.

2.6.1. Resilience attributes

The quantification of system's resilience is achieved by measuring the *rapidity*, *robustness*, *redundancy* and *resourcefulness* attributes. According to Cimellaro et al., (2009) *rapidity* represents the slope of the functionality curve (**Figure 2.12(a)**) during the recovery time and can be expressed as the average recovery rate (in percentage) in time: L/T_{RE}, where L is the total loss

after the extreme event and T_{RE} is the recovery time. The second parameter, *robustness*, can be related to the residual functionality right after the extreme event (**Figure 2.12(b)**) and can be expressed as: $R= (1-L)$, where L is the total loss. It is possible to incorporate uncertainties in the calculation of robustness by expressing the losses (L) as a function of the mean (m_L) and dispersion (σ_L) corresponding to a specific level of losses. The last two quantities *redundancy* and *resourcefulness* refer to the system properties that allow for alternate options or substitutions and to the capacity of the society to identify the problems and to mobilize the needed resources. While the influence of *rapidity* and *robustness* is clear, the influence of the other two parameters is more complex, being strongly coupled, yet very difficult to quantify because they depend on human factors and available resources (Cimellaro et al., 2009).

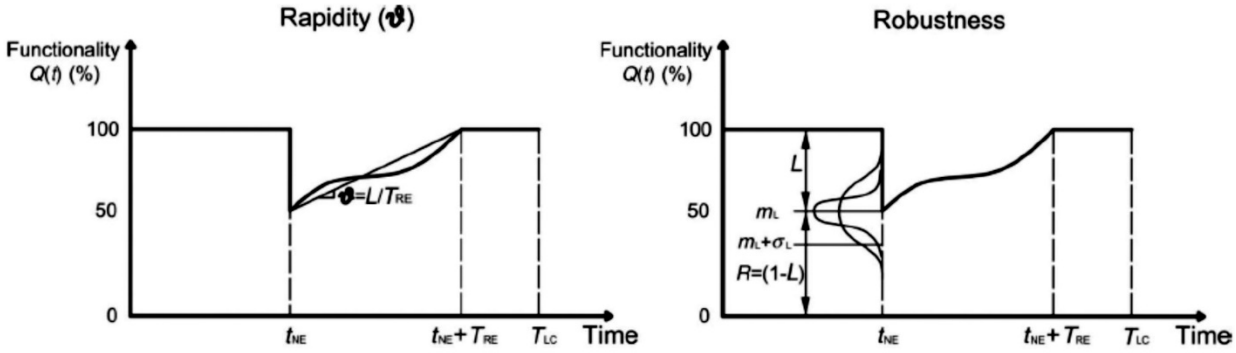

(a) (b)

Figure 2.12 Resilience attributes: (a) Rapidity; (b) Robustness (Cimellaro et al., 2009)

2.6.2. Loss estimation

Because loss estimation models generally produce results in terms of expected $ losses, they do not measure directly the resilience. In addition, this type of losses are highly uncertain and depend on different scenarios considered. However, there are some common parameters that influence the loss calculation. In fact, the loss function $L(I,T_{RE})$ is expressed as a function of earthquake intensity I, and recovery time, T_{RE}. According to Cimellaro et al. (2006) losses are divide in two groups: Structural losses (L_S) and Nonstructural losses (L_{NS}). The latter can be divided in four categories: i) Direct economic losses $L_{NS,DE}$ (loss of content);ii) Direct casualties losses $L_{NS,DC}$; iii) Indirect economic losses $L_{NS,IE}$; (business interruption losses);iv) Indirect casualties losses $L_{NS,IC}$.

The evaluation of damage (losses) is expressed in terms of economic cost ($) or repair cost ratio defined as the ratio of the cost of retrofit and reinstatement of building to the cost of fully replaced

(Coburn and Spencer, 2002). However, the estimation of losses is reported according to the previously defined damage states (e.g. *very light*, *light*, etc) expressed as a function of the associated structural and nonstructural building performance as depicted in **Figure 2.10**. The nonstructural components are drift-sensitive (e.g. partition walls, cladding, ceiling, etc.) and acceleration-sensitive (e.g. mechanical equipment, piping, electrical system, etc.). The physical structural losses can be determined using **Eq. (2.31)** according to the methodology provided by HAZUZ (FEMA, 2003):

$$L_S = \sum_1^N CS_{DS} = BRC * \sum_1^N POSTR_{DS} * RCS_{DS} \tag{2.31}$$

where: CS_{DS} is the cost of the structural damage computed for the considered damage state; BRC is the building replacement cost; $POSTR_{DS}$ is the probability of being in a given damage state, DS; RCS_{DS} is the structural repair cost ratio in a damage state, DS; while N is the number of damage states considered. A similar calculation can be performed to assess L_{NS}.

2.6.3. Recovery functions

As depicted in **Figure 2.12** the recovery time T_{RE} and the recovery path are essential for evaluation of seismic resilience but the information on comprehensive models describing the recovery process is limited. However, three different recovery functions shown in **Eq. (2.32)** can be chosen depending on system and society response: i) linear; ii) exponential (Kafali and Grigoriu, 2005) and iii) trigonometric (Chang and Shinozuka, 2004).

i) $$f_{rec}(t, T_{RE}) = (1 - \frac{t - t_{0E}}{T_{RE}})$$

ii) $$f_{rec}(t) = \exp[-(t - t_{0E}) * ln200/T_{RE}] \tag{2.32}$$

iii) $$f_{rec}(t) = 0.5 * \{1 + \cos[\pi(t - t_{0E})/T_{RE}]\}$$

The linear recovery is the simplest form of recovery, and can be used when there is no information regarding the society response. On the other hand, when the society response to an event is very fast having an initial flow of resources, the exponential recovery function is more suitable. However, the rapidity of recovery decreases slowly. Lastly the trigonometric recovery function is used when the society response is very slow initially, due to the lack of organization; but after, the rapidity of recovery increases gradually. All three types of recovery functions are illustrated in **Figure 2.13**.

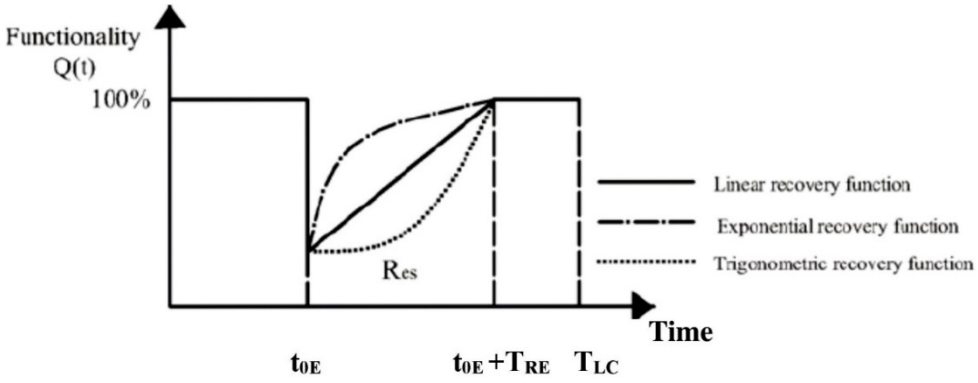

Figure 2.13 Recovery functions (Cimellaro et al., 2006)

2.7. Conclusions

This Chapter emphasizes the quantification of seismic resilience of buildings constructed prior to modern codes. The following findings are reported:

- In terms of seismic hazard, the western and eastern Canada is prone to high and moderate risk.
- The first probabilistic seismic hazard map (2nd generation) was conceived for 100 years return period (50%/50 years) and was released in the 1970 edition of NBCC. It was followed by the 3rd and 4th generation of seismic map developed for 475 and 2475 years return period, respectively. The 3rd generation was released in the 1985 edition of NBCC and the 4th generation in the 2005 edition. Furthermore, capacity design and special detailing provisions were not incorporated in CSA S16 standard prior to '89.
- Existing building stock, designed and built prior to 1970 was proportioned to carry gravity and wind load only, while that constructed between 1970 -1985 was designed to withstand lower seismic forces in comparison with those required today.
- From the map of non-residential buildings distribution by year of construction considering the 1920 – 1999 time span, the 1980-1989 building stock is the largest: 25% (QC) and 21% (BC). In addition, sorted by non-residential occupancy, the office building stock is the largest. Within the 1980-1989 building stock, the low-rise represent the dominant segment followed by the middle-rise. Among them, the percentage of existing CBF buildings is representative only for eastern Canada.
- To assess the seismic performance of existing buildings the methodology given in FEMA P695 can be employed. In this light, the collapse safety of a structure is characterized by the Collapse Margin Ratio (CMR) which is determined by means of Incremental Dynamic Analysis (IDA).

Additionally, using collapse data obtained from IDA results, a collapse fragility function can be defined through a cumulative distribution function (CDF), relating the ground motion intensity to the probability of collapse. However, the seismic vulnerability of existing buildings can be reduced with appropriate rehabilitation schemes according to the methodology given in ASCE 41-13 standard.

- The concept of seismic resilience is defined as the capability of a system to maintain a level of functionality or performance in the aftermath of an earthquake event. Resilience is characterized by performance metrics such as: fragility, loss, and recovery functions developed for structural systems designed to withstand the corresponding seismic hazard level.

CHAPTER 3. DESIGN OF CONCENTRICALLY BRACED FRAME (CBF) BUILDINGS IN ACCORDANCE WITH 1980 CODE REQUIREMENTS

3.1. Proposed Methodology

The purpose of this study is to quantify the seismic resilience of existing low- and middle-rise CBF office buildings. In this light, a methodology is presented below and is also illustrated in **Figure 3.1**:

- First, the seismic assessment of building is based on the Equivalent Static Force Procedure (*ESFP*) and all structural members and components (e.g. braces, beams, columns, and brace connections) are evaluated in terms of demand-to-capacity ratios according to the current code provisions (NBCC 2010 and CSA/S16-09 standard).
- Second, to assess the collapse safety of a structure expressed in term of Collapse Margin Ratio (*CMR*), the Incremental Dynamic Analysis (*IDA*) is employed. This procedure requires Nonlinear Time-History Analysis where an ensemble of ground motions are scaled and incremented stepwise until collapse is reached. Herein, the *CMR* is defined as the ratio between the median collapse intensity of employed ground motions (determined from IDA), and the ordinate of design spectrum that corresponds to the first-mode period of the building.
- At this stage of building assessment, decision makers can judge if the retrofit action is recommended or they accept the risk and keep the building "as is".
- When the retrofit action is decided, the Rehabilitation Objective Class is defined according to ASCE/SEI 41-13 standard. In addition, based on the selected Rehabilitation Objective Class and Targeted Performance levels the retrofit technique is selected.
- The final step consists in the quantification of seismic resilience of the pre- and post-retrofit office buildings. Resilience is characterized by performance metrics such as: fragility, loss and recovery functions developed for structural systems designed to withstand the corresponding seismic hazard level. Thus, using collapse data obtained from IDA results, a collapse fragility function is defined through a cumulative distribution function (CDF). Then, the loss and recovery functions are estimated.

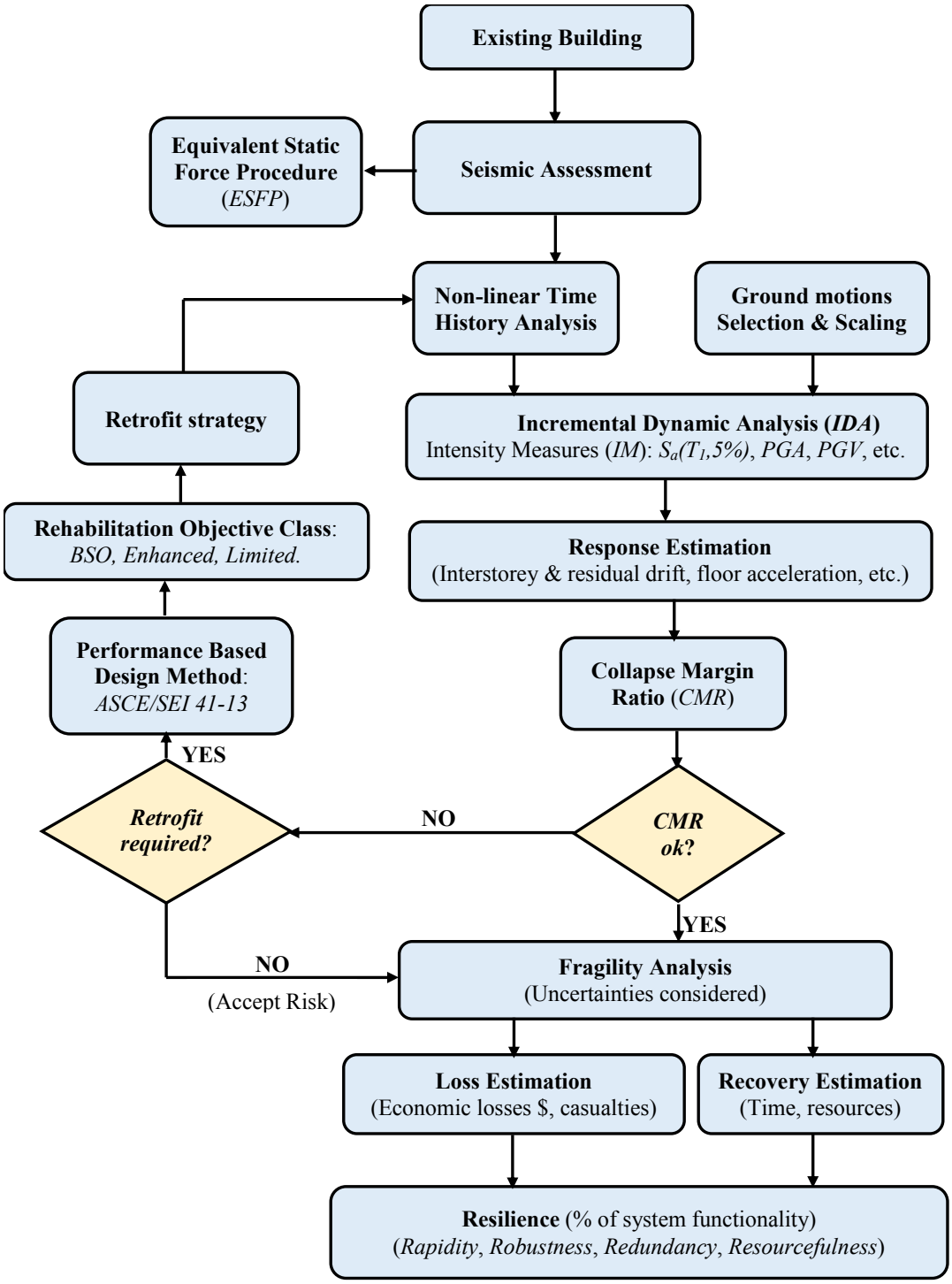

Figure 3.1 Flowchart of the proposed methodology

3.2. Building description and load definitions

To quantify the seismic vulnerability of the 1980 low- and middle-rise CBF office building structures, two 3- and 6-storey fictitious buildings with identical plan layout located in Quebec City and Vancouver were selected for investigation. The total height of the 3-and 6-storey building

is $h_n = 11.7\ m$ and $h_n = 22.5\ m$, respectively. The typical floor height is $h_{typ} = 3.6\ m$, while the ground floor height is $h_{gf} = 4\ .5\ m$. Both buildings are located on firm soil (site class C) and cover a rectangular area of 30 x 60 m^2. The plan view and frame elevations are shown in **Figure 3.2**.

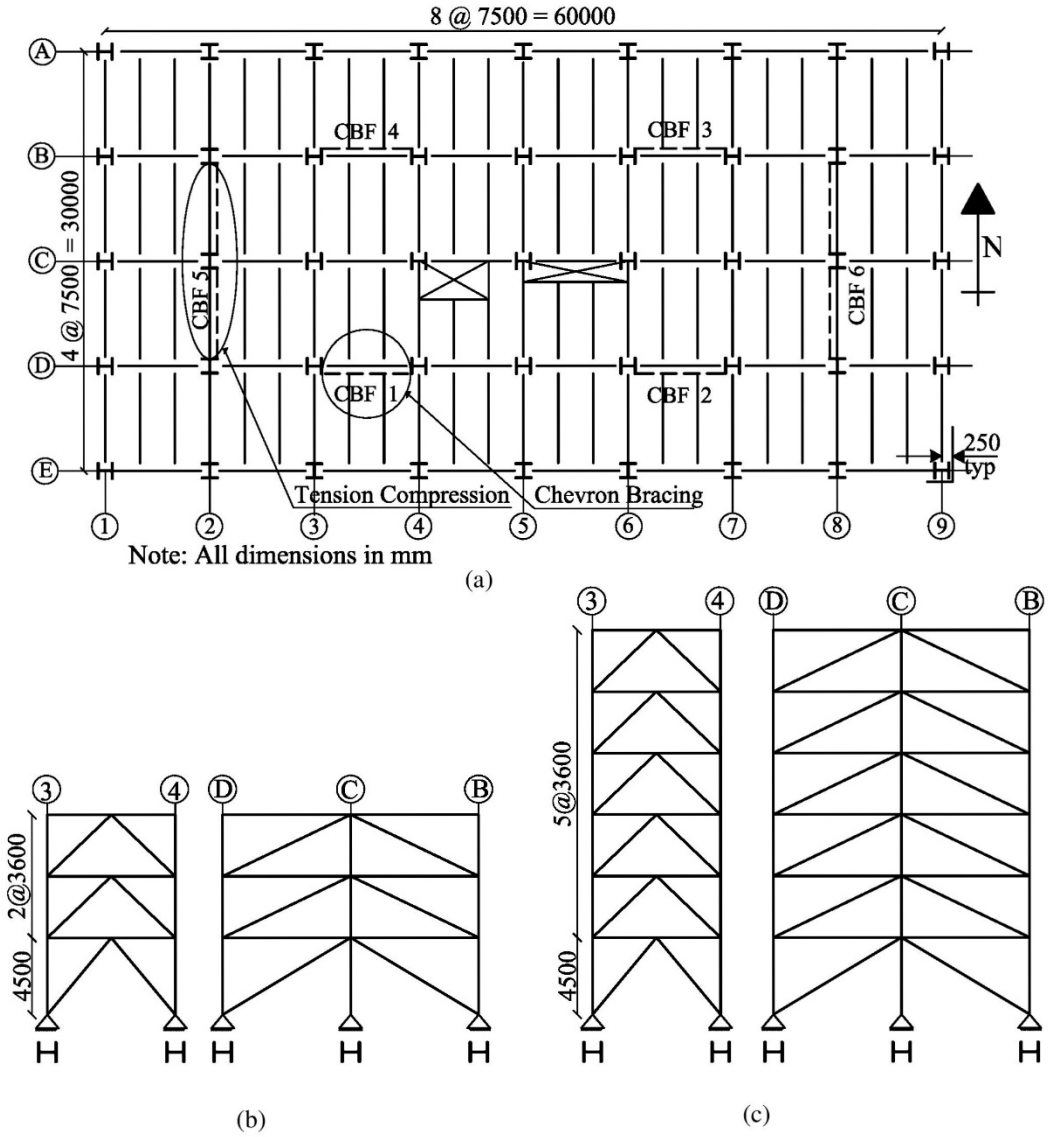

Figure 3.2 Studied buildings: (a) plan view; (b) E-W and N-S direction elevations for 3-storey building; (c) E-W and N-S direction elevations for 6-storey building.

As illustrated, both buildings are braced in both principal directions. Hence, there are four CBFs in chevron bracing configuration located in the East-West (E-W) direction on gridlines B-34, B-67, D-34 and D-67 and two times two adjacent CBFs in tension-compression diagonal bracing located in the North-South (N-S) direction, on axis 2-BD and 8-BD respectively. Furthermore, the buildings were considered simple constructions which assumes that ends of beams, girders,

columns and braces are free to rotate (pinned connection) under loads in the plane of loading. In addition, all columns and beams were assumed made of CSA G40.21-300W steel with a nominal yield strength $F_y = 300\ MPa$ and $F_u = 450\ MPa$ while for braces $F_y = 345\ MPa$ was considered.

As mentioned previously, the design was based on the 1980 NBCC in conjunction with CSA/S16.1-M78 standard. Therefore, according to Part 4 of NBCC 1980, the minimum specified uniformly distributed gravity loads for the structure design for both 3- and 6-storey buildings are given in **Table 3.1**. In addition, all the studied buildings have a normal importance category.

Table 3.1 Dead and live loads for the building

DL on the Roof (kPa)	
Steel deck with 100 mm concrete on the top	1.9
5 mm plate gravel fleck	0.3
Ceiling	0.1
Mechanical	0.2
10 mm insulation	0.1
Concrete for roof slope	0.4
Total	**3.0**
DL on Typical Floor (kPa)	
Steel deck with 100 mm concrete on the top	1.9
Partition	1.0
Mechanical	0.2
Ceiling	0.1
Flooring	0.2
Total	**3.4**
DL on the walls (kPa)	
Cladding	1.22
LL on the roof (kPa)	
Snow load- Quebec City	2.24
Snow load- Vancouver	1.52
LL on Typical Floor (kPa)	
Commercial floor load	2.4

DL=Dead load; LL=Live load.

According to Part 4 of NBCC 1980, structural members were designed using the load combinations given in **Eq. (2.10)**. Further, the minimum lateral seismic force V, assumed to act non-concurrently in any direction of the building was calculated using **Eq. (2.2)**. The value of the design acceleration ratio A corresponds to peak ground accelerations based on 50% probability of exceedance in 50 years, which corresponds to a return period of 100 years and was assumed constant within each seismic zone defined in the Commentary on Effects of Earthquakes in NBC Supplement No. 4.

The seismic zones, the ratio of horizontal ground acceleration to the gravity acceleration and the acceleration ratio *A* respectively, are presented in **Table 3.2.** According to the 1970 seismic map, both Quebec and Vancouver were in the same seismic zone 3, thus the corresponding acceleration ratio was *0.08 g*, for the selected 3- and 6-storey buildings.

Table 3.2 Definition of seismic zones

Seismic Zone	Ratio of horizontal ground acceleration to the acceleration due to gravity		Acceleration Ratio, A
0	Less than	0.01	0.00
1	Equal to or greater than to less than	0.01 0.03	0.02
2	Equal to or greater than to less than	0.03 0.06	0.04
3	Equal to or greater than	0.06	0.08

3.3. Design of a 3-storey office building located in Quebec City (3Q) according to NBCC 1980 and CSA/S16.1-M78 standard

According to NBCC 1980, the minimum design base shear *V*, was calculated using **Eq. (2.2)**. The seismic response factor *S,* was taken *1.0* for both E-W and N-S direction and the value was calculated according to **Eq. (2.7)**. As shown, the seismic response factor cannot exceed the value of *1.00* and depends on the fundamental vibration period of the structure which has the value *0.136 s* in the E-W direction and, *0.192 s* in the N-S direction. The empirical expression of the fundamental period T_{emp}, for steel braced frames is given as: $T_{\mathrm{emp}} = 0.09h_n/D^{1/2}$; where h_n is the total building height and *D* represents the dimension of the building in the direction parallel to the applied seismic force. Alternatively, *S* can be determined using the period computed from methods of mechanics, without any prescribed upper limit.

Frames with tension–compression diagonal bracing or chevron are also considered to form a ductile structural system requiring *K=1.0* while for tension only braces *K=1.3*. The importance factor *I=1.0* for office buildings and the foundation factor *F* is equal to *1.0* for the assumed site type (firm soil). For the 3-storey building located in Quebec City (3Q), the total seismic weight including 25% design snow load was *W= 20918 kN*. Substituting all values in **Eq. (2.2)** the resulted minimum lateral earthquake design force at the base of the structure was *1674 kN* for the E-W direction, corresponding to a force of *418 kN* per each frame in the aforementioned direction;

whereas for the N-S direction the total base shear was *1674 kN* which is distributed between the two Seismic Force Resisting Systems (SFRS), resulting a value of *837 kN* per two adjacent CBFs.

It is noted that for regular structures, which is the case for this study, NBCC 1980 allows to determine the earthquake induced forces using the static equivalent force method. According to this procedure, a concentrated load F_t given in **Eq. (2.8)**, which cannot exceed $0.15V$ was applied at the roof level when the ratio $h_n/D_s > 3$ (otherwise $F_t=0$). According to the calculations $F_t = 0$ for both E-W and N-S directions. The remaining seismic load, $V\text{-}F_t$, was distributed along the building height as a function of the relative product of the seismic weight and the elevation from the ground at the level under consideration in accordance with **Eq. (2.9)**. Additionally, torsional moments in the horizontal plan of the building were computed for each storey using **Eq. (2.4)** according to the design eccentricity e_x, calculated with **Eq. (2.5)** or **(2.6)**, whichever provides the greater effect. On the other hand, if e_x exceeds $D_n/4$ then a dynamic analysis is required or the computed torsional moment needs to be doubled. The computed design eccentricity for E-W direction was *1.5 m* while for the N-S direction was *3 m*. It is noted that the dynamic analysis was not required.

The sway effects produced by the vertical loads acting on the structure on its displaced configuration were accounted directly in the analysis by means of $P\text{-}\Delta$ effects. Herein, the additional shear due to $P\text{-}\Delta$ effects, V' was obtained using **Eq. (3.1)** in which h_i, represents the storey height, Δ_i, is the storey deflection due to the application of the lateral forces determined from an elastic first order analysis and P_i represents the total gravity load supported by the columns of the SFRS (E-W or N-S direction) under the 1.25DL + 0.7(1.5LL + 1.5Q) load combination.

$$V`_i = \sum P_i(\Delta_{i+1} - \Delta_i)/h_i \tag{3.1}$$

3.3.1. Gravity System design

According to **Figure 3.2** there are two secondary beams in each bay of *7.5 m*, having a tributary width of *2.5 m*. The most unfavorable effect under the gravity loads, which corresponds to load combination: 1.25DL+1.5LL was considered for the gravity system design. Thus, the maximum beam deflection has to be smaller than $l/360$ where l represents the total beam length in millimetres. Additionally, beams were selected such that the factored moment resistance of the member $M_r > M_{max}$ where M_{max} is the maximum bending moment due to the gravity loads. The secondary beams and girders design summary for the 3-storey building in Quebec City is illustrated in **Table 3.3.**

Table 3.3 Design summary for secondary beams and girders (3-Storey Quebec City)

ST	Sec. beams		Girders	
	M_{max}	Selected Beam	M_{max}	Selected Beam
	*kN*m*	-	*kN*m*	-
3	125	W310x33	333	W460x52
2	138	W310x33	368	W460x60
1	138	W310x33	368	W460x60

Further, the gravity columns were designed choosing a section that has the factored axial compressive resistance C_r larger than the axial compressive force in the column, C_f. It is noted that when a structural member supports a tributary floor area $> 20\ m^2$ for any use or occupancy other than those used for storage, manufacturing, retail stores, garage or assemblies, the design live load due to use and occupancy, excluding snow, is reduced with a factor *f*, called live load reduction factor given in **Eq. (3.2)**. On the other hand, when the tributary area exceeds $80\ m^2$ the live load reduction factor is given in **Eq. (3.3)**.

$$f = 0.3 + \sqrt{9.8/B} \tag{3.2}$$

$$f = 0.5 + \sqrt{20/A} \tag{3.3}$$

where, *A* and *B* is the tributary area in square meters for this type of use and occupancy, excluding the area supporting snow. For any tributary areas smaller than $20\ m^2$ there is no live load reduction. Moreover CSA/S16.1-M78 standard, limits the slenderness ratio which is taken as the ratio of effective length (*KL*) to the corresponding radius of gyration (*r*) to *200* for compression members while for tension members the maximum value is *300*. Note that, for gravity members there is no restriction in selecting the class of section. The design summary for the gravity columns is presented in **Appendix I** where the factored axial compressive resistance C_r, was calculated as per **Eq. (2.17)** considering $F_y = 300\ MPa$.

3.3.2. Design of the CBF in the E-W direction according to NBCC 1980 and CSA/S16.1-M78

The factored shear force per frame with and without torsion and additional shear from *P-Δ* effects computed for each loading case (see **Eq. (2.10)**) for the 3-storey building in Quebec City is

summarized in **Table 3.4**. As illustrated, by adding the torsion and *P-Δ* effects the total base shear per frame increased by *11%*.

Table 3.4 Shear force per 3-storey CBF in E-W direction (Quebec City)

St	Shear force: Q	Case 2: 1.50 Q	Case 3: 1.05Q	Case 2: 1.50 (Q+T+ PΔ)	Case 3: 1.05 (Q+T+ PΔ)
	kN	*kN*	*kN*	*kN*	*kN*
3	199	299	209	303	212
2	340	510	357	546	382
1	420	630	441	701	490

Q- earthquake; T-torsion effect; *PΔ*- additional shear from P-Δ effects.

3.3.2.1. SFRS brace design

Braces were made of square Hollow Structural Sections (HSS) and comply with CSA G40.21-345W Class C steel (cold formed) having $F_y = 345\ MPa$ and $F_u = 448\ MPa$ as per 1980's. Additionally, braces were selected such as $C_f \leq C_r$ computed according to **Eq. (2.17)**. The most unfavorable load combination for brace design was: (1.25DL + 1.5Q) and the design values are given in **Figure 3.3** (for E-W direction). Moreover, braces were also verified to satisfy the condition: $T_f \leq T_r$, where T_r was calculated using **Eq. (2.16)**. For this case $F_y/F_u = 0.77$ which implies $A_n = 0.9A_g$. The selected HSS brace sections together with their C_r and T_r values are given in **Table 3.5** where "80" symbol was used to refer to the "1980's design". The gross cross-sectional area A_g; radius of gyration r; the width-to-thickness ratio b/t where b is the nominal outside dimension less four times the wall thickness t, together with the slenderness ratio KL/r and slenderness λ, are also given in **Table 3.5**. It is noted that the effective length of the brace was considered as $0.9L$ to account for the connections between brace and frame.

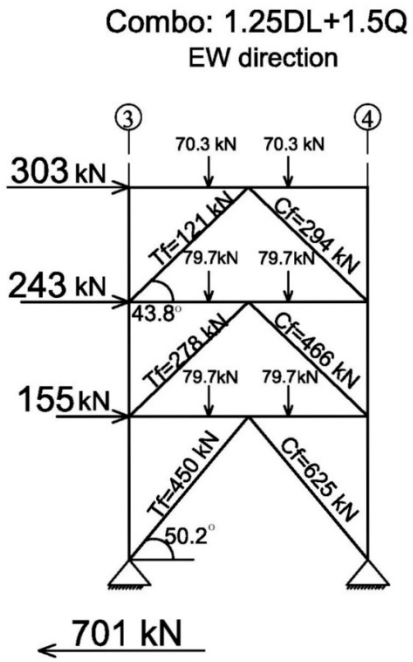

Figure 3.3 Axial compressive forces in braces under 1.25DL+1.5Q load combination for the 3-storey CBF in E-W direction (Quebec City)

Thus, for the E-W direction the effective length is *5265 mm* for braces at ground floor and *4678 mm* for those at typical floor. In addition, the selected braces are Class 1 of section where $b/t < 420/F_y^{0.5} = 22.5$ as per *Section 11.2* of CSA/S16.1-M78. Regardless of the selected cross-sections, the term C_f/C_r is called *demand-to-capacity ratio* which should be ≤ 1.0.

Table 3.5 Design summary of 3-storey CBF braces in E-W direction (Quebec City)

St	Section*	A_g	r	b/t	KL/r	λ	$C_{f\text{-}80}$	$C_{r\text{-}80}$	$T_{r\text{-}80}$	$C_{f\text{-}80}/C_{r\text{-}80}$
	mm x mm x mm	*mm^2*	*mm*	-	*< 200*	-	*kN*	*kN*	*kN*	*< 1.00*
3	102x102x9.5	3280	36.9	6.7	127	1.7	294	304	917	0.97
2	127x127x8.0	3620	47.2	11.9	99	1.3	466	477	1012	0.98
1	152x152x8.0	4430	58.4	15	90	1.2	625	665	1238	0.94

*Square tubular section (HSS): b x h x t

3.3.2.2. Beams and column design of 3-storey CBF

All beams and columns are made of W-shape complying with CSA G40.21-300W where $F_y=300$ *MPa* and $F_u= 450$ *MPa* as commonly used in the 1980s. Each member section was proportioned to satisfy the strength and stability conditions for axial compression/tension and bending as per

Eqs. (3.4) to (**3.7)** of CSA/S16.1-M78 standard. As previously stated, the ends of beams are pinned connected to columns. However, beams were laterally supported by the composite steel deck over the full beam length.

$$\frac{M_{fx}}{M_{rx}} \leq 1.0 \tag{3.4}$$

$$\frac{C_f}{C_r} + \frac{0.85M_{fx}}{M_{rx}} \leq 1.0, \text{ where } C_r = \phi A F_y \tag{3.5}$$

$$\frac{C_f}{C_{rx}} + \frac{\omega_x M_{fx}}{M_{rx}\left(1-\frac{C_f}{C_{ex}}\right)} \leq 1.0 \tag{3.6}$$

$$\frac{T_f}{T_r} + \frac{M_{fx}}{M_{rx}} \leq 1.0 \tag{3.7}$$

In the above equations M_f, the factored bending moment computed for each of the three combinations considered, is given in **Table 3.6** together with the factored axial compression C_f, and tension T_f in the members. The factored compressive resistance of the beams about the strong axis C_{rx} was computed using **Eq. (2.17).** When the interaction **Eq. (3.5)** was used, C_r was considered equal to ϕAF_y, where $\phi = 0.9$ and A is the cross-sectional area. The factored moment resistance about x-x axis M_{rx}, is: $M_{rx}=\phi ZF_y$, where Z represents the plastic modulus of the section. Additionally, the parameter ω_x was taken as *1.00* while C_{ex} is the Euler buckling load taken as: $C_{ex} = \pi^2 EI/L^2$, where I is the moment of inertia of the section and L represents the clearance of the beam. The selected 3-storey CBF beams in E-W direction are summarized in **Table 3.7**. In addition, all beams are Class 1 and 2 according to CSA/S16.1-M78 standard requirements.

Table 3.6 Design loads for the 3-storey CBF beams in E-W direction (Quebec City)

St	Combo:1.25DL+1.5LL			Combo:1.25DL+1.5Q			Combo:1.25DL+1.05LL+1.05Q		
	M_f *kNm*	T_f *kN*	C_f *kN*	M_f *kNm*	T_f *kN*	C_f *kN*	M_f *kNm*	T_f *kN*	C_f *kN*
3	93	N/A	N/A	49	149	149	79	104	104
2	102	N/A	N/A	55	328	203	88	287	85
1	102	N/A	N/A	55	414	272	88	353	128

Table 3.7 Design summary of 3-storey CBF beams in E-W direction (Quebec City)

St	Section	Class	1.25DL+1.5LL				1.25DL+1.5Q				1.25DL+1.05LL+1.05Q			
	-	-	Eq. (3.4)	Eq. (3.5)	Eq. (3.6)	Eq. (3.7)	Eq. (3.4)	Eq. (3.5)	Eq. (3.6)	Eq. (3.7)	Eq. (3.4)	Eq. (3.5)	Eq. (3.6)	Eq. (3.7)
3	W310x33	1	0.7	N/A	N/A	N/A	0.4	0.5	0.6	0.5	0.6	0.6	0.8	0.7
2	W310x39	2	0.6	N/A	N/A	N/A	0.3	0.4	0.6	0.6	0.5	0.5	0.6	0.8
1	W360x33	1	0.7	N/A	N/A	N/A	0.4	0.6	0.7	0.8	0.6	0.6	0.8	0.97

The 3-storey CBF columns were designed such that $C_f \leq C_r$. It is noted that a live load reduction factor as described previously was applied for live loads triggered in the columns. The demand to capacity ratio $C_{f\text{-}80}/C_{r\text{-}80}$ computed for the 3-storey CBF columns (E-W direction) is presented in **Table 3.8**. According to the calculation, the governing loading combination was 1.25DL+1.05LL+1.05Q. The cross-sectional area A, radius of gyration about y-y axis r_y, the width-to-thickness ratios $b/2t_f$ and h/w for the flanges and web, together with the slenderness ratio KL/r and λ, are also given in **Table 3.8**.

Table 3.8 Design summary of 3-storey CBF columns in E-W direction (Quebec City)

St	Section	A	r_y	$b/2t_f$	h/w	Cls.	KL/r	λ	$C_{f\text{-}80}$	$C_{r\text{-}80}$	$C_{f\text{-}80}/C_{r\text{-}80}$
	S1	mm^2	*mm*	-	-	-	< 200	-	*kN*	*kN*	*kN*
3	W200x31	4000	32.0	6.57	29.6	1	113	1.39	400	424	0.94
2	W200x52	6650	51.8	8.10	22.9	1	69	0.86	882	1255	0.70
1	W250x80	10200	65.0	8.17	23.9	1	69	0.85	1475	1930	0.80

It is noted that columns are pinned at the base and were selected to be Class 1 of section. Hence, the class of section verification depends on the maximum width-to-thickness ratios of the elements subjected to compression according to CSA/S16.1-M78 standard. The factored axial compressive resistance C_r has been computed for effective lengths (KL) with respect to the least radius of gyration using **Eq. (2.17)**. For ground-floor columns the effective length was *4500 mm* while for those at typical floor the considered length was *3600 mm*.

3.3.2.3. Design of CBF brace connections

According to Clause 20.4 of CSA/S16.1-M78 standard, the connections at ends of tension or compression members should develop the force due to the factored loads. However, the

connections have to be designed for not less than 50% of the tensile / compressive resistance of the brace member. Thus the actual dimensions and thickness of the gusset plates at each floor were established using the Whitmore width approach. Whitmore (1952) defined the effective width referred in text as "Whitmore width" W_w, as the "length of the line passing through the bottom row of fasteners and intercepted by two 30° lines originated at the outside fasteners of the first row". In this study, the effective Whitmore width W_w, was determined as the length of the line passing through the end of the brace and intercepted by two 30° lines starting from the intersection of the brace and the gusset plate as illustrated in **Figure 3.4**.

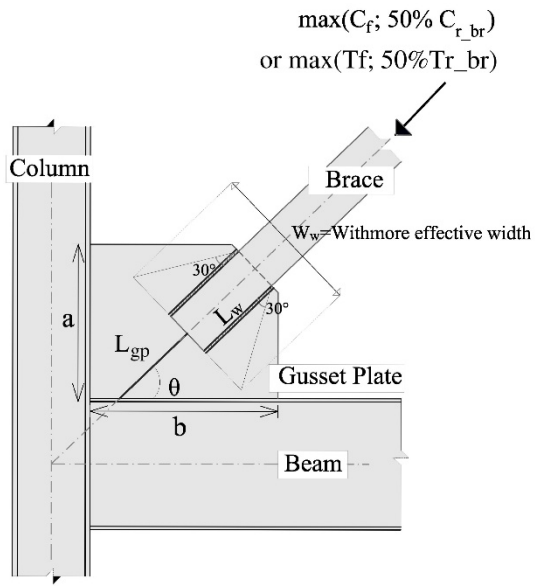

Figure 3.4 Brace- to-frame connection detail according to CSA/S16.1-M78

Brace connection design should consider the factored resistance of the welds and tensile/ compression resistance of gusset plate. Thus, the design of each component should follow the possible failure modes examined according to CSA/S16.1-M78 requirements for connections. In this study, all gusset plates were assumed to be made of steel having the yielding strength *Fy=300 MPa* and were designed such that the factored resistance of the gusset plate in tension and compression to exceed the factored tension force $T_{fgp} = max(T_f ; 50\%T_{r\_br})$ or the factored compressive force $C_{fgp}=max(C_f ; 50\%C_{r\_br})$, as required by CSA/S16.1-M78 standard. The symbols T_{r_br} and C_{r_br} refer to the factored tensile and compressive resistance of the brace given in **Table 3.5**. The electrode type used for welding was *E480 XX*, having the ultimate strength X_u = *480 MPa*, and the weld leg width was considered D_w=*8.0 mm.*

The factored shear resistance of the fillet weld resulted from the consideration of the minimum value of two failure modes: i) fracture of the weld metal through the weld throat, calculated using the equation: $V_r=0.5\phi A_w X_u$ and ii) yielding at the weld-to-base metal interface obtained from: $V_r=0.66\phi A_m F_y$. The shear area of a fillet weld was taken as $A_w=0.707 D_w L_w$ and the interface area was calculated as: $A_m=D_w L_w$. The required length of the fillet weld L_w, was obtained substituting V_r with max($C_{f\_br}/4$; $50\% T_{r\_br}/4$) and solving for L_w. It is noted that the HSS brace was connected to the gusset plate by means of four fillet welds. The gusset plate thickness t_{gp}, was obtained from the factored tension T_{fgp} and compression force C_{fgp} triggered in gusset, and the largest resulted t_{gp} value was selected. The factored tensile resistance of gusset plate T_{rgp}, was computed as per **Eq. (3.8)**, with $\phi = 0.9$ while the factored compressive resistance C_{rgp} was obtained from **Eq. (2.17)**. Moreover, the gusset slenderness is $\lambda = KL/r\ (F_y/\pi^2 E)^{0.5}$, where the effective length factor K was considered 0.67; the effective length L, was calculated from the gusset plate geometry according to **Figure 3.4** and $r=(I/A_{gp})^{0.5}$ is the radius of gyration. Further, the gusset plate area is $A_{gp} = W_w t_{gp}$, where W_w is the Whitmore width and $I = W_w * t_{gp}^3/12$ represents the moment of inertia of the gusset plate.

$$T_r = \phi F_y W_w t_{gp} \tag{3.8}$$

Besides the aforementioned verifications, the connections between brace and frame were verified for net rupture of brace due to the reduction of cross-sectional area at slotted brace end (A_{net}) as per **Eq. (2.16)**. In **Table 3.9** is summarized the gusset plate design for 3-storey chevron CBF frames in E-W direction. As illustrated, the table contains the selected welding length, L_w, gusset plate geometry: height a, width b (as shown in **Figure 3.4**), thickness t_{gp}, and area A_{gp}, together with Whitmore width and critical length L_g. The reserve capacity of the connections, as well as, the demand-to-capacity ratios at each floor for each verification case are given in **Table 3.10**. A detailed design example of the brace-to-frame connection calculation for the 3-storey building located in Quebec City is given in **Appendix II.** It is noted that the block shear check was introduced in later editions of S16.

Table 3.9 Design summary of brace-to-frame gusset plate connections of 3-storey CBF in E-W direction (Quebec City)

St	L_w	a	b	t_{gp}	W_w	A_{gp}	L_{gp}
	mm	*mm*	*mm*	*mm*	*mm*	mm^2	*mm*
3	120	194	264	9.5	240.6	2291.37	151
2	120	197	298	9.5	265.6	2529.50	148
1	150	448	251	9.5	325.2	3097.58	221

Table 3.10 Summary of brace-to-frame gusset plate connection verification for the 3-storey CBF in E-W direction (Quebec City)

St.	Shear resistance of welding (kN)		Tensile resistance of metal base (kN)		Yielding of gusset plate (kN)		Buckling of gusset plate (kN)		Net Fracture of brace (kN)	
	V_r	C_{fgp}/V_r	$T_{r.mb}$	$T_{fgp}/T_{r.mb}$	T_{rgp}	T_{fgp}/T_{rgp}	C_{rgp}	C_{fgp}/C_{rgp}	$T_{r.br\text{-}net}$	$T_{fgp}/T_{r.br\text{-}net}$
3	489	0.60	617	0.74	619	0.74	556	0.54	917	0.50
2	489	0.95	617	0.82	683	0.74	616	0.76	1011	0.50
1	635	0.98	772	0.80	836	0.74	672	0.93	1238	0.50

3.3.3. Design of the 3-storey CBF in the N-S direction

The factored shear force per frame with and without torsion and additional shear from *P-Δ* effects, computed for each loading case of the 3-storey building in Quebec City as per the 1980 NBCC requirements is summarized in **Table 3.11,** for N-S direction. As illustrated, by adding the torsion and P-Δ effects the total base shear per frame increased by 17%.

Table 3.11 Shear force per CBF in N-S direction (3-storey Quebec City)

St	Shear force: Q	Case 2: 1.50 Q	Case 3: 1.05Q	Case 2: 1.50 (Q+T+ PΔ)	Case 3: 1.05 (Q+T+ PΔ)
	kN	*kN*	*kN*	*kN*	*kN*
3	397	595	417	610	427
2	678	1017	712	1111	778
1	837	1255	879	1461	1023

Q- earthquake; T-torsion effect; PΔ- additional shear from P-Δ effects.

3.3.3.1. Brace design of 3-storey CBF in N-S direction (Quebec City)

Brace cross-sections were selected such that $C_f \leq C_r$ computed according to **Eq. (2.17)**. Thus, the total factored axial load in brace was determined from the most unfavorable load combination (1.25DL + 1.5Q) and the critical design values are indicated in **Figure 3.5** for N-S directions. Additionally, the selected HSS brace sections together with the factored axial compressive and tensile resistance C_r, T_r are given in **Table 3.12**.

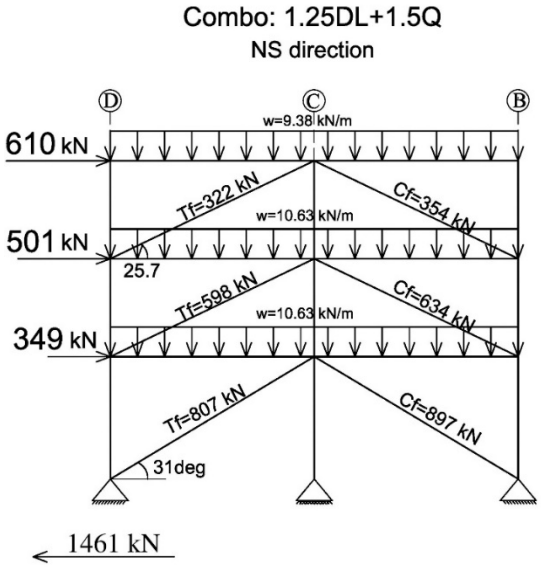

Figure 3.5 Axial compressive forces in braces under 1.25DL+1.5Q load combination for the 3-storey CBF in N-S direction (Quebec City)

Table 3.12 Design summary of 3-storey CBF braces in N-S direction (Quebec City)

St	Section*	A_g	r	b/t	KL/r	λ	C_f	$C_{r\text{-}80}$	$T_{r\text{-}80}$	$C_f/C_{r\text{-}80}$
	mm x mm x mm	*mm^2*	*mm*	-	*< 200*	-	*kN*	*kN*	*kN*	*< 1.00*
3	152x152x7.95	4430	58.4	7.5	128	1.7	354	405	1238	0.87
2	178x178x9.53	6180	68.0	14.7	110	1.5	634	704	1727	0.90
1	203x203x9.53	7150	78.4	17.3	100	1.3	897	926	1998	0.97

*Square tubular section (HSS): b x h x t

For the N-S direction the effective length of brace (*0.9L*) was *7871 mm* and *7488 mm* for ground and typical floor, respectively. In addition, the selected braces were selected to be Class 1 section and regardless of the selected section, the *demand-to-capacity ratio*, C_f/C_r, has to be ≤ *1.00*.

3.3.3.2. Beams and column design of 3-storey CBF in N-S direction (Quebec City)

All beams were proportioned to satisfy the strength and stability conditions for axial compression/tension and bending as per **Eqs. (3.4)** to (**3.7)** and CSA/S16.1-M78 standard requirements. Thus, the factored bending moment M_f, computed for each of the three loading combinations considered is given in **Table 3.13** together with the total factored axial compression C_f, and tension T_f in the members. Beams cross-sections of 3-storey CBF (N-S direction) in Quebec City are summarized in **Table 3.14** while the design summary for 3-storey CBF columns in N-S direction is given in **Table 3.15**. In addition, all beams and columns are Class 1 and 2 sections according to CSA/S16.1-M78 standard. For CBF columns design, the governing case was the gravity combination (i.e. 1.25DL+1.5LL) for the middle column; while for the side column the most critical combination was: 1.25DL+1.05LL+1.05Q.

Table 3.13 Design loads for the 3-storey CBF beams in N-S direction (Quebec City)

	Combo:1.25DL+1.5LL			Combo:1.25DL+1.5Q			Combo:1.25DL+1.05LL+1.05Q		
St	M_f	T_f	C_f	M_f	T_f	C_f	M_f	T_f	C_f
	kNm	*kN*	*kN*	*kNm*	*kN*	*kN*	*kNm*	*kN*	*kN*
3	125	0	0	66	305	305	107	213	213
2	138	0	0	75	570	541	119	412	366
1	138	0	0	75	747	714	119	538	484

Table 3.14 Design summary of 3-storey CBF beams in N-S direction (Quebec City)

	Section	Class	1.25DL+1.5LL				1.25DL+1.5Q				1.25DL+1.05LL+1.05Q			
St	-	-	Eq. (3.4)	Eq. (3.5)	Eq. (3.6)	Eq. (3.7)	Eq. (3.4)	Eq. (3.5)	Eq. (3.6)	Eq. (3.7)	Eq. (3.4)	Eq. (3.5)	Eq. (3.6)	Eq. (3.7)
3	W360x33	1	0.9	N/A	N/A	N/A	0.5	0.7	0.84	0.77	0.7	0.8	0.99	0.96
2	W360x45	2	0.7	N/A	N/A	N/A	0.4	0.7	0.83	0.79	0.6	0.7	0.91	0.88
1	W410x46	1	0.6	N/A	N/A	N/A	0.3	0.7	0.89	0.87	0.5	0.7	0.90	0.90

Table 3.15 Design summary of 3-storey CBF columns in N-S direction (Quebec City)

St	Section S2/S3	A mm^2	r_y mm	$b/2t_f$ -	h/w -	Cls. -	KL/r < 200	λ -	$C_{f\text{-}80}$ kN	$C_{r\text{-}80}$ kN	$C_{f\text{-}80}/C_{r\text{-}80}$ kN
N-S direction- side column											
3	W200x31	4000	32.0	6.57	29.6	1	113	1.39	400	424	0.94
2	W200x42	5310	41.2	7.03	25.2	1	87	1.08	798	795	0.98
1	W250x80	10200	65.0	8.17	23.9	1	69	0.85	1304	1146	0.70
N-S direction- middle column											
3	W200x31	4000	32.0	6.57	29.6	1	113	1.39	400	424	0.94
2	W200x42	5310	41.2	7.03	25.2	1	87	1.08	784	795	0.98
1	W200x59	7560	52.0	7.22	19.9	1	87	1.07	1119	1263	0.97

3.3.3.3. Design of 3-storey CBF brace connections (N-S direction)

The same approach as presented in *Section 3.3.2.3* was used to design the brace-to-frame connections of 3-storey CBF in the N-S direction. Therefore, the steel strength for gusset plates was F_y=*300 MPa* and the type of electrode used for welding was *E480 XX* with X_u = *480 MPa.* Note that, brace connections were designed for the triggered maximum factored load or 50% of brace tensile/compressive resistance which one is larger. Additionally, brace connection design should consider the factored resistance of the weld, gusset plate as well as the connected brace as described previously. In **Table 3.16** are summarized the end brace gusset plate dimensions of the 3-storey CBF from N-S direction. As illustrated, the table contains the selected welding length and width L_w, and D_w respectively; gusset plate geometry: height *a*, width *b* (as shown in **Figure 3.4**), thickness t_{gp}, and area A_{gp}, together with Whitmore width and critical length L_{gp}.

Table 3.16 Design summary of brace-to-frame gusset plate connections of 3-storey CBF in N-S direction (Quebec City)

St	D_w mm	L_w mm	a mm	b mm	t_{gp} mm	W_w mm	A_{gp} mm^2	L_{gp} mm
3	8	120	296	632	9.53	291.0	2771.43	328
2	8	150	350	765	11.11	351.0	3900.54	391
1	8	210	416	345	11.11	445.7	4952.70	248

Furthermore, the reserve capacity of the connections as well as the demand-to-capacity ratios for each verification case according to the 1980 design is given in **Table 3.17** for each storey.

Table 3.17 Summary of brace-to-frame gusset plate connection verification for the 3-storey CBF in N-S direction (Quebec City)

St.	Shear resistance of welding (kN)		Tensile resistance of metal base (kN)		Yielding of gusset plate (kN)		Buckling of gusset plate (kN)		Net Fracture of brace (kN)	
	V_r	C_{fgp}/V_r	$T_{r.mb}$	$T_{fgp}/T_{r.mb}$	T_{rgp}	T_{fgp}/T_{rgp}	C_{rgp}	C_{fgp}/C_{rgp}	$T_{r.br\text{-}net}$	$T_{fgp}/T_{r.br\text{-}net}$
3	489	0.72	617	0.99	748	0.83	464	0.76	1238	0.50
2	635	0.99	900	0.96	1053	0.82	639	0.99	1727	0.50
1	929	0.97	1260	0.79	1337	0.75	1091	0.82	1998	0.50

3.4. Design of a 6-storey office building in Quebec City according to NBCC 1980 and CSA/S16.1-M78 standard

The plan view and frame elevations of the 6-storey building (6Q) are given in **Figure 3.2**. In addition, the building has the same plan view and characteristics as the 3-storey CBF office building. The minimum lateral seismic force *V*, assumed to act non-concurrently in any direction of the building was calculated using **Eq. (2.2)**, in the same way as the 3-storey building located in Quebec City. Hence, the seismic response factor *S,* was taken as *0.98* and *0.82* for E-W and N-S direction respectively and the values were calculated according to **Eq. (2.7)**. As previously noted, the seismic response factor cannot exceed the value of *1.00* and depends on the fundamental vibration period of the structure which has the value *0.261 s*and *0.370 s* for E-W and N-S direction, respectively. The ductility related factor *K*, the importance factor *I,* and foundation factor *F,* were taken as *1.0* as discussed for the 3Q building. Lastly, the seismic weight for the 6-storey building located in Quebec City was computed as *W= 42068 kN*. The resulted minimum lateral earthquake design force at the base of the structure, *V* was *3292 kN* for the E-W direction which implies *823 kN* per each CBF frame in the aforementioned direction; whereas for the N-S direction the total base shear was *2768 kN* which was distributed equally between the two CBFs *i.e*. *1384 kN* per two adjacent CBFs. According to the calculations $F_t = 0$ for both E-W and N-S directions and the seismic load *V,* was distributed along the building height as a function of the relative product of the seismic weight and the elevation from the ground at the level under consideration in accordance

with **Eq. (2.9)**. Similar with the 3Q building, torsional moments in the horizontal plan of the building and additional shear due to *P-Δ* effects were also considered.

3.4.1. Gravity System design

The same loading scheme as for the 3-storey CBF building applies for secondary beams and girders of the 6-storey buildings. The selected secondary beam for all floors was *W310x33* while girders were: *W460x52* for roof and *W460x60* for typical floor. Note that the beam selection for the 6Q building is consistent with that for the 3Q building given in **Table 3.3**. Further, gravity columns were designed considering $C_f \leq C_r$. It is noted that columns are continuous over two storeys. The design summary of interior gravity columns is presented in **Table 3.18** while that for the edge and corner columns is given in **Table 3.19**. Design steps are described in detail in Appendix II.

Table 3.18 Design summary for gravity interior column S4 (A_t= *56.25 m²*)

St	C_{fmax}	Section	A	r_x	r_y	KL/r	λ	C_r	$b/2t_f$	h/w	Class
	kN	*S4*	*mm²*	*mm*	*mm*	-	-	*kN*	-	-	-
6	400	W200x42	5310	87.7	41.2	83.74	1.03	841	7.03	25.2	1
5	784	W200x42	5310	87.7	41.2	83.74	1.03	841	7.03	25.2	1
4	1119	W250x67	8550	110	51.0	67.65	0.83	1644	6.50	25.3	1
3	1446	W250x67	8550	110	51.0	67.65	0.83	1644	6.50	25.3	1
2	1768	W250x89	11400	112	65.1	52.99	0.66	2488	7.40	21.1	1
1	2088	W250x89	11400	112	65.1	66.82	0.82	2210	7.40	21.1	1

Table 3.19 Design summary for gravity edge and corner column S5 and S6 (A_t= *28.13 m²*)

St	C_{fmax}	Section	A	r_x	r_y	KL/r	λ	C_r	$b/2t_f$	h/w	Class
	kN	*S5/S6*	*mm²*	*mm*	*mm*	-	-	*kN*	-	-	-
6	200	W150x30	3790	67.3	38.3	90.32	1.11	546	8.23	21.0	2
5	410	W150x30	3790	67.3	38.3	90.32	1.11	546	8.23	21.0	2
4	584	W200x42	5310	87.7	41.2	105.60	1.30	615	7.03	25.2	1
3	753	W200x42	5310	87.7	41.2	105.60	1.30	615	7.03	25.2	1
2	919	W200x59	7560	89.9	52.0	66.35	0.82	1472	7.22	20.0	1
1	1083	W200x59	7560	89.9	52.0	83.65	1.03	1199	7.22	20.0	1

3.4.2. Design on the 6-storey CBF in the E-W direction (Quebec City)

The factored shear force per frame with and without torsion and additional shear from *P-Δ* effects, computed for each loading case of the 6-storey CBF office building in Quebec City as per the 1980s design requirements is summarized in **Table 3.20** for E-W direction. As illustrated, by adding the torsion and *P-Δ* effects the total base shear per frame increases by *19%*.

Table 3.20 Shear force per 6-storey CBF in E-W direction (Quebec City)

St	Shear force: Q	Case 2: 1.50 Q	Case 3: 1.05Q	Case 2: 1.50 (Q+T+ PΔ)	Case 3: 1.05 (Q+T+ PΔ)
	kN	*kN*	*kN*	*kN*	*kN*
6	224	336	235	359	251
5	416	624	437	697	488
4	573	860	601	973	681
3	693	1040	727	1214	850
2	776	1164	815	1382	968
1	823	1235	864	1465	1026

Q- earthquake; T-torsion effect; PΔ- additional shear from P-Δ effects.

3.4.2.1. Brace design of 6-storey CBF in E-W direction (Quebec City)

Braces were selected to comply with G40.21-345W Class C steel, cold formed HSS cross-sections with F_y*=345 MPa* and F_u*= 448 MPa.* Additionally, braces were selected such that $C_f \leq C_r$. The factored axial load in the brace was determined from the most unfavorable load combination (1.25DL + 1.5Q) and the critical design values are given for the E-W direction in **Figure 3.6**. The selected HSS braces cross-sections together with the factored axial compressive and tensile resistance C_r, and T_r are given in **Table 3.21**. The gross area of the section A_g; radius of gyration *r*; the width-to-thickness ratio *b/t*, together with the slenderness ratio *KL/r* and λ, are also given. It is noted that the effective length of the brace was considered as *0.9L* to account for the connections between brace and frame. In addition, the selected braces were selected to be Class 1 of section.

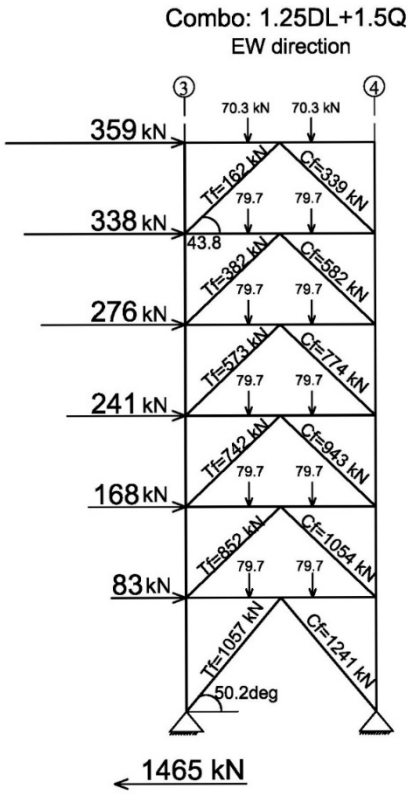

Figure 3.6 Axial compressive forces in braces under 1.25DL+1.5Q load combination for the 6-storey CBF in E-W direction (Quebec City)

Table 3.21 Design summary of 6-storey CBF braces in E-W direction (Quebec City)

St	Section*	A_g	r	b/t	KL/r	λ	$C_{f\text{-}80}$	$C_{r\text{-}80}$	$T_{r\text{-}80}$	$C_{f\text{-}80}/C_{r\text{-}80}$
	mm x mm x mm	*mm^2*	*mm*	-	*< 200*	-	*kN*	*kN*	*kN*	*< 1.00*
6	127x127x6.4	2960	48.8	15.8	96	1.27	339	409	827	0.84
5	127x127x11	4840	46.4	7.5	101	1.33	582	623	1353	0.93
4	152x152x8.0	4430	58.4	15	80	1.06	774	780	1238	0.99
3	152x152x11	5970	56.8	9.8	82	1.09	943	1012	1668	0.93
2	178x178x8.0	5240	68.8	18.3	68	0.90	1054	1096	1464	0.96
1	178x178x11	7100	67.2	12.2	78	1.04	1241	1287	1984	0.96

*Square tubular section (HSS) : b x h x t

3.4.2.2. Beams and columns design of 6-storey CBF in E-W direction (Quebec City)

The factored bending moment computed for beams M_f, from each of the three loading combinations is given in **Table 3.22** together with the triggered factored axial compression force C_f, and tension force T_f. In addition, the selected CBF beams cross-sections in E-W direction are summarized in **Table 3.23**. Moreover, all selected beams are Class 1 and 2 sections according to CSA/S16.1-M78 standard requirements.

Table 3.22 Design loads for the 6-storey CBF beams in E-W direction (Quebec City)

	Combo:1.25DL+1.5LL			Combo:1.25DL+1.5Q			Combo:1.25DL+1.05LL+1.05Q		
St	M_f	T_f	C_f	M_f	T_f	C_f	M_f	T_f	C_f
	kNm	*kN*	*kN*	*kNm*	*kN*	*kN*	*kNm*	*kN*	*kN*
6	93	N/A	N/A	49	181	181	79	126	126
5	102	N/A	N/A	55	411	284	88	345	143
4	102	N/A	N/A	55	558	413	88	453	228
3	102	N/A	N/A	55	680	535	88	537	312
2	102	N/A	N/A	55	760	615	88	596	371
1	102	N/A	N/A	55	808	663	88	625	400

Table 3.23 Design summary of 6-storey CBF beams in E-W direction (Quebec City)

	Section	Class	1.25DL+1.5LL				1.25DL+1.5Q				1.25DL+1.05LL+1.05Q			
St	-	-	Eq. (3.4)	Eq. (3.5)	Eq. (3.6)	Eq. (3.7)	Eq. (3.4)	Eq. (3.5)	Eq. (3.6)	Eq. (3.7)	Eq. (3.4)	Eq. (3.5)	Eq. (3.6)	Eq. (3.7)
6	W310x33	1	0.7	N/A	N/A	N/A	0.4	0.5	0.62	0.57	0.6	0.6	0.79	0.74
5	W310x39	2	0.6	N/A	N/A	N/A	0.3	0.5	0.64	0.70	0.5	0.6	0.70	0.84
4	W310x45	1	0.5	N/A	N/A	N/A	0.3	0.5	0.67	0.72	0.5	0.5	0.68	0.81
3	W360x45	2	0.5	N/A	N/A	N/A	0.3	0.6	0.72	0.80	0.4	0.6	0.70	0.83
2	W360x45	2	0.5	N/A	N/A	N/A	0.3	0.6	0.79	0.84	0.4	0.6	0.75	0.87
1	W360x51	1	0.4	N/A	N/A	N/A	0.2	0.6	0.73	0.78	0.4	0.5	0.68	0.79

The 6-storey CBF columns are continuous over two storeys and were designed such that: $C_f \leq C_r$. It is noted that a live load reduction factor as described previously was applied for the design live loads. The summary of CBF design (E-W direction), as well as, the demand-to-capacity ratio $C_{f\text{-}80}/C_{r\text{-}80}$ is presented in **Table 3.24**. According to the calculations, the governing loading combination was 1.25DL+1.05LL+1.05Q. The area of the column cross-section A, radius of gyration about y-y axis r_y, the width-to-thickness ratios $b/2t_f$ and h/w for the flanges and web, together with the slenderness ratio KL/r and slenderness λ, are also given in the table.

Table 3.24 Design summary of 6-storey CBF columns in E-W direction (Quebec City)

St	Section	A	r_y	$b/2t_f$	h/w	Cls.	KL/r	λ	$C_{f\text{-}80}$	$C_{r\text{-}80}$	$C_{f\text{-}80}/C_{r\text{-}80}$
	S1	*mm^2*	*mm*	-	-	-	*< 200*	-	*kN*	*kN*	*kN*
6	W200x52	6650	51.8	8.10	22.9	1	69	0.86	343	1255	0.27
5	W200x52	6650	51.8	8.10	22.9	1	69	0.86	902	1255	0.72
4	W250x89	11400	65.1	7.40	21.1	1	55	0.68	1551	2444	0.64
3	W250x89	11400	65.1	7.40	21.1	1	55	0.68	2287	2444	0.94
2	W310x158	20100	78.9	6.18	17.9	1	46	0.56	3101	4619	0.67
1	W310x158	20100	78.9	6.18	17.9	1	57	0.71	3970	4251	0.94

3.4.2.3. Design of brace connections

The same approach as showed in *Section 3.3.2.3* was applied to design the brace-to-frame connections of the 6-storey CBF office building located in Quebec City (E-W direction). All gusset plates were assumed to be made of steel with *Fy=300 MPa* and were designed such that the factored resistance of the gusset plate in tension and compression to exceed the factored tension force $T_{fgp}= max(T_f; 50\%T_{r\text{-}br})$ or the factored compressive force $C_{fgp}=max(C_f; 50\%C_{r\_br})$. The symbols T_{r_br} and C_{r_br} refer to the factored tensile and compressive resistance of the brace given in **Table 3.21**. The electrode type used for welding was *E480 XX*, having the ultimate strength X_u *= 480 MPa.* In **Table 3.25** is summarized the brace gusset plate design for the 6-storey CBF in E-W direction. The reserve capacity of the connections, as well as, the demand-to-capacity ratios for each verification case as per 1980s design requirements are given for each floor in **Table 3.26**.

Table 3.25 Design summary of brace-to-frame gusset plate connections of 6-storey CBF in E-W direction (Quebec City)

St	D_w	L_w	a	b	t_{gp}	W_w	A_{gp}	L_{gp}
	mm	*mm*	*mm*	*mm*	*mm*	*mm*	mm^2	*mm*
6	6	120	218	259	9.5	266	2529.50	164
5	8	150	242	287	9.5	300	2859.45	182
4	8	190	282	379	11.11	371	4127.11	219
3	9	200	291	387	11.11	383	4255.42	225
2	8	240	355	389	11.11	455	5057.61	262
1	9	260	608	357	12.7	478	6073.42	312

Table 3.26 Summary of brace-to-frame gusset plate connection verification for the 6-storey CBF in E-W direction (Quebec City)

St.	Shear resistance of welding (kN)		Tensile resistance of metal base (kN)		Yielding of gusset plate (kN)		Buckling of gusset plate (kN)		Net Fracture of brace (kN)	
	V_r	C_{fgp}/V_r	$T_{r.mb}$	$T_{fgp}/T_{r.mb}$	T_{rgp}	T_{fgp}/T_{rgp}	C_{rgp}	C_{fgp}/C_{rgp}	$T_{r.br\text{-}net}$	$T_{fgp}/T_{r.br\text{-}net}$
6	367	0.92	617	0.67	683	0.61	602	0.56	827	0.50
5	635	0.92	772	0.88	772	0.88	663	0.88	1353	0.50
4	831	0.93	1140	0.54	1114	0.56	948	0.82	1238	0.50
3	990	0.95	1200	0.69	1149	0.73	970	0.97	1668	0.50
2	1075	0.98	1440	0.59	1366	0.62	1089	0.97	1464	0.58
1	1320	0.94	1783	0.59	1640	0.64	1284	0.97	1984	0.53

3.4.3. Design of the 6-storey CBF in the N-S direction (Quebec City)

The factored shear force per frame with and without torsion and additional shear from *P-Δ* effects was computed for each loading case of the 6-storey CBF office building in Quebec City, in accordance with the 1980 NBCC requirements and is summarized in **Table 3.27** for N-S direction. As illustrated, by adding the torsion and *P-Δ* effects the total base shear per frame increased by 29%.

Table 3.27 Shear force per 6-storey CBF in N-S direction (Quebec City)

St	Shear force: Q	Case 2: 1.50 Q	Case 3: 1.05Q	Case 2: 1.50 (Q+T+ PΔ)	Case 3: 1.05 (Q+T+ PΔ)
	kN	*kN*	*kN*	*kN*	*kN*
6	377	566	396	596	417
5	700	1050	735	1163	814
4	963	1445	1012	1679	1175
3	1165	1747	1223	2123	1486
2	1305	1957	1370	2479	1735
1	1384	2076	1453	2686	1880

Q- earthquake; T-torsion effect; PΔ- additional shear from P-Δ effects.

3.4.3.1. Brace design of 6-storey CBF in N-S direction (Quebec City)

Brace cross-sections were selected such that $C_f \leq C_r$. Thus, the critical design values computed for the 6-storey CBF in the N-S direction are illustrated in **Figure 3.7**. The selected HSS brace cross-sections together with the factored axial compressive and tensile resistance C_r, and T_r are given in **Table 3.28**. In addition, the selected braces are Class 1 section and the effective length of the brace was considered *0.9L*.

Table 3.28 Design summary of 6-storey CBF braces in N-S direction (Quebec City)

St	Section*	A_g	r	b/t	KL/r	λ	$C_{f\text{-}80}$	$C_{r\text{-}80}$	$T_{r\text{-}80}$	$C_{f\text{-}80}/C_{r\text{-}80}$
	mm x mm x mm	*mm^2*	*mm*	-	*< 200*	-	*kN*	*kN*	*kN*	*< 1.00*
6	152x152x8.0	4430	58.4	15.2	128	1.70	352	405	1238	0.87
5	178x178x9.5	6180	68.0	12.2	110	1.46	671	704	1727	0.95
4	203x203x9.5	7150	78.4	17.3	96	1.26	959	992	1998	0.97
3	203x203x12.7	9260	76.9	12.0	97	1.29	1207	1251	2588	0.96
2	254x254x8.0	7660	99.9	19.1	75	0.99	1406	1466	2141	0.96
1	254x254x11	10500	98.4	19.1	80	1.06	1648	1851	2934	0.90

*Square tubular section (HSS): b x h x t

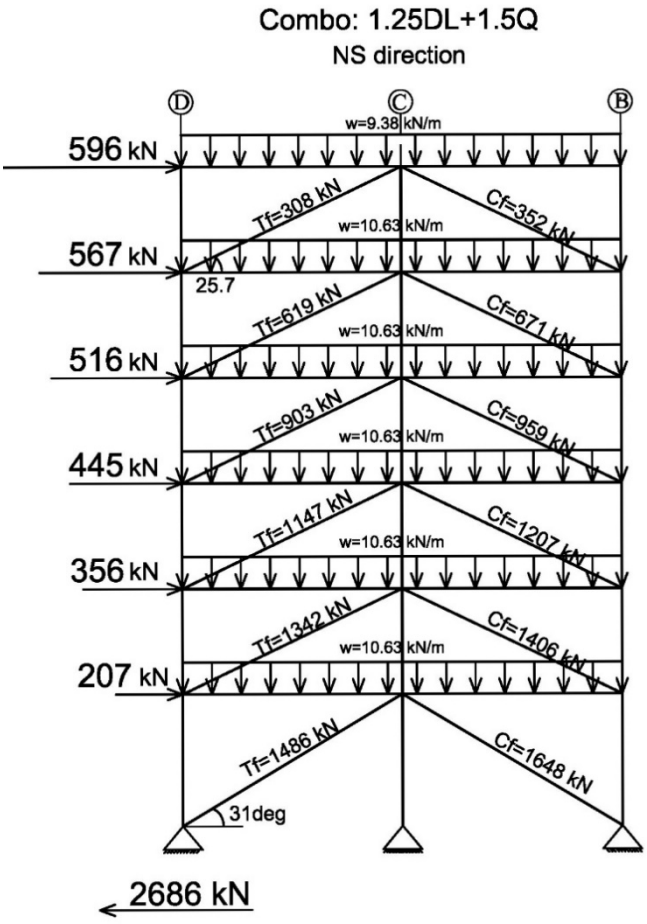

Figure 3.7 Axial compressive forces in braces under 1.25DL+1.5Q load combination for the 6-storey CBF in N-S direction (Quebec City)

3.4.3.2. Beams and column design of 6-storey CBF in N-S direction (Quebec City)

The factored bending moment M_f, of 6-storey CBF beams computed for each of the three loading combinations are given in **Table 3.29** together with the factored axial compression C_f, and tension force T_f triggered in beam members. The selected cross-sections for the 6-storey CBF beams in N-S direction are summarized in **Table 3.30**. On the other hand, the cross-sections for the 6-storey columns in N-S direction are given in **Table 3.31.** In addition, all beams and columns were selected Class 1 and 2 type according to S16.1-1978 standard requirements.

Table 3.29 Design loads for the 6-storey CBF beams in N-S direction (Quebec City)

St	Combo:1.25DL+1.5LL			Combo:1.25DL+1.5Q			Combo:1.25DL+1.05LL+1.05Q		
	M_f *kNm*	T_f *kN*	C_f *kN*	M_f *kNm*	T_f *kN*	C_f *kN*	M_f *kNm*	T_f *kN*	C_f *kN*
6	125	N/A	N/A	66	298	298	107	208	208
5	138	N/A	N/A	75	602	562	119	437	376
4	138	N/A	N/A	75	863	816	119	623	551
3	138	N/A	N/A	75	1087	1036	119	782	704
2	138	N/A	N/A	75	1266	1212	119	909	826
1	138	N/A	N/A	75	1372	1314	119	983	897

Table 3.30 Design summary of 6-storey CBF beams in N-S direction (Quebec City)

St	Section	Class	1.25DL+1.5LL				1.25DL+1.5Q				1.25DL+1.05LL+1.05Q			
	-	-	Eq. (3.4)	Eq. (3.5)	Eq. (3.6)	Eq. (3.7)	Eq. (3.4)	Eq. (3.5)	Eq. (3.6)	Eq. (3.7)	Eq. (3.4)	Eq. (3.5)	Eq. (3.6)	Eq. (3.7)
6	W310x39	2	0.8	N/A	N/A	N/A	0.4	0.6	0.73	0.66	0.7	0.7	0.90	0.84
5	W310x45	1	0.7	N/A	N/A	N/A	0.4	0.7	0.93	0.85	0.6	0.8	0.99	0.96
4	W310x52	1	0.6	N/A	N/A	N/A	0.3	0.7	0.98	0.89	0.5	0.8	0.99	0.93
3	W360x57	1	0.5	N/A	N/A	N/A	0.3	0.8	0.98	0.93	0.4	0.7	0.94	0.91
2	W360x64	1	0.4	N/A	N/A	N/A	0.2	0.8	0.97	0.92	0.4	0.7	0.90	0.87
1	W360x72	1	0.4	N/A	N/A	N/A	0.2	0.7	0.91	0.87	0.3	0.7	0.84	0.82

Note that for middle columns of CBF in the N-S direction the governing loading case was 1.25DL+1.5LL and for the side columns the 1.25DL+1.05LL+1.05Q combination governed.

Table 3.31 Design summary of 6-storey CBF columns in N-S direction (Quebec City)

St	Section	A	r_y	$b/2t_f$	h/w	Cls.	KL/r	λ	$C_{f\text{-}80}$	$C_{r\text{-}80}$	$C_{f\text{-}80}/C_{r\text{-}80}$
	S2/S3	*mm^2*	*mm*	-	-	-	*< 200*	-	*kN*	*kN*	*kN*
N-S direction- side column											
6	W200x42	5310	41.2	7.03	25.2	1	87	1.08	400	795	0.50
5	W200x42	5310	41.2	7.03	25.2	1	87	1.08	799	795	0.99
4	W200x86	11000	53.3	5.07	13.9	1	68	0.83	1317	2117	0.62
3	W200x86	11000	53.3	5.07	13.9	1	68	0.83	1917	2117	0.98
2	W310x129	16500	78	7.48	21.1	1	46	0.57	2591	3779	0.69
1	W310x129	16500	78	7.48	21.1	1	58	0.71	3391	3471	0.98
N-S direction- middle column											
6	W200x42	5310	41.2	7.03	25.2	1	87	1.08	400	795	0.50
5	W200x42	5310	41.2	7.03	25.2	1	87	1.08	784	795	0.99
4	W250x67	8550	51.0	6.50	25.4	1	71	0.87	1119	1595	0.70
3	W250x67	8550	51.0	6.50	25.4	1	71	0.87	1446	1595	0.91
2	W250x89	11400	65.1	7.40	21.07	1	55	0.68	1771	2444	0.73
1	W250x89	11400	65.1	7.40	21.07	1	69	0.85	2088	2160	0.99

3.4.3.3. Design of 6-storey CBF brace-to-frame connections in N-S direction (Quebec City)

The same approach as that presented in Section 3.3.2.3 was used to design the brace-to-frame connections of the 6-storey CBF office building in N-S direction located in Quebec City. All gusset plates were made of steel having the yielding strength $F_y=300\ MPa$, while the same electrode type *E480 XX*, was used for welds. In **Table 3.32** is summarized the gusset plate design. Additionally, the reserve capacity of the brace gusset plate connections as well as the demand-to-capacity ratios for each verification case according to the 1980 design requirements is given for each floor in **Table 3.33**.

Table 3.32 Design summary of brace-to-frame connections of 6-storey CBF in N-S direction (Quebec City)

St	D_w	L_w	a	b	t_{gp}	W_w	A_{gp}	L_{gp}
	mm	*mm*	*mm*	*mm*	*mm*	*mm*	mm^2	*mm*
6	8	130	303	617	9.5	302	2877.61	340
5	8	160	361	695	11.1	363	4028.86	378
4	8	220	446	832	14.3	457	6532.73	502
3	10	220	446	820	15.9	457	7258.59	502
2	8	310	586	955	17.5	612	10686.30	637
1	10	290	508	420	17.5	589	10283.02	305

Table 3.33 Summary of brace-to-frame gusset plate connection verification for the 6-storey CBF in N-S direction (Quebec City)

St.	Shear resistance of welding (kN)		Tensile resistance of metal base (kN)		Yielding of gusset plate (kN)		Buckling of gusset plate (kN)		Net Fracture of brace (kN)	
	V_r	C_{fgp}/V_r	$T_{r.mb}$	$T_{fgp}/T_{r.mb}$	T_{rgp}	T_{fgp}/T_{rgp}	C_{rgp}	C_{fgp}/C_{rgp}	$T_{r.br\text{-}net}$	$T_{fgp}/T_{r.br\text{-}net}$
6	538	0.65	669	0.93	777	0.80	462	0.76	1238	0.50
5	684	0.98	960	0.90	1088	0.79	684	0.98	1727	0.50
4	978	0.98	1697	0.59	1764	0.57	1073	0.89	1998	0.50
3	1222	0.99	1886	0.69	1960	0.66	1315	0.92	2588	0.50
2	1417	0.99	2923	0.46	2885	0.47	1667	0.84	2141	0.63
1	1650	0.99	2735	0.54	2776	0.54	2439	0.68	2934	0.51

3.5. Design of a 3-storey office building located in Vancouver (3V) according to NBCC 1980 and CSA/S16.1-M78 standard

For comparison purposes, the same 3-storey CBF office building designed in Quebec City (3Q) was also designed in Vancouver, BC (3V). The plan view and frame elevations are given in **Fig. 3.2** while the specified gravity loads for the structure design are given in **Table 3.1.** Note that the only difference between Quebec building and Vancouver building is the snow load which is *S=1.52 kPa* for Vancouver and *S=2.24 kPa* for Quebec City. Since the snow load at the roof level is smaller for Vancouver, the calculated seismic weight was in turn slightly smaller compared with

Quebec City. Hence, for the 3V building, the total seismic weight was *W= 20675 kN*. Substituting all the values in **Eq. (2.2)** the resulted minimum lateral earthquake design force at the base of the structure was *1654 kN* for the E-W direction which implies *414 kN* base shear per each CBF in the aforementioned direction. In the N-S direction the total base shear was *1654 kN* which means *827 kN* per two adjacent CBF frames. Note that these values are very close to those obtained for the 3Q building.

3.5.1. Gravity System design

The gravity system of the 3-storey CBF office building located in Vancouver is similar to that in Quebec City. Since the difference between 3Q and 3V buildings consisted only in the *snow load* at the roof level, the sections selected for the 3Q building automatically satisfy the strength and serviceability conditions for the gravity system of the 3V building. For simplicity, the same cross-sections as those considered for the 3-storey CBF office building in Quebec City were selected for the gravity system of the 3V building.

3.5.2. Design of the CBF system

The factored shear force per frame with and without torsion and additional shear from *P-Δ* effects, computed for each loading case of the 3-storey CBF office building in Vancouver is summarized in **Table 3.34** for both E-W and N-S directions. As illustrated, by adding the torsion and *P-Δ* effects the total base shear per frame increased by *11%* for E-W direction, whereas for N-S the increment is *17%*.

Table 3.34 Shear force per CBF of the 3-storey building located in Vancouver

St	Shear force: Q		Case 2: 1.50 Q		Case 3: 1.05Q		Case 2: 1.50 (Q+T+ PΔ)		Case 3: 1.05 (Q+T+ PΔ)	
	E-W	N-S	E-W	N-S	E-W	N-S	E-W	N-S	E-W	N-S
3	191	381	286	572	200	400	289	584	203	409
2	333	666	500	999	350	699	530	1089	371	762
1	414	827	620	1241	434	868	690	1440	483	1008

Q- earthquake; T-torsion effect; PΔ- additional shear from P-Δ effects. (Units: kN)

3.5.2.1. Brace design of 3-storey CBF building in E-W and N-S direction (Vancouver)

The factored axial load in braces was determined from the most unfavorable load combination (1.25DL + 1.5Q) and the critical design values are indicated in **Figure 3.8** for both E-W and N-S directions. As illustrated, the design values for the 3-storey building located in Vancouver are very close to those for the 3-storey building located in Quebec City. For this reason, the brace sections were selected to be the same as for the 3Q building. Thus, the selected HSS brace for the 3V building are given in **Table 3.5** and **Table 3.12** for E-W and N-S direction, respectively.

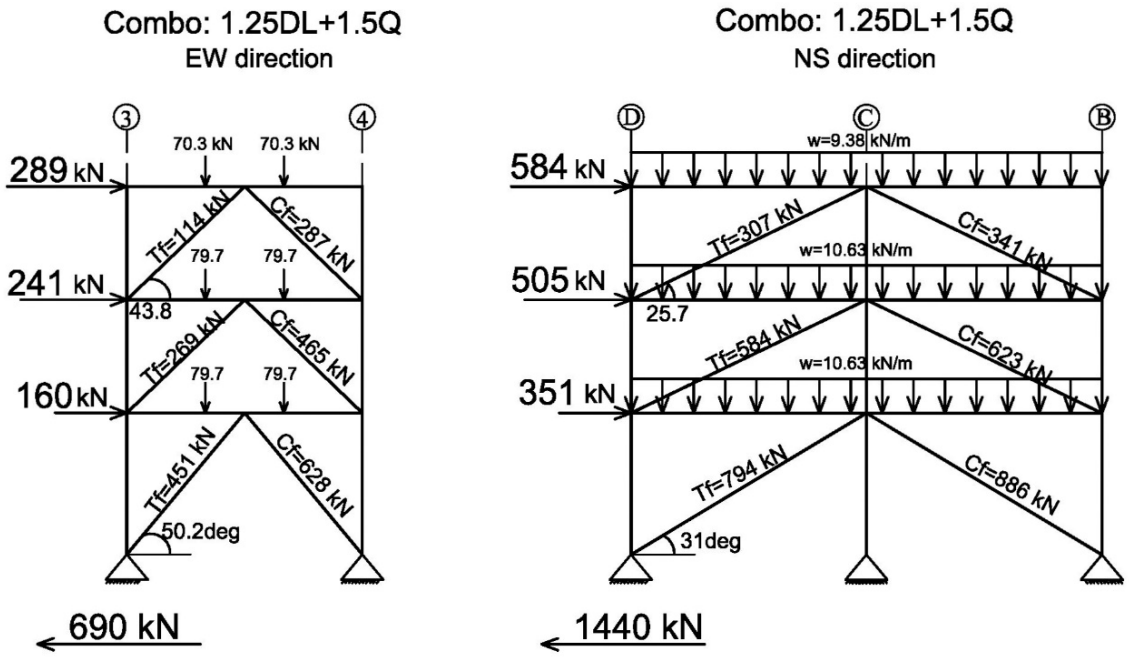

Figure 3.8 Axial compressive forces in braces of the 3-storey CBF office building in Vancouver

In addition, the selected braces are Class 1 section and the slenderness ratio limitation for all compression members is 200 while for the tension members the limitation is 300.

3.5.2.2. Beams and Column design of 3-storey CBF in Vancouver

Each selected member cross-section was proportioned to satisfy the strength and stability conditions for axial compression/tension and bending, given in **Eqs. (3.4)** to (**3.7)** according to CSA/S16.1-M78 standard. The factored bending moment of the beams M_f, computed for each of the three considered loading combinations is given in **Table 3.35** and **Table 3.36** for both E-W and N-S directions. Additionally these tables contain information regarding the factored axial compression C_f, and tension T_f in members. As illustrated in **Table 3.35** and **Figure 3.8**, the design values for the 3-storey building located in Vancouver are very close to those for the 3Q building.

Table 3.35 Design loads for the 3-storey CBF beams in E-W direction (Vancouver)

St	Combo:1.25DL+1.5LL			Combo:1.25DL+1.5Q			Combo:1.25DL+1.05LL+1.05Q		
	M_f	T_f	C_f	M_f	T_f	C_f	M_f	T_f	C_f
	kNm	*kN*	*kN*	*kNm*	*kN*	*kN*	*kNm*	*kN*	*kN*
3	79	N/A	N/A	49	144	144	70	102	102
2	102	N/A	N/A	55	327	202	88	274	97
1	102	N/A	N/A	55	416	275	88	354	129

Table 3.36 Design loads for the 3-storey CBF beams in N-S direction (Vancouver)

St	Combo:1.25DL+1.5LL			Combo:1.25DL+1.5Q			Combo:1.25DL+1.05LL+1.05Q		
	M_f	T_f	C_f	M_f	T_f	C_f	M_f	T_f	C_f
	kNm	*kN*	*kN*	*kNm*	*kN*	*kN*	*kNm*	*kN*	*kN*
3	106	0	0	66	292	292	94	204	204
2	138	0	0	75	560	529	119	403	360
1	138	0	0	75	737	702	119	529	478

The governing loading combination for the CBF columns in E-W and N-S directions was 1.25DL+1.05LL+1.05Q for side columns and 1.25DL+1.5LL for middle columns. In addition, all beams and columns are Class 1 or Class 2 sections according to CSA/S16.1-M78 standard.

3.5.2.3. Design of 3-storey CBF brace-to-frame connections (Vancouver)

The same approach as that presented in *Section 3.3.2.3* was used for the design of brace-to-frame connections of the 3-storey CBF office building in Vancouver. Because the design forces in braces of the 3-storey CBF building in Vancouver were very close to those for the 3-storey building located in Quebec City, the same dimensions for the gusset plates were considered (see **Table 3.9** for the E-W direction and **Table 3.16** for the N-S direction). Each case verification is given in **Table 3.10** and **Table 3.17** for brace connections of CBF located in the E-W and N-S direction, respectively.

3.6. Design of a 6-storey office building located in Vancouver (6V) according to NBCC 1980 and CSA/S16.1-M78 standard

The plan view and CBF elevations of the 6-storey office building (6V) are given in **Figure 3.2**. In addition, the building has the same plan view and characteristics as the 6-storey CBF office building located in Quebec. Note that the only difference regarding the applied loads between 6Q and 6V building consists in the snow load value. Therefore, for the 6-storey CBF building located in Vancouver, the total seismic weight was *W= 41624 kN* which is slightly smaller compared with 6Q building. The resulted minimum lateral earthquake design force at the base of the structure was *3256kN* for the E-W direction of the 6V building which implies a base shear force of *814 kN* per CBF in the aforementioned direction; whereas for the N-S direction the base shear per 6V building was *2738 kN* or *1369 kN* per two adjacent CBFs.

3.6.1. Gravity System design

The gravity system design for the 6V building is similar to the design of the gravity system for 6Q building. For simplicity, the same member cross-sections were selected for the 6V building as those selected for the 6Q building.

3.6.2. Design of the 6-storey CBF system in Vancouver

The factored shear force per frame with and without torsion and additional shear from *P-Δ* effects, is summarized in **Table 3.37** for both E-W and N-S directions. As depicted, by adding the torsion and *P-Δ* effects the total base shear per frame increased by 19% for the CBFs from E-W direction, while for the braced frames from N-S the increment is 29%.

Table 3.37 Shear force per CBF of the 6-storey building located in Vancouver

St	Shear force: Q		Case 2: 1.50 Q		Case 3: 1.05Q		Case 2: 1.50 (Q+T+ PΔ)		Case 3: 1.05 (Q+T+ PΔ)	
	E-W	N-S	E-W	N-S	E-W	N-S	E-W	N-S	E-W	N-S
6	214	361	322	541	225	379	339	553	237	387
5	407	685	611	1027	427	719	667	1114	467	780
4	564	948	846	1422	592	996	951	1658	665	1160
3	684	1150	1025	1725	718	1207	1182	2115	828	1481
2	767	1290	1151	1935	805	1354	1350	2437	945	1706
1	814	1369	1221	2054	855	1438	1439	2669	1007	1868

Q- earthquake; T-torsion effect; PΔ- additional shear from P-Δ effects, (Units: kN).

3.6.2.1. Brace design of 6-storey CBF office building in Vancouver

Brace design procedure follows the same principles described previously for other buildings. In addition, all braces have the same steel properties (F_y, F_u) like the other buildings (3Q, 6Q, 3V). The factored axial load in the brace was determined from the most unfavorable load combination (1.25DL + 1.5Q) and the critical design values are indicated in **Figure 3.9** for both direction.

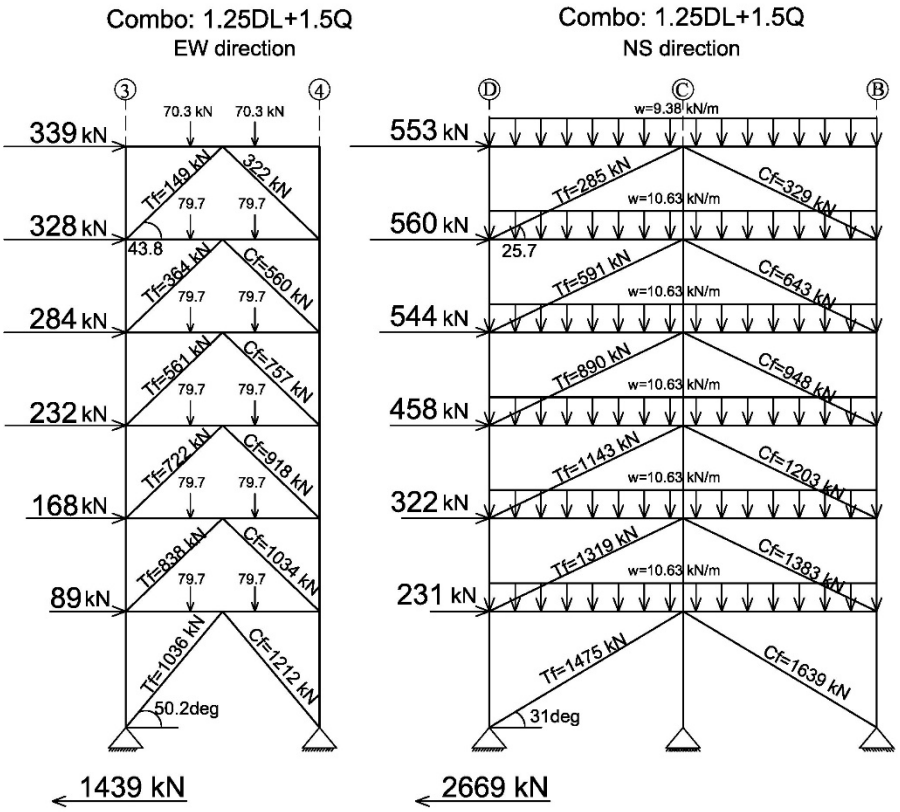

Figure 3.9 Axial compressive forces in braces of 6-storey CBF office building in Vancouver

As mentioned above, the design forces of the 6-storey CBF building located in Vancouver are almost similar to those for the 6-storey CBF office building located in Quebec City. For this reason, the brace cross-sections of the 6-storey CBFs in Vancouver are the same as those selected for the 6-storey CBFs in Quebec City (**Table 3.21** gives brace cross-sections of CBF in E-W direction and **Table 3.28** gives braces of CBF in N-S direction).

3.6.2.2. Beams and Column design of 6-storey CBF building in Vancouver

Each selected beam cross-sections of 6-storey CBFs were proportioned to satisfy the strength and stability conditions for axial compression/tension and bending. The factored bending moment M_f, together with the factored axial compression C_f, and tension force T_f computed for each of the three

loading combinations considered, are given in **Table 3.38** and **Table 3.39** for both E-W and N-S directions. As illustrated in **Table 3.38** and **Figure 3.9**, the design forces for the 6V building are very close to those for the 6-storey building located in Quebec City. For this reason, the beam and column (Class 1 or 2) sections were selected to be the same as those for the 6Q building.

Table 3.38 Design loads for the 6-storey CBF beams in E-W direction (Vancouver)

	Combo:1.25DL+1.5LL			Combo:1.25DL+1.5Q			Combo:1.25DL+1.05LL+1.05Q		
St	M_f	T_f	C_f	M_f	T_f	C_f	M_f	T_f	C_f
	kNm	*kN*	*kN*	*kNm*	*kN*	*kN*	*kNm*	*kN*	*kN*
6	79	N/A	N/A	49	169	169	70	119	119
5	102	N/A	N/A	55	396	271	88	322	145
4	102	N/A	N/A	55	546	405	88	445	220
3	102	N/A	N/A	55	662	520	88	526	301
2	102	N/A	N/A	55	746	605	88	585	360
1	102	N/A	N/A	55	790	649	88	616	391

Table 3.39 Design loads for the 6-storey CBF beams in N-S direction (Vancouver)

	Combo:1.25DL+1.5LL			Combo:1.25DL+1.5Q			Combo:1.25DL+1.05LL+1.05Q		
St	M_f	T_f	C_f	M_f	T_f	C_f	M_f	T_f	C_f
	kNm	*kN*	*kN*	*kNm*	*kN*	*kN*	*kNm*	*kN*	*kN*
6	106	N/A	N/A	66	277	277	94	194	194
5	138	N/A	N/A	75	577	537	119	420	360
4	138	N/A	N/A	75	852	805	119	615	545
3	138	N/A	N/A	75	1084	1032	119	779	702
2	138	N/A	N/A	75	1246	1192	119	895	812
1	138	N/A	N/A	75	1363	1305	119	977	891

Thus, the selected sections for the CBF beams are given in **Table 3.23** while the column sections are given in **Table 3.24** for the E-W direction; whereas for the N-S direction the beams of the braced frames are given in **Table 3.30** and the CBF column sections are given in **Table 3.31**.

3.6.2.3. Design of 6-storey CBF brace-to-frame connections (Vancouver)

As illustrated above, design forces computed for the 6-storey CBF office building located in Vancouver are very close to those of the 6-storey CBF building located in Quebec City. For this reason, the brace-to frame connections of the 6-storey CBF are the same to those computed for the 6-storey CBF in Quebec City. **Table 3.25** and **Table 3.26** summarize the gusset plate design and the reserve capacity of the connections together with the demand-to-capacity ratios for each considered verification for braces of CBFs in E-W direction. In addition, **Table 3.32** and **Table 3.33** show the summary of gusset plate design and its reserve capacity of CBF brace connections located in the N-S direction.

3.7. Conclusions

This chapter presents the design of fictitious 3- and 6-storey CBF office buildings located in representative locations of eastern Canada i.e. Quebec City (3Q, 6Q), and western Canada: i.e. Vancouver, BC (3V, 6V)- that were designed according to the 1980 NBCC and CSA/S16.1-M78 standard. Even though the percentage of CBF buildings in B.C. is low, the 3- and 6-storey buildings located in Vancouver were considered for comparison purposes. It is noted that both Quebec and Vancouver were in the same seismic zone 3 according to the first seismic zoning map from 1970. Under these circumstances, the design seismic force for the 3Q and 6Q buildings was slightly larger compared with 3V and 6V buildings. In other words, the only difference consists in the snow load applied at the roof level, i.e. for Quebec City the snow load is $S = 2.24\ kPa$ whereas for Vancouver the design snow load is $S = 1.52\ kPa$. As a consequence, all CBF members and brace-to-frame connections of the 3V and the 6V buildings were selected to be the same as that of the 3Q and 6Q buildings, respectively.

CHAPTER 4. SEISMIC ASSESSMENT OF 1980 CBF BUILDINGS ACCORDING TO CURRENT CODE DEMAND

4.1. Introduction

In this Chapter, the existing low- and middle-rise CBF office buildings designed using NBCC 1980 and CSA/S16.1-M78 standard, are evaluated in order to identify possible seismic deficiencies. To quantify the level of deficiency, the structural system was divided into bins, labelled performance groups (FEMA P695, 2009) which reflect changes in seismic behaviour of an existing structural system when comparing it to a similar system, proportioned to comply with current code provisions. The collapse safety of the studied buildings was evaluated for each performance group (e.g. braces, beams, columns and brace-to-frame-connections) in terms of demand-to-capacity ratios, where the demand was as per current code and standard (NBCC 2010 and CSA S16-2009). Specifically, the assessment process can be conducted using the Equivalent Static Force Procedure (ESFP) and also the nonlinear time-history analysis by means of IDA, as documented in Chapter 2 of this thesis.

4.2. Seismic Assessment of studied buildings located in Quebec City

Several major changes were incorporated in the 2005 edition of NBCC based on the release of the 4th generation seismic map which was carried in the following 2010 edition. In this light, the seismic map is based on the Uniform Hazard Spectrum (UHS) approach and provides site-specific response spectral accelerations at specified periods for each city in Canada. The UHS was developed for a probability of exceedance of 2% in 50 years corresponding to a return period of 2475 years. Thus, according to NBCC 2010, the minimum lateral earthquake design force at the base of the structure *V,* is calculated using **Eq. (2.11)**. In the equation, the design spectral acceleration corresponding to the first-mode period of the building $S(T_a)$, replaces the seismic zone factor *A* from NBCC 1980 with spectral ordinates given at specified periods of *0.2*, *0.5*, *1.0* and *2.0 s* for each city in Canada. For Quebec City, these values are: 0.55g, 0.32g, 0.15g and 0.052g respectively.

Another change between NBCC 2010 and NBCC 1980 refers to load combinations and consists in a factor load for earthquake induced forces taken as *1.0* instead of *1.5* and the load combination as per current code is given in **Eq. (4.1):**

$$1.0DL + 0.5LL + 0.25S + 1.0E \tag{4.1}$$

where *S* and *E* represent the snow and earthquake load, respectively.

According to NBCC 2010, the roof snow load was calculated using **Eq. (4.2)**, where I_a is the importance factor; S_s and S_r represent the ground snow load and the associated rain load, while C_b, C_w, C_s, and C_a represent the basic roof snow, wind exposure, slope and shape factors, respectively.

$$S = I_a[S_s(C_b C_w C_s C_a) + S_r] \tag{4.2}$$

For Quebec City, the ground snow load is S_s=*3.6 kPa* and S_r =*0.6 kPa*, as per NBCC 2010 Table C-2. Further, the basic roof snow load factor C_b, was taken *0.8* and all remaining terms I_a, C_w, C_s, and C_a are equal to unity. The resulting snow load for Quebec City was *S= 3.48 kPa*. On the other hand, the snow load calculated according to NBCC 1980 and presented in *Section 3.2* of this study, was *S=2.24 kPa*; thus an increase of 55% can be observed, regarding the snow load calculation.

4.2.1. Base shear evaluation for the 3Q building

The design spectrum $S(T_a)$ was determined at the fundamental vibration period of the structure using linear interpolation between the values given in **Eq. (2.13)**, having the site modification factors F_a=F_v=*1.0 (*soil class C*)*. In addition, for braced frames, the empirical equation for the fundamental period of the structure T_{emp} is given in **Eq. (2.14)**. According to the calculations, for the 3-storey office building located in Quebec City, resulted T_{emp}=*0.293 s*. Alternatively, a dynamic analysis can be used to determine the first-mode period which cannot exceed $2T_{emp}$ = *0.585 s*. For this reason, a numerical model of the structure was created using ETABS computer program (CSI, 2009) to determine the dynamic response of the structure based on the modal response spectrum method which has become a widely accepted practice nowadays. The resulted 1st mode dynamic period of the structure in E-W direction was *0.559 s* while for the N-S direction, the period was *0.593 s*. It is noted that according to 1980's design, the first-mode period in the E-W direction was *0.136 s* and in the N-S direction was *0.192 s*.

Further, for base shear calculation according to NBCC 2010, the higher mode effects factor M_v, and the importance factor I_E, were taken as *1.00*. Additionally, the seismic weight *W*, was calculated as a summation of all dead loads acting on the structure plus 25% of the design roof snow loads. Thus, for the 3-storey office building located in Quebec City (3Q), the total seismic weight was *W= 21557 kN*. In consequence, a 3% increase in the seismic weight resulted due to the increase in the snow load. Lastly, the ductility-related force modification factor, R_d and the

overstrength-related force modification factor R_o, were considered $R_d = 1.5$ and $R_o = 1.3$ which correspond to conventional construction type (CC) as described in *Section 2.3.2* of this thesis. Substituting all the values in **Eq. (2.11)**, the resulted minimum lateral earthquake design force at the base of the structure was $V_{f,10} = 3219\ kN$, which implies a force of *805 kN* and *1609 kN* per each frame in the E-W and N-S direction, respectively. It is noted, that the calculated base shear has to be larger than the base shear determined at a period of *2.0 s* according to **Eq. (2.12)** and should not exceed $2/3[S(0.2)I_E W/R_d R_o]$. In **Table 4.1** is summarized the base shear calculation based on the equivalent static force procedure (ESFP) according to NBCC 1980 and NBCC 2010 for the 3Q building. Additionally, the table contains values for the seismic weight *W*, together with the fundamental period of vibration according to the empirical equation (T_{emp}) and linear dynamic analysis ($T_{1,dyn}$), respectively.

Table 4.1 Base shear computed for the 3Q building based on the ESF procedure

3Q	T_{emp} (s)		$T_{1,dyn}$ (s)		W (kN)	V (kN)
	E-W	N-S	E-W	N-S	E-W&N-S	E-W &N-S
NBCC 1980	0.136	0.192	N/A	N/A	20918	1674
NBCC 2010	0.293	0.293	0.559	0.593	21557	3219

Similarly to 1980s design, a concentrated load, $F_t = 0.07T_1V$ which cannot exceed $0.25V$ was applied at the roof level when the first-mode period of the building is $T_1 \geq 0.7\ s$ (otherwise $F_t = 0$ kN). As shown in **Table 4.1** the resulted 1st mode dynamic period of the structure for both directions is less than *0.7 s*, therefore $F_t = 0$. The remaining seismic load (V-F_t), was distributed along the building height in accordance with **Eq. (2.9).** Additionally, the torsional effects were considered by applying torsional moments at each level, according to **Eq. (2.15)**. Moreover, the 3Q building was checked for torsional sensitivity by calculating the maximum ratios $B_x = \delta_{max}/\delta_{ave}$ (at each level x), as described in *Section 2.2*.1. From ETABS model the maximum ratio resulted at the roof for both directions, i.e. $B_3 = 1.1$ for E-W and $B_3 = 1.33$ for N-S which are both less than *1.7*; thus the building is not torsional sensitive. For this reason, the dynamic base shear V_{dyn} resulted from modal response spectrum analysis (linear dynamic analysis) in ETABS should not be lower than $80\%V_f$, where V_f is the base shear obtained based on the equivalent static force method from **Eq. (2.11)**.

According to NBCC 2010, the earthquake-induced forces, shears, overturning moments and torsional moments calculated at each storey level are to be multiplied by an amplification factor $U_2=1+\theta_x$ to allow for P-Δ effects, where θ_x is a stability factor given in **Eq. (4.3)**.

$$\theta_{\mathrm{x}} = \frac{\sum_{i=x}^{n} Wi}{R_0 \sum_{i=x}^{n} F_{\mathrm{i}}} \frac{\Delta_{\mathrm{mx}}}{H_{\mathrm{s}}} \tag{4.3}$$

In the above expression $\sum_{i=x}^{n} F_{\mathrm{i}}$ is the seismic design shear force at the level under consideration; $\sum_{i=x}^{n} W_i$ represents the portion of factored dead plus live load above storey under consideration; Δ_{mx} is the maximum interstorey drift, while H_s and R_o represent the storey height and overstrength-related force modification factor, respectively. However, if the stability factor θ_x is less than *0.10,* (i.e. $U_2=1.1$) then, P-Δ effects can be ignored. According to the calculations, the P-Δ effects can be ignored for both directions.

The un-factored base shear distribution per CBF based on ESFP according to NBCC 1980 (1Q) and NBCC 2010 (1E) is given for the 3Q building in **Table 4.2**. In addition, the dynamic base shear obtained from the linear dynamic analysis (ETABS) is also given.

Table 4.2 Base shear distribution along the CBF height of 3Q building according to NBCC'80 and NBCC'10

St.	NBCC 1980		NBCC 2010					
	*V_{80}=ASKIFW, (kN)		**$V_{f,10}$=S(T_a)$M_v I_E$W/$R_d R_0$, (kN)		0.8$V_{f,10}$, (kN)		V_{dyn}, (kN)	
	E-W	N-S	E-W	N-S	E-W	N-S	E-W	N-S
3	202	407	435	986	348	789	439	978
2	364	741	722	1636	577	1309	686	1520
1	467	974	883	2003	707	1602	861	1879

* torsion and P-Δ included; ** torsion included and P-Δ neglected because $\theta < 0.1$

It is mentioned that in the N-S direction the shear force is given for two adjacent CBFs. Additional forces from torsion and P-Δ effects (only for 1980s design) were also included in the base shear calculation. In the above table, "80" symbol was used to refer to the 1980's design, while "10" refers to the 2010 design.

As illustrated in **Table 4.2**, the current base shear demand which was selected as $max(0.8V_{f,10}; V_{dyn})$, is higher than the lateral base shear computed according to NBCC 1980 in both directions. In other words, the *demand-to-capacity* ratio between the current design base shear and 1980s design is *1.84* for the *CBFs* from E-W direction, while for the N-S direction the ratio is *1.93* as shown in **Figure 4.1**. Therefore, the seismic demand has considerably increased. However, V_{80} given in **Table 4.2** was taken with factor *1.00*, although according to NBCC 1980 the earthquake force factor was *1.05* and *1.5* as per controlling combination.

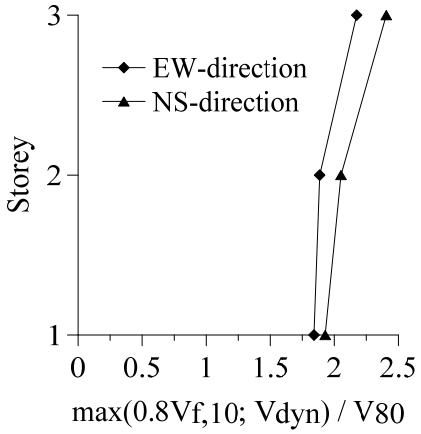

Figure 4.1 Storey shear demand-to-capacity ratio for the 3Q building

4.2.2. Seismic assessment of the 3-storey CBF components (3Q building) in the E-W direction

4.2.2.1. Assessment of CBF members

In order to quantify seismic deficiencies of 3Q building, all existing CBF members and components (e.g. braces, beams, columns and brace-to-frame connections) were assessed against the current design requirements (NBCC 2010 and S16.1-2009). Thus, the demand is that required by the current code while the capacity was computed for the existing member sizes resulted according to 1980 design. When the *demand-to-capacity ratio > 1* means that the CBF member does not possess sufficient resistance to respond to the current demand.

In this study, the axial force demand triggered in braces was determined from the load combination $1.0DL + 0.5LL + 0.25S + 1.0E$ where E is the earthquake load obtained from dynamic analysis conducted in ETABS. The resulted axial compression and tension forces ($C_{f,10}$, $T_{f,10}$) in CBF braces of E-W direction are given in **Figure 4.2**. In addition, according to S16.1-2009 standard, the factored tensile resistance T_r, as well as, the factored compressive resistance C_r, were computed according to **Eq. (2.18)** and **Eq. (2.19)**, respectively. In agreement with the capacity design

method, bracing members are expected to develop the probable resistance, both in tension and compression (T_u, C_u). In this regard, the demand-to-capacity ratios of CBF braces $C_{f,10}/C_{r,10}$; $T_{f,10}/T_{r,10}$ as well as $C_{f,10}/C_u$; $T_{f,10}/T_u$ were computed and are illustrated in **Figure 4.3(a)**. It is noted that the probable tensile resistance T_u, and the probable compressive resistance C_u, were determined based on **Eq. (4.4)** and **(4.5)** respectively, while $C_{r,10}$ and $T_{r,10}$ were calculated with values of $\phi=1.0$ instead of $\phi=0.9$ such that the results are closer to real response.

$$T_u = A_g R_y F_y \tag{4.4}$$

$$C_u = \min[\, A_g R_y F_y ; 1.2 A_g R_y F_y (1 + \lambda^{2n})^{-1/n}] \tag{4.5}$$

Although the value of R_y is usually taken as *1.1* for W-shape members, the product $R_y F_y$ in the above equations (probable yield stress) cannot be taken less than *460 MPa* for HSS members as per Clause *27.1.7* of CSA/ S16.1-2009 standard; A_g represents the gross area of the member.

It is noted that the design of CBFs members such as: beams, columns and brace-to-frame connections, need to sustain in elastic range the development of the probable brace resistance in tension and compression (T_u and C_u).

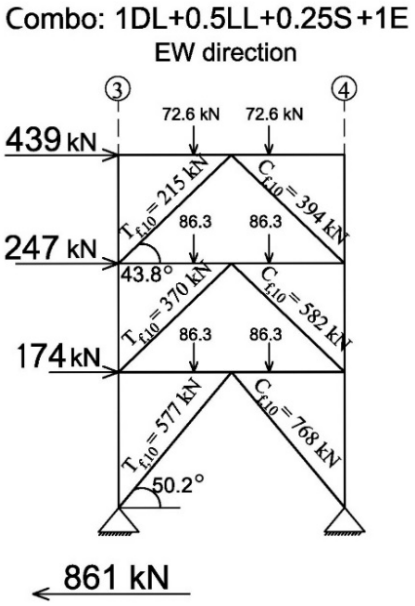

Figure 4.2 Axial forces triggered in 3-storey CBF braces in E-W direction according to NBCC 2010 demand (Quebec City)

Beams of CBFs were made of I-shape cross-sections and were verified as beam-column elements for three limit states such as: cross-sectional strength (*CSS*), overall member strength (*OMS*) and

combined tensile axial force and bending moment (*AT&B*). On the other hand, the torsional buckling strength was not verified because beams are laterally supported by the composite steel deck. According to CSA/S16-09 standard, the interaction equation used to check member strength and stability under axial compression and bending for Class 1 and Class 2, I-shaped cross-sections is given below. In addition, the capacity of the member for *CSS* and *OMS* was verified based on **Eq. (4.6)**, while for axial tension and bending **Eq. (4.7)** was used.

$$\frac{C_f}{C_r} + \frac{0.85U_1M_f}{M_r} \leq 1.0 \tag{4.6}$$

$$\frac{T_f}{T_r} + \frac{M_f}{M_r} \leq 1.0 \tag{4.7}$$

For the *CSS* verifications, the value of C_r is given in **Eq. (2.19)** with $\lambda=0$. Conversely, for *OMS*, C_r was calculated based on the axis of bending according to the corresponding λ value. Moreover, the factored bending moment resistance M_r was calculated as: $M_r=\phi ZF_y$ for all limit states, while U_1 was obtained from the following equation: $U_1 = \omega_1/(1-C_f/C_e)$, where ω_1 depends on the loading type between supports and C_e is the Euler buckling load described by: $C_e = \pi^2EI/L^2$; where I is the moment of inertia of the section and L represents the clearance of the beam. It is specified that, for *CSS* verifications the values for U_1 should not be taken less than *1.00*. In addition, $\omega_1=1.0$ for members subjected to distributed loads or series of point loads between supports.

According to S16.1-09, the CBF beams should be designed to resist bending moments due to gravity loads, and to act as a collector to transfer seismic inertial forces into the braced bays. Thus, the effect of load redistribution due to brace buckling and yielding was considered for the seismic assessment. For this reason, two possible loading scenarios were analyzed: i) the compression acting braces attain their probable compressive resistance C_u, while the tension acting braces develop their probable tensile resistance, T_u and ii) the compression acting braces attain their probable post-buckling compression resistance calculated as $C'_u= min(0.2A_gR_yF_y; A_gR_yF_y (1+\lambda^{2n})^{-1/n})$ in conjunction with the tension acting braces which develop their probable tensile resistance, T_u.. In other words, chevron bracing members provide or do not provide vertical support for the attached beams. It is noted that in the case of buildings not exceeding four storeys, CSA/S16-09 standard allows the tension brace force to be taken as $0.6T_u$, provided that beams are Class 1 section. For the 3Q building, all CBF beams were Class 1 section. Thus, a reduction in the

probable tensile resistance was applied. The seismic assessment of beam members given in terms of demand-to-capacity ratio corresponding to the following limit states: *CSS, OMS* and *AT&B* is shown in **Figure 4.3(b)**. According to the calculation, the most critical case was obtained when braces attain their probable post-buckling compression resistance and no vertical support was provided for CBF beams.

Similarly to beams, columns of CBFs in the E-W direction are subjected to axial compression and bending, as well as axial tension and bending. Therefore, the capacity of the members was examined for: overall member strength (*OMS*), lateral torsional buckling (*LTB*) and axial tension and bending (*AT&B*). In addition, the same interaction equations as for the beams assessment were used, i.e. **Eq. (4.6)** for *OMS* and *LTB* verifications, while **Eq. (4.7)** was used for the *AT&B* limit state. All the interaction equation parameters were calculated similarly with the parameters for the beams, however the C_r for the *LTB* limit state was calculated based on the weak-axis of the column cross-section besides the fact that the values for U_1 should not be taken less than 1.00. It is noted that, for the column assessment, $\omega_1=0.6$ because column members are not subjected to transverse loads between supports and the columns were considered pinned at each floor. According to CSA/S16-09 standard, the total axial force in columns was determined from the brace probable resistances projection (e.g. T_u and C_u) combined with the forces from gravity (applied on the tributary area of each member) and the factored seismic forces obtained from $R_dR_0=1.3$ combined with the effect of gravity loads -whichever occurs first. It is noted that for *OMS* and *LTB* the total axial force in columns C_f, was obtained from the projection of the probable resistances plus the axial load from the gravity forces, while for the AT&B verifications the total axial tension was given by the seismic forces from $R_dR_0=1.3$ which were reduced with the axial compression from the gravity effect. Additionally, a bending moment $M_f=0.2ZF_y$ in the direction of the braced bay was also considered for each verification. Thus, columns assessment is presented in **Figure 4.3(c)** in terms of demand-to-capacity ratio.

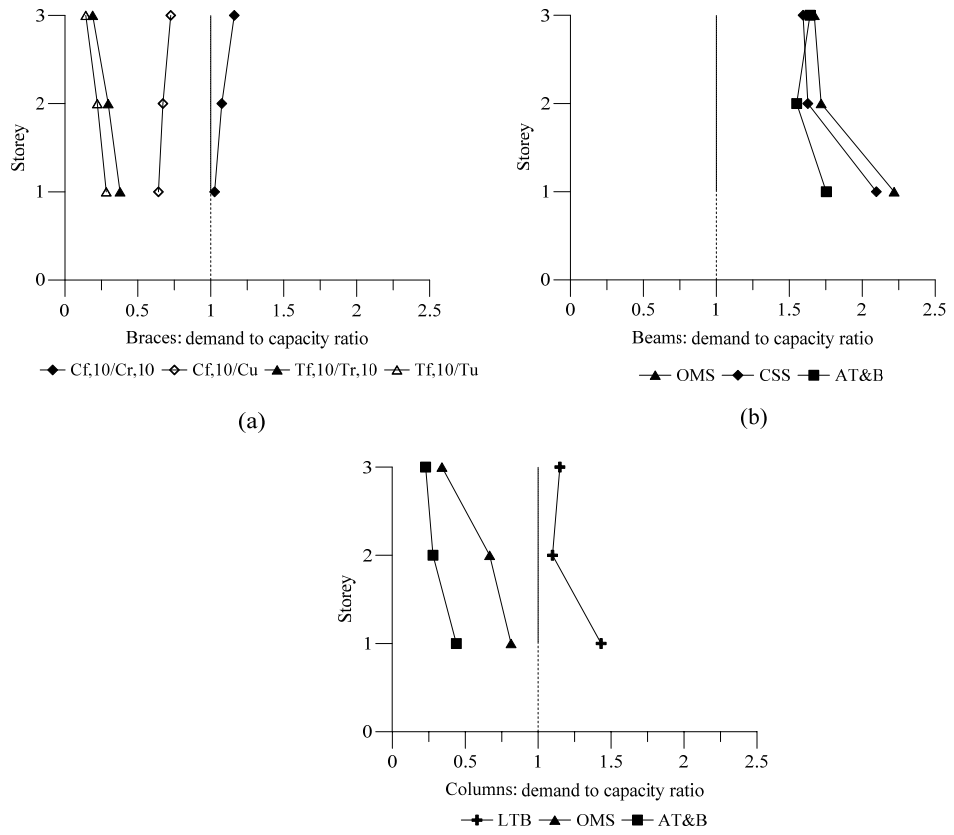

Figure 4.3 Seismic assessment of structural members of 3-storey CBF in E-W direction (3Q): (a) braces; (b) beams (c) columns.

As illustrated in **Figure 4.3** , braces at the 3rd floor are more likely to encounter some damage ($C_{f,10}/C_{r,10} > 1.0$), while the $C_{f,10}/C_{r,10}$ ratio computed for braces at the 2nd and ground floor is *1.08* and *1.03*, respectively. However, if the calculation of brace capacity is based on the probable compressive resistance (C_u) the demand to capacity ratio is significantly reduced, having the values below *1.0* for all braces. Comparing $T_{f,10}/T_{r,10}$ and $T_{f,10}/T_u$ ratios, the bracing members strength seems to be adequate. Conversely, none of the beams have sufficient capacity to withstand the required limit states, in addition, the larger demand resulted for the *OMS* verification. Furthermore, the columns in the E-W direction of the 3-storey building located in Quebec City are prone to instability due to lateral torsional buckling having the demand to capacity ratio *>1* for all storeys.

4.2.2.2. Brace-to- frame connection assessment

Past studies (Wang, 2014; Jiang, 2013) had shown that structural components that are most likely to fail when capacity design principles apply, are the brace-to-frame connections. According to CSA/S16-09 standard, a clearance of $2t_{gp}$ is necessary below the Whitmore width to allow the

plastic hinge formation in the gusset plate in order to allow braces to buckle out-of-plane. In addition, to avoid HSS brace fracture at the end portion containing the slotted hole, the current standard requires a cover-plate at the location of the slotted HSS bracing member. However, these requirements were not stipulated in CSA/S16.1-M78 standard. Thus, for the seismic assessment, the existing connections designed according to CSA/S16.1-M78 standard were checked against the current requirements. It is noted that besides the typical verifications according to 1980's design, the block shear failure and the shear lag effect were introduced as new verifications in CSA/S16-09 standard.

For this reason, the welding length (L_w), the weld leg width (D_w), as well as the Whitmore effective width (W_W) and the gusset plate thickness (t_{gp}) are the values obtained according to 1980's design and are given in *Chapter 3* (see **Table 3.9)**. Similarly to the old code design, the factored shear resistance of the fillet weld V_r, resulted from the consideration of the minimum value of two failure modes: i) fracture of the weld metal through the weld throat calculated using the equation $V_r=0.67\phi_w A_w X_u$ and ii) yielding at the weld-to-base metal interface as per the following equation $V_r=0.67\phi_w A_m F_u$. Thus, the factored coefficient has changed from *0.5* (weld metal) and *0.66* (base metal) to *0.67* in CSA/S16-09 standard. In addition, the welding resistance factor ϕ_w, has changed from *0.9* in CSA/S16.1-M78 standard to *0.67* in CSA/S16-09 standard. However, the shear area A_w, the interface area A_m, and the ultimate strength of the electrode X_u were calculated the same as in the *Section 3.3.2.3*.

On the other hand, the factored tensile resistance of gusset plate T_{rgp} was calculated according to **Eq. (3.8)** with $\phi = 0.9$. The factored compression resistance of gusset plate C_{rgp} was obtained from **Eq. (2.19)** based on the slenderness $\lambda = KL_{ave}/r\,(F_y/\pi^2 E)^{0.5}$, where the effective length factor K was considered *0.67* and the critical effective length L_{ave}, was calculated as an average value between the three lengths (L_1, L_2, L_3) resulted from the gusset plate geometry according to **Figure 4.4** (Hsiao et al., 2013). Additionally, the radius of gyration was taken as $r= (I/A_{gp})^{0.5}$, where A_{gp} and I, represent the area and the moment of inertia of the gusset plate, respectively, as explained in *Section 3.3.2.3* of this thesis.

Another key modification is the calculation of tensile resistance of the HSS bracing member due to the block shear failure, given in **Eq. (2.20),** where Φ_u is a factor taken as *0.75* for steel, U_t represents the efficiency factor taken as *1.0* for symmetrical blocks, which is the case for this study;

while A_n and A_{gv} represent the net area in tension and the gross area along the shear failure plane, respectively.

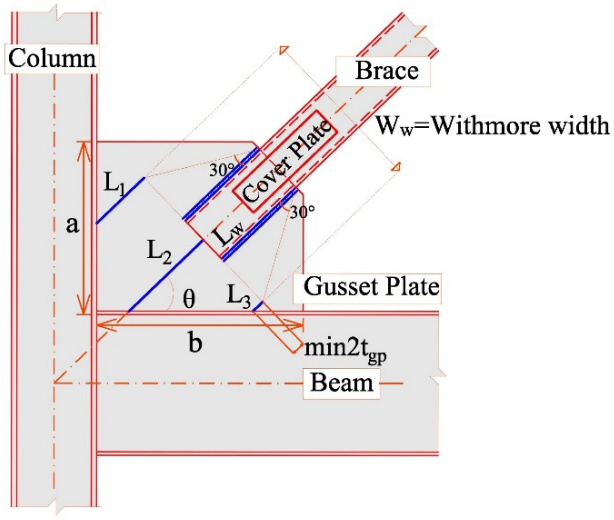

Figure 4.4 HSS brace-to-frame connection detail according to CSA/S16-09

Moreover, based on the research conducted by Martinez-Saucedo and Packer (2009), and documented in Chapter 2 (*Section 2.3.2*), a new clause *12.3.3.4* has been added in the upcoming edition of CSA/S16-14 standard, in order to specifically address the shear lag factor U for all slotted HSS welded connections with a single concentric gusset plate. Although the *block-shear* may control the tensile limit state for short welding lengths, the "circumferential" fracture of the HSS with the consideration of shear lag effect, where the gusset plate tears out of the HSS by forming a fracture through the HSS walls was also verified. Thus, for the *circumferential fracture* of the HSS brace, the following equation should be satisfied: $T_{NR} = 0.85\Phi A_{ne} F_u$ where A_{ne} is the effective net area reduced with the shear lag factor U computed as $A_{ne}=A_{n2}U$, in which A_{n2} is given bellow for elements connected by longitudinal welds along two parallel edges. On the other hand, the shear lag factor U, was calculated using **Eq. (2.22)** and **Eq. (2.23)** depending on $\bar{x}'/L_w$.

(i) when $L_w \geq 2w$, where L_w represents the welding length while w and t are the width and thickness of the HSS bracing member.

$$A_{n2} = 1.00wt$$

(ii) when $2w > L_w \geq w$: $A_{n2} = 0.5wt + 0.25L_w t$ (4.8)

(iii) when $w > t$: $A_{n2} = 0.75L_w t$

The seismic assessment of brace-to-frame connections of 3-storey CBF in the E-W direction of the 3Q building is summarized in **Table 4.3** It is noted that the values of T_u and C_u in braces, given by **Eq. (4.4)** and **(4.5)**, were used to calculate the seismic demand for HSS brace connections according to the current code. In addition, the tensile resistance for the metal base resistance $T_{r,mb}$ was calculated the same as for the 1980s design. As illustrated in the table, the failure occurs due to the shear failure of welding followed by the tensile failure of the metal base, which are both brittle failure modes. Therefore, all brace to frame connections should be replaced in order to provide: the $2t_g$ clearance, sufficient welding lengths to carry the brace capacity and strength to sustain brace buckling and yielding.

Table 4.3 HSS brace-to-frame connections assessment for E-W direction of 3-storey CBF (3Q)

St.	Shear resistance of welding,(kN)			Metal base resistance,(kN)		Yielding of gusset plate,(kN)		Buckling of gusset plate,(kN)		Net Rupture and block shear of brace with shear lag,(kN)		
	V_r	C_u/V_r	T_u/V_r	$T_{r.mb}$	$T_u/T_{r.mb}$	T_{rgp}	T_u/T_{rgp}	C_{rgp}	C_u/C_{rgp}	T_{NR}	$T_{r\text{-}BS}$	$T_u/\min(T_{NR}, T_{r\text{-}BS})$
3	585	0.93	2.58	617	2.44	619	2.44	603	0.90	969	772	1.95
2	585	1.48	2.85	617	2.70	683	2.44	663	1.31	851	648	2.57
1	731	1.64	2.79	772	2.64	836	2.44	737	1.62	1064	810	2.52

4.2.3. Seismic assessment of the 3-storey CBF components (3Q building) in the N-S direction

4.2.3.1. Assessment of CBF members

The process of seismic assessment of members of CBFs located in N-S direction is similar with that in E-W direction. Thus, the response of braces, beams and columns was analysed in terms of demand-to-capacity-ratios where the demand was based on the current design provisions (NBCC 2010 and S16.1-09). The factored compression and tension forces in braces ($C_{f,10}$, $T_{f,10}$) are given for the N-S direction in **Figure 4.5**.

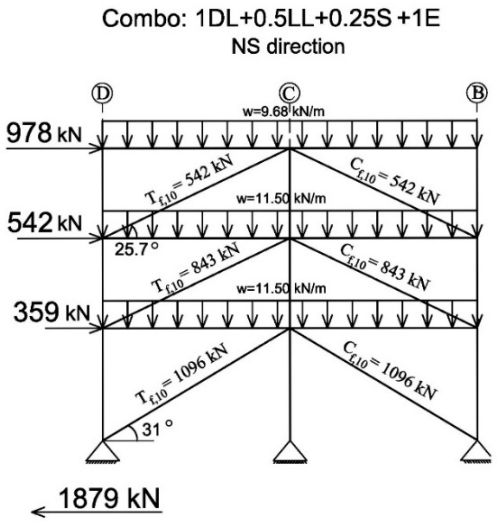

Figure 4.5 Axial forces triggered in 3-storey CBF braces in N-S direction according to NBCC 2010 demand (Quebec City)

The demand-to-capacity ratios for braces, beams and columns are illustrated in **Figure 4.6.** Similar with members of chevron CBF (E-W direction), beams of the two adjacent CBFs were verified as beam-column elements for three limit states (i.e. *CSS*, *OMS* and *AT&B)*. To summarize, the demand-to-capacity ratios for braces are given in **Figure 4.6(a)**, for beams in **Figure 4.6(b)** while for both side columns (*SC*) and middle column (*MC*) in **Figure 4.6(c)** which corresponds to *LTB*, *OMS* and *AT&B*. It is noted that only the compression acting braces attaining the probable compressive resistance C_u, in conjunction with the tension acting braces assumed to reach the probable tensile resistance T_u, were considered for beams assessment. In addition, the $0.6T_u$ reduction in the probable tensile resistance of the bracing members was not applied for the N-S direction.

The same approach as for the E-W direction was used to determine the axial load in the SC and MC columns. It is noted that for evaluating the *OMS* and *LTB* the total factored axial force (C_f) in columns was obtained from the projection of brace probable resistances plus the axial load from the gravity forces. On the other hand, for the *AT&B* verification, the governing loading scenario corresponds to seismic forces computed with $R_dR_0=1.3$ and the axial compression force due to the gravity load component. However, the *AT&B* verification was performed only for the side columns, as the middle column is subjected to axial compression only. Additionally, a bending moment of $M_f=0.2ZF_y$ in the direction of the braced bay was also considered for column verification.

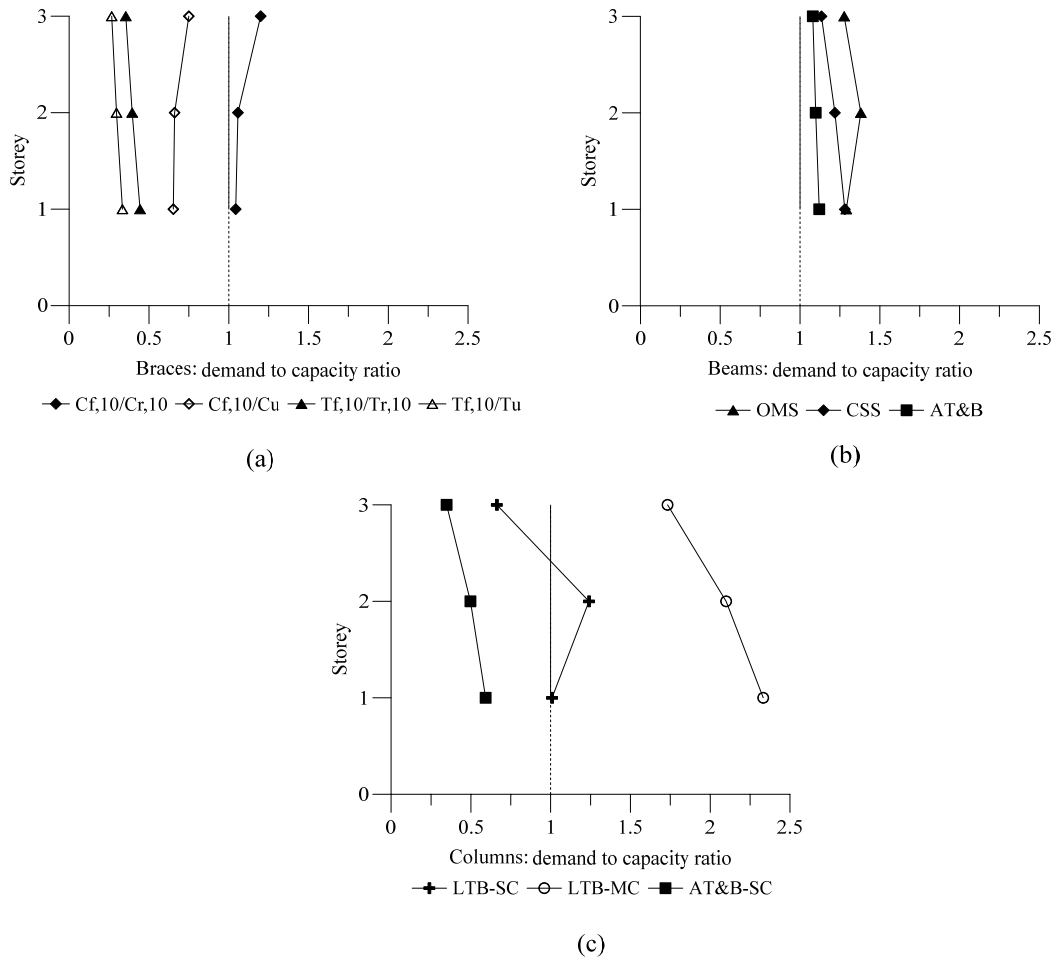

Figure 4.6 Seismic assessment of structural members of 3-storey CBF in N-S direction (3Q): (a) braces; (b) beams (c) columns.

As illustrated in the figure, based on $C_{f,10}/C_{r,10}$ ratio the braces at the 3rd floor were more likely to encounter some damage, while for braces at the 2nd and ground floor the ratio slightly exceeded *1.0*. However, if the calculation of brace capacity is based on the probable compressive resistance (C_u) the demand-to-capacity ratio was significantly reduced and the ratio was less than *1.0* for all braces. Compared with chevron braces (E-W direction) the ratios for CBF braces in the N-S direction were slightly larger. Furthermore, CBF beams do not have sufficient capacity to withstand the required limit states and the larger demand resulted for the *OMS* verification. Compared with the chevron beams (E-W direction), the demand-to-capacity ratios for CBF beams in N-S direction were smaller because beams were not supported by the diagonal braces. On the other hand, the side columns of CBFs in the N-S direction (3Q building) were prone to instability due to lateral torsional buckling. Their demand-to- capacity ratio was >1.0 for the bottom two columns and all middle columns.

4.2.3.2. Brace-to- frame connection assessment

In this section, the existing connections designed according to CSA/S16.1-M78 standard were checked against the current requirements similar with the connections of CBF braces in E-W direction. The seismic assessment of brace-to-frame connections is summarized in **Table 4.4** for the 3Q frames from N-S direction. As illustrated in the table, the failure occurs due to the shear failure of welding followed by the tensile failure of metal base, which are both brittle failure modes. Therefore, all brace-to-frame connections should be replaced in order to provide the $2t_g$ clearance, however sufficient welding lengths to carry the brace capacity and strength to sustain brace buckling and yielding, are also required.

Table 4.4 HSS brace-to-frame connections assessment of 3Q building in N-S direction, according to S16-09

St.	Shear resistance of welding,(kN)			Metal base resistance,(kN)		Yielding of gusset plate,(kN)		Buckling of gusset plate,(kN)		Net Rupture and block shear of brace with shear lag,(kN)		
	V_r	C_u/V_r	T_u/V_r	$T_{r.mb}$	$T_u/T_{r.mb}$	T_{rgp}	T_u/T_{rgp}	C_{rgp}	C_u/C_{rgp}	T_{NR}	$T_{r\text{-}BS}$	$T_u/\min(T_{NR}, T_{r\text{-}BS})$
3	585	1.24	3.48	617	3.30	748	2.72	494	1.46	787	644	3.16
2	731	1.74	3.89	900	3.16	1053	2.70	677	1.88	1389	1127	2.52
1	1024	1.64	3.21	1260	2.61	1337	2.46	1288	1.31	1739	1351	2.43

It is noted that the calculation of the shear resistance of welding (V_r), yielding and buckling of the gusset plate (T_{rgp}, C_{rgp}) together with the net rupture and block shear failure of the brace due to shear lag effects (T_{NR}, T_{BS}) were explained in *Section 4.2.2.2* for the E-W direction.

4.2.4. Base shear evaluation for the 6Q building

The same approach as that used in *Section 4.2.1* was applied for the 6Q building. The calculated base shear is given in **Table 4.5** together with the seismic weight W, the fundamental period of vibration according to the empirical equation (T_{emp}) and linear dynamic analysis ($T_{1,dyn}$), respectively. The minimum lateral earthquake design force at the base of the structure V, was calculated using **Eq. (2.11)** and resulted $V= 3707\ kN$ which corresponds to $927\ kN$ per frame in the E-W direction and $1854\ kN$ per two adjacent CBFs in the N-S direction. Further, the higher mode effect factor was taken as $M_v=1.07$ for high seismic areas with Sa(0.2)/Sa(2.0) ≥ 8 while the importance factor was kept $I_E=1.0$. Lastly, the force modification factors, R_d and R_o were kept 1.5 and 1.3, respectively - similar with the 3Q building. It is noted that NBCC 2010 limits the total

building height of CC type to *15 m*. However, according to *Clause 27.11.3* of CSA/S16-09 standard the building may exceed this limit if certain conditions are met. Thus, the base shear was linearly increased (as a function of the building height) by 2% per meter of height above *15m*, without exceeding the seismic forces determined with $R_dR_o = 1.3$. It is noted that the calculated base shear has to be larger than the base shear determined at a period of *2.0 s* according to **Eq. (2.12)**.

Table 4.5 Base shear resulted for the 6Q building according to ESF procedure

6Q	T_{emp}, (s)		$T_{1,dyn}$, (s)		W, (kN)	V, (kN)	
	E-W	N-S	E-W	N-S	E-W&N-S	E-W	N-S
NBCC 1980	0.261	0.370	N/A	N/A	42068	3292	2767
NBCC 2010	0.563	0.563	1.00	1.02	42506	3707	3707

As shown in **Table 4.5** the resulted 1st mode dynamic period of the structure for both directions was larger than *0.7 s*, therefore the concentrated load calculated as $F_t = 0.07T_1V = 260\ kN < 0.25V$ was applied at the roof level. Subsequently, the remaining seismic load, $V\text{-}F_t$ was distributed along the building height using **Eq. (2.9).** In addition, the torsional effect given by **Eq. (2.15)** was also included. Moreover, similarly with the 3Q building, the 6Q building was also checked for torsional sensitivity. However, based on the dynamic analysis using ETABS, the building was not found to be torsional sensitive. **Table 4.6** presents the un-factored base shear distribution based on ESFP for the CBFs for E-W and N-S direction, according to NBCC 1980 (e.g. earthquake is taken as 1Q) and NBCC 2010 (e.g. earthquake taken as 1E) while **Figure 4.7** shows the demand-to-capacity ratio for the base shear. Similar with the 3Q building, the current base shear demand was selected as $max(0.8V_{f,10}; V_{dyn})$ where V_{dyn} was the shear resulted from the linear dynamic analysis. In the table, "80" symbol was used to refer to the 1980's design, while "10" referrers to the 2010 design. It is noted that the P-Δ effects according to NBCC 2010 were neglected for both directions because the stability factor θ_x calculated with **Eq. (4.3)** was < 0.10. Additional forces from torsion and P-Δ effects (only for 1980s design) were also included for the base shear calculation.

Table 4.6 Base shear distribution along the CBF height of 6Q building according to NBCC'80 and NBCC'10

St.	NBCC 1980		NBCC 2010					
	*V_{80}=ASKIFW, (kN)		**$V_{f,10}$=S(T_a)$M_v I_E$W/$R_d R_0$, (kN)		0.8$V_{f,10}$, (kN)		V_{dyn}, (kN)	
	E-W	N-S	E-W	N-S	E-W	N-S	E-W	N-S
6	240	397	345	768	276	615	403	829
5	465	775	556	1238	445	990	551	1201
4	649	1119	727	1619	582	1295	646	1457
3	809	1416	858	1911	687	1529	743	1684
2	921	1653	949	2114	759	1691	875	1944
1	977	1791	1001	2228	801	1783	990	2135

* torsion and P-Δ included; ** torsion included and P-Δ neglected because $\theta < 0.1$

As depicted in **Figure 4.7** the ratio between the current and 1980s design base shear (taken with factor 1.0) is *1.01* for the CBFs in E-W direction and 1.20 for the CBF in N-S direction.

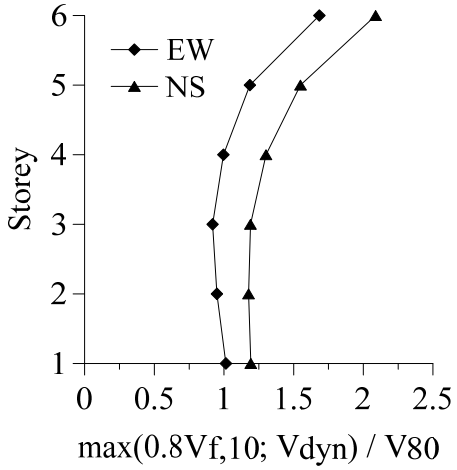

Figure 4.7 Storey shear demand-to-capacity ratio for the 6Q building

4.2.5. Seismic assessment of CBF's components of 6Q building in E-W direction

4.2.5.1. Assessment of CBF members

The seismic assessment of structural members of the 6Q building (E-W direction) is similar with the assessment conducted for the 3Q building. The factored axial tension and compression forces triggered in braces as per the current code demand ($C_{f,10}$, $T_{f,10}$) are given in **Figure 4.8**.

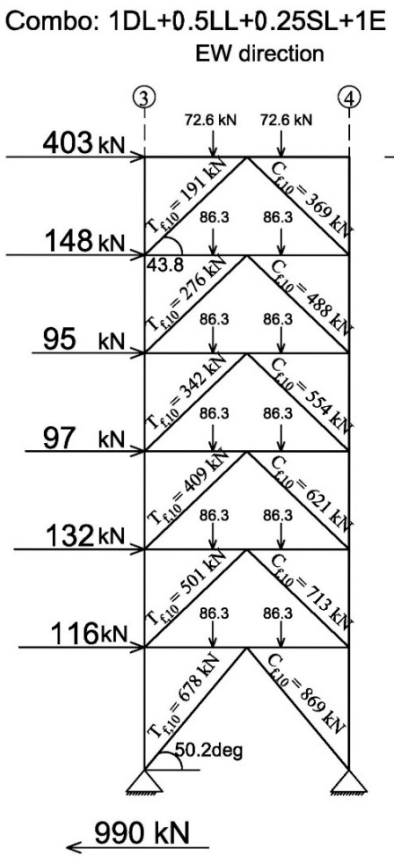

Figure 4.8 Axial forces triggered in 6-storey CBF braces in E-W direction according to NBCC 2010 demand (Quebec City)

The demand-to-capacity ratios for braces, beams and columns were computed and are illustrated in **Figure 4.9**. As illustrated in **Figure 4.9(a)**, the demand-to-capacity ratio for braces is less than *1.00.* The explanation is given in two points: i) the empirical period computed according to NBCC 2010 is much larger than that given in the NBCC 1980 and the resulted base shear is very similar (*1001 kN* as per NBCC 2010 vs *977 kN* as per NBCC 1980) and ii) the earthquake load combination given in NBCC 1980 is different compared to NBCC 2010 (1.25DL +1.5Q versus 1.25DL+0.5LL+0.25SL+1E) which implies a factored base shear of *1465 kN* vs *1001 kN* (see **Table 4.6**). Because the building is regular, the NBCC 2010 allows considering in design 80% of the base shear resulted from the equivalent static force procedure if a dynamic analysis is employed. Using ETABS, the resulted base shear from dynamic analysis (*990 kN*) was retained in design.

Conversely, for the beams and columns, the demand-to-capacity ratio is *>1.00*. It is noted that the critical case for CBF beams was obtained when braces attained their probable post-buckling

compression resistance C_u' in the compression side and the probable tension resistance T_u in the tensile side (**Figure 4.9 (b)**). Thus, beams do not have sufficient capacity to withstand the required limit states, with the larger demand resulted for the *OMS* verification. The governing axial force demand (C_f) in CBF columns for all limit states resulted from the projection of the seismic forces triggered in braces when $R_dR_0=1.3$, in addition to the associated axial forces generated from the gravity load component. The larger demand occurred due to lateral torsional buckling where a demand-to-capacity ratio >1.00 was recorded at all storeys except the top floor (**Figure 4.9(c)**). A bending moment of $M_f=0.2ZF_y$ in the direction of the braced bay was also considered for columns verification as per CSA/S16-09 requirements

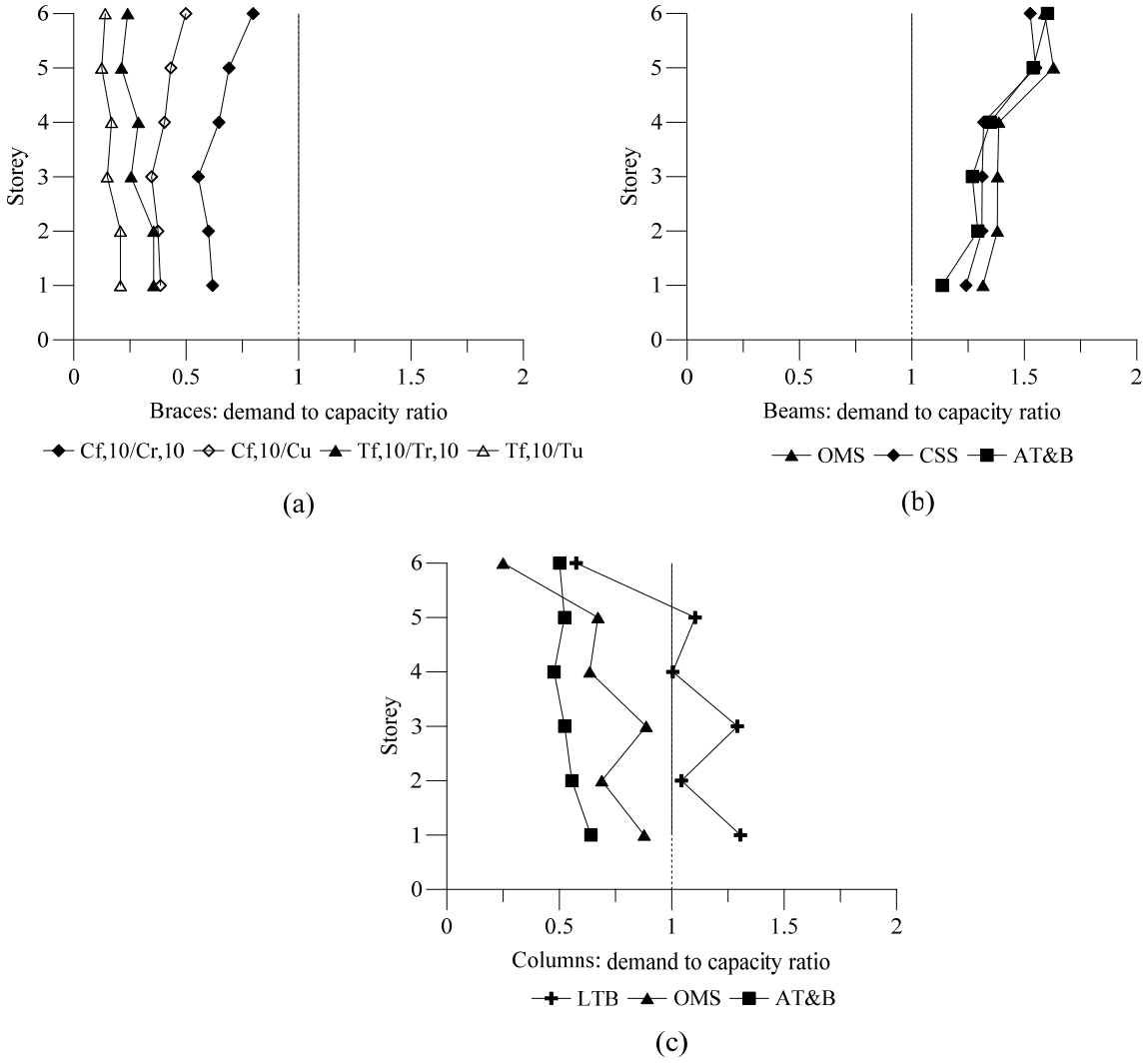

Figure 4.9 Seismic assessment of structural members of 6-storey CBF in E-W direction (6Q): (a) braces; (b) beams (c) columns.

4.2.5.2. Brace-to- frame connection assessment

In this section the existing connections designed according to CSA/S16.1-M78 standard were checked against the current requirements similar with the verifications illustrated for the 3Q building. The seismic assessment of brace-to-frame connections is summarized in **Table 4.7** for the E-W chevron braced frame of the 6Q building. As depicted, the failure occurs due to the shear failure of welding which is a brittle failure mode. Therefore, all brace to frame connections should be replaced in order to provide sufficient welding lengths and the required $2t_g$ clearance which is part of seismic detailing.

Table 4.7 HSS brace-to-frame connections assessment of 6Q building in E-W direction, according to S16-09

St.	Shear resistance of welding,(kN)			Metal base resistance,(kN)		Yielding of gusset plate,(kN)		Buckling of gusset plate,(kN)		Net Rupture and block shear of brace with shear lag,(kN)		
	V_r	C_u/V_r	T_u/V_r	$T_{r.mb}$	$T_u/T_{r.mb}$	T_{rgp}	T_u/T_{rgp}	C_{rgp}	C_u/C_{rgp}	T_{NR}	$T_{r\text{-}BS}$	$T_u/\min(T_{NR}, T_{r\text{-}BS})$
6	439	1.69	3.10	617	2.21	683	1.99	668	1.11	692	518	2.63
5	731	1.55	3.04	772	2.89	772	2.88	751	1.51	1369	1114	2.00
4	926	1.48	2.20	1140	1.79	1114	1.83	1073	1.28	1251	1026	1.99
3	1097	1.64	2.50	1200	2.29	1149	2.39	1104	1.63	1749	1485	1.85
2	1170	1.63	2.06	1440	1.67	1366	1.77	1322	1.44	1521	1296	1.86
1	1426	1.58	2.29	1783	1.83	1640	1.99	1446	1.56	2183	1931	1.69

4.2.6. Seismic assessment of CBF's components of 6Q building in N-S direction

4.2.6.1. Assessment of CBF members

Seismic assessment of the 6-storey CBF members and connections in the N-S direction of loading is similar with that presented for the 3Q building. The factored axial forces computed according to NBCC 2010 and triggered in CBF braces ($C_{f,10}$, $T_{f,10}$) are given in **Figure 4.10**. Moreover, the demand-to-capacity ratios for braces, beams and columns are illustrated in **Figure 4.11**.

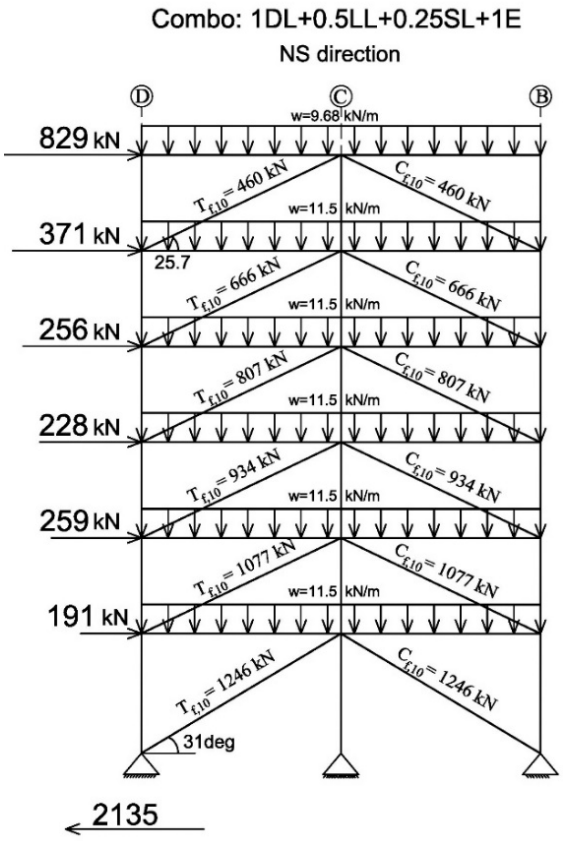

Figure 4.10 Axial forces triggered in 6-storey CBF braces in N-S direction according to NBCC 2010 demand (Quebec City)

As illustrated in **Figure 4.11(a)**, the demand-to-capacity ratio computed for braces is less than *1.0*, except the $C_{f,10}/C_{r,10}$ ratio of top floor braces which is *1.02*; hence HSS braces possess enough strength to carry the demand as per the current code.

The CBF beams were verified as beam-column elements for the three limit states defined previously: *CSS*, *OMS* and *AT&B*. As depicted in **Figure 4.11(b)**, the *OMS* limit state governs the assessment of upper floors beams (i.e. 4^{th} to 6^{th}), while the *AT&B* limit state governs the assessment of bottom floors beams. Compared with demand-to-capacity ratios resulted for beams of CBFs in E-W direction (see **Figure 4.9(b)**) in this case the ratios are smaller because these beams are not supported by the braces as for chevron configuration.

The demand-to-capacity ratios corresponding to *LTB*, *OMS* and *AT&B* for side columns (*SC*) and the middle column (*MC*) are presented in **Figure 4.11(c)**. As resulted, the demand-to-capacity ratios larger than 1 were obtained under the *LTB* (lateral torsional buckling) verification. Thus, the side columns of the 6-storey building located in Quebec City are prone to instability at ground

floor, 3rd and 5th floor while the middle column is prone to failure at all floors, but especially at the ground floor and the 3rd floor level.

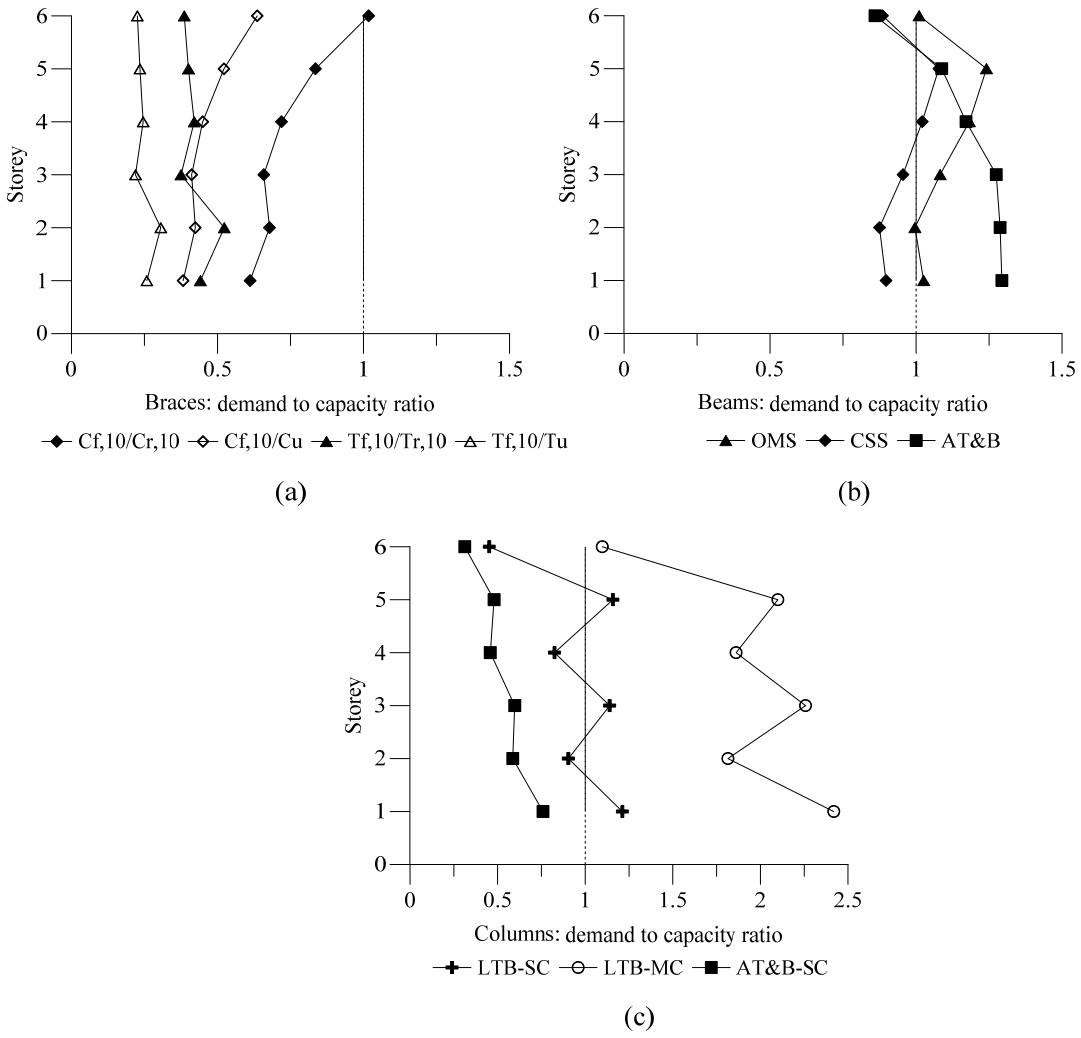

Figure 4.11 Seismic assessment of structural members of 6-storey CBF in N-S direction (6Q): (a) braces; (b) beams (c) columns

Note that the factored compression force (C_f) in columns for all limit states resulted from the case $R_dR_0=1.3$ combined with the tributary axial forces from the gravity load component. In the case of middle column, the total axial compression was determined based on the projection of the probable brace resistances combined with the forces from the gravity component

4.2.6.2. Brace-to-frame connections assessment

The seismic assessment of brace-to-frame connections is summarized in **Table 4.8** for the 6-storey building located in Quebec City, and loaded in the N-S direction. As illustrated in the table, the failure occurs due to the shear failure of welding which is a brittle failure mode. Therefore, all

brace to frame connections should be replaced in order to provide sufficient welding lengths and the $2t_g$ clearance because the gusset plate has to sustain brace buckling and yielding. It is noted that the calculation of the shear resistance of welding (V_r), yielding and buckling of the gusset plate (T_{rgp}, C_{rgp}) together with the net rupture and block shear failure of the brace due to shear lag effects (T_{NR}, T_{BS}) were explained in *Section 4.2.2.2* for the 3Q building.

Table 4.8 HSS brace-to-frame connections assessment of 6Q building in N-S direction, according to S16-09

St.	Shear resistance of welding,(kN)			Metal base resistance,(kN)		Yielding of gusset plate,(kN)		Buckling of gusset plate,(kN)		Net Rupture and block shear of brace with shear lag,(kN)		
	V_r	C_u/V_r	T_u/V_r	$T_{r.mb}$	$T_u/T_{r.mb}$	T_{rgp}	T_u/T_{rgp}	C_{rgp}	C_u/C_{rgp}	T_{NR}	$T_{r\text{-}BS}$	$T_u/\min(T_{NR}, T_{r\text{-}BS})$
6	634	1.14	3.22	669	3.05	777	2.62	517	1.40	883	702	2.90
5	780	1.63	3.64	960	2.96	1088	2.61	757	1.68	1310	1029	2.76
4	1072	1.68	3.07	1697	1.94	1764	1.86	1264	1.42	1831	1415	2.32
3	1341	1.69	3.18	1886	2.26	1960	2.17	1514	1.50	2424	1886	2.26
2	1511	1.68	2.33	2923	1.21	2885	1.22	2113	1.20	2098	1674	2.10
1	1767	1.84	2.73	2735	1.77	2776	1.74	2722	1.20	2723	2153	2.24

4.3. Assessment of the 3- and 6-storey CBF buildings located in Vancouver

The spectral acceleration ordinates of design spectrum for Vancouver corresponding to 2% in 50 years probability of exceedance is given according to Appendix C of NBCC 2010 in **Table 4.9** together with the snow load coefficients.

Table 4.9 Design data for Vancouver buildings according to NBCC 2010

Location	Snow load , (kPa)		Seismic Data, (g)				
	S_s	S_r	$S_a(0.2)$	$S_a(0.5)$	$S_a(1.0)$	$S_a(2.0)$	PGA
Vancouver	1.8	0.2	0.94	0.64	0.33	0.17	0.46

In addition, the snow load for the buildings in Vancouver (3V and 6V) was calculated based on **Eq. (4.2**) and the resulted value was *S= 1.64 kPa* which is *8%* larger than the snow load calculated according to NBCC 1980 (i.e. *S=1.52 kPa*). It is noted that the same load combinations as those used for seismic assessment of Quebec City buildings were considered**.**

4.3.1. Base shear evaluation for buildings located in Vancouver

The base shear evaluation procedure for buildings located in Vancouver was similar with that for buildings in Quebec City**.** Therefore, **Table 4.10** and **Table 4.11** show the base shear calculation for the 3V and 6V building conducted based on the equivalent static force procedure according to NBCC 1980 and NBCC 2010. In addition, these tables contains values for the seismic weight W together with the fundamental period of vibration according to the empirical equation (T_{emp}) and linear dynamic analysis ($T_{1,dyn}$), respectively. It is noted that the minimum lateral earthquake design force at the base of the structure (V) for the current design was obtained using **Eq. (2.11)**, while $T_{1,dyn}$, resulted from ETABS. However the higher mode factor was taken $M_v=1.00$ because Sa(0.2)/Sa(2.0) < 8 for Vancouver.

Table 4.10 Base shear computed for the 3V building based on the ESF procedure

3V	T_{emp}, (s)		$T_{1,dyn}$, (s)		W, (kN)	V, (kN)	
	E-W	N-S	E-W	N-S	E-W&N-S	E-W	N-S
NBCC 1980	0.136	0.192	N/A	N/A	20675	1654	1654
NBCC 2010	0.293	0.293	0.540	0.570	20729	6243	6243

Table 4.11 Base shear computed for the 6V building based on the ESF procedure

6V	T_{emp}, (s)		$T_{1,dyn}$, (s)		W, (kN)	V, (kN)	
	N-S	E-W	N-S	N-S	E-W&N-S	E-W	N-S
NBCC 1980	0.261	0.370	N/A	N/A	41624	3256	2738
NBCC 2010	0.563	0.563	0.98	0.99	41678	7645	7645

For comparison purposes, the load factor for the resulted base shear was taken as 1.00 for both 1980 and 2010 designs. Thus, the base shear distribution along the 3-storey CBF height is given in the N-S and E-W direction in **Table 4.12**. The base shear was computed using the ESF procedure according to NBCC 1980 and NBCC 2010. Similar calculations were conducted for the 6V building and results are given in **Table 4.13**. In addition, the base shear demand-to-capacity ratios for both 3- and 6-storey buildings are given in, **Figure 4.12**. Similar with the 3Q and 6Q buildings, the current base shear demand was selected as $max(0.8V_{f,10};V_{dyn})$ where V_{dyn} was the shear resulted from the linear dynamic analysis. It is noted that the P-Δ effects according to NBCC 2010 were

ignored for both directions because the stability factor θ_x calculated according to **Eq. (4.3)** was less than *0.10*. Moreover, based on the analysis conducted in ETABS the building was not found to be torsional sensitive.

Table 4.12 Base shear distribution along the CBF height of 3V building according to NBCC'80 and NBCC'10

St.	NBCC 1980		NBCC 2010					
	*V_{80}=ASKIFW, (kN)		**$V_{f,10}=S(T_a)M_vI_EW/R_dR_0$, (kN)		$0.8V_{f,10}$, (kN)		V_{dyn}, (kN)	
	E-W	N-S	E-W	N-S	E-W	N-S	E-W	N-S
3	193	389	780	1734	624	1387	783	1719
2	353	726	1359	3020	1087	2416	1312	2855
1	460	960	1685	3746	1348	2997	1666	3564

* torsion and P-Δ included; ** torsion included and P-Δ neglected because $\theta < 0.1$

Table 4.13 Base shear distribution along the CBF height of 6V building according to NBCC'80 and NBCC'10

St.	NBCC 1980		NBCC 2010					
	*V_{80}=ASKIFW, (kN)		**$V_{f,10}=S(T_a)M_vI_EW/R_dR_0$, (kN)		$0.8V_{f,10}$, (kN)		V_{dyn}, (kN)	
	E-W	N-S	E-W	N-S	E-W	N-S	E-W	N-S
6	226	369	667	1489	533	1191	749	1546
5	445	742	1116	2493	893	1994	1136	2452
4	634	1105	1482	3309	1185	2647	1401	3092
3	788	1410	1761	3933	1409	3146	1630	3626
2	900	1625	1956	4367	1565	3493	1883	4151
1	959	1779	2065	4612	1652	3690	2084	4506

* torsion and P-Δ included; ** torsion included and P-Δ neglected because $\theta < 0.1$

As illustrated in **Figure 4.12** the ratio between the current (2010) and 1980 design base shear (unfactored) for the 3V building was *3.62* for the CBFs in E-W direction and *3.71* for the CBFs in N-S direction. On the other hand, for the 6V building the ratios were *2.17* and *2.53*, for the CBFs from E-W and N-S direction, respectively. Therefore the seismic demand has increased almost 4 times for the 3-storey building while for the 6-storey building the seismic demand doubled.

Comparing the base shear ratios illustrated in **Figure 4.12** with the values for 3Q and 6Q buildings (**Figure 4.1** and **Figure 4.7**) it can clearly be seen that the seismic demand is almost double for Vancouver. It is noted that according to NBCC 1980 both locations were in the same seismic zone, thus having the same demand at that time. It can be concluded that the demand is much higher for the low rise buildings in Vancouver, especially for the N-S direction.

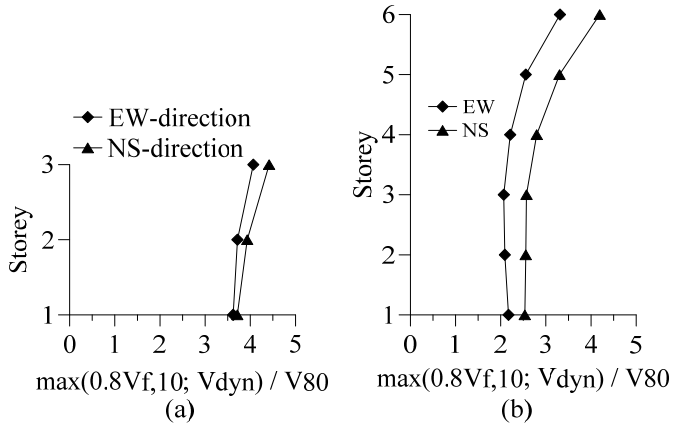

Figure 4.12 Storey shear demand-to-capacity ratio: (a) 3V; (b) 6V

4.3.2. Seismic assessment of CBF's components of 3V building

4.3.2.1. Assessment of CBF members

The seismic assessment procedure of CBF members of 3V building is similar with the assessment done for the 3Q building. Thus, forces triggered in braces, beams and columns versus member capacity were analysed in terms of demand-to-capacity-ratios based on the new values obtained according to the current design provisions (NBCC 2010 and S16.1-09). The demand-to-capacity ratios for braces are illustrated in **Figure 4.13(a)** and **Figure 4.13(b)** for braces of CBFs located in the E-W and N-S direction. As depicted, none of the bracing members possess the sufficient strength to pass the current code design requirement, whereas the factored axial force in braces exceeds the probable buckling capacity of braces (C_u) with almost 20% for all storeys. Seismic assessment of CBF beams is illustrated in **Figure 4.13(c)** and **Figure 4.13(d)** for CBFs located in the E-W and N-S direction, respectively. As resulted, beams do not have sufficient capacity to withstand the required limit states, while the larger demand resulted for the *OMS* verification.

The demand-to-capacity ratios for CBF columns are presented in **Figure 4.13(e)** and **Figure 4.13(f)** for the E-W and N-S direction, respectively. As depicted, CBF columns in E-W direction are prone to instability due to lateral torsional buckling. It is noted that for the E-W direction and all considered limit states, the total axial force in columns C_f resulted from the projection of the

probable brace resistances (C_u, T_u) combined with the axial forces from the associated gravity component.

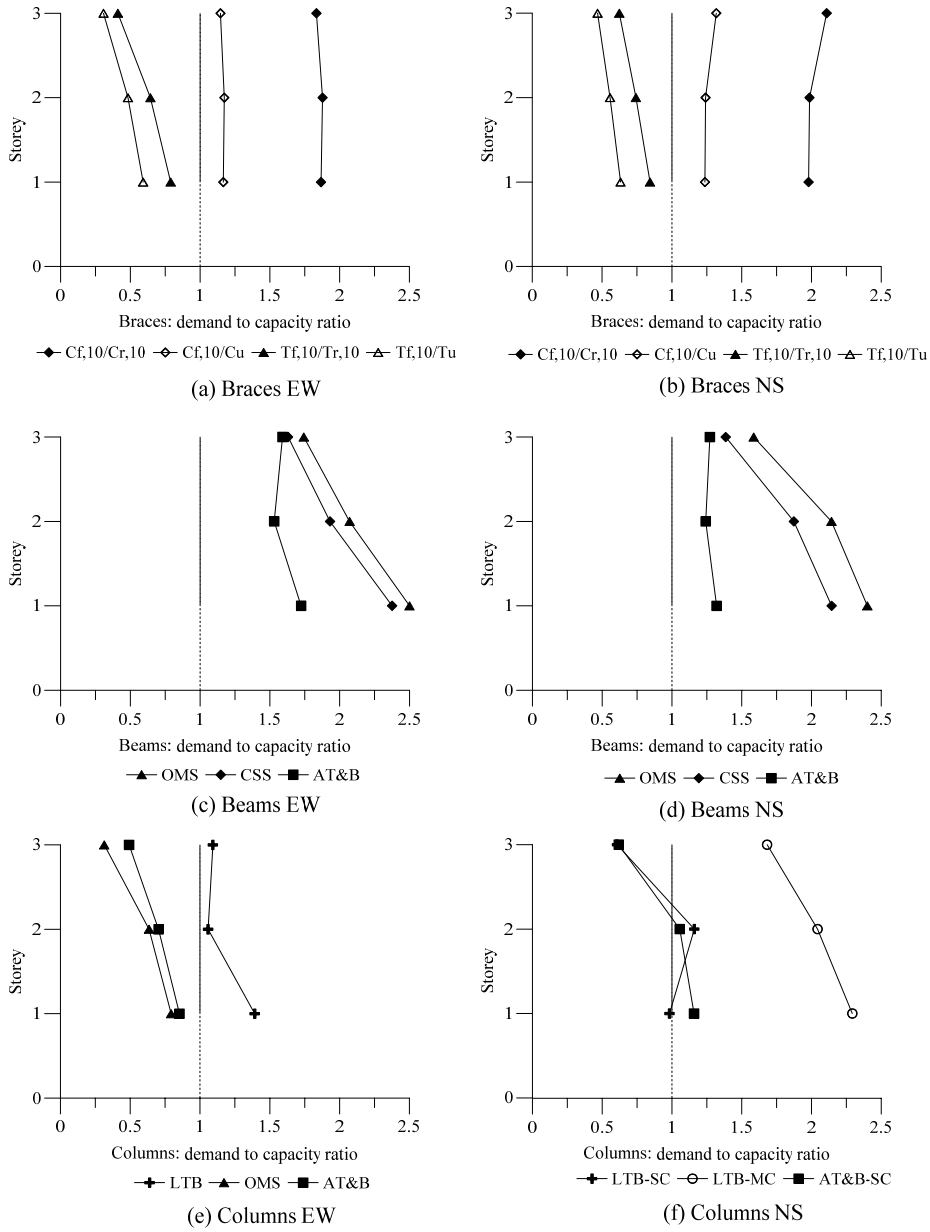

Figure 4.13 Seismic assessment of CBF members of 3V building: (a) braces E-W; (b) braces NS; (c) beams E-W; (d) beams N-S; (e) columns E-W; (f) columns N-S.

Conversely, for the N-S direction, the side columns were prone to damage due to AT&B at the ground floor level, while at the 2nd floor the lateral torsional buckling verification governs. Additionally, the middle column was the most vulnerable having the demand-to-capacity ratio *>1.0* at all floors. Important to note that for the N-S direction the total axial force triggered in the side columns resulted from the projection of the probable brace resistances (C_u, T_u) combined with

the associated axial force from gravity component. In this case, the *LTB* verification was not satisfied at the 2nd floor. For *AT&B* verification, the total axial force resulted from the consideration of $R_dR_0=1.3$ combined with the forces from the gravity component. The demand was larger at the ground floor and slightly larger at the 2nd floor. However, the largest demand was encountered by the middle column where the demand-to-capacity ratio was larger than 2 at the ground floor and 2nd floor in the case of *LTB* limit state verification.

4.3.2.2. Brace-to- frame connections assessment

It is noted that the brace-to-frame connections for the 3-storey building located in Vancouver were selected to be the same with those of the 3Q building. For this reason, the assessment procedure described in *Section 4.2.2.2* and *Section 4.2.3.2* was applied for the connections assessment of the 3V building and the results are given in **Table 4.3** and **Table 4.4** for both E-W and N-S directions, respectively.

4.3.3. Seismic assessment of CBF's components of the 6V building

4.3.3.1. Assessment of CBF members

Seismic assessment procedure of the CBF structural members of the 6V building was similar with the assessment done for the 6Q building and the demand-to-capacity ratios for braces, beams, and columns for both E-W and N-S directions are illustrated in **Figure 4.14.** As illustrated in the figure none of the bracing members possess the sufficient strength to pass the current code design based on $C_{f,10}/C_{r,10}$ ratio. However, if the calculation of brace capacity is based on the probable compressive resistance (C_u) the demand to capacity ratio is significantly reduced.

It is noted that for the E-W direction the critical case for CBF beams was obtained when the braces attain their probable post-buckling compression resistance and no vertical support was provided. However, all beams of E-W and N-S CBFs do not have sufficient capacity to withstand the required limit states, while the larger demand resulted for the *OMS* verification.

The factored axial force (C_f) demanded in the upper floor columns (3rd to 6th) resulted from the projection of the probable brace resistances (C_u, T_u) combined with the associated gravity force component. This case governed for the *LTB* and *OMS* limit state verifications. Conversely, for the bottom two columns, the demanded axial force in columns resulted from the distributed seismic

forces computed with $R_d R_0 = 1.3$, in addition to the associated gravity force component. The latter was found to be governing for the *AT&B* verification for all storeys.

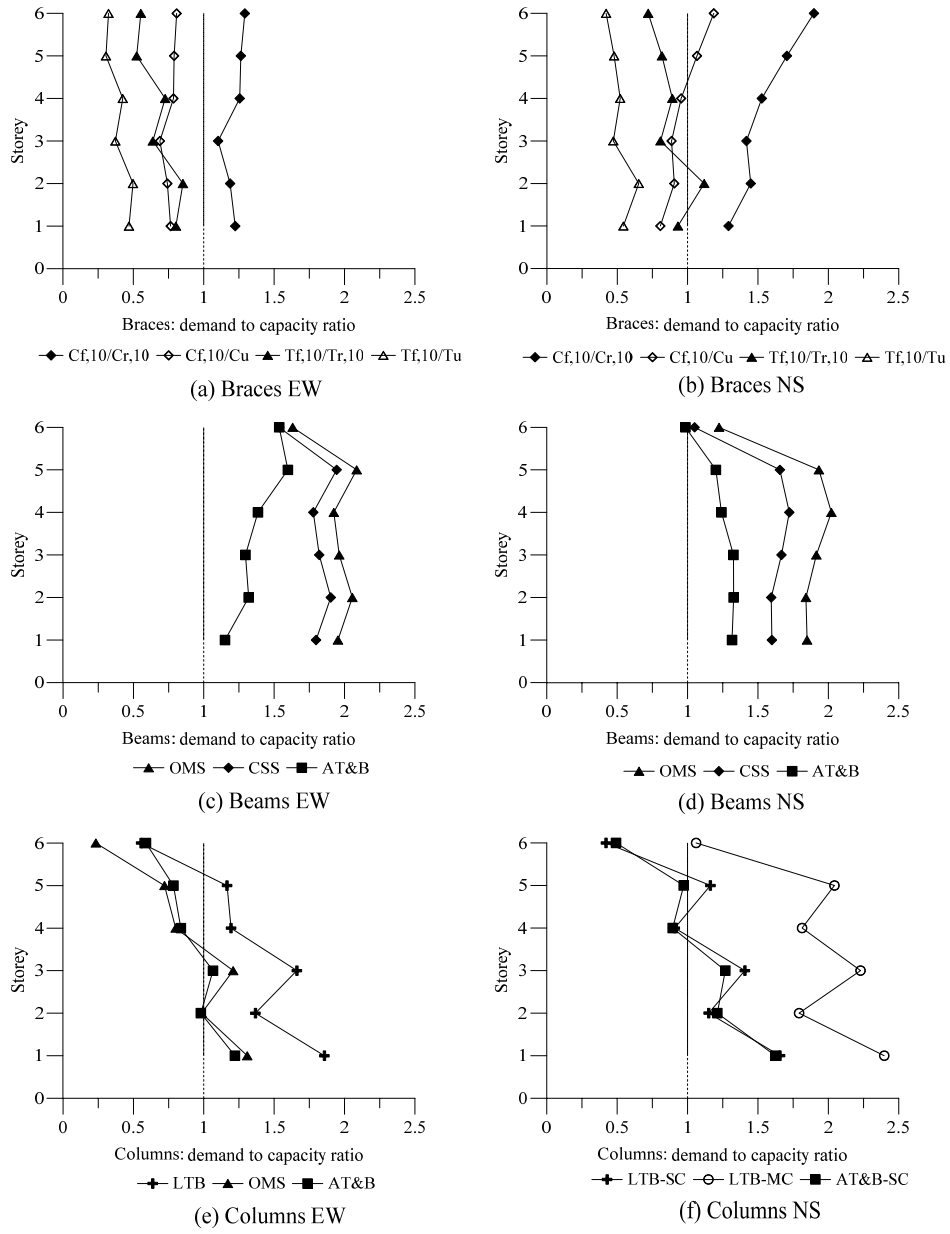

Figure 4.14 Seismic assessment of CBF members of 6V building: (a) braces E-W; (b) braces N-S; (c) beams E-W; (d) beams N-S; (e) columns E-W; (f) columns N-S.

As depicted from the above figure, the CBF columns in the E-W direction are prone to instability (except the 6th floor column) due to lateral torsional buckling. In the case of CBF columns located in the N-S direction, the demanded axial force in the side columns resulted from the projection of the probable brace resistance combined with the associated axial force from gravity component and the demand-to-capacity ratio corresponding to *LTB* limit state verification is larger than *1.0* at

the ground floor, 2nd, 3rd and 5th floors. For the AT&B verification the demanded axial force was given by the seismic forces considering $R_dR_0=1.3$ combined with associated forces from the gravity loads component. The middle column of CBF in N-S direction was the most vulnerable having the demand-to-capacity ratio >1.5 at all floors except at top floor, where *LTB* limit state governed.

4.3.3.2. Brace-to-frame connection assessment

It is noted that HSS brace-to-frame connections of the 6-storey CBF building located in Vancouver were selected to be the same with those of the 6Q building. For this reason, the assessment procedure described in *Section 4.2.5.2* and *Section 4.2.6.2* applies for the connections assessment of the 6V building and the results are given in **Table 4.7** and **Table 4.8** for both E-W and N-S directions, respectively**.**

4.4. Seismic assessment based on Nonlinear Time-History Analysis

In the previous section, the studied buildings were assessed based on the ESF procedure and some deficiencies were identified at the level of structural members in terms of demand-to-capacity ratios. However, to better assess the seismic performance, as well as the failure hierarchy of the structural members of the studied buildings, a comprehensive nonlinear dynamic analysis was carried out. For this reason, a detailed numerical model was developed and subjected to nonlinear time-history analysis using the OpenSees framework (Mazzoni et al.). Furthermore, to assess the collapse margin ratio, the incremental dynamic analysis (IDA) was employed. Because of the large volume of computations only the 3- and 6-storey building located in Quebec City were further analysed and the 3- and 6-storey buildings located in Vancouver were considered for comparison purposes. Hence, the Opensees modelling, together with the ground motion selection and the results from the IDA are presented hereafter.

4.4.1. Modelling of the CBF office buildings in OpenSees

Tensile yielding, buckling and post-buckling behavior of CBF braces are highly nonlinear. For this reason, a numerical 2D line-element model with the option for braces to deform out-of-plane, was developed. Due to the building symmetry, the structural system in the E-W direction was constructed for one quarter of the building footprint area and in the N-S direction for half, as shown in **Figure 4.15(a)**. Simplified discrete component models including linear and nonlinear beam-column elements and concentrated springs were used to simulate the behaviour of the system

illustrated in **Figure 4.15(b)** and **Figure 4.15(c)** for the E-W and N-S direction, respectively. As illustrated, the *P-Δ* effect on the CBF system was taken into account by employing leaning columns (gravity columns) which were connected at each floor by truss elements with large stiffness (link beams).

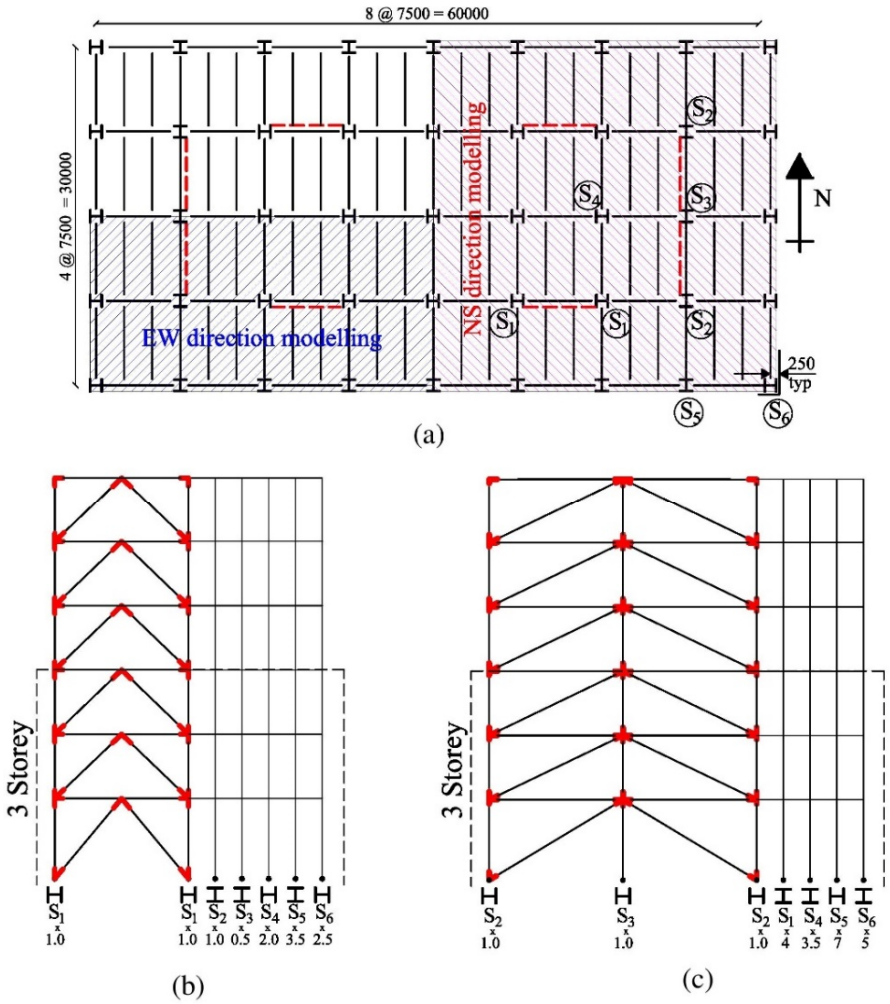

Figure 4.15 OpenSees model of the 3- and 6-storey CBF: (a) modelling assumptions; (b) E-W model; (c) N-S model

It is noted that columns of the 6-storey building, as well as, the leaning columns were assumed continuous over two storeys, while those of the 3-storey were considered pinned at each floor. The leaning columns, link beams and all rigid link segments incorporated in the model were modeled with elastic beam-column elements while the brace connections and beam-column connections were modeled by springs assigned in the Zero-Length elements. In addition, the seismic mass was applied at each floor on every column of the braced frame and the associated lumped gravity load was applied to each column (including the leaning columns) and to the beams of CBFs.

4.4.1.1. Modelling of braces, beams and columns

Braces, beams and columns were modelled as non-linear forced-based beam-column elements with distributed plasticity, having three integration points per element and fiber cross-section formulations. The constitutive law used for all members was Giuffre-Menegotto-Pinto model (Steel02) which captures very well the Bauschinger effect and the residual stresses (Lamarche and Tremblay, 2008). Furthermore, the Steel02 material parameters were those given in Aguero et al. (2006). In addition, the effect of rigid end zones was also considered for the beam-column and beam-column-brace connections. Hence, the considered rigid links were simulated using elastic beam-column elements with extremely large stiffness. Moreover, to simulate brace fracture, fatigue material was assigned to parental material of HSS braces (Steel02) and each brace member was discretized into 16 elements along the brace length. The value of strain at which one cycle will cause failure (ε_o) and the slope of Coffin-Manson curve in log-log space (m) are required as input parameters in the definition of fatigue material in OpenSees. In this study, the parameters used to define the fatigue material were calculated using **Eq. (4.9)**, according to Tirca and Chen (2014), which proposed the equation for a wide range of slenderness ratios of square HSS brace cross-sections, $50< KL/r <150$. The ductility coefficient $m= -0.5$ was considered constant for all braces. Additionally, an initial out-of-straightness having the shape of a sine function with the apex equal to 1/500 of the length of the brace was used to efficiently simulate the brace buckling behaviour. The brace out-of-straightness was assigned out-of-plane.

$$\varepsilon_o = 0.006\left(\frac{KL}{r}\right)^{-0.859}\left(\frac{b_0}{t}\right)^{-0.6}\left(\frac{E}{F_y}\right)^{0.1} \tag{4.9}$$

In the above equation, $b_0=b-4t$, where b is the effective width of the HSS tube and t represents the thickness.

On the other hand, four elements having three integration points and no out-of-plane imperfection was used for the W-shape beam members, while the W-shape column member was discretized into 8 elements having the initial out of plane imperfection equal to 1/1000 of the length of the column.

To simulate the nonlinear behaviour of the CBF members, the HSS brace cross-section was divided into four quadrilateral and four circular (for the rounded corners) patches, each quadrilateral patch was discretized using 5 fibers along the thickness and 8 across, while for the circular patches a total of 20 fibers / patch (4 circumferential direction by 5 radial direction) were used as illustrated

in **Figure 4.16(a)**. In total, 240 fibers were used for HSS braces. For both beams and columns, the W-shape cross- section was discretized using 5 fibers along the thickness and 8 fibers along the length within each flange and web (two quadrilateral patches for the flanges and one for the web) as shown in **Figure 4.16(b)**. As a result, a total number of 120 fibers were considered through the beam and column cross sections.

The beam-column connections were modelled as shear-tab connections and were simulated as zero-length nonlinear spring elements having the capacity to transfer up to 20% of the beam plastic bending moment to the rigid link (Liu and Astaneh-Asl, 2004).

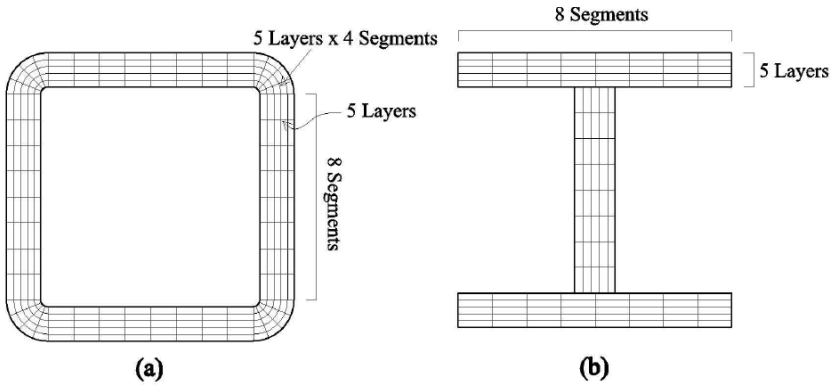

Figure 4.16 Fiber cross-section discretization: (a) HSS cross-section; (b) W-shape cross-section

4.4.1.2. Gusset plate connections

Several studies have shown (Hsiao, 2014) that the gusset plate connections have a significant effect on the stiffness, resistance and inelastic deformation capacity of the CBF braces. For this reason, an accurate simulation of these connections is required. Thus, a zero-length element was used to simulate the behaviour of the gusset plate. The zero-length element connects the brace to the rigid link. To simulate the out-of-plane deformational stiffness of the connection at the brace end a nonlinear spring element using Steel02 material model having one torsional (direction 4) and one rotational spring (direction 5) was used. The stiffness of the rotational spring was based upon the geometry and properties of the gusset plate as shown in **Figure 4.17** (Hsiao, 2012), while the torsional spring stiffness is given by: $K_{torsion}=GJ/L_{ave}$; where G is the shear modulus taken as *77000 MPa,* L_{ave} is the average value between the L_1, L_2, L_3 lengths given bellow, and J is the torsion constant. The post-yield stiffness of the rotational spring was considered as *1%* of the initial rotational stiffness. As illustrated in **Figure 4.17**, three rigid end zones were used, hence the gusset plate has a minimal in plane deformation relative to other deformation modes of the frame. In

addition, the rigid links were simulated using elastic beam-column elements with very large stiffness.

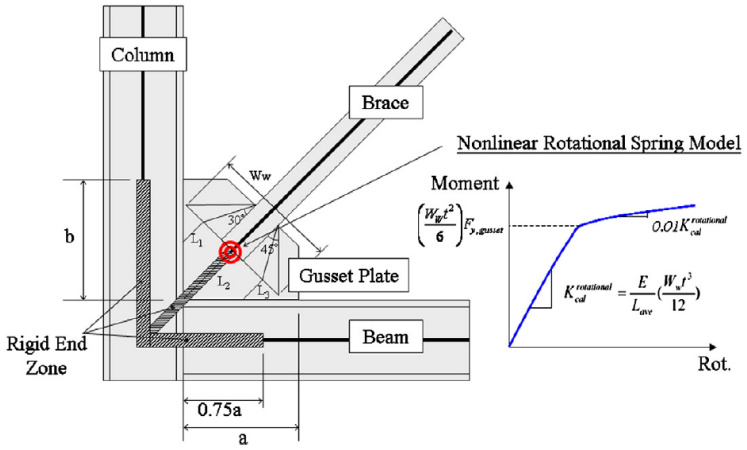

Figure 4.17 Brace to frame connection model (Hsiao et al., 2012)

To capture the failure of the gusset plate, in the same zero-length element which defines the gusset plate connection on the axial direction (direction 1), a MinMax material was defined. This material returns zero values for the tangent stress (decouples the brace) if the strain or the deformation ever falls below or above certain threshold values. The minimum and the maximum threshold values for the strain/deformation were calculated based on the gusset plate capacity and the axial stiffness of the gusset plate. As described in the previous *Sections*, shearing of welds was the controlling failure mode of brace-to-frame connections designed according to 1980s. When this occurs, the gusset plate will be decoupled due to the addition of MinMax material.

4.4.2. Earthquake selection and scaling

For Eastern Canada, the contribution to seismic hazard are moderate crustal earthquakes of magnitudes M6 - M7 which are compatible with the NBCC 2010 uniform hazard spectrum (*UHS*) developed for 2% probability of exceedance in 50 years (Atkinson, 2009). On the other hand, the seismic events registered in Eastern Canada occur at depths varying from surface to 30 km (shallow earthquakes) and are concentrated in specific clusters as described in *Section 2.1.1*. The set of 10 records comprises three historical records from the 1988 Saguenay earthquake and seven artificial accelerograms compatible with the design spectrum of Quebec City developed by Atkinson (2009). These artificial accelerograms can be accessed at www.seismotoolbox.com. The characteristics of the selected ground motions including the magnitude M_w, epicentral distance R, peak ground velocity and acceleration *PHV* and *PHA,* respectively together with the Trifunac

duration t_D and the predominant and average period of ground motion T_p and T_m are given in **Table 4.14.**

Table 4.14 Ground motion characteristics

Event	Mw	Station	R	Comp	PHV	PHA	PHV/PHA	tD	Tp	Tm
			km	*[◦]*	*cm/s*	*cm/s²*	*s*	*s*	*s*	*s*
M6C1-10.7	6.0	simulated	10.7	-	18.93	547.0	0.035	2.39	0.06	0.20
M6C1-12.8	6.0	simulated	12.8	-	30.58	753.0	0.041	1.29	0.12	0.19
M6C1-16.6	6.0	simulated	16.6	-	17.43	429.0	0.041	1.95	0.12	0.23
M7C1-20.1	7.0	simulated	20.1	-	22.39	467.0	0.048	6.81	0.12	0.26
M7C1-25.2	7.0	simulated	25.2	-	18.65	379.0	0.049	7.32	0.06	0.24
M7C1-25.8	7.0	simulated	25.8	-	17.56	288.0	0.061	7.31	0.08	0.28
M7C2-41.6	7.0	simulated	41.6	-	14.49	224.0	0.065	7.61	0.14	0.31
Saguenay(S8.EN1)	5.8	La Malbaie		63	4.37	126.8	0.034	10.5	0.12	0.19
Saguenay(S9.EN1)	5.8	St-Pascal		0	2.61	45.7	0.057	21.5	0.14	0.23
Saguenay(S10.EN2)	5.8	Riviere-Ouelle		270	3.833	56.29	0.068	12.52	0.14	0.27

It is noted that there are no specific provisions in NBCC 2010 regarding scaling of ground motions. However, it is mentioned that all selected ground motions should be scaled to match the uniform hazard spectrum (UHS) at the fundamental period of the structure and to fit or be above the UHS at all points corresponding to the period of higher modes. On the other hand, ASCE/SEI-7 provisions requires that the mean of the 5% damped response spectra of a minimum of seven ground motions to match or be above the *UHS* in any point over the interval $0.2T_1 – 1.5T_1$. Herein, the scaling methodology proposed by Reyes and Kalkan (2011) which consist in minimizing the discrepancy between the scaled acceleration response spectrum of each record and the UHS, over the $0.2T_1 – 1.5$T1 period range, was employed. The response spectra of the scaled records together with the mean and design spectrum of Quebec City corresponding to 2%, 10% and 50% probability of exceedance in 50 years are plotted in **Figure 4.18**.

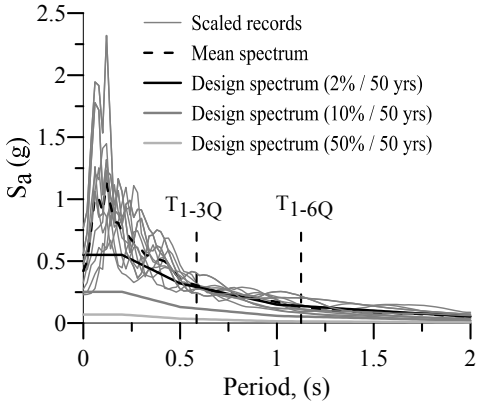

Figure 4.18 Response spectrum of scaled ground motions (Quebec City)

Note that design spectra for the probability of exceedance *10%/50 years* and *50%/50 years* were derived based on the spectral accelerations obtained using the attenuation relations from NBCC 2010 and the values are given in **Table 4.15** for Quebec City as well as for Vancouver, for comparison purposes.

Table 4.15 Spectral acceleration values for 10%/50 years and 50%/50 years probability of exceedance for Quebec City and Vancouver

Location	10% in 50 years, *(g)*				50% in 50 years, *(g)*			
	$S_a(0.2)$	$S_a(0.5)$	$S_a(1.0)$	$S_a(2.0)$	$S_a(0.2)$	$S_a(0.5)$	$S_a(1.0)$	$S_a(2.0)$
Quebec City	0.252	0.130	0.058	0.019	0.069	0.036	0.015	0.006
Vancouver	0.491	0.333	0.172	0.087	0.19	0.130	0.065	0.033

4.4.3. Incremental Dynamic Analysis for buildings located in Quebec City

The 3- and 6- storey buildings located in Quebec City were subjected to Incremental Dynamic Analysis (IDA) using OpenSees. Thus, each analysis was repeated by applying successively a stepwise incremental scaling factor (0.05g) to the selected ground motion records until failure was observed. The IDA method is suitable for identifying the boundary parameters that define the performance levels such as: *Immediate Occupancy* (*IO*), *Life-Safety* (*LS*), *Collapse prevention* (*CP*) and *Global Instability*. As documented in Chapter 2 (*Section 2.5.2*), the structural response was transposed into an incremental dynamic curve, referred herein as IDA curve; which represents a graph with the abscissa consisting of an engineering demand measure parameter (EDM) and the ordinate axis consisting of a given intensity measure parameter (IM). For this study, the selected EDM and IM were the maximum interstorey drift over the building height, δ_{max} and the $S_a(T_1,5\%)$,

respectively, where T_1 represents the first mode period resulted from rigorous eigen value analysis in OpenSees. **Table 4.16** presents a comparison between the first mode period from OpenSees ($T_{1dyn\text{-}OS}$), the $2T_{emp}$ according to **Eq. (2.14)** and modal response spectrum ($T_{1,dyn}$) from ETABS. Note that, the spectral acceleration values corresponding to each period are also given in the table. As expected, the first mode period resulted from OpenSees and ETABS are very close.

Table 4.16 Comparisons of the first mode vibration period of the studied buildings

ID	OpenSees				ESF				ETABS			
	$T_{1,dyn\text{-}OS}$, (s)		$S_a(T_{1,dynOS})$,(g)		$2T_{emp}$, (s)		$S_a(2T_{emp})$,(g)		$T_{1,Etabs}$, (g)		$S_a(T_{1,Etabs})$, (g)	
	E-W	N-S	E-W	N-S	E-W	N-S	E-W	N-S	E-W	N-S	E-W	N-S
3Q	0.554	0.630	0.302	0.256	0.585	0.585	0.304	0.304	0.559	0.593	0.316	0.300
6Q	0.930	1.135	0.177	0.137	1.125	1.125	0.130	0.130	1.00	1.02	0.167	0.161

4.4.3.1. IDA results for 3-st CBF building

The IDA curves for the 3-storey building located in Quebec City are given in **Figure 4.19** for both E-W and N-S direction. In addition, the variation between IDA curves reflects the ground motion signature. As depicted, the 3Q building cannot pass the current demand (2% in 50 years hazard level), yet for 10% and 50% in 50 years hazard level, the response of the building is in the elastic range except for two ground motions in the N-S direction. On the other hand, for the 50% in 50 years hazard level, the response is in the elastic range as expected. It is noted that 50% in 50 years was an equivalent seismic demand as required by the 1980 code. Compared to the response in the E-W direction, the capacity of the CBFs located in N-S direction was lower because the demand-to-capacity ratios were larger for members of CBFs in the N-S direction. As shown in the figure bellow, the first point of nonlinearity corresponds to the first brace buckling or first brace-to-frame connection failure, whichever occurs first.

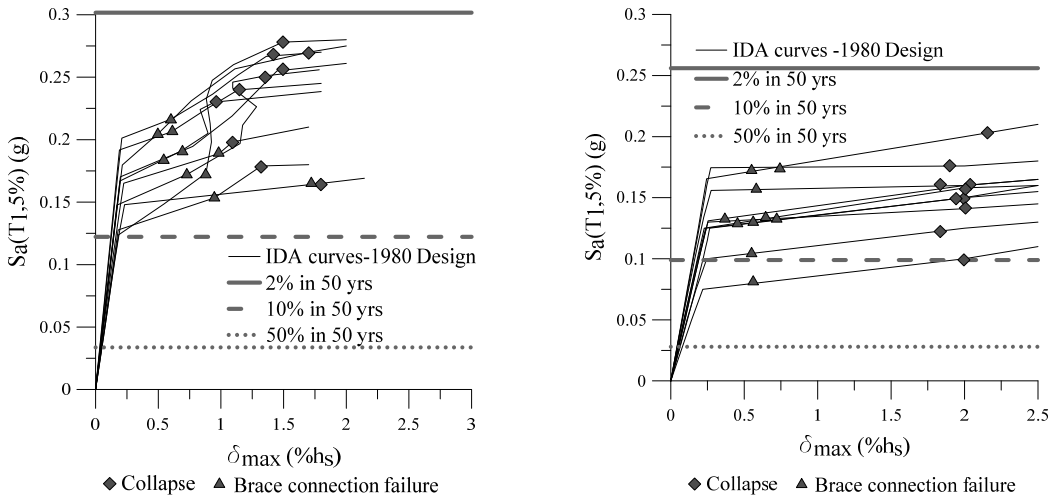

Figure 4.19 IDA curves for the 3Q building: (a) E-W direction; (b) N-S direction

In general, for the E-W direction, the 3rd floor brace reached buckling, triggering the connection at the ground floor to fail. This scenario was observed under the Saguenay S8.EN1 ground motion and is illustrated in **Figure 4.20(a)**. Once the gusset plate connection fails due to shearing of welds (brittle failure), the ground floor braces cannot dissipate any energy making the CBF to lose stiffness (very flexible) and to experience large interstorey drifts. On the other hand, the 3-storey CBF in the N-S direction experienced the first brace buckling at the 3rd floor (left brace) and start triggering the bottom connection of the right brace (side column) to fail in tension due to shearing of the welds (**Figure 4.20(b)** as discussed in *Section 4.2.3.2* of this thesis. Thus, damage is concentrated at the critical floor leading to the storey mechanism formation causing total or partial building failure. According to the results of the nonlinear time history analysis, damage concentration was observed at the ground floor for the 3Q building.

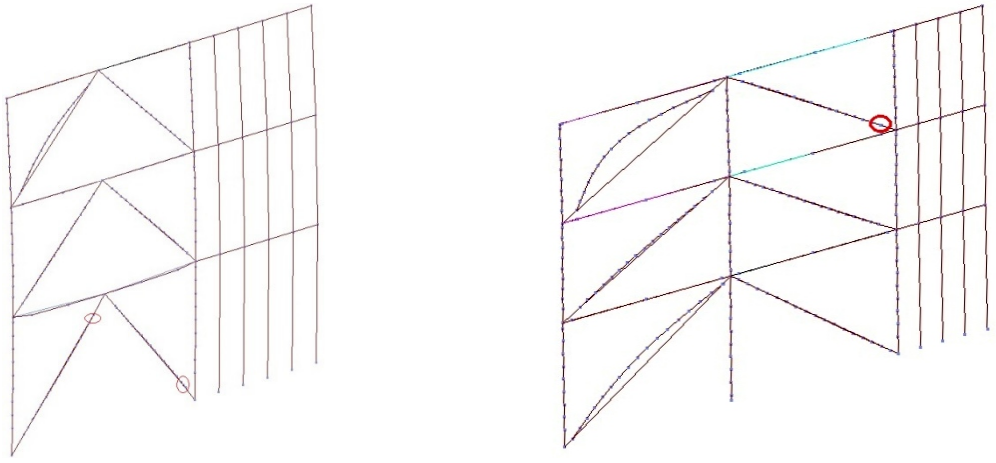

(a) (b)

Figure 4.20 First brace-to-frame connection failure under S8.EN1 ground motion (SF=2.0) for the 3Q building: (a) E-W direction; (b) N-S direction.

However, it is impossible to predict precisely when or how the building will collapse, therefore the collapse assessment is made using a combination of structural analysis and engineering judgement. It is suggested that the non-convergence of the time-integration scheme is the safest numerical equivalent of the actual dynamic collapse, but this in turn can suffer from the quality of the numerical code, stepping or even round-off error of the integration process. However, in FEMA 350 (2000) it was proposed a 20% tangent slope approach, in which the last point on the curve with a tangent slope equal to 20% of the elastic slope is defined as the capacity point. Herein, the flattening of the curve is an indicator of dynamic instability. For this study, the collapse points were verified based on the interaction equation of the axial compression and bending moment, according to CSA/S16-09 standard. In other words, the columns do not possess sufficient axial compression and bending capacity, leading to dynamic instability due to P-Δ effects at large interstorey drifts. This behaviour was observed in the Opensees model. As shown in IDA curves, the onset of dynamic instability (collapse) is strongly correlated with the 20% of the initial (elastic) slope approach-where a relatively small increase in the *IM* produces a large increment in the buildings response.

4.4.3.2. IDA results for 6-st CBF building

The IDA curves for the 6Q building are presented in **Figure 4.21**. As depicted, the building cannot pass the current demand (2% in 50 years hazard level), however for 10% and 50 % in 50 years hazard level, the response of the building is in the elastic range. In general, for the E-W direction of the 6-storey building, the left brace at the 6th floor reached buckling and triggered the connection at the 5th floor to fail, leading to the storey mechanism formation causing partial building failure. The scenario depicted in **Figure 4.22** resulted under the effect of Saguenay ground motion S8.EN1. According to the results obtained from nonlinear time history analyses, damage concentration was observed at the 5th and 6th floor for the 6Q building when the E-W was the loading direction. On the other hand, for the N-S direction, the first connection failure was recorded at the second floor, causing damage concentration and storey mechanism formation (**Figure 4.22(b)**). As the earthquake demand was incremented (increasing the scaling factor), the second connection failed at the 6th floor causing non-convergence of the time-integration scheme resulting large interstorey drifts at all floors, thus causing the dynamic instability of the building (collapse).

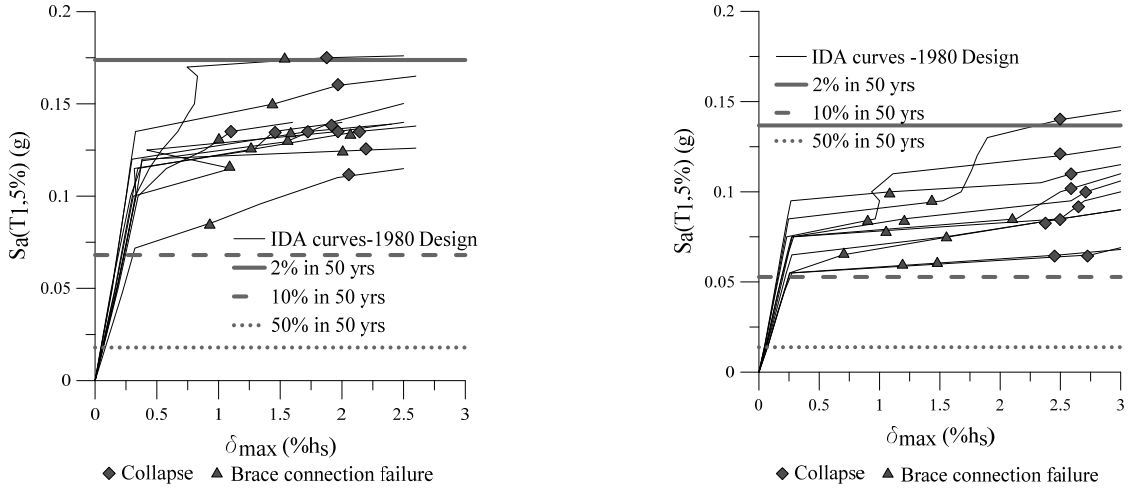

Figure 4.21 IDA curves for the 6Q building: (a) E-W direction; (b) N-S direction

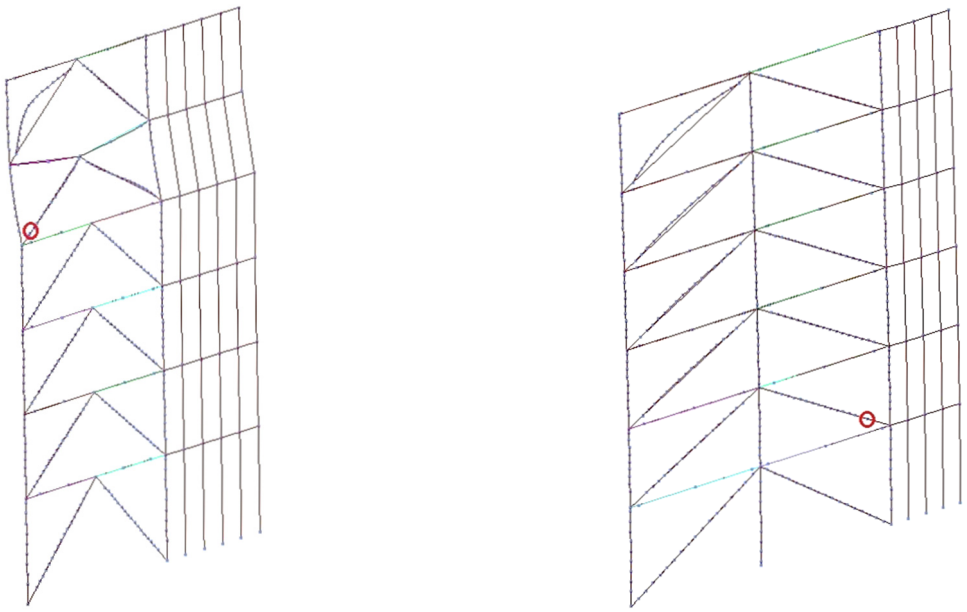

(a) SF=3.8 (b) SF= 2.5

Figure 4.22 First brace-to-frame connection failure under S8.EN1 ground motion for the 6Q building: (a) E-W direction; (b) N-S direction

4.4.3.3. Collapse Margin Ratio for the buildings located in Quebec City

One primary parameter to characterize the collapse safety of a structure is the Collapse Margin Ratio (CMR). According to FEMA P695, the median collapse was defined as the ground motion intensity in which half of the records in the selected set cause collapse of the structure. Thus, the ratio between the median collapse capacity, $\hat{S}_{CT}$ and maximum design ground motion intensity S_{MT}, was defined as the CMR. It is noted that the maximum design ground motion intensity was obtained from the response spectrum of the design level ground motions (2% in 50 years), at the fundamental period $T_{1,dyn\text{-}OS}$, given in **Table 4.16**. On the other hand, the median collapse capacity of the ten ground motions, $\hat{S}_{CT,}$ and the CMR are given in **Table 4.17** for both 3- and 6-storey buildings located in Quebec City.

Table 4.17 Collapse Margin Ratio for the buildings located in Quebec City

ID	E-W direction		N-S direction	
	$\hat{S}_{CT}$, (g)	**CMR**	$\hat{S}_{CT}$, (g)	**CMR**
3Q	0.236	**0.78**	0.152	**0.59**
6Q	0.137	**0.79**	0.098	**0.71**

As illustrated in the table all the CMR ratios are less than *1.0*, that means both 3- and 6-storey buildings do not possess sufficient strength to pass the current code demand (2% in 50 years hazard level), especially for the N-S direction of the 3Q building. Therefore retrofit action is required.

4.5. Conclusions

In this Chapter, the existing low- and middle-rise CBF office buildings designed using NBCC 1980 and CSA/S16.1-M78 standard were evaluated in order to identify possible seismic deficiencies. The collapse safety of the studied buildings was evaluated for each performance group in terms of demand-to-capacity ratios. Specifically, the assessment process was done based on the ESF procedure and nonlinear time-history analysis by means of IDA. According to the results from the ESF procedure, both the 3- and the 6- storey buildings located in Quebec City and Vancouver- show deficiencies at the level of structural members, especially the buildings located in Vancouver. Moreover, all brace-to-frame connections have insufficient strength and show failure due to shearing of the welds. In addition, the IDA analysis was performed only for Quebec City buildings using OpenSees. As reported from IDA curves, all studied buildings experienced collapse when subjected to ground motion intensities in agreement with the current code demand. However under 50% in 50 years hazard level, which was the seismic demand according to NBCC 1980, all buildings showed adequate strength having the response in the elastic range. Nevertheless, the collapse safety of the structure is described by the collapse margin ratio (CMR) computed as the ratio between the ground motion intensity at which the median collapse capacity is reached and the acceleration spectrum intensity corresponding to the fundamental period of the building. Based on the results from IDA, both low- and middle-rise office buildings located in Quebec City have a collapse safety bellow *1.0*, especially for the N-S direction of the 3Q building. It is noted that the results from the ESF procedure are consistent with the results from nonlinear time-history analysis.

CHAPTER 5. IMPROVING THE SEISMIC RESILIENCE OF EXISTING CBF BUILDINGS USING A CONVENTIONAL RETROFIT STRATEGY

5.1. Introduction

This Chapter presents the selection of retrofit strategy for the studied low- and middle-rise office buildings located in Quebec City that were designed according to NBCC 1980. Herein, the seismic resilience of the retrofitted buildings was computed based on nonlinear time-history analysis by means of IDA and fragility curves.

5.2. Selection of retrofit scheme for buildings located in Quebec City

As previously stated in *Section 2.5.4*, the Rehabilitation Objective Class needs to be selected according to ASCE 41-13 standard. In this light, the Rehabilitation Objective Class for office buildings is *Basic Safety*. As illustrated in **Figure 2.9**, the targeted performance limits associated to the Basic Safety Objective (BSO) are *Life Safety* (*LS*) and *Collapse Prevention* (*CP*). In other words, buildings meeting the BSO are expected to respond to: i) *LS* performance level when subjected to frequent, moderate earthquakes (10% in 50 years probability of exceedance) and ii) *CP* performance level when subjected to more severe rare events (2% in 50 years probability of exceedance). Therefore, there are accepted little damage from frequent, moderate earthquakes for *LS* and significant damage but no collapse for *CP* level. To rehabilitate the studied buildings located in Quebec City, a conventional retrofit strategy was selected, which is specified in ASCE 41-13. It consists of strengthening or replacing the CBF components that are prone to damage and local strengthening of remaining components. Hence, local strengthening of CBF members consists in cover plating steel columns and beams. In the studied cases, the replacement of (HSS braces) gusset plate connections was required. Thus, all brace-to-frame connections were re-designed in order to carry the forces associated with the probable tensile/ compression resistance of HSS braces and were re-detailed to present the $2t_{gp}$ clearance, where t_{gp} is the thickness of the gusset plate. Having a sufficiently strong connection, the HSS braces can dissipate the earthquake induced energy through yielding and buckling.

5.2.1. Retrofit strategy for the 3-storey building located in Quebec City

5.2.1.1. Brace to frame connection retrofit

To re-design the brace-to-frame connections, the same verifications as those given in Chapter 4 were used. It is noted that a clearance of $2t_{gp}$ was considered in detailing the gusset plate in order

to allow the plastic hinge formation in the gusset upon out-of pane buckling of braces. The effective length of the gusset plate was taken as the average of L_1, L_2, L_3 illustrated in **Figure 4.4**. Further, the welding length L_w, was selected such that the shear resistance of welding and the tensile resistance of gusset plate to be larger than the probable tension resistance of attached brace. Additionally, it was verified that the failure mode of connection, if occurs, to be a ductile failure mode such as: yielding of gusset or block shear. **Table 5.1** and **Table 5.2** summarize the new gusset plate design for the braced frames in E-W and N-S direction respectively. As illustrated, the tables contain the selected welding length L_w; the weld leg width D_w; gusset plate geometry: height a, width b; thickness t_{gp}, and area A_{gp}, together with Whitmore effective width and the lengths L_1, L_2, L_3.

Table 5.1 Brace-to-frame connections design parameters of CBF in E-W direction (3Q building)

St	D_w	L_w	a	b	t_{gp}	W_w	A_{gp}	L_1	L_2	L_3
	mm	*mm*	*mm*	*mm*	*mm*	*mm*	mm^2	*mm*	*mm*	*mm*
3	8	330	371	439	12.7	483	6135	101	264	25.4
2	8	370	412	514	12.7	554	7039	144	301	25.4
1	8	440	732	506	19.05	660	12574	38.1	415	341

Table 5.2 Brace-to-frame connections design parameters of CBF in N-S direction (3Q building)

St	D_w	L_w	a	b	t_{gp}	W_w	A_{gp}	L_1	L_2	L_3
	mm	*mm*	*mm*	*mm*	*mm*	*mm*	mm^2	*mm*	*mm*	*mm*
3	8	440	629	1058	12.7	660	8388	823	701	25.4
2	10	480	697	1209	15.9	732	11621	955	778	31.8
1	8	685	888	885	19.05	994	18939	400	698	38.1

Further, the reserve capacity of the connections as well as the demand-to-capacity ratios for each verification case according to the current design is given in **Table 5.3** and **Table 5.4** for both E-W and N-S direction. A detailed design example of the brace-to-frame connection of 3-st CBF building located in Quebec City is given in **Appendix III.**

Table 5.3 Design verification of brace-to-frame connections of CBF in E-W direction, according to CSA/S16-09 (3Q building)

St.	Shear resistance of welding,(kN)			Metal base resistance,(kN)		Yielding of gusset plate,(kN)		Buckling of gusset plate,(kN)		Net Rupture and block shear of brace with shear lag,(kN)		
	V_r	C_u/V_r	T_u/V_r	$T_{r.mb}$	$T_u/T_{r.mb}$	T_{rgp}	T_u/T_{rgp}	C_{rgp}	C_u/C_{rgp}	T_{NR}	$T_{r\text{-}BS}$	$T_u/\min(T_{NR}, T_{r\text{-}BS})$
3	1642	0.33	0.92	2263	0.67	1656	0.91	1615	0.34	1333	2123	1.13
2	1841	0.47	0.90	2537	0.66	1900	0.88	1823	0.47	1393	1998	1.20
1	2190	0.55	0.93	4526	0.45	3395	0.60	3207	0.37	1667	2376	1.22

Table 5.4 Design verification of brace-to-frame connections of CBF in N-S direction, according to CSA/S16-09 (3Q building)

St.	Shear resistance of welding,(kN)			Metal base resistance,(kN)		Yielding of gusset plate,(kN)		Buckling of gusset plate,(kN)		Net Rupture and block shear of brace with shear lag,(kN)		
	V_r	C_u/V_r	T_u/V_r	$T_{r.mb}$	$T_u/T_{r.mb}$	T_{rgp}	T_u/T_{rgp}	C_{rgp}	C_u/C_{rgp}	T_{NR}	$T_{r\text{-}BS}$	$T_u/\min(T_{NR}, T_{r\text{-}BS})$
3	2190	0.33	0.93	3018	0.68	2265	0.90	1154	0.63	1661	2361	1.23
2	2986	0.43	0.95	4115	0.69	3138	0.91	1777	0.72	2713	3606	1.05
1	3409	0.49	0.96	7047	0.47	5114	0.64	4433	0.38	2655	4406	1.24

As illustrated in the above tables, after retrofitting the connections resulted that braces are prone to net rupture due to the reduction of the cross-sectional area at the gusset plate slot. Therefore, in order to strengthen the net section of the brace, a cover plate should be added at the location of slotted HSS segment. All cover plates were selected to be G40.21-300W steel grade, having F_y=*300 MPa.* The summary of cover plate design is presented in **Table 5.5** and **Table 5.6** for braces of CBF located in both, E-W and N-S directions. As illustrated, these tables contain information about the dimensions of the selected cover plates (*thickness* x *width*), centroid, the ratio between the center of gravity and welding length $\bar{x}'/L_w$, and shear lag factor *U*. It is noted that the resistance of slotted HSS brace cross-sections reinforced with cover plates T_{rb} has to be equal to or larger than the probable tensile resistance of brace T_u. The value of T_{rb} was obtained with **Eq. (5.1)** which was also used by Haddad and Tremblay (2006) and originates from the AISC standard (2005).

$$T_{rb} = U(\Phi_r R_t A_{nb} F_{u,b} + \Phi A_{gCP} F_{u,CP}) \tag{5.1}$$

In the above equation, A_{nb} represents the cross-sectional area of the brace with the consideration of the gusset plate slot; A_{gCP} is the gross cross-sectional area of the added cover plate; while U is the shear lag factor, given in **Eq. (2.22)** or **Eq. (2.23)** depending on $\bar{x}'/L_w$. On the other hand, R_t was taken as *1.1*, while the coefficients Φ_r and Φ were taken as *0.75* and *1.0* respectively. In addition a *1.5 mm* cutting space between brace and gusset plate slot was also considered**.**

Table 5.5 Cover plate design of HSS braces of CBF in E-W direction (3Q building)

St.	Cover plate dimensions		Centroid	$\bar{x}'/L_w$	U	T_{rb}	T_u/T_{rb}
	$t_{CP,}$ *(mm)*	$W_{CP,}$ *(mm)*	*(mm)*	-	-	*(kN)*	-
3	10	50	42	0.108	0.99	1539	0.96
2	10	75	54	0.128	0.97	1866	0.89
1	10	100	65	0.127	0.97	2342	0.87

Table 5.6 Cover plate design of HSS braces of CBF in N-S direction (3Q building)

St.	Cover plate dimensions		Centroid	$\bar{x}'/L_w$	U	T_{rb}	T_u/T_{rb}
	$t_{CP,}$ *(mm)*	$W_{CP,}$ *(mm)*	*(mm)*	-	-	*(kN)*	-
3	10	100	65	0.133	0.97	2365	0.86
2	10	120	73	0.136	0.96	3094	0.92
1	10	150	86	0.111	0.99	3794	0.87

5.2.1.2. Retrofit of CBF members (3Q)

As presented in Chapter 4 of this thesis, for the 3Q building, the braces do not need any retrofit since the ratio between the actual demand and brace capacity (probable brace resistance, C_u) is below *1.00* for both E-W and N-S direction. For this reason, all HSS braces of the 3Q building remained unchanged. The beams on the other hand, experienced failure when braces attain their probable post-buckling compression resistance and the larger demand resulted for the *OMS* verification. In addition, for the chevron braced frames in the E-W direction the most critical case was recorded when braces do not provide vertical support for the beams. Thus, to overcome this drawback, beams were reinforced by adding two longitudinal steel plates to each side of the I-shaped web as illustrated in **Figure 5.1**. According to demand-to-capacity ratios of beams presented in **Figure 4.3(b)** for CBF in the E-W direction and **Figure 4.6(b)** for the N-S direction all I-shape beams were found to have insufficient capacity. Thus, all CBF beams were retrofitted and the dimensions of the attached steel plates are given in **Table 5.7** and **Table 5.8** for the CBF in E-W and N-S direction, respectively**.** Additionally, the factored moment resistance of the beam

cross-section before and after retrofit M_r, and $M_{r,retrofit}$ together with the associated interaction equations for the axial compression and bending are also given. It is noted that the interaction equation for Class 1 and Class 2 sections was given by **Eq. (4.6)**. The selected strategy used to retrofit the I-shape beams was to maintain its symmetrical cross-section and to have enough space to add the additional plates shown in **Figure 5.1**.

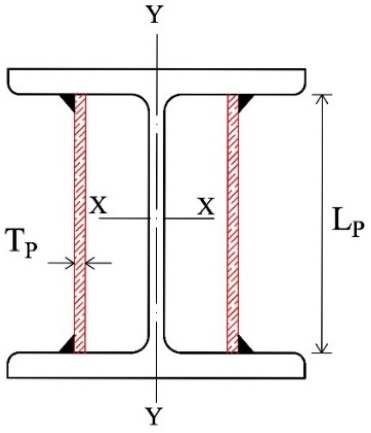

Figure 5.1 Retrofitted I-shape beam cross-section

Table 5.7 Retrofit summary for beams of the CBF in E-W direction (3Q building)

St	Steel plate dimensions		Section Class	M_r	$M_{r,retrofit}$	Interaction Eq.	Interaction Eq. retrofit
	T_P, (mm)	*L_P, (mm)*	-	*(kN*m)*	*(kN*m)*	-	-
3	8.0	291.4	1	130	291	1.67	0.91
2	9.5	290.6	2	165	271	1.72	0.92
1	9.5	332.0	1	146	284	2.22	0.93

Table 5.8 Retrofit summary for beams of the CBF in N-S direction (3Q building)

St	Steel plate dimensions		Section Class	M_r	$M_{r,retrofit}$	Interaction Eq.	Interaction Eq. retrofit
	T_P, (mm)	*L_P, (mm)*	-	*(kN*m)*	*(kN*m)*	-	-
3	5.0	332.0	1	146	217	1.28	0.70
2	5.0	332.4	2	210	281	1.38	0.78
1	5.0	380.6	1	239	332	1.42	0.78

Regarding the strategy to retrofit the CBF columns, they were designed to perform under axial compression and bending due to lateral loading. Although the beam-column connection is a shear tab connection, this connection was considered to allow transferring an additional bending moment having the value 20% of the beam plastic moment. According to **Figure 4.3(c)** columns in the E-

W direction of the 3-storey building located in Quebec City were prone to instability, due to lateral torsional buckling having the demand-to-capacity ratio *>1.00* for all storeys; however after increasing the gusset plate dimensions based on the current code demand the columns became stiffer having a smaller effective length. On the other hand, calculating conservatively the axial compressive resistance C_r as per **Eq. (2.19)** with $\phi=1.00$ instead of *0.9*, reduces the demand-to-capacity ratios considerably. In addition, after running the nonlinear time-history analysis for the N-S direction some damage concentration was observed at the middle columns. For this reason, it was decided that only the middle column in the diagonal tension/compression braced frame (N-S direction) needs to be retrofitted. In this light, additional steel plates were added to the flange of the I-shaped column cross-section, as illustrated in **Figure 5.2**, where T_P and L_P are the thickness and width of the steel cover plate, respectively.

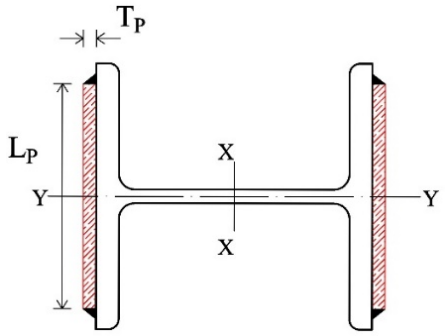

Figure 5.2 Retrofitted I-shape column cross-section

The retrofit summary for the middle columns in the diagonal tension/compression braced frame (N-S direction) is given in **Table 5.9**. As illustrated, the table contains information about the steel plates welded on the flanges, class of section, the factored compressive resistance, as well as the associated interaction equation before and after retrofit, based on **Eq. (4.6)**. It is noted, for the middle column the most critical case was given by lateral torsional buckling as discussed in *Section 4.2.3*. As depicted from the table, after retrofit, the interaction equation for the middle column is below *1.00* and the axial compressive resistance significantly improved for all columns.

Table 5.9 Retrofit summary for middle columns of the CBF in N-S direction (3Q building)

St	Steel plate dimensions		Section Class	C_r	$C_{r,retrofit}$	Interaction Eq.	Interaction Eq. retrofit
	T_P, *(mm)*	L_P, *(mm)*	-	*(kN)*	*(kN)*	-	-
3	5.00	140	1	510	1005	1.73	0.95
2	9.53	185	1	919	2122	2.10	0.95
1	19.05	200	1	1310	3378	2.33	0.95

5.2.2. Retrofit strategy for the 6-storey building located in Quebec City

5.2.2.1. Brace to frame connection retrofit

The same approach as in *Section 5.2.1.1* was applied for the 6-storey building located in Quebec City. Thus, it was verified that the failure mode of connection, if occurs, to be a ductile failure mode such as: yielding of gusset or block shear. In **Table 5.10** and **Table 5.11** is summarized the new gusset plate design for the braced frames in E-W and N-S direction, respectively. As illustrated, the tables contain the selected welding length L_w; the weld leg width D_w; gusset plate geometry together with Whitmore effective width and the lengths L_1, L_2, L_3.

Table 5.10 Brace-to-frame connections design parameters of CBF in E-W direction (6Q building)

St	D_w	L_w	a	b	t_{gp}	W_w	A_{gp}	L_1	L_2	L_3
	mm	*mm*	*mm*	*mm*	*mm*	*mm*	*mm²*	*mm*	*mm*	*mm*
6	6	390	437	480	9.53	577	5499	75	310	19.05
5	8	470	506	554	12.70	670	8505	86	361	25.4
4	8	440	488	587	12.70	660	8383	143	356	25.4
3	9	520	541	657	15.90	752	11945	120	407	31.8
2	8	520	589	625	15.90	778	12358	80	421	31.8
1	9	610	927	443	15.90	882	14008	31.8	546	434

Table 5.11 Brace-to-frame connections design parameters of CBF in N-S direction (6Q building)

St	D_w	L_w	a	b	t_{gp}	W_w	A_{gp}	L_1	L_2	L_3
	mm	*mm*	*mm*	*mm*	*mm*	*mm*	*mm²*	*mm*	*mm*	*mm*
6	8	430	280	994	12.7	649	8236	786	688	25.4
5	8	600	399	1157	14.3	871	12439	972	921	28.6
4	8	690	457	1200	15.9	1000	15874	1108	1057	31.8
3	12	595	402	1100	19.1	890	16959	1010	946	38.1
2	8	730	538	1200	19.1	1097	20897	1126	1162	38.1
1	11	726	762	949	19.1	1092	20809	416	744	38.1

Further, the reserve capacity of the connections as well as the demand-to-capacity ratios for each verification case according to the current design standard is given in **Table 5.12** and **Table 5.13** for E-W and N-S direction, respectively. It is noted that all verifications considered for brace-to-

frame connections are similar with those considered for the 3Q building. For this reason the reader is referred to **Appendix III** of this thesis, where a detailed design example of the brace-to-frame connection for the 3-storey building located in Quebec City is described step-by-step**.**

Table 5.12 Design verification of brace-to-frame connections of CBF in E-W direction, according to CSA/S16-09 (6Q building)

St.	Shear resistance of welding, (kN)			Metal base resistance, (kN)		Yielding of gusset plate, (kN)		Buckling of gusset plate, (kN)		Net Rupture and block shear of brace with shear lag, (kN)		
	V_r	C_u/V_r	T_u/V_r	$T_{r.mb}$	$T_u/T_{r.mb}$	T_{rgp}	T_u/T_{rgp}	C_{rgp}	C_u/C_{rgp}	T_{NR}	$T_{r\text{-}BS}$	$T_u/\min(T_{NR}, T_{r\text{-}BS})$
6	1456	0.51	0.94	2006	0.68	1485	0.92	1399	0.53	1114	1685	1.22
5	2339	0.48	0.95	3223	0.69	2296	0.97	2202	0.51	1915	3490	1.16
4	2190	0.63	0.93	3018	0.68	2263	0.90	2141	0.64	1667	2376	1.22
3	2911	0.62	0.94	4458	0.62	3225	0.85	3110	0.58	2292	3861	1.20
2	2588	0.74	0.93	4458	0.54	3337	0.72	3232	0.59	1952	2808	1.23
1	3415	0.66	0.96	5229	0.62	3782	0.86	3197	0.70	2684	4529	1.22

Table 5.13 Design verification of brace-to-frame connections of CBF located in N-S direction, according to CSA/S16-09 (6Q building)

St.	Shear resistance of welding, (kN)			Metal base resistance, (kN)		Yielding of gusset plate, (kN)		Buckling of gusset plate, (kN)		Net Rupture and block shear of brace with shear lag, (kN)		
	V_r	C_u/V_r	T_u/V_r	$T_{r.mb}$	$T_u/T_{r.mb}$	T_{rgp}	T_u/T_{rgp}	C_{rgp}	C_u/C_{rgp}	T_{NR}	$T_{r\text{-}BS}$	$T_u/\min(T_{NR}, T_{r\text{-}BS})$
6	2140	0.34	0.95	2949	0.69	2224	0.92	1177	0.61	1667	2322	1.22
5	2986	0.43	0.95	4629	0.61	3359	0.85	1513	0.84	2323	3860	1.22
4	3434	0.52	0.96	5915	0.56	4286	0.77	1858	0.97	2655	4439	1.24
3	4441	0.51	0.96	6121	0.70	4579	0.93	2759	0.82	3538	5101	1.20
2	3633	0.70	0.96	7510	0.47	5642	0.62	2872	0.89	2786	3942	1.26
1	4968	0.66	0.96	7468	0.65	5618	0.86	4775	0.68	3830	5391	1.26

Similar with the 3Q building, after retrofitting the connections, the brace is prone to net rupture due to the reduction of the cross-sectional area at the gusset plate slot. Therefore, in order to strengthen the net section of the brace, a cover plate was necessary. Thus the cover plate design summary is presented in **Table 5.14** and **Table 5.15** for both directions. It is noted that the resistance of the sections reinforced with cover plates T_{rb} was obtained using **Eq. (5.1)**. In addition,

a detailed example of the design of cover plates at brace-to-gusset connection is presented in **Appendix III** as well.

Table 5.14 Cover plate design of HSS braces of CBF in E-W direction (6Q building)

St.	Cover plate dimensions		Centroid	$\bar{x}'/L_w$	U	T_{rb}	T_u/T_{rb}
	$t_{CP,}$ *(mm)*	$W_{CP,}$ *(mm)*	*(mm)*	-	-	*(kN)*	-
6	10	70	54	0.127	0.97	1620	0.84
5	10	75	52	0.097	1.00	2336	0.95
4	10	100	65	0.132	0.97	2336	0.86
3	10	100	63	0.105	0.99	2937	0.94
2	10	120	76	0.130	0.97	2817	0.86
1	10	120	73	0.107	0.99	3525	0.93

Table 5.15 Cover plate design of HSS braces of CBF in N-S direction (6Q building)

St.	Cover plate dimensions		Centroid	$\bar{x}'/L_w$	U	T_{rb}	T_u/T_{rb}
	$t_{CP,}$ *(mm)*	$W_{CP,}$ *(mm)*	*(mm)*	-	-	*(kN)*	-
6	10	100	65	0.135	0.97	2358	0.86
5	10	120	74	0.112	0.98	3205	0.89
4	10	150	85	0.112	0.98	3813	0.86
3	10	150	83	0.124	0.97	4456	0.96
2	10	200	109	0.136	0.96	4339	0.81
1	10	200	106	0.132	0.97	5324	0.91

5.2.2.2. Retrofit of CBF members (6Q)

According to demand-to-capacity ratios of W-shape beams of CBF in E-W direction presented in **Figure 4.9(b)** and N-S direction shown in **Figure 4.11(b)** it was found that especially the beams of CBFs in the E-W direction have insufficient capacity. For this reason all beams belonging to the CBF in the E-W direction and only the bottom three beams for the CBFs in the N-S direction were retrofitted and the dimensions of the attached steel plates are given in **Table 5.16** and **Table 5.17** for both loading directions**.** Additionally, in these tables are given the factored moment resistance of the beam section before and after retrofit M_r, and $M_{r,retrofit}$ together with the associated interaction equations.

Table 5.16 Retrofit summary for beams of the CBF in E-W direction (6Q building)

St	Steel plate dimensions		Section Class	M_r	$M_{r,retrofit}$	Interaction Eq.	Interaction Eq. retrofit
	T_P, (mm)	*L_P, (mm)*	-	*(kN*m)*	*(kN*m)*	-	-
6	6.4	291.4	1	130	201	1.59	0.96
5	8.0	290.6	2	165	254	1.63	0.95
4	5.0	290.6	1	191	246	1.39	0.97
3	5.0	332.4	2	210	281	1.38	0.93
2	5.0	332.4	2	210	281	1.38	0.93
1	5.0	331.8	1	241	312	1.32	0.89

Table 5.17 Retrofit summary for beams of the CBF in N-S direction (6Q building)

St	Steel plate dimensions		Section Class	M_r	$M_{r,retrofit}$	Interaction Eq.	Interaction Eq. retrofit
	T_P, (mm)	*L_P, (mm)*	-	*(kN*m)*	*(kN*m)*	-	-
6	-	-	2	165	165	0.90	0.90
5	-	-	1	191	191	1.02	1.02
4	-	-	1	227	227	0.95	0.95
3	5.0	331.8	1	273	343	1.27	0.84
2	5.0	320.0	1	308	369	1.29	0.89
1	5.0	319.8	1	346	407	1.29	0.92

In addition, once the full compression capacity of the brace was reached, large forces were transferred to the adjacent columns which did not possess sufficient compression and bending strength. Hence, local strengthening of columns (welding steel cover plates to the W-shape flanges as illustrated in **Figure 5.2**) was required. The retrofit summary for columns of CBFs in E-W and N-S direction is given in **Table 5.18** and **Table 5.19** respectively. These tables contain information about the steel plate dimensions that were welded to the flanges, class of section, the factored compressive resistance, as well as the most critical interaction equation used before and after retrofit according to **Eq. (4.6)**. It is noted that, columns of the 6Q building were critical loaded and prone to failure due to lateral torsional buckling. As depicted, after retrofit the interaction equation for these columns is below *1.00* and the axial compressive resistance has significantly improved.

Table 5.18 Retrofit summary for columns of the CBF in E-W direction (6Q building)

St	Steel plate dimensions		Section Class	C_r	$C_{r,retrofit}$	Interaction Eq.	Interaction Eq. retrofit
	T_P, *(mm)*	L_P, *(mm)*	-	*(kN)*	*(kN)*	-	-
6	6.4	190	1	1412	2255	0.56	0.35
5	6.4	190	1	1412	2257	1.03	0.70
4	6.4	240	1	2781	3890	0.94	0.83
3	15.9	240	1	2781	5251	1.20	0.90
2	12.7	300	1	5293	7785	0.98	0.86
1	19.05	300	1	4806	8473	1.22	0.96

Table 5.19 Retrofit summary for columns of the CBF in N-S direction (6Q building)

Side Column							
St	Steel plate dimensions		Class	C_r	$C_{r,retrofit}$	Interaction Eq	Interaction Eq. Retro.
	T_P, *(mm)*	L_P, *(mm)*	-	*(kN)*	*(kN)*	-	-
6	-	-	1	919	919	0.43	0.43
5	5.0	60	1	919	1153	1.07	0.88
4	-	-	1	2384	2384	0.76	0.76
3	5.0	150	1	2384	3002	1.04	0.85
2	-	-	1	4329	4329	0.83	0.83
1	5.0	240	1	3921	4812	1.11	0.90
Middle Column							
6	-	-	1	919	919	0.98	0.98
5	8.0	150	1	919	1687	2.10	0.95
4	5.0	140	1	1794	2333	1.86	0.92
3	11.1	190	1	1794	3167	2.26	0.93
2	5.0	220	1	2781	3601	1.81	0.92
1	12.7	250	1	2414	4352	2.42	0.94

5.3. Incremental Dynamic Analysis for retrofitted buildings located in Quebec City

To verify the performance of retrofitted buildings, the incremental dynamic analysis (IDA) was employed. As illustrated in **Table 5.20** the dynamic proprieties of post-retrofit buildings slightly vary when comparing to those of pre-retrofit buildings. It can be concluded that the selected retrofit strategy does not modify to much the building period, which might be seen as a good thing because the structure does not add any extra loads at the foundation level, thus no need to do additional work to reinforce the building foundations.

Table 5.20 First mode vibration period of the investigated buildings before and after retrofit

ID	Pre-retrofit				Post-retrofit			
	T_1 , (s)		$S_a(T_1)$, (g)		T_1 , (s)		$S_a(T_1)$, (g)	
	E-W	N-S	E-W	N-S	E-W	N-S	E-W	N-S
3Q	0.554	0.690	0.302	0.256	0.543	0.642	0.306	0.272
6Q	0.930	1.135	0.177	0.137	0.880	1.032	0.191	0.147

5.3.1. IDA results for the CBF in E-W direction (3Q)

The IDA curves of retrofitted frames in E-W direction are illustrated in **Figure 5.3** with red line. In addition, the variation between IDA curves reflect the ground motion signature. As depicted in **Figure 5.3**, before retrofit, the gusset plate connection fails at a critical floor and the brace cannot dissipate any energy making the CBF to lose stiffness and to experience large interstorey drifts. After the brace-to-frame connections were re-designed and detailed, braces were able to dissipate the earthquake induced energy through buckling and yielding. In general, not all braces attached to CBF column reach yielding at the same time sequence during the ground motion excitation. Based on this observation, columns were not strengthened to carry the full braces capacity in tension which further requires the strengthening of foundations. As resulted from **Figure 5.3**, the post-retrofit building was able to withstand the earthquake loads computed for a probability of exceedance of 2%/50 yrs.

For this study, the collapse assessment is made using a combination of structural analysis and engineering judgement. It is suggested that the non-convergence of the time-integration scheme is the safest numerical equivalent of the actual dynamic collapse, but this in turn can suffer from the quality of the numerical code. Hence, the collapse points were also verified using the interaction equation of the axial compression and bending moment according to CSA/S16-09 standard. In other words, a laterally supported member fails when it reaches its in-plane moment capacity, reduced for the presence of axial load. On the other hand, a laterally unsupported member may fail by lateral-torsional buckling or a combination of weak-axis buckling and lateral buckling. In addition, when subjected to axial load only, the column axial compressive resistance (which represents a fraction of the yield load) depends on its slenderness ratio and below this yield load

the column will fail by buckling. Note that column buckling represents a bifurcation problem and not a bending strength problem.

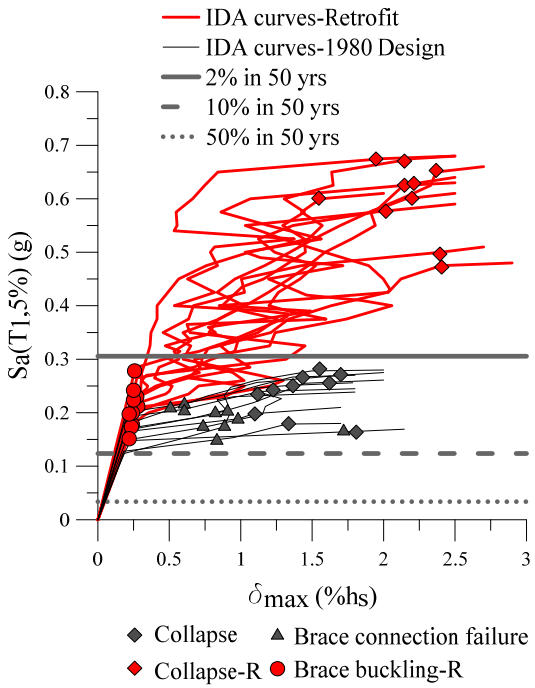

Figure 5.3 IDA curves of existing and retrofitted CBFs in E-W direction (3Q)

Additionally, Pillai (1974) proposed a simplified interaction equation based on the theoretical relations, derived from the fully plastic stress distribution of the cross section which is both satisfactory and far less conservative. According to his research, for uniaxial bending about the x-x axis, the interaction equation for wide flange beam-column sections has the following expression:

$$M_x \leq M_{px}, \text{ for } 0 \leq \frac{C}{C_y} \leq 0.15 \text{ and,}$$

$$M_x \leq 1.18\left(1 - \frac{C}{C_y}\right) M_{px}, \text{ for } 0.15 < \frac{C}{C_y} \leq 1.0 \qquad (5.2)$$

where M_{px} is the plastic moment about the strong axis and C_y is taken as $\phi A_g F_y$; where A_g represents the cross-sectional area of the member.

Therefore, the axial load and bending moment of each column were picked up from the time-history analysis in order to calculate the interaction equation ratio. Thus, the pairs of M_f/M_{rx} and C_f/C_{ry}, points recorded at the 2nd and 3rd floor column under the *M7C2-41.6* ground motion, (near collapse) are presented in **Figure 5.4(a)** and **Figure 5.4(b)**, respectively. In other words, the

columns do not possess sufficient axial compression and bending capacity, leading to dynamic instability due to P-Δ effects at large interstorey drifts.

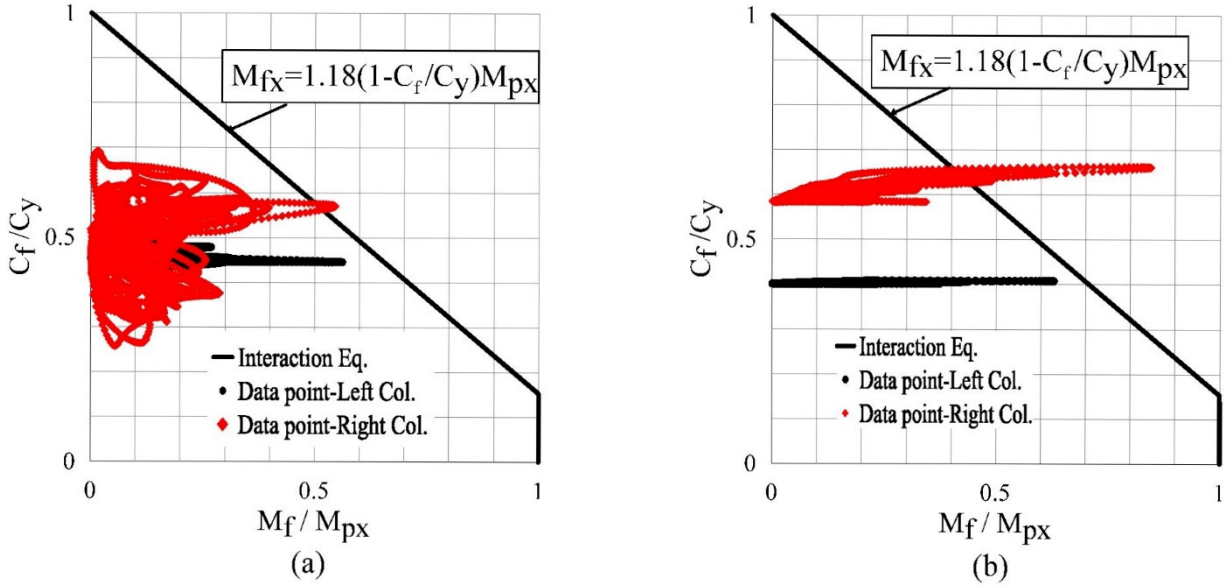

Figure 5.4 Axial load – bending moment interaction diagram, under M7C2-41.6 ground motion scaled to CP performance level for: (a) 2nd floor columns; (b) 3rd floor columns

Note that a similar procedure can be applied to plot the axial force and bending moment developed in the beams of CBFs. However, from the above figure it can be seen clearly that the dynamic instability already happened at the column level, thus partial failure of the upper two floors can be observed. In general, for the E-W direction of the 3Q building this collapse points were correlated with the non-convergence of the time-integration scheme.

One advantage of the IDA approach is that performance levels corresponding to a given earthquake hazard level can be defined on such IDA curve by acceptable ranges of deformation demand on structural and nonstructural components which imply probable levels of damage. Damage levels namely*: Very Light, Light, Moderate* and *Severe* vary as a continuous function of building deformation and are associated with the defined building performance levels as illustrated in **Figure 2.10**. In addition, ASCE/SEI 41-13 provides suggested maximum interstorey drift and maximum residual interstorey drift values for each performance level. In this study, the displacement capacity point (last point) on the IDA curve associated to the *CP* performance level corresponds to storey mechanism and the point associated to the *IO* level corresponds to the first brace buckling. However, the *LS* performance level is difficult to define (Wen et al., 2004).

Based on qualitative approaches, the *LS* performance level can be defined when braces yield or buckle but do not fail, while the maximum residual interstorey drift is about $0.5\%h_s$. The seismic response of the CBFs from the E-W direction is presented in detail herein.

5.3.1.1. Seismic Response of the CBF in E-W direction

Before retrofit, the brace-to-frame connections fail due to shearing of welds making the existing building vulnerable when subjected to the current code demand. In the case of post-retrofit building, all braces are able to dissipate energy, through buckling and yielding. However, the columns and beams were not strengthened to withstand a seismic demand larger than the current code demand without hinging. For this reason, hinging in beams/columns occurs before braces exhibit any fracture due to low-cycle fatigue. The hysteretic response of CBF braces subjected to M7C2-41.6 ground motion scaled to *CP* limit state is depicted in **Figure 5.5** where the axial force in braces is plotted versus the axial deformation of HSS brace members. As illustrated in the figure, almost all braces buckled except the left braces of the 2nd and ground floor which were triggered in tension. However, this behaviour depends on the ground motion signature. In addition, from **Figure 5.5(a)** and **Figure 5.5(b)** it can be seen that the 3rd floor shows a larger interstorey drift since the axial deformation of the corresponding braces is considerably higher. Thus, the 3rd floor columns, more precisely the right column, experiences higher demand being prone to failure due to axial compression and bending, as depicted in **Figure 5.4(b).**

It is noted that the values of the calculated probable compressive resistance C_u, of braces are very close with the values obtained from the nonlinear time history analysis in OpenSees. However, the latter values are slightly smaller (approx. 10-15 %) because of the effective brace length, which was reduced with the rigid extensions from the gusset plate connections.

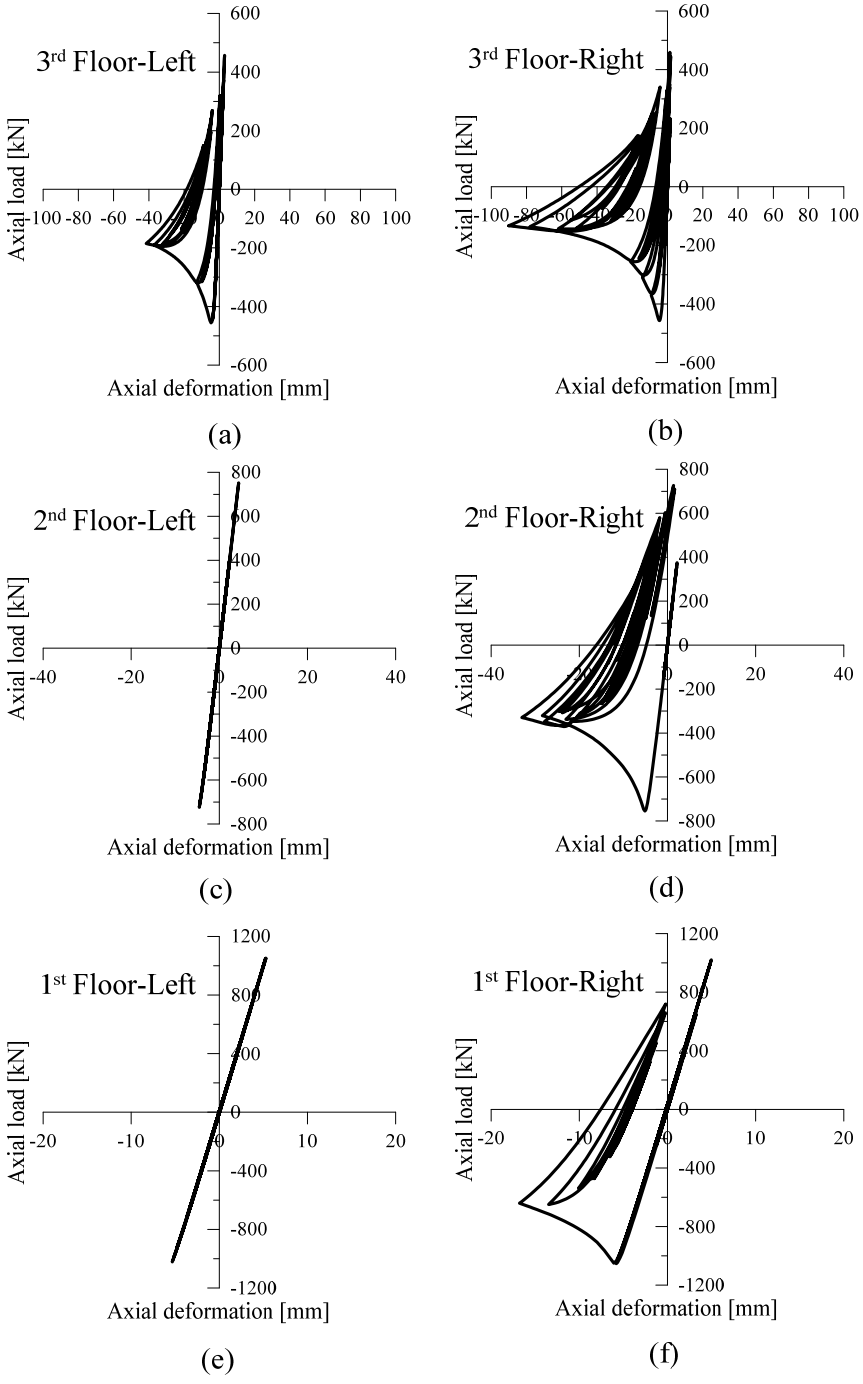

Figure 5.5 Hysteretic response of CBF braces (E-W direction) associated to CP limit state under M7C2-41.6 ground motion (3Q)

Furthermore, each performance level can be defined for each considered seismic ground motion on the computed IDA curve based on acceptable ranges of deformation demand on structural and nonstructural components. Therefore, the 50th and 84th fractiles of the recorded engineering demand parameters such as: interstorey drift (δ_{max}), residual drift ($\delta_{max.res}$) and floor acceleration

(a_{max}) resulted from nonlinear analysis of retrofitted CBF in E-W direction for each performance levels (*IO*, *LS*, *CP*) are illustrated in **Figure 5.6**. As depicted from **Figure 5.6(b)** the overall residual drift is concentrated at the bottom floors for both: collapse prevention and life safety-performance levels. It is noted that for *Immediate Occupancy*- the resulted remanent drift was very small, thus was not represented in the figure. In addition, the maximum floor acceleration, a_{max}, was added in order to assess the failure of acceleration-sensitive nonstructural components.

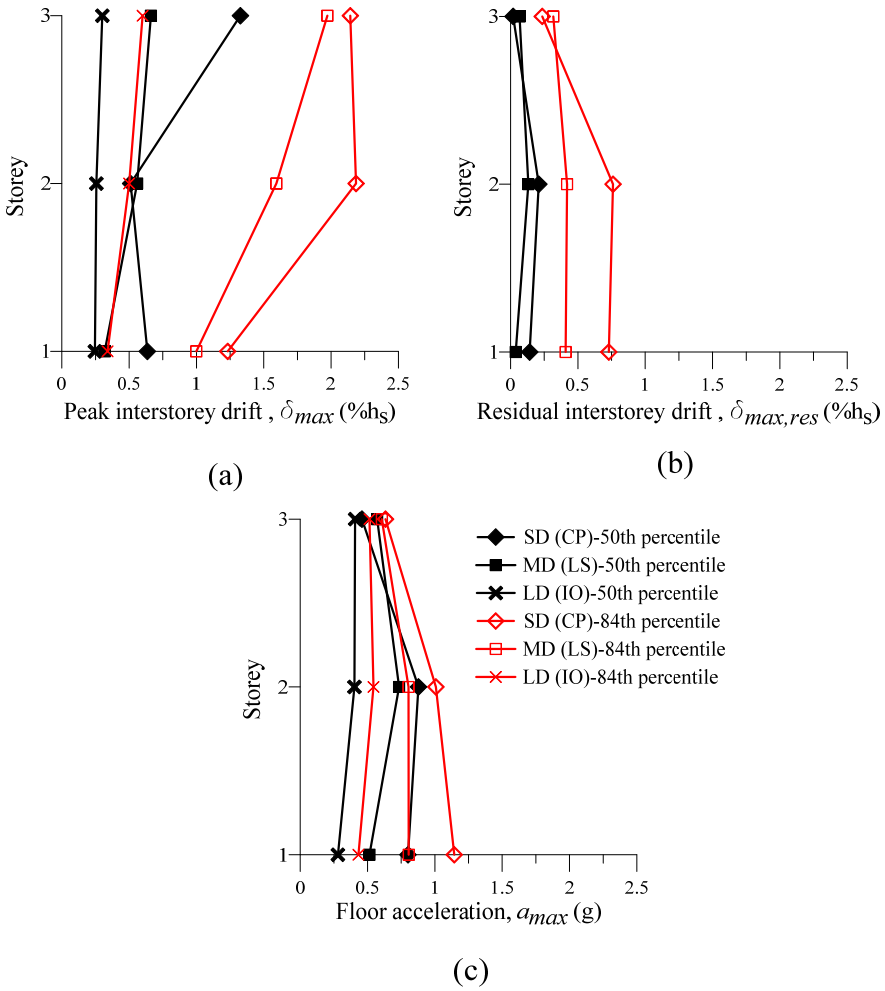

Figure 5.6 The 50th and 84th percentile of EDP of 3Q (E-W) computed from IDA for performance levels *IO*, *LS*, *CP*: (a) Peak interstorey drift; (b) Residual interstorey drift; (c) Floor acceleration. (Legend: *SD-Severe damage*; *MD- Moderate damage*; *LD- Light Damage*)

5.3.2. IDA results for the CBF in N-S direction (3Q)

The IDA curves for the retrofitted frames in N-S direction are illustrated in **Figure 5.7** with red line. The CBF building response is similar with that resulted in the E-W direction.

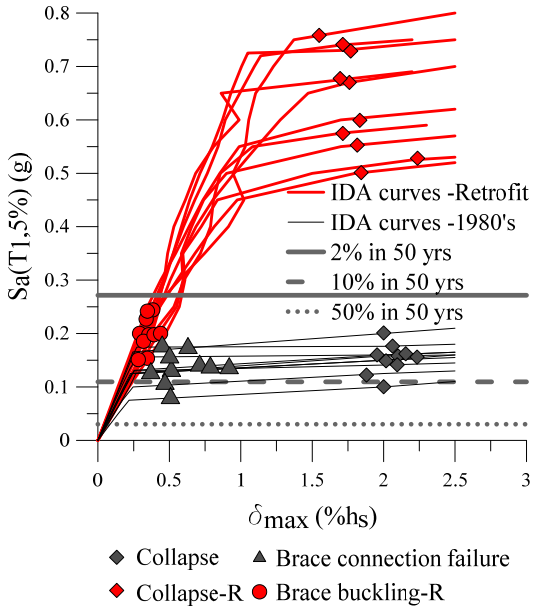

Figure 5.7 IDA curves of existing and retrofitted CBFs in N-S direction (3Q)

In general, for the CBF in N-S direction, the 3rd floor brace buckled first and in consequence the interstorey drift increases. In addition, the 3rd floor column reached buckling and the most vulnerable column was found to be the middle column. This example is illustrated in **Figure 5.8** when the CBF was subjected to S8.EN1 ground motion. It is noted that at the collapse points all column members buckled due to the large interstorey drifts. The collapse points from the IDA curve were defined in the same way as were defined on the IDA curves of CBF in E-W direction.

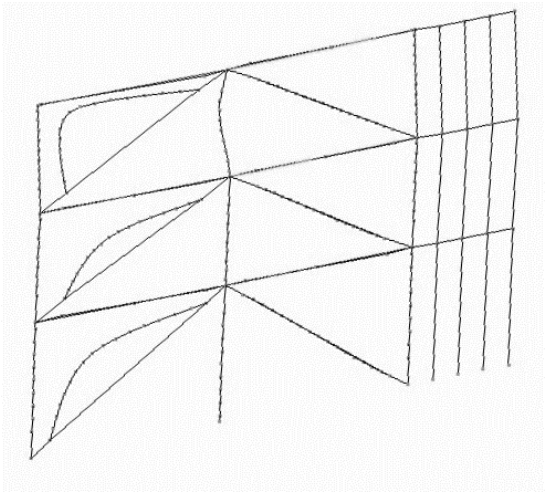

Figure 5.8 Deflected shape associated to CP limit state of CBF in N-S direction under S8.EN1 ground motion (3Q building)

Therefore, the axial load and bending moment of each column were recorded from the time-history analysis in order to calculate the interaction ratio. Thus, the pairs of M_f/M_{rx} and C_f/C_{ry}, points recorded at the ground floor for the middle column under the *M7C1-25.8* ground motion corresponding to *CP* limit state are presented in **Figure 5.9**. In other words, the columns do not possess sufficient axial compression and bending capacity, leading to dynamic instability due to P-Δ effects. In general, for the N-S direction, the dynamic instability was recorded at the ground floor level.

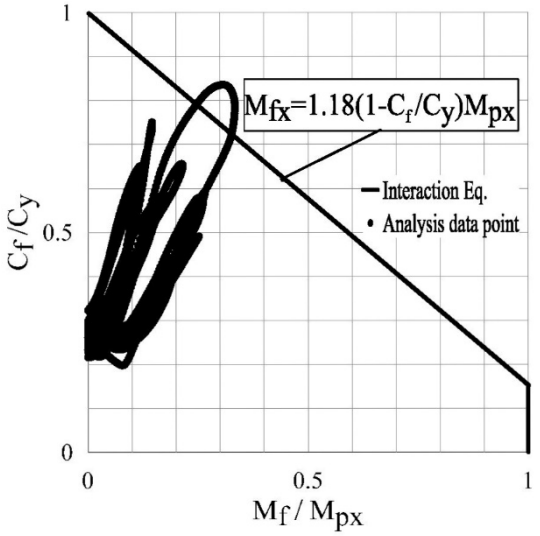

Figure 5.9 Axial load – bending moment interaction diagram recorded for middle column at ground floor level under M7C1-25.8 ground motion scaled to CP performance level

5.3.2.1. Seismic Response of the CBF in N-S direction

Similar with the response of CBF in E-W direction, performance levels corresponding to a given earthquake hazard level, were defined on the computed IDA curves. An example of the CBF brace behaviour (N-S direction) associated to *CP* limit state under the M7C1-25.8 ground motion is depicted in **Figure 5.10** in terms of axial load in the brace versus its axial deformation. As illustrated, all braces were able to dissipate energy when exhibited several tension-compression excursions. Note that the number of cycles, load magnitude and axial deformation of the brace depends on the ground motion signature and also on the brace properties. It can be seen in **Figure 5.10** that large interstorey drift was triggered at the ground floor level. Thus, the ground floor middle column, has experienced higher demands as depicted in **Figure 5.9**.

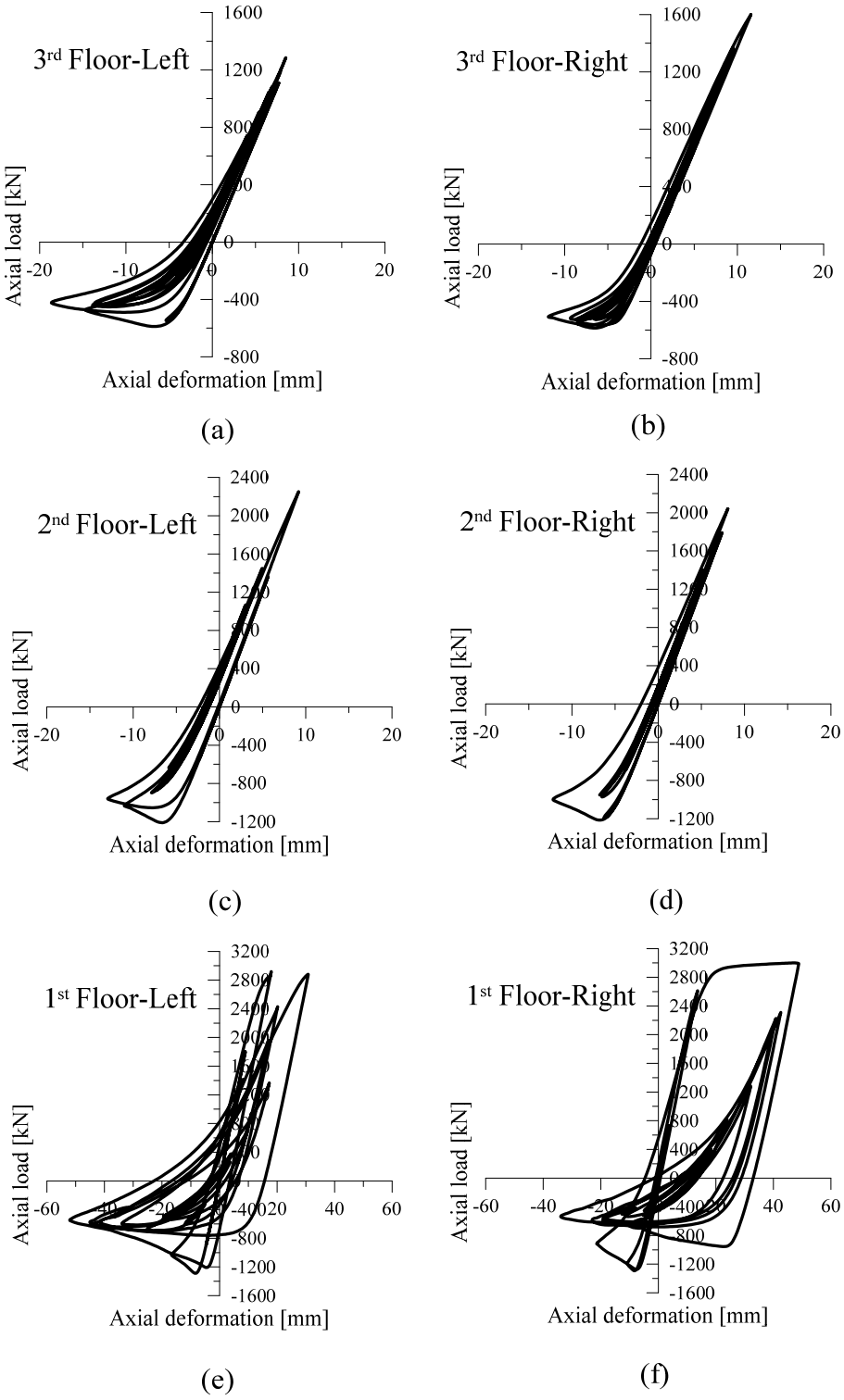

Figure 5.10 Hysteretic response of CBF braces (N-S direction) associated to the CP limit state resulted under M7C1-25.8 ground motion (3Q).

It is noted that the values of the calculated probable compressive resistance C_u, of braces are very close with the values obtained from the nonlinear time history analysis in OpenSees. However, the latter values are slightly smaller (approx. 10-15%) because of the effective brace length, which was reduced with the rigid extensions from the gusset plate connections.

In addition, the response of CBF (N-S) expressed as 50th and 84th fractiles of recorded engineering demand parameters such as: interstorey drift (δ_{max}), residual drift ($\delta_{max.res}$) and floor acceleration (a_{max}) resulted for each performance level (IO, LS, CP) are illustrated in **Figure 5.11**.

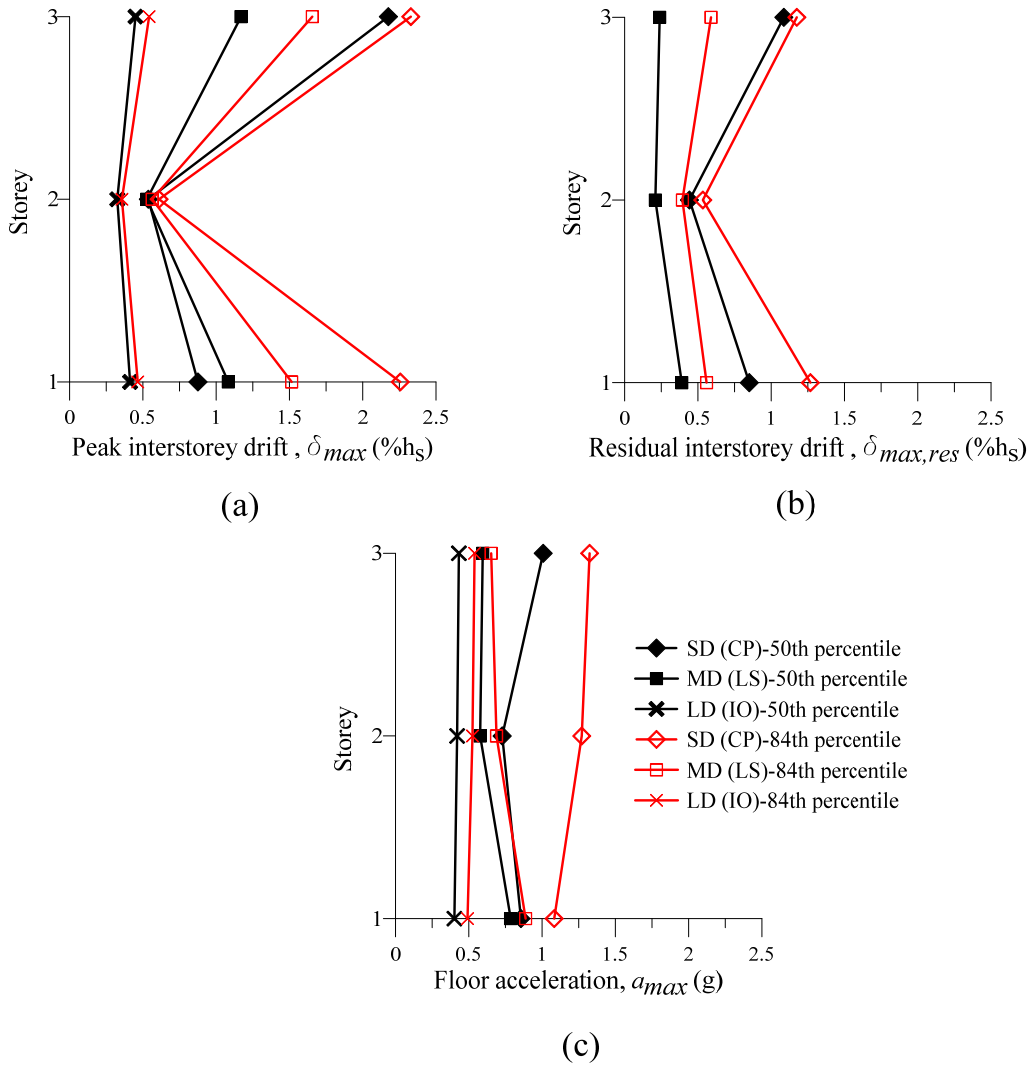

Figure 5.11 The 50th and 84th percentile of EDP of 3Q (N-S) computed from IDA for performance levels *IO*, *LS*, *CP*: (a) Peak interstorey drift; (b) Residual interstorey drift; (c) Floor acceleration. (Legend: *SD-Severe damage*; *MD- Moderate damage*; *LD- Light Damage*)

As depicted from **Figure 5.11(b),** the overall residual drift is concentrated at the bottom and top floor for both: *collapse prevention* and *life safety* performance levels. It is noted that for *immediate occupancy*, the resulted remanent drift was very small and was not represented in the figure.

5.3.3. IDA results for the CBF in E-W direction (6Q)

The IDA curves for the retrofitted 6Q building (E-W direction) are illustrated in **Figure 5.12** with red line. The response is similar with that resulted for the 3Q building and the performance of retrofitted building was significantly improved.

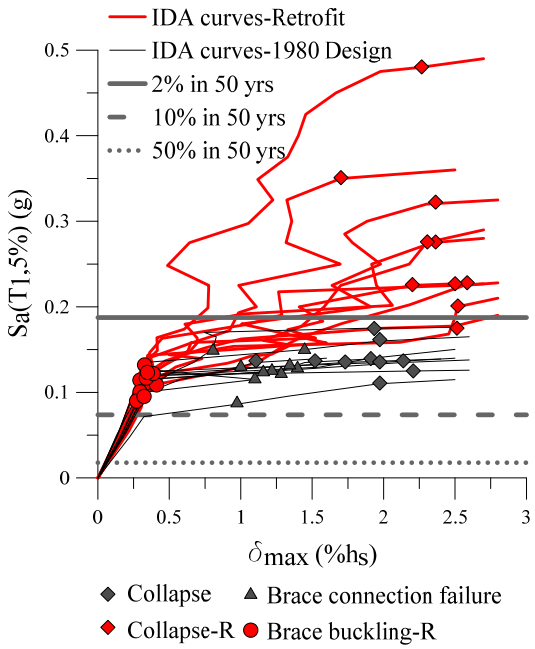

Figure 5.12 IDA curves of existing and retrofitted CBFs in E-W direction (6Q)

As illustrated in the above figure, the first brace buckling of the post-retrofit 6-storey building was initiated at a spectral acceleration of 0.12g while the collapse points are scattered above the current code demand (i.e. 2% in 50 years hazard level). As resulted from IDA, the building behaves inelastically when subjected to the code demand level and damage was concentrated mostly at the upper two floors. Similar with the 3Q building, the axial load and bending moment of each column were recorded from time-history analysis in order to calculate the interaction ratio. Thus, the pairs of M_f/M_{rx} and C_f/C_{ry} points recorded at the 5th floor columns under the *S8.EN1* ground motion at the *CP* limit state are presented in **Figure 5.13**, which clearly shows that columns do not possess sufficient axial compression and bending capacity, leading to dynamic instability due to P-Δ

effects. In general, for the E-W direction, the dynamic instability was recorded at the 5th floor columns

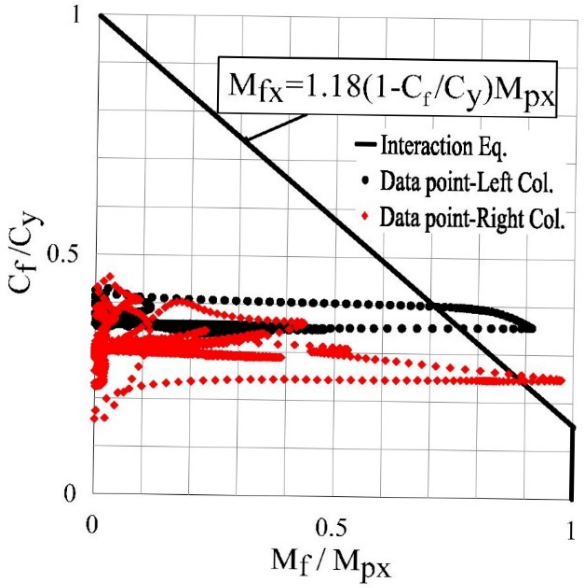

Figure 5.13 Axial load – bending moment interaction diagram recorded for the 5th floor columns under S8.EN1 ground motion scaled to CP limit state

5.3.3.1. Seismic Response of the CBF in E-W direction

An example of CBF brace behavior at the CP limit state is depicted in **Figure 5.14** and **Figure 5.15** for the upper and bottom three floor braces, respectively. As illustrated in **Figure 5.14(a)**, the left brace at the top floor fractures due to low-cycle fatigue where the brace experiences several tension-compression excursions. In addition, the rest of the braces are in tension except the left braces at 5th floor and ground floor. As depicted in **Figure 5.16(a)** which represents the accelerogram of a ground motion that caused fracture (i.e. M7C1-41.6), the top floor left brace experiences rupture right after the ground motion peak. In other words, the brace cannot dissipate energy anymore, leading to large interstorey drifts as shown in **Figure 5.16(b)** which in turn leads to column hinging and eventually the formation of the storey mechanism. It is noted that brace fracture failure due to low-cycle fatigue is the desirable failure mode, and was observed only at the 6-storey CBF in the E-W direction. However, brace failure is strongly dependent on brace effective length, its slenderness ratio and width-to-thickness ratio according to **Eq. (4.9)**.

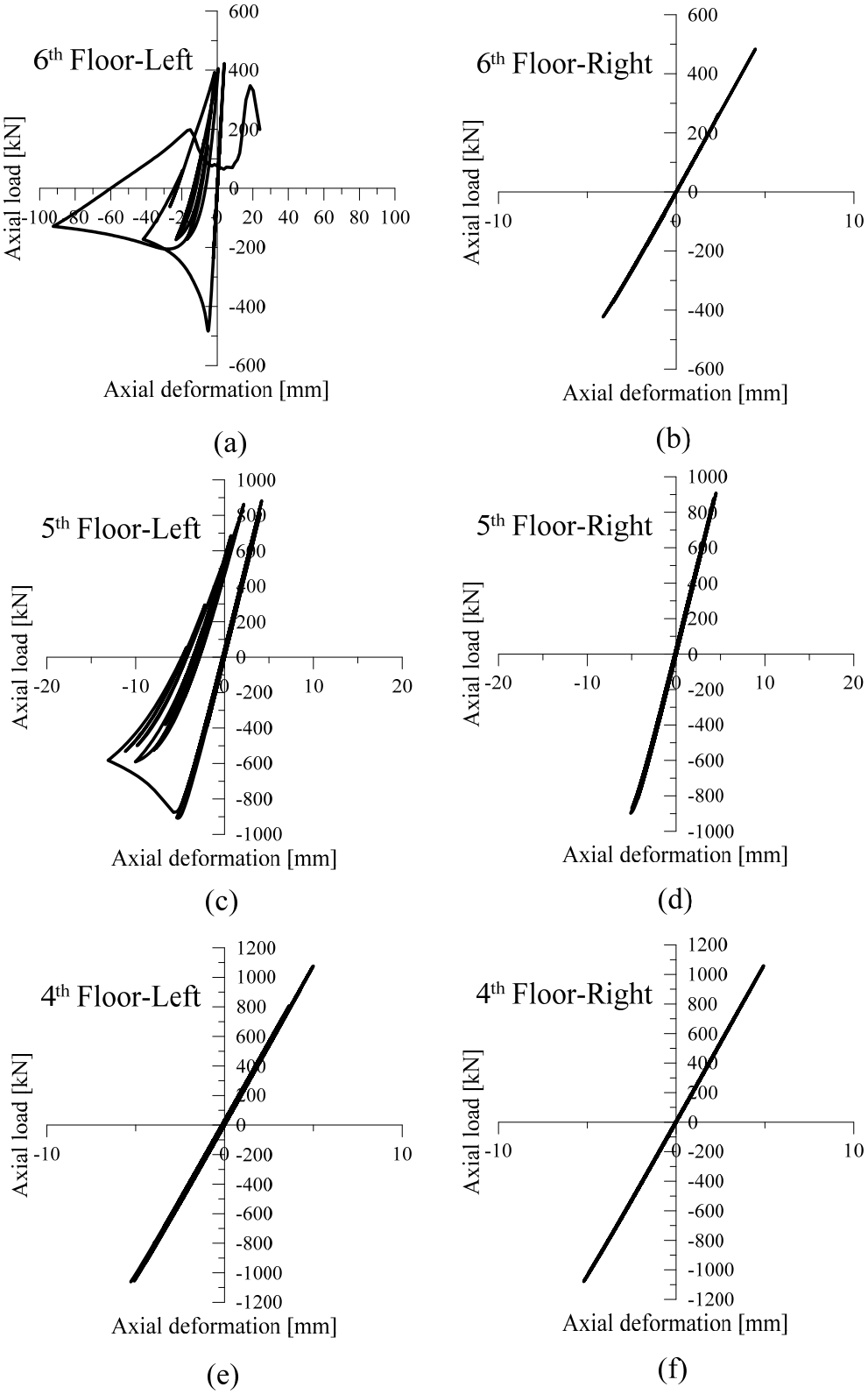

Figure 5.14 Hysteretic response of the 6th- 4th floor braces of CBF (E-W direction) under M7C2-41.6 ground motion scaled to CP (6Q).

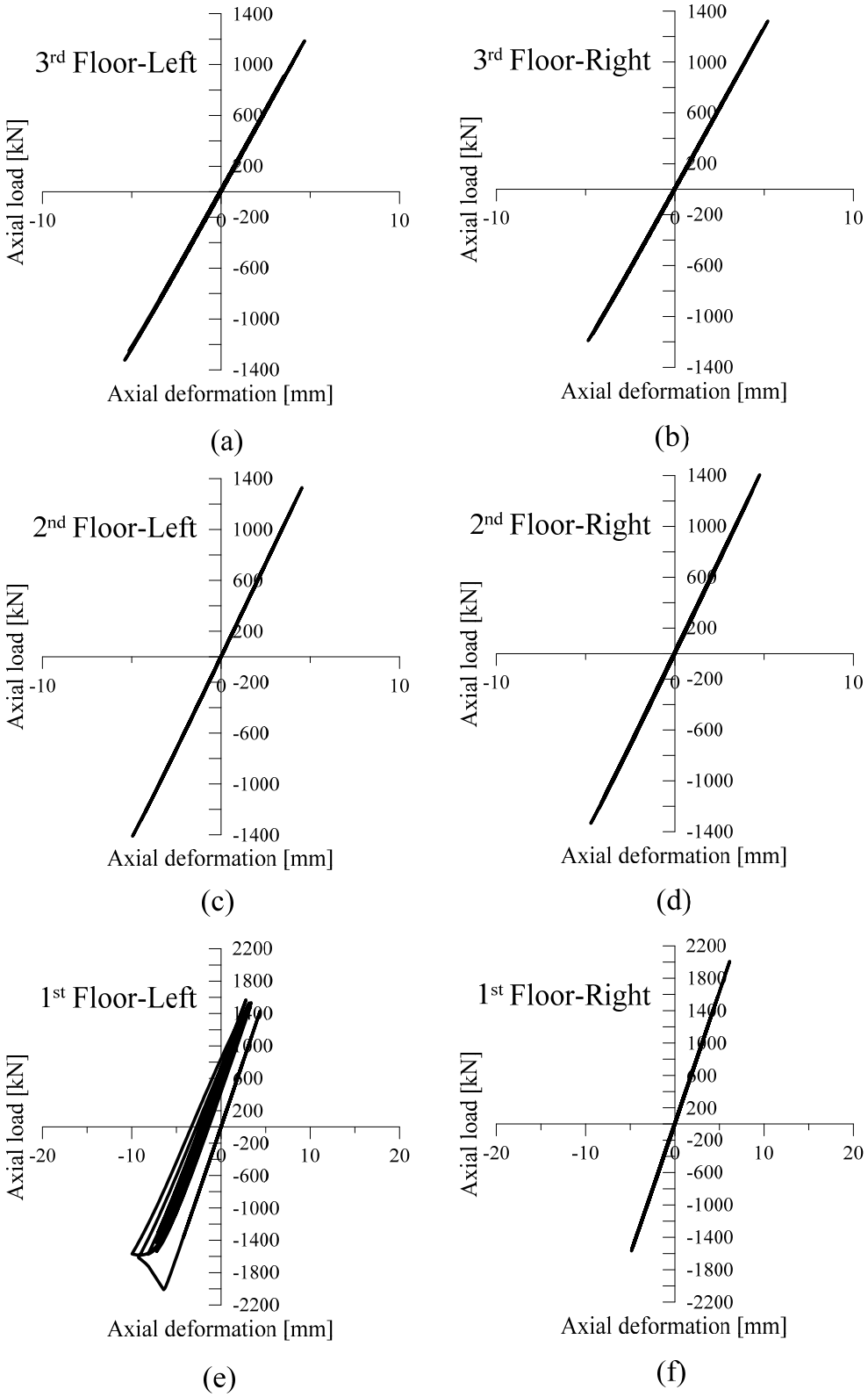

Figure 5.15 Hysteretic response of the 3rd– 1st floor braces (E-W direction) under M7C2-41.6 ground motion scaled to CP limit state (6Q).

It is noted that the values of the calculated probable compressive resistance C_u of braces are very close with the values obtained from the nonlinear time-history analysis using OpenSees. However, the latter values are slightly smaller (approx. 10-15%) because of the effective brace length, which was reduced with the rigid extensions from the gusset plate connections.

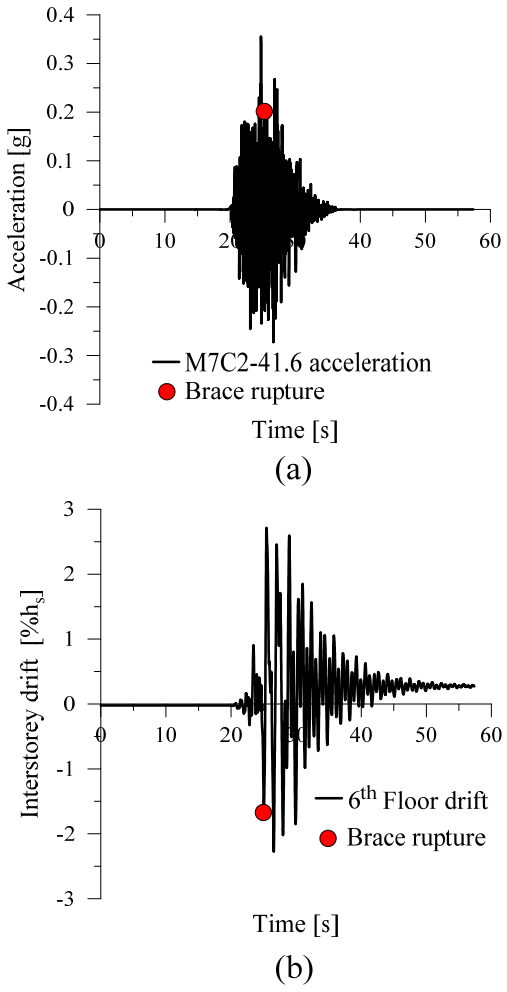

Figure 5.16 Top floor brace rupture due to low-cycle fatigue under simulated ground motion M7C2-41.6 scaled to CP limit state: (a) ground motion acceleration; (b) 6th floor interstorey drift.

Similar with the 3Q building, performance levels corresponding to a given earthquake hazard level, can be defined on the computed IDA curves by acceptable ranges of deformation demand on structural and nonstructural components which imply probable levels of damage. Hence, the response of CBF (E-W) expressed as the 50th and 84th fractiles of the recorded engineering demand

parameters such as: interstorey drift (δ_{max}), residual drift ($\delta_{max.res}$) and floor acceleration (a_{max}) resulted for each performance levels (*IO*, *LS*, *CP*) are illustrated in **Figure 5.17**. As depicted, the overall damage is concentrated at the top floors especially for: *collapse prevention* and *life safety* performance levels. In addition, the maximum floor acceleration, a_{max}, was added in order to assess the failure of acceleration-sensitive nonstructural components.

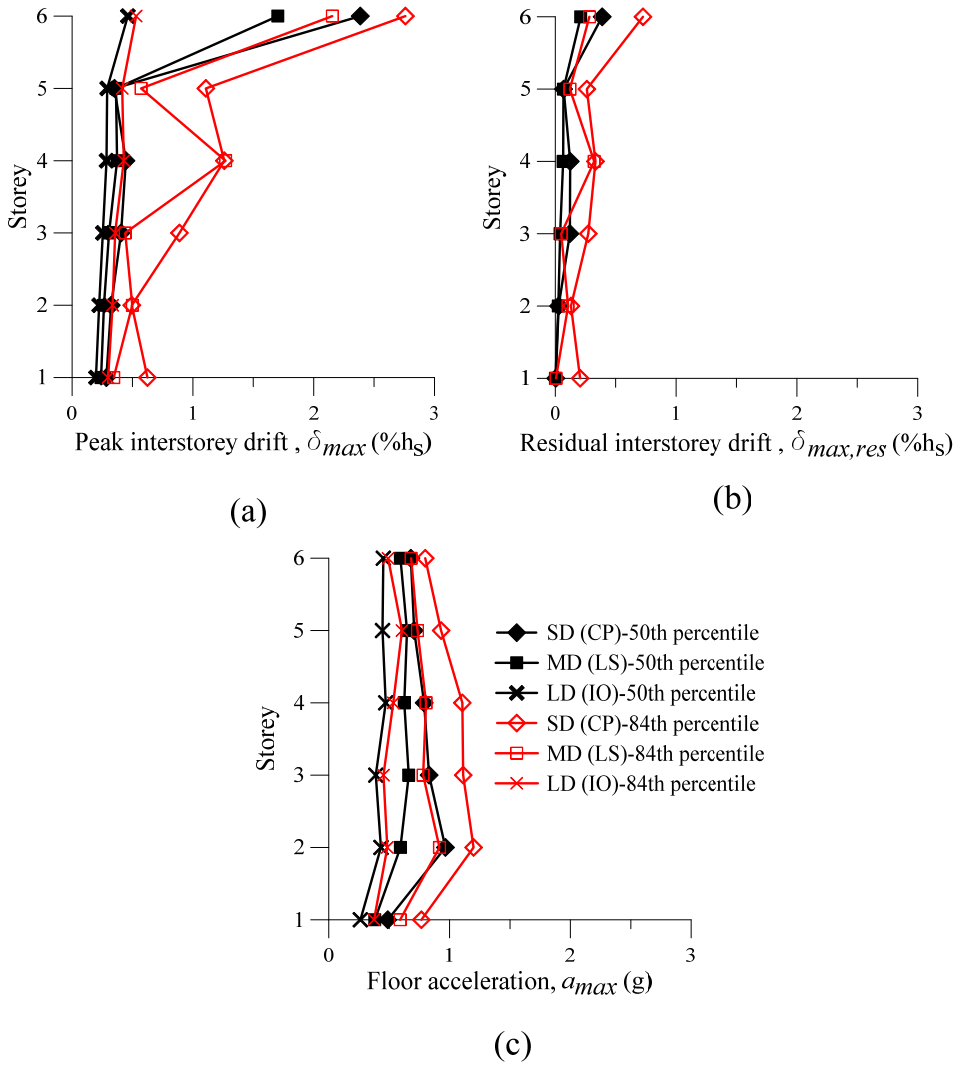

Figure 5.17 The 50th and 84th percentile of EDP of 6Q (E-W) computed from IDA for performance levels (IO, LS, CP) : (a) Peak interstorey drift; (b) Residual interstorey drift; (c) Floor acceleration. (Legend: *SD-Severe damage*; *MD- Moderate damage*; *LD- Light Damage*)

5.3.4. IDA results for the CBF in N-S direction (6Q)

The IDA curves for the retrofitted 6Q building (E-W direction) are illustrated in **Figure 5.18** with red line. The response is similar with that resulted in E-W direction and the performance of retrofitted building was significantly improved.

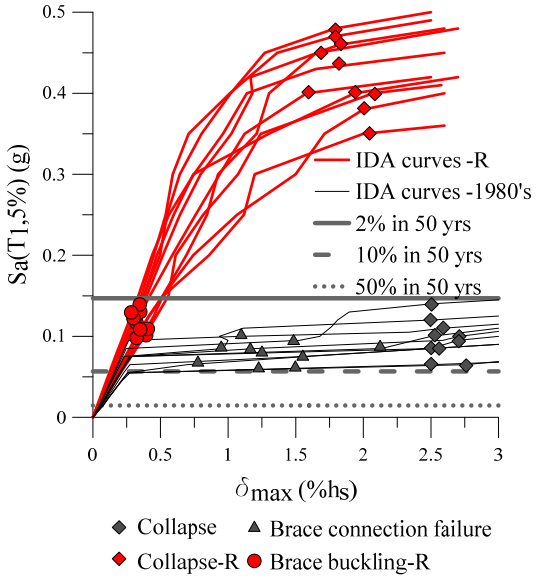

Figure 5.18 IDA curves of existing and retrofitted CBFs in N-S direction (6Q)

As illustrated in the above figure, the first brace buckling of the post-retrofit 6-storey building was initiated at a spectral acceleration of 0.12g while the collapse points are scattered above the current code demand (i.e. 2% in 50 years hazard level). It is noted that the damage concentration in the case of CBF in N-S direction was observed at the upper floors (e.g. 6^{th} to 3^{rd}). The most vulnerable column was found to be the middle one as illustrated in **Figure 5.19** which represents a print screen from OpenSees analysis with the response of the frame under S8.EN1 ground motion corresponding to CP limit state.

An example of column failure is shown in **Figure 5.20** where the axial load and bending moment of the ground floor middle column were recorded from time-history analysis in order to calculate the interaction ratio. Thus, the pairs of M_f/M_{rx} and C_f/C_{ry}, resulted after running a historical ground motion (i.e. S8.EN1) scaled to CP limit state prove that the middle columns do not possess sufficient axial compression and bending capacity, leading to dynamic instability due to P-Δ effects.

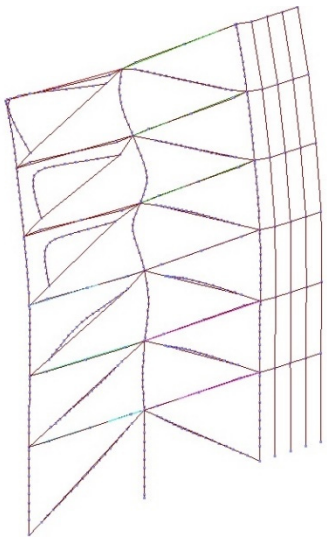

Figure 5.19 Behavior of the CBF from N-S direction under S8.EN1 ground motion scaled to CP level (6Q building)

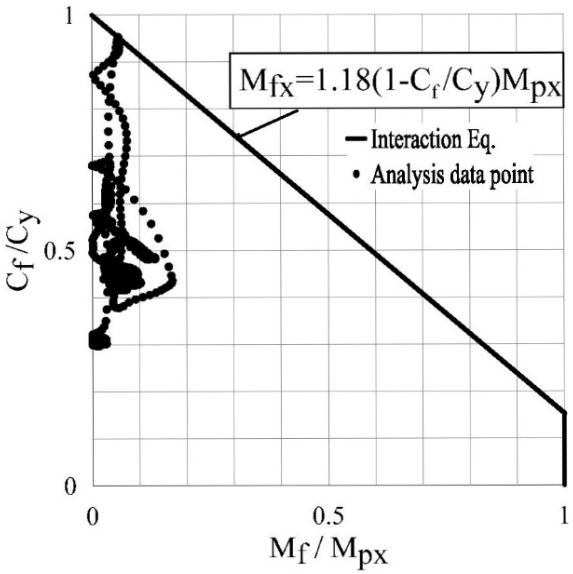

Figure 5.20 Axial load – bending moment interaction diagram, for ground floor middle column, under S8.EN1 ground motion scaled to CP limit state

5.3.4.1. Seismic Response of the CBF in N-S direction (6Q)

An example of CBF braces behaviour corresponding to *CP* is depicted in **Figure 5.21** and **Figure 5.22** for the upper and bottom three floor braces, respectively. As illustrated, all braces are able to dissipate energy while exhibiting several tension-compression excursions, especially at the top floors braces.

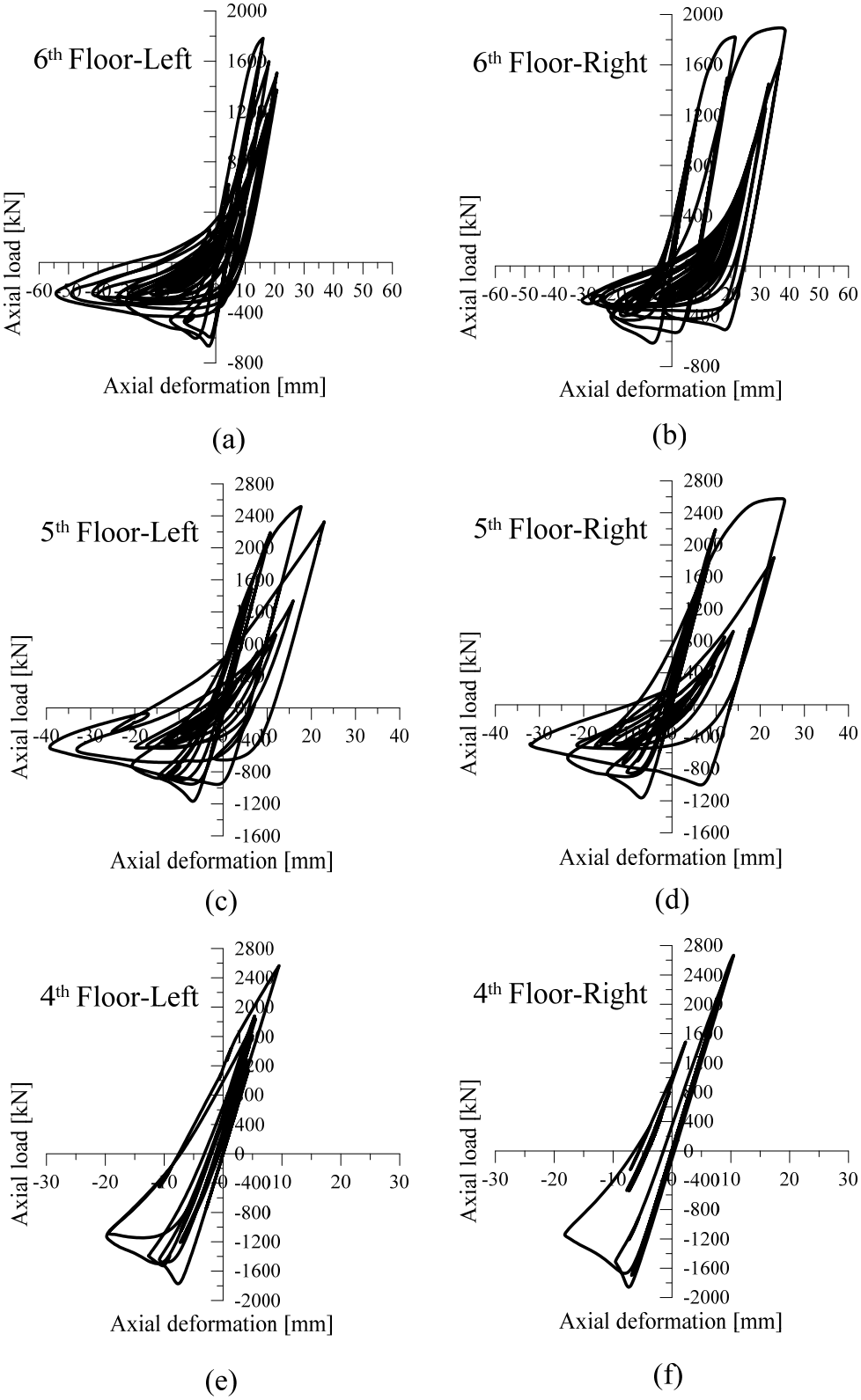

Figure 5.21 Hysteretic response of CBF braces of the 6th- 4th floor (N-S direction) under M7C2-41.6 ground motion scaled to the CP limit state (6Q).

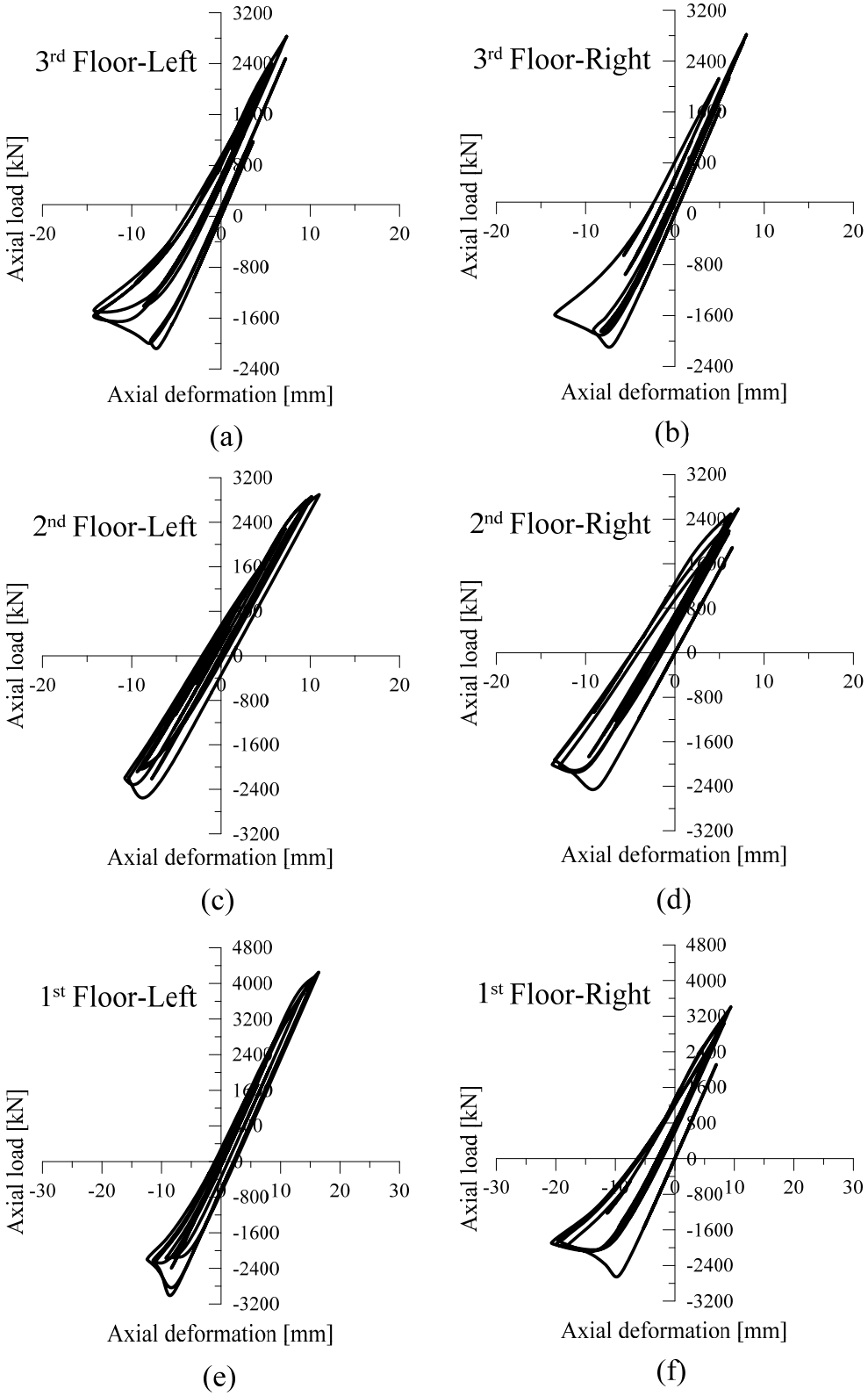

Figure 5.22 Hysteretic response of CBF braces of 3rd- 1st floor (N-S direction) under M7C2-41.6 ground motion scaled to CP limit state (6Q).

It is noted that brace fracture failure due to low-cycle fatigue is the desirable failure mode, and was observed only at the 6-storey CBF in the E-W direction. Similar with the E-W direction and with the 3Q building, the 50th and 84th fractiles of the recorded engineering demand parameters such as: interstorey drift (δ_{max}), residual drift ($\delta_{max.res}$) and floor acceleration (a_{max}) resulted for each performance levels (*IO*, *LS*, *CP*) are illustrated in **Figure 5.23**. As depicted the overall damage is concentrated at the top floors especially for: *collapse prevention* and *life safety* performance levels. In addition, the maximum floor acceleration, a_{max}, was added in order to assess the failure of acceleration-sensitive nonstructural components.

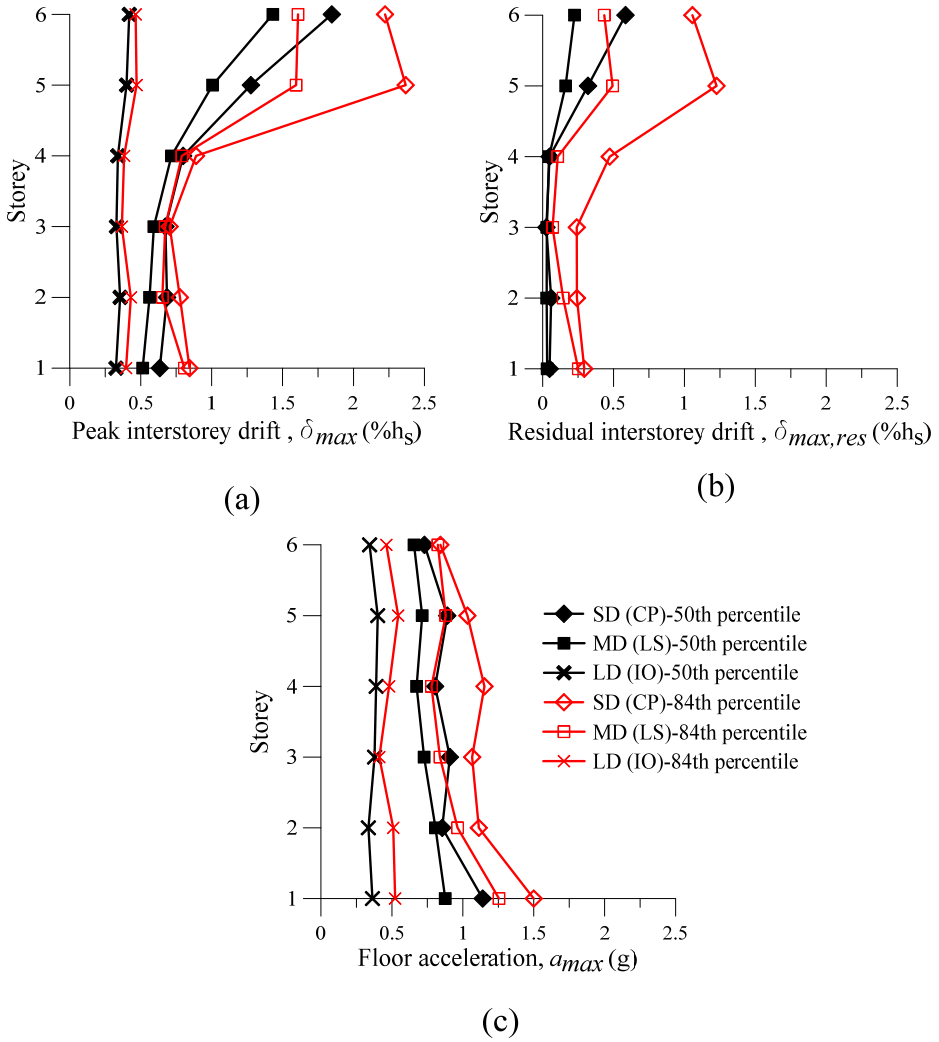

Figure 5.23 The 50th and 84th percentile of EDP of 6Q (N-S) computed from IDA for performance levels (IO, LS, CP): (a) Peak interstorey drift; (b) Residual interstorey drift; (c) Floor acceleration. (Legend: *SD-Severe damage*; *MD- Moderate damage*; *LD- Light Damage*)

5.3.5. Collapse Margin Ratio for the retrofitted buildings located in Quebec City

As previously stated in *Section 4.4.3.3*, the CMR is the ratio between the median collapse capacity, $\hat{S}_{CT}$ and maximum design ground motion intensity S_{MT}. It is noted that the maximum design ground motion intensity is obtained from the response spectrum of the design level ground motions (2% in 50 years) which corresponds to the fundamental period, T_1 given in **Table 5.20**. The median collapse capacity of the ten ground motions $\hat{S}_{CT,}$ and the CMR are given in **Table 5.21** for both 3- and 6-storey buildings located in Quebec City. As illustrated in the table, all CMR ratios are larger than *1.0*, which means the performance of retrofitted buildings has significantly improved and the retrofit action was efficient. Note that the selection of retrofit technique depends on the level of expected building performance. Thus, a higher performance level translates into extended retrofit actions. Unlike the Moment Resisting Frames (MRF), the CBF buildings are not prone to large interstorey drifts, being more suitable for moderate seismic zones.

Table 5.21 Collapse Margin Ratio for the retrofitted buildings located in Quebec City

ID	E-W direction		N-S direction	
	$\hat{S}_{CT,}$ *(g)*	**CMR**	$\hat{S}_{CT,}$ *(g)*	**CMR**
3Q	0.600	**1.96**	0.630	**2.30**
6Q	0.275	**1.47**	0.410	**2.70**

5.4. Fragility Analysis for the buildings located in Quebec City

A key factor to describe the seismic performance also the risk assessment of structures is *fragility*, a term that describes the probability of failure to meet a performance level as a function of demand on the system. In addition, the fragility analysis can also be used to determine probabilistic safety margins against specific identified events for decision purposes (Wen et al., 2004). On the other hand, the fragility not only defines the probability of exceeding pre-defined damage states but also is required for estimating expected or maximum probable losses, in order to quantify the buildings resilience.

In this study, fragility functions were derived from parameters estimated using IDA curves. Thus, fragility curves corresponding to different damage levels were derived for the structural system using **Eq. (2.24)**. As described in *Section 2.5.3* of this thesis, the fragility is assumed to follow a lognormal cumulative distribution, which is defined by a median value and a dispersion. Because

the concept of risk involves hazard, there is a level of uncertainty in the response of the buildings, due to the inherent randomness in the ground motion itself concerning: peak intensity, time-varying amplitude, duration, as well as frequency content besides the local design and construction practices. For fragility analysis of buildings located in Quebec City two sources of uncertainties were incorporated: aleatoric uncertainty and epistemic uncertainty (Ellingwood et al., 2007). Aleatoric uncertainty measures the inherent randomness in the seismic capacity of the structure while epistemic uncertainty depends on the quality of the analysis and supporting databases. More specifically, the value of β_R in **Eq. (2.24)** was replaced by the square root of the sum of the squares of β_{RR} and β_{RU}, where β_{RR} is the aleatoric component of uncertainty given in **Eq. (2.26)** and β_{RU} is the modeling (epistemic) uncertainty taken as *0.20*, as suggested by Ellingwood et al. (2007). Note that sources of uncertainties in structural material properties were not considered. The computation of fragility curves as well as of β_{RR} is presented in detail in the following sub-sections for each studied building.

5.4.1. Fragility results for the structural components of the 3-st CBF in E-W direction (3Q)

In order to calculate the aleatoric uncertainty (β_{RR}) for the CBF frames in E-W direction, **Eq. (2.26)** was used. As depicted, β_{RR} depends on the uncertainty in capacity of the structure (βc) which in turn depends on the considered Performance Level. In addition, the aleatoric uncertainty also depends on the seismic demand uncertainty calculated from the nonlinear time history analysis. To calculate the seismic demand uncertainty, $\beta_{D|Sa}$, the N generated paired values $\{(IM_i, \delta_{max.i}), i = 1,..., N\}$ for each of the defined performance levels (e.g. *IO, LS, CP*) were identified from IDA curves. Herein, N is the number of selected ground motions. Because of the highly nonlinear nature and large scatter of the response due to record-to-record variation, a nonlinear regression analysis of the power-law form given in **Eq. (2.27)** was used to assess $\beta_{D|Sa}$. A logarithmic transform of **Eq. (2.27)** reduces it to a linear form as given in **Eq. (2.28)**, where a and b are constants which can be determined using a simple linear regression analysis. Note that the engineering demand parameter used to generate the IDA curves was the maximum interstorey drift δ_{max}, while the *IM* selected for this study was the 5% damped spectral acceleration at the structure first mode period ($Sa(T_1, 5\%)$).

For example, **Figure 5.24(a)** illustrates the results for the retrofitted CBFs in E-W direction where the response for different performance levels (*IO*, *LS* and *CP*) are plotted using different symbols.

It is noted that the vertical axis was plotted using δ_{max} and not the logarithm of δ_{max}. According to the calculations, for the CBF in E-W direction, $a=4.6$, $b=1.55$ while $\beta_{D|Sa}=0.36$. Additionally, the value of βc was considered 0.25 similar with the value used by Ellingwood et al. (2007). Substituting all the values into **Eq. (2.25)** the resulted total dispersion is $\beta_R=0.48$. Fragility curves for the structural components derived for the studied CBF are given in **Figure 5.24(b)**. Three damage states were considered such as: light damage (*LD*), moderate damage (*MD*), and severe damage (*SD*) which were defined using the recommended δ_{max} values given in **Figure 2.10**. As illustrated in **Figure 5.24(b)** the results clearly show that the existing pre-retrofitted building is vulnerable to earthquakes while the vulnerability decreased significantly after the retrofit action. Note that for 2% in 50 years hazard level, the associated spectral acceleration value is $S_a=0.3g$ while for 10% in 50 years $S_a=0.124g$.

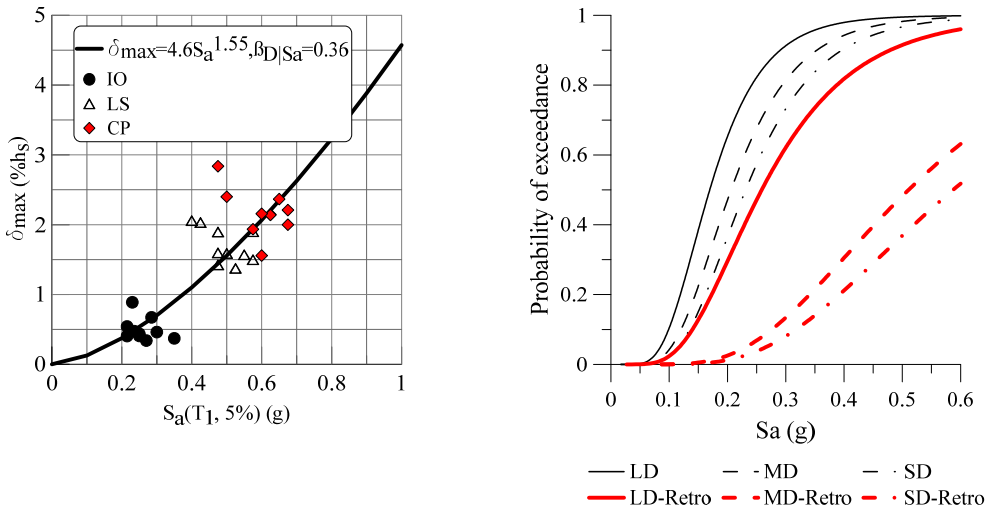

(a) (b)

Figure 5.24 Fragility of the structural components for the CBF in E-W direction (3Q): (a) Regression analysis for the retrofitted 3Q building; (b) Fragility curves;

Because the existing building designed according to 1980s code has a non-ductile behavior and brittle failure of brace-to-frame connections leads to collapse, the seismic demand uncertainty is hard to be estimated and large uncertainty value can be predicted. For this reason, according to FEMA P695, the total uncertainty for the pre-retrofitted building was assumed 0.625.

5.4.2. Fragility results for the structural components of the 3-st CBF in N-S direction (3Q)

For retrofitted CBF in N-S direction, based on the regression analysis illustrated in **Figure 5.25(a)**, the resulted parameters for the power-law function are: $a=3.5$, $b= 1.43$ while $\beta_{D|Sa}= 0.28$. Similar with the response of CBF in E-W direction, the value for the uncertainty in capacity of the structure was taken as $\beta c=0.25$, thus the value for the aleatoric uncertainty is $\beta_{RR}=0.38$. Substituting all the values into **Eq. (2.25),** the resulted total dispersion is $\beta_R= 0.43$. Fragility curves for the structural components computed for the studied CBF in N-S direction are given in **Figure 5.25(b)**. Thus, the same damage states as those presented for CBF in E-W direction were considered: light damage (*LD*), moderate damage (*MD*), and severe damage (*SD*). As depicted, the results clearly showed that the existing pre-retrofitted building is vulnerable to earthquakes while the vulnerability decreased significantly after the retrofit action. Note that for 2% in 50 years hazard level, the associated spectral acceleration value is $S_a= 0.27g$ while for 10% in 50 years $S_a= 0.11g$.

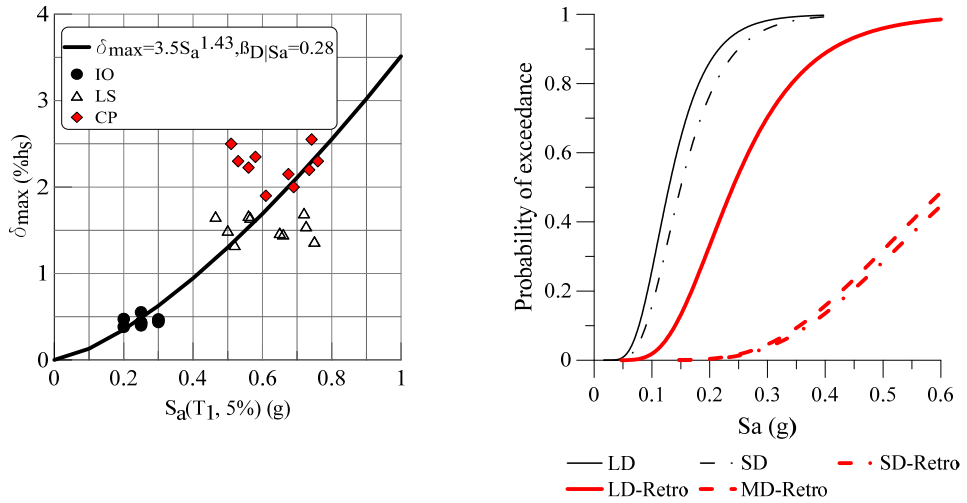

(a) (b)

Figure 5.25 Fragility of the structural components for the CBF in N-S direction (3Q): (a) Regression analysis for the retrofitted 3Q building; (b) Fragility curves;

Because the existing building is non-ductile and brittle failure of brace-to-frame connections leads to collapse, there is no a gradual transition between damage states. Thus, the *SD* state occurs suddenly after the structure response exceeds the elastic state characterised by *LD*. Hence, the existing CBF structure is not able to sustain large inelastic response and the pre-retrofitted building is prone to *SD* right after *LD*. For this reason, the seismic demand uncertainty is hard to be estimated and large uncertainty value can be predicted. It is noted that for the pre-retrofitted building the total uncertainty was assumed *0.625* according to FEMA P695.

5.4.3. Fragility results for the structural components of the 6-st CBF in E-W direction (6Q)

For the 6-storey building frames from the E-W direction, based on the regression analysis shown in **Figure 5.26(a)**, the resulted parameters for the power-law function are: $a= 11.4$, $b= 1.38$ while $\beta_{D|Sa}= 0.54$. Similar with the 3Q building the value for the uncertainty in capacity of the structure was taken as $\beta c= 0.25$, thus the value for the aleatoric uncertainty resulted $\beta_{RR}= 0.59$. Substituting all the values into **Eq. (2.25)** the resulted total dispersion is $\beta_R= 0.63$. Fragility curves for structural components computed for the studied CBF in E-W direction are given in **Figure 5.26(b)**, for the same damage states: light damage (*LD*), moderate damage (*MD*), and severe damage (*SD*). As depicted, the results clearly show that the existing pre-retrofitted building is prone to severe damage when subjected to current code intensities, while the vulnerability decreased significantly after the retrofit action. Note that for 2% in 50 years hazard level, the associated spectral acceleration value is $S_a= 0.19g$ while for 10% in 50 years, $S_a= 0.074g$. Similar with the 3Q building, for the pre-retrofitted building the total uncertainty was assumed *0.625* according to FEMA P695.

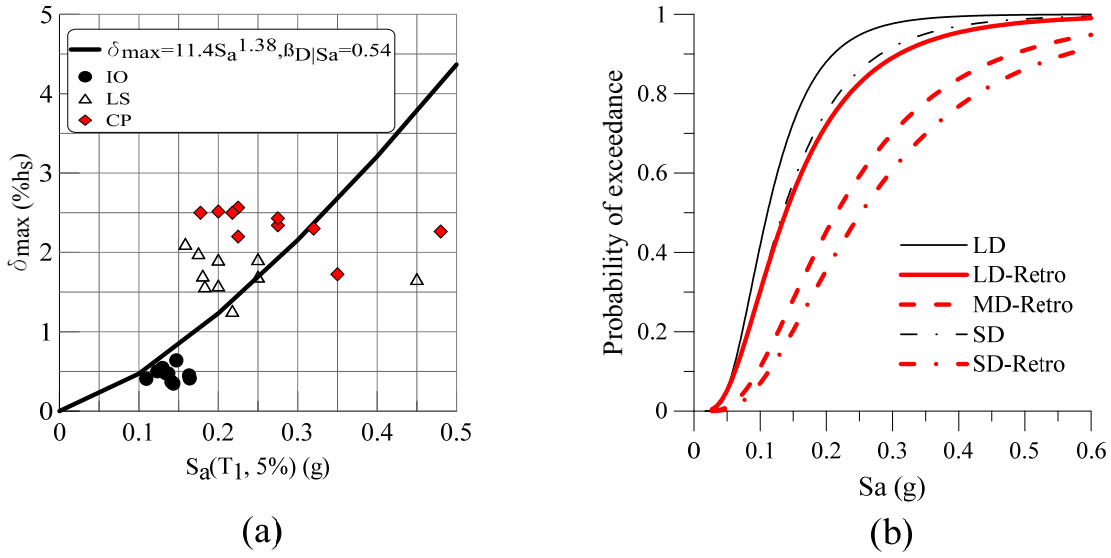

Figure 5.26 Fragility of the structural components for CBF in E-W direction (6Q):
(a) Regression analysis for the retrofitted building; (b) Fragility curves

5.4.4. Fragility results for the structural components of the 6-st CBF in N-S direction (6Q)

For the frames from the N-S direction, based on the regression analysis shown in **Figure 5.27(a)**, the resulted parameters for the power-law function are: $a= 5.8$, $b= 1.28$ while $\beta_{D|Sa}= 0.21$. Similar with the CBF in E-W direction, the value for the uncertainty in capacity of the structure was taken

as $\beta c = 0.25$, thus the value for the aleatoric uncertainty resulted $\beta_{RR} = 0.33$. Substituting all the values into **Eq. (2.25)** the resulted total dispersion is $\beta_R = 0.38$. Therefore, the structural fragility curves computed for the studied CBF in N-S direction are given in **Figure 5.27(b)**, for the previously defined damage states (light damage - *LD*, moderate damage - *MD*, severe damage - *SD*). As depicted, the results clearly show that the existing pre-retrofitted building is prone to severe damage when subjected to current code intensities, while the vulnerability decreased significantly after the retrofit action. Note that for 2% in 50 years hazard level, the associated spectral acceleration value is $S_a = 0.15g$ while for 10% in 50 years $S_a = 0.057g$. Similar with the E-W direction, for the pre-retrofitted building, the total uncertainty was assumed *0.625* according to FEMA P695.

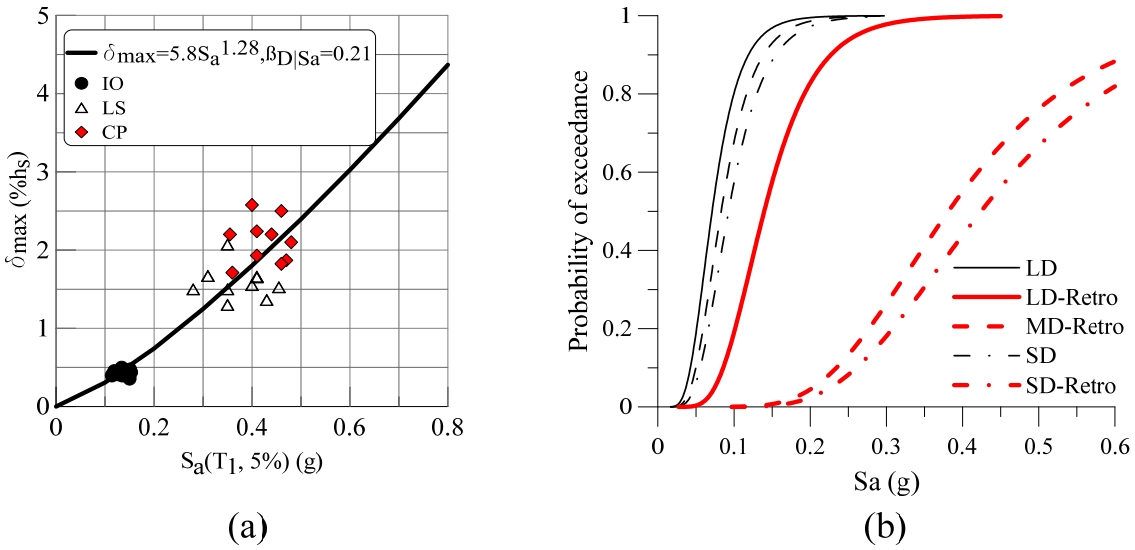

Figure 5.27 Fragility of the structural components for CBF in N-S direction (6Q):
(a) Regression analysis for the retrofitted building; (b) Fragility curves

5.5. Response of studied buildings (3Q, 6Q) in N-S and E-W directions

When the critical floor happens to be the bottom floor, the overall building failure is more likely to occur. Conversely, if the roof floor becomes unstable, it may be only a floor failure or partial collapse of the building. The median of peak interstorey drift, the median of peak residual interstorey drift and the median of peak floor acceleration resulted for the 3Q and 6Q buildings is given in **Table 5.22**.

Table 5.22 Median of peak: interstorey drift, residual interstorey drift and floor acceleration

Building ID (retrofitted)	IO			LS			CP		
	$\delta_{max.}$ *(%h_s)*	$\delta_{max\_res.}$ *(%h_s)*	$a_{max.}$ *(g)*	$\delta_{max.}$ *(%h_s)*	$\delta_{max\_res.}$ *(%h_s)*	$a_{max.}$ *(g)*	$\delta_{max.}$ *(%h_s)*	$\delta_{max\_res.}$ *(%h_s)*	$a_{max.}$ *(g)*
3Q E-W	0.45	0.08	0.49	1.59	0.41	0.72	2.15	0.74	0.80
3Q N-S	0.47	0.01	0.47	1.53	0.52	0.79	2.26	1.14	1.13
6Q E-W	0.46	0.08	0.50	1.70	0.15	0.69	2.39	0.30	1.04
6Q N-S	0.43	0.02	0.46	1.54	0.32	0.88	2.2	0.65	1.31

For better understanding the fragility of structural members showed in **Figure 5.24(b) –Figure 5.27(b)**, the probabilities of exceeding or reaching a given damage state corresponding to spectral accelerations for hazard levels of *2%/50 years* and *10%/50 year*s are listed in **Table 5.23**. It is noted that, damage probabilities due to *50%/50 years* hazard are close to zero because the excitations are low and are not represented.

Table 5.23 Damage probabilities for different hazard levels as resulted from fragility analysis for structural components

ID	2%/50yrs			10%/50yrs		
	LD (%)	MD (%)	SD (%)	LD (%)	MD (%)	SD (%)
3Q/ 3Q-R (E-W)	92/ 63	82/ 14	74/ 9	23/ 6	11/ 0	7/ 0
3Q/3Q-R (N-S)	96/ 62	NA/ 3	91/ 2	25/ 3	NA/ 0	15/ 0
6Q/ 6Q-R (E-W)	83/ 68	NA/ 42	70/ 33	17/ 16	NA/ 5	12/ 3
6Q/ 6Q-R (N-S)	95/ 55	89/ 0.6	84/0.3	23/ 0.9	13/ 0	8/ 0

As depicted in the above table, the probabilites for *LD* for the retrofitted buildings complying with the current code demand (NBCC 2010) are relatively larger compared with those for *MD* and *SD*. In addition, the probability for all retrofitted buildings to develop *SD* is bellow 10%, except for the E-W direction of the retrofitted 6-storey building wich has a probability of exceedance of 33%.

As previously stated, based on the results from the ESF procedure, both the 3- and the 6- storey buildings located in Quebec City and Vancouver showed deficiencies at the level of structural members, especially the buildings located in Vancouver. It is noted that Quebec City and Vancouver were in the same seismic zone based on the 1970 map, thus having the same demand

at that time. However, according to the current code, the seismic demand considerably increased (more than double). For this reason, applying a traditional retrofit method for the buildings located in Vancouver would not satisfy the *Basic Safety Objective* (Tirca et al., 2015). Thus, the required type of action is either building replacement or other enhanced retrofit strategies. It is suggested to double the number of CBFs such that the buildings located in Vancouver to pass the current code requirements.

5.6. Fragility curves for nonstructural components of retrofitted buildings

Similar with structural damage described by means of fragility curves depicted above, the same four damage states were used to describe nonstructural damage: *Very Light*, *Light*, *Moderate* and *Severe*. However, for this study, nonstructural damage was considered to be independent of the structural model building type (i.e. partitions, ceilings, cladding etc. were assumed to incur the same damage when subjected to the same interstorey drift or floor acceleration). Besides, damage to drift-sensitive nonstructural components can be described in general as a function of interstorey drift while for acceleration-sensitive components (e.g. mechanical equipment) damage was defined as a function of the floor acceleration. For this reason, the nonstructural building components, were grouped into drift-sensitive and acceleration sensitive component groups and damage functions for each group was assumed to be "typical" for each sub-components, according to the methodology given in HAZUS (FEMA, 2003).

In the same way with the fragility for structural elements, each nonstructural fragility curve was assumed to follow a lognormal cumulative distribution, which is characterized by a median value (mean) and a dispersion (β). Based on HAZUS methodology, the median values of fragility curves together with lognormal standard deviation (β) for each damage states and for each nonstructural building compnents defined as drif-sensitive and acceleration-sensitive are given in **Table 5.24** for the retrofitted low- and middle-rise steel braced frames office buildings. Note that, median values of nonstructural drift sensitive components fragility were based on building drift ratios that describe the threshold of damage states while the median values of acceleration-sensitive components were based on peak floor acceleration. On the other hand, the total variability of each nonstructural drift- and acceleration-sensitive damage state was modeled by the combination of three contributors to damage variability: uncertainty in the damage state threshold of nonstructural

components, variability in response-capacity of the model and uncertainty in the ground motion demand similarly with the total uncertainty for the structural elements.

Table 5.24 Drift- and acceleration-sensitive parameters of fragility curve for nonstructural components of retrofitted buildings

Building	Drift-Sensitive non-struct. components						Acc.-Sensitive non-struct. components					
	Light (*LD*)		Moderate (*MD*)		Severe (*SD*)		Light (*LD*)		Moderate (*MD*)		Severe (*SD*)	
	Mean (%)	β	Mean (%)	β	Mean (%)	β	Mean (g)	β	Mean (g)	β	Mean (g)	β
3Q	0.4	0.84	0.8	0.90	2.5	0.97	0.3	0.67	0.6	0.67	1.2	0.67
6Q	0.4	0.71	0.8	0.74	2.5	0.74	0.3	0.69	0.6	0.66	1.2	0.66

From the IDA, the mean values resulted for the interstorey drift for a seismic hazard level of 2% in 50 years were: *0.82%* and *0.46%* for the E-W and N-S direction of the 3Q building while for the 6Q building the interstorey drift values were: *1.5%* and *0.41%* respectively. Conversely, for the seismic hazard level of 10% in 50 years, the mean drift values were: *0.15%*, *0.17%*, *0.23%* and *0.15%* for 3Q in E-W, 3Q in N-S, 6Q in E-W and 6Q in N-S, respectively. Regarding the floor acceleration values, they were also extracted from IDA. Thus, for 2% in 50 years seismic demand the mean values were: *0.59g*, *0.50g*, *0.65g* and *0.45g* for each 3Q in E-W, 3Q in N-S, 6Q in E-W and 6Q in N-S, respectively. Furthermore, the floor acceleration values associated with 10% in 50 years hazard as resulted from IDA in the same order were: *0.23g*, *0.19g*, *0.37g* and *0.15g*. The fragility curves for drift- and acceleration- sensitive nonstructural components for each previously described damage state are illustrated in **Figure 5.28** and **Figure 5.29** for the 3- and 6-storey retrofitted buildings located in Quebec City, while the parameters of fragility curves for nonstructural components of retrofitted buildings are given in **Table 5.25**.

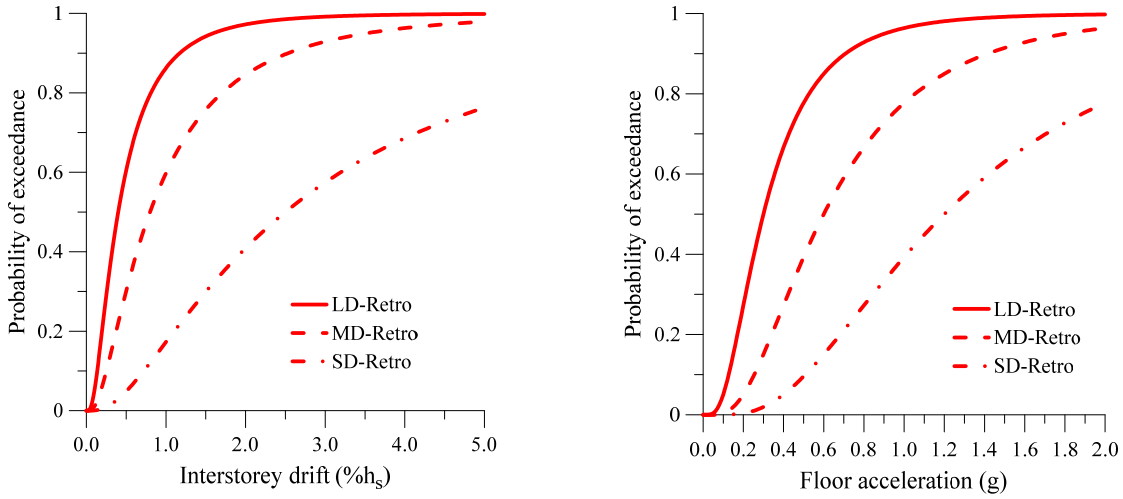

Figure 5.28 Fragility curves for Nonstructural components of the retrofitted 3-storey building located in Quebec City: (a) Drift-sensitive; (b) Acceleration-sensitive

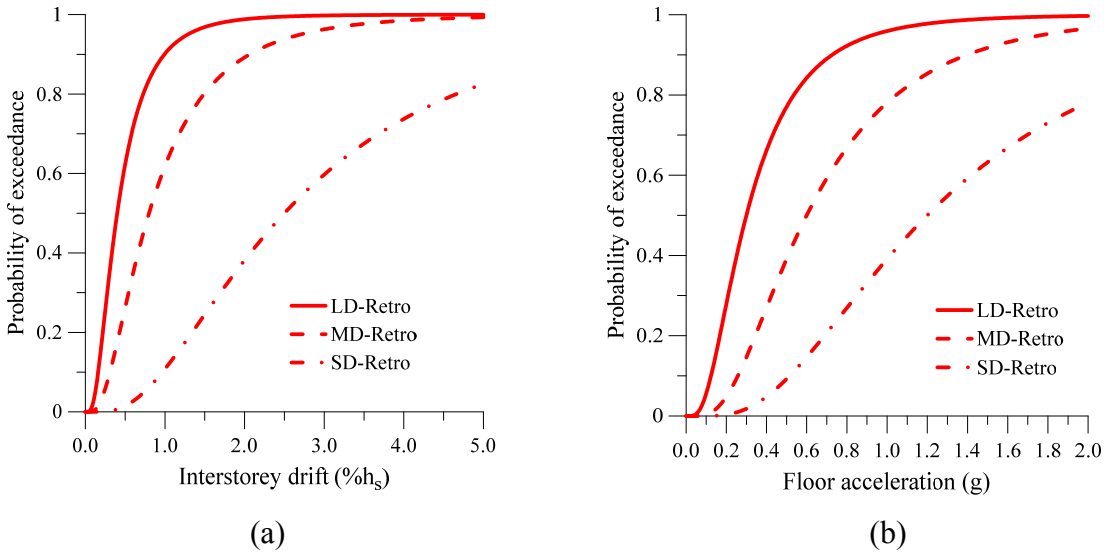

Figure 5.29 Fragility curves for Nonstructural components of the retrofitted 6-storey building located in Quebec City: (a) Drift-sensitive; (b) Acceleration-sensitive

For better understanding the fragility of nonstructural components, the probabilities of exceeding or reaching a given discrete damage state corresponding to spectral accelerations for hazard levels of *2%/50 years* and *10%/50 years* are listed in **Table 5.25** for the drift- sensitive components, while **Table 5.26** presents the probability at a given *discrete* damage state for acceleration-sensitive components. Note that this values were used further to estimate the total nonstructural losses.

Table 5.25 Damage probabilities for different hazard levels for drift-sensitive components

ID	2%/50yrs			10%/50yrs		
	LD (%)	MD (%)	SD (%)	LD (%)	MD (%)	SD (%)
3Q-R (E-W)	80.0	51.0	13.0	12.00	3.00	0.20
3Q-R (N-S)	56.6	26.9	4.04	15.42	4.30	0.30
6Q-R (E-W)	96.9	80.2	24.5	21.80	4.60	0.07
6Q-R (N-S)	51.4	18.3	0.73	8.40	1.20	0.007

Table 5.26 Damage probabilities for different hazard levels for acceleration-sensitive components

ID	2%/50yrs			10%/50yrs		
	LD (%)	MD (%)	SD (%)	LD (%)	MD (%)	SD (%)
3Q-R (E-W)	84.96	50.00	15.04	34.60	7.62	0.70
3Q-R (N-S)	77.70	39.30	9.60	27.25	5.00	0.40
6Q-R (E-W)	86.90	54.80	17.70	66.20	26.95	4.80
6Q-R (N-S)	72.16	33.15	6.90	15.80	1.80	0.08

5.7. Loss estimation and Recovery time for the retrofitted buildings located in Quebec City

Loss estimation, specifically the losses associated with extreme events- require some damage descriptors that can be translated into monetary terms. Because the concept of risk involves hazard, consequences and context, the loss estimation procedure by itself represents a source of uncertainty, however this has been taken into account in *Section 5.4*. In addition, earthquake losses are by their nature highly uncertain being different for each specific analysed scenario. As previously discussed in Chapter 2 (*Section 2.6*) the evaluation of resilience requires a loss estimation model and a recovery function model. Furthermore, in **Eq. (2.30)** which was used to calculate the buildings functionality, it can be seen that the loss function $L(I, T_{RE})$ is expressed as a function of earthquake intensity I and recovery time T_{RE}. Therefore, the total loss, L is composed of structural losses, L_S and nonstructural losses L_{NS}. The latter, are divided in four categories: i)

Direct economic losses $L_{NS,DE}$ (loss of content); ii) Direct casualties losses $L_{NS,DC}$; iii) Indirect economic losses $L_{NS,IE}$ (business interruption losses); iv) Indirect casualties losses $L_{NS,IC}$.

However, direct and indirect casualties losses (deaths, injuries), as well as the replacement of building contents, building relocation expenses, business interruption and others indirect economic losses were not considered in this study. Note that, complete structural losses are equivalent to the replacement cost of structure, while the structural repair cost refers to the replacement of structural components such as: connections, braces, beams and columns. Herein, the losses associated with the structural damage L_S, were evaluated using **Eq. (2.31)** that was adopted from HAZUS. A similar calculation was performed for nonstructural damage. Thus, nonstructural damage was broken down into drift- sensitive damage L_{NSD}, (partitions, exterior walls, ornamentation and glass) and acceleration-sensitive damage L_{NSA}, (damage to ceilings, mechanical and electrical equipment, piping and elevators) as depicted in **Eq. (5.3)**. Similar with the structural losses, the calculation of drift and acceleration sensitive damage is given by **Eq. (5.4**) and **Eq. (5.5)**, respectively.

$$L_{NS} = L_{NSD} + L_{NSA} \tag{5.3}$$

$$L_{NSD} = \sum_1^N CNSD_{DS} = BRC * \sum_1^N PONSD_{DS} * RCD_{DS} \tag{5.4}$$

$$L_{\mathrm{NSA}} = \sum_1^N CNSA_{DS} = BRC * \sum_1^N PONSA_{DS} * RCA_{DS} \tag{5.5}$$

where: $CNSD_{DS}$ and $CNSA_{DS}$ represent the cost of nonstructural drift and acceleration sensitive damage, respectively, computed for the considered damage state; BRC is the building replacement cost; $PONSD_{DS}$ and $PONSA_{DS}$ is the probability of being in nonstructural drift and acceleration sensitive damage state DS, respectively; RCD_{DS} and RCA_{DS} represent the drift and acceleration sensitive repair and replacement ratio in damage state DS; while N is the number of damage states considered.

The repair cost ratios for each damage state are given in **Table 5.27**, for structural and nonstructural components (drift- and acceleration-sensitive). Additionally, the total cost of building damage (total loss) was obtained as a summation of the structural and nonstructural damage.

Table 5.27 Structural and NonStructural repair cost ratios (in % of building replacement cost)

Components	Damage State , *DS*		
	Light	Moderate	Severe
Structural	0.4	9.6	19.2
Nonstructural drift sensitive	0.7	3.3	16.4
Nonstructural acc. sensitive	0.9	4.8	14.4

The office building replacement cost *BRC,* was calculated based on the average cost per square meter (*$/m²*) estimated for representative projects according to Toronto market (RS Means, 2014). Herein, costs are presented based on gross floor area, and are shown for each building element with its proportion to the total cost in **Table 5.28**. As depicted, the structural cost represents around *15%* from the total building cost while for the nonstructural elements and other fees is close to *85%*. Note that, the gross floor area of studied buildings was taken as *1800 m²* whereas the total average cost per square meter was taken as *$2,402.10*.

Table 5.28 Gross building replacement cost

Description	Components	% of total	Cost / square meter ($/m²)		
			Low	Average	High
Corporate office complex	Structure	15.1		361.52	
	Exterior enclosure	14.2		340.17	
	Interior construction	19.6		470.42	
	Mechanical	20.0		481.53	
	Electrical	19.1		459.84	
	General requirements & fee	12.0		288.62	
Complete Building		100.0	2161.89	**2402.10**	2642.31

For this study, the total losses were evaluated for the retrofitted buildings subjected to 2%/50years earthquake. For comparison purpose, losses due to earthquakes with probability of exceedance of *10%/50 years* were also calculated and are presented in **Table 5.29.** It is noted that, probability for structural components exceeding or reaching a given damage state (*DS) POSTR*$_{DS}$, was determined based on fragility curves, i.e., results given in **Table 5.23** were used to determine the probability at a given *discrete* damage state. On the other hand, the probabilities of being in nonstructural

damage state (e.g. $PONSD_{DS}$ and $PONSA_{DS}$) are listed in **Table 5.25** and **Table 5.26** for both drift- and acceleration-sensitive components. Additionally, the losses due to damage to structural, drift- and acceleration-sensitive nonstructural components of retrofitted buildings, together with the estimated *BRC* are also given in **Table 5.29**.

As depicted from **Table 5.29**, losses computed for the 6-story building are relatively large compared to the 3-storey building. Such a result is expected because higher buildings are normally more vulnerable to earthquakes than lower buildings. Another remark is about the total cost of buildings due to damage from *10%/50 years* hazard level, which is significantly smaller than that from *2%/50 years* earthquakes.

Table 5.29 Estimated losses for the retrofitted buildings

Hazard level	ID	Replacement cost, *BRC*	Structural losses, L_s	Nonstructural losses		Total cost
				Drift-sensitive components, L_{NSD}	Acc.-sensitive components, L_{NSA}	
2%/50 yrs	3Q-EW	$12,971,340	$431,167	$567,496	$730,442	$1,729,106
	3Q-NS	$12,971,340	$119,336	$252,482	$539,621	$911,439
	6Q-EW	$25,942,680	$2,760,301	$1,904,945	$1,638,358	$6,303,604
	6Q-NS	$25,942,680	$86,960	$281,068	$874,849	$1,242,877
10%/50 yrs	3Q-EW	$12,971,340	$3,113	$27,992	$102,728	$133,833
	3Q-NS	$12,971,340	$1,557	$38,789	$71,453	$111,799
	6Q-EW	$25,942,680	$290,558	$81,522	$694,382	$1,066,462
	6Q-NS	$25,942,680	$934	$25,825	$62,794	$89,553

Regarding the recovery path and recovery time $T_{RE,}$ these parameters are essential in order to evaluate the seismic resilience. The latter, was defined (Cimellaro et al., 2006) as the necessary time to restore the functionality of a system to a desired level which can be the same, bellow, or better than the original one. However, this parameter is a random variable with large uncertainties which depends on the level of hazard (earthquake intensity), building type considered and the availability of resources. For this reason, the recovery time is the most difficult quantity to predict. Despite these difficulties, HAZUS provides a basis for establishing the building recovery (repair) time in crude terms, assuming that within one year everything returns to normal. Moreover, according to the methodology given in HAZUS the time to repair a damaged building can be

divided in two parts: construction and clean-up time, and necessary time to obtain financing, permits, etc. Thus, the maximum recovery time for corporate office buildings was adjusted from *360 days* to *480 days*.

5.8. Seismic Resilience of studied buildings

The building resilience is a non-dimensional parameter (percentage) that measures its remaining functionality after an earthquake. Further, as documented in Chapter 2 (*Section 2.6*), the evaluation of seismic resilience is based on an analytical function which includes the total losses and the recovery path over a period of interest. For instance, resilience is *100%* for an un-damaged system, whereas for total loss of the building the resilience is *0%*.

The control period of the system T_{LC} was assumed 50 years and usually is based on the decision maker's interest in the evaluation of the retrofit alternatives. In addition, the control time is consistent with the period used for the hazard level (i.e. 2% probability of exceedance in 50 years), and the retrofit strategy becomes more cost-effective. In general, seismic losses associated with the hazard level are larger if longer control periods are considered.

5.8.1. Resilience of the retrofitted 3-storey building located in Quebec City

In **Figure 5.30** is summarized the quantification of seismic resilience for the retrofitted 3-storey office building located in Quebec City. As depicted the vertical axis represents the building functionality calculated based on losses associated with structural and nonstructural elements according to **Eq. (2.30)**, while the horizontal axis represents the time (days). **Figure 5.30(a)** and **Figure 5.30(b)** show the functionality of the retrofitted building for E-W and N-S direction, respectively- when subjected to a 2% in 50 years earthquake intensity. On the other hand, **Figure 5.30 (c)** and **Figure 5.30(d)** represent the functionality when the building is exposed to a hazard level of 10% in 50 years. Graphically, the resilience was defined as the normalised area under the *Q(t)* function. Important to note that, before the extreme event happens, the building functionality was *100%*. Subsequently, at the initial time when the extreme event happens (selected arbitrary as 30 days) the functionality drops to a certain value depending on the total amount of losses. It is noted that, in the functionality expression given in **Eq. (2.30)**, *H(t)* is the Heaviside step function whose value is zero for negative argument and one for positive argument. In addition, all the functionality curves illustrated in **Figure 5.30** were constructed based on the exponential recovery function given in **Eq. (2.32(ii))**. The exponential recovery function is usually used when the

response of the society is fast at the beginning having the adequate resources, however the rapidity of recovery decreases in time.

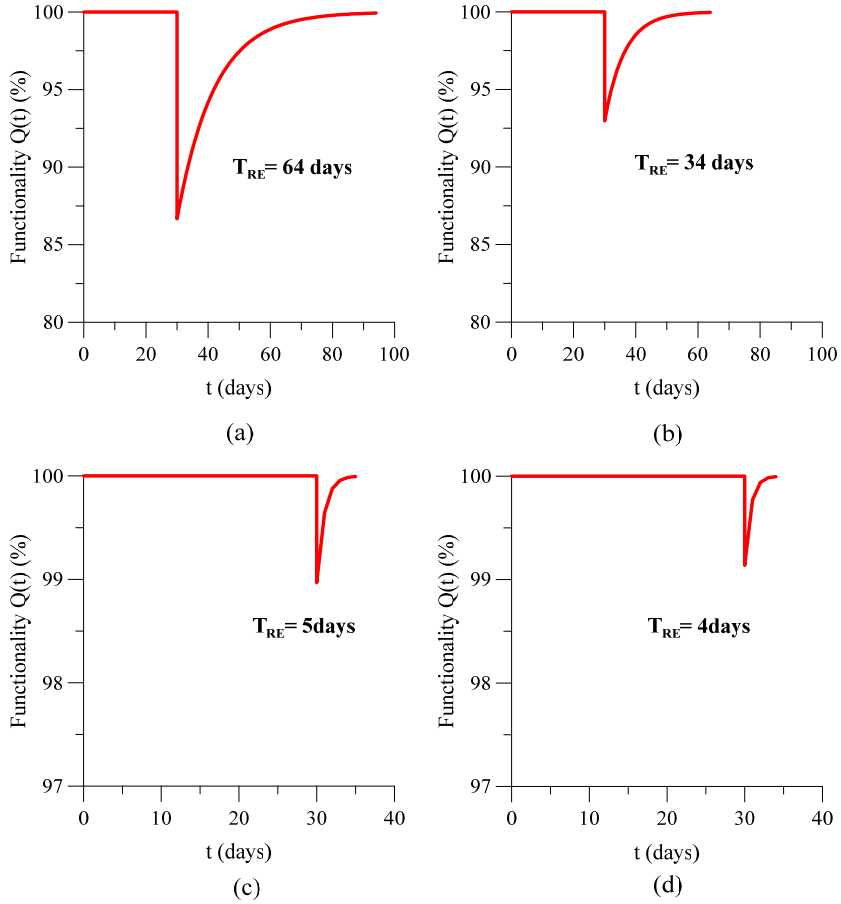

Figure 5.30 Functionality curves of retrofitted 3-storey building having exponential recovery: (a) E-W direction-2%/50 yrs; (b) N-S direction-2%/50 yrs; (c) E-W direction-10%/50 yrs; (d) N-S direction-10%/50 yrs

As depicted from **Figure 5.30**, the 3-storey retrofitted building located in Quebec City has a functionality of *86.67%* and *92.97%* for *2% in 50 years* hazard level for the E-W and N-S direction, respectively. Moreover if the building is subjected to more often earthquakes having the probability of exceedance of *10% in 50 years*, the building shows a functionality of *98.97%* and *99.14%* for E-W and N-S direction, respectively. It can be seen that the retrofit strategy was efficient for both directions of the 3-storey building. Moreover, due to the retrofit level, the damages for the N-S direction are smaller compared with the E-W direction for *2%/50 years* hazard, while for *10%/50* years the difference is very small.

5.8.2. Resilience of the retrofitted 6-storey building located in Quebec City

Similar with the 3-storey buildings, the functionality curves for the retrofitted 6-storey buildings located in Quebec City were computed based on **Eq. (2.30)** and are illustrated in **Figure 5.31** having an exponential recovery. **Figure 5.31(a)** and **Figure 5.31(b)** show the functionality of the retrofitted building for E-W and N-S direction, respectively, when subjected to a *2% in 50 years* earthquake intensity. On the other hand, **Figure 5.31(c)** and **Figure 5.31(d)** represent the functionality when the building is exposed to a hazard level of *10% in 50 years*. Graphically, the resilience was defined as the normalised area under the *Q(t)* function. In addition, the recovery time T_{RE} is also given for each case.

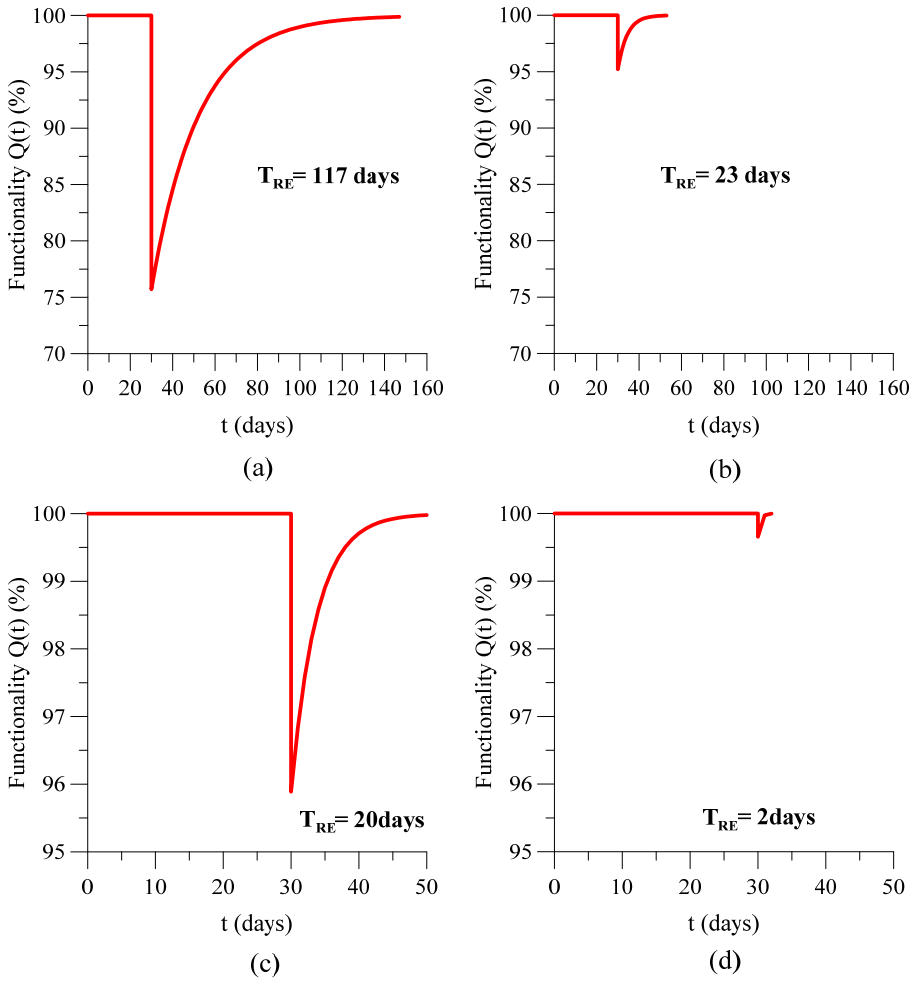

Figure 5.31 Functionality curves of retrofitted 6-storey building having exponential recovery: (a) E-W direction-2%/50 yrs; (b) N-S direction-2%/50 yrs; (c) E-W direction-10%/50 yrs; (d) N-S direction-10%/50 yrs

As depicted from **Figure 5.31,** the 6-storey retrofitted building located in Quebec City has a functionality of *75.70%* and *95.20%* for *2% in 50 years* hazard level for the E-W and N-S direction, respectively. In addition, if the building is subjected to more often earthquakes having the probability of exceedance of *10% in 50 years*, the building shows a functionality of *95.89%* and *99.65%* for E-W and N-S direction, respectively. It can be seen that the retrofit strategy was efficient for both directions of the 6-storey building. Furthermore, due to the increased retrofit level, the damages for the N-S direction are smaller compared with the E-W direction for both *2%/50 years* and *10%/50* years hazard levels.

5.8.3. Resilience attributes

According to Cimellaro et al., (2009) the resilience attributes are: *Rapidity*, *Robustness*, *Redundancy* and *Resourcefulness*. While the influence of rapidity and robustness is clear, the influence of the other two parameters is more complex, being strongly coupled, yet very difficult to quantify because they depend on human factors and available resources. For that reason no analytical function is provided at this time. It is noted that the estimated recovery time, T_{RE} for *2%/50 years* and *10%/50 years* earthquake hazard levels, as well as the computed resilience attributes: rapidity (υ) and robustness (R) are given for retrofitted buildings in **Table 5.30**.

Regarding the rapidity attribute corresponding to *2%/50 years*, the post-retrofit 3-storey Quebec City building shows a slightly larger average recovery rate in E-W direction when compared with the N-S direction (*0.207 %* vs *0.205%*). On the other hand, for *10%/50 years* hazard level, the rapidity is larger for the post-retrofit 3Q building in the N-S direction. Conversely, the 6-storey building shows a higher recovery rate if subjected to a *2% /50 years* earthquake intensity in the N-S direction. However for a *10% /50 years* hazard level, the rapidity increases when the 6Q building is analysed in the E-W direction. Note that, the rapidity represents the slope of the functionality curve during the recovery time and is expressed as the average recovery rate in time: L/T_{RE} (in percentage), where L is the total loss after the extreme event and T_{RE} represents the recovery time.

Table 5.30 Summary of the results from resilience analysis for the retrofitted buildings

ID	2% /50 years			10% /50 years		
	T_{RE} (days)	$\upsilon(\%)$	R (%)	T_{RE} (days)	$\upsilon(\%)$	R (%)
3Q-EW	64	0.2072	86.67	5	0.205	98.97
3Q-NS	34	0.2056	92.97	4	0.215	99.14
6Q-EW	117	0.2066	75.70	20	0.204	95.88
6Q-NS	23	0.2073	95.20	2	0.172	99.65

Another key attribute of resilience can be identified in system's robustness which can be seen as the ability to withstand a given demand without suffering degradation, and can be referred to the residual functionality right after the extreme event. As depicted in **Table 5.30**, the CBFs in N-S direction shows a larger robustness when compared with those in the E-W direction for both 3- and 6-storey buildings. These results can be attributed in general to the increased level of retrofit for CBFs in the N-S direction.

5.9. Conclusions

This Chapter describes the retrofit strategies, the computation of fragility curves and the quantification of seismic resilience of the investigated buildings, built and designed according to 1980 code and standards (i.e. NBCC 1980, S16.1-19878). Therefore, a typical Rehabilitation Objective Class for the office buildings is Basic Safety. To reach the Basic Safety objective, the retrofitted building should sustain light damage from *10%/50 years* earthquakes and severe damage from *2%/50 years* hazard level. In this study, the selected retrofit strategy consists of local replacement and strengthening of structural components (e.g. replacement of brace-to-frame connections, columns and beam strengthening by adding cover plates, etc.). Such measures increased the strength of the components and allowed them to resist the demanded earthquake forces before failure.

The performance level corresponding to a given earthquake hazard level, was defined on each IDA curve by acceptable ranges of deformation demand on structural and nonstructural components, which imply probable levels of damage. Damage levels namely*: Very Light, Light, Moderate* and *Severe* vary as a continuous function of building deformation and are associated to the defined building performance levels in the same order: *Operational* (*O*), *Immediate Occupancy* (*IO*) , *Life Safety* (*LS*) and *Collapse Prevention* (*CP*).

The evaluation of damage (losses) was expressed in terms of economic cost (*$*) or repair cost ratio defined as being the ratio of the cost of retrofit and reinstatement of building to the cost of fully replaced. However, the estimation of losses was reported according to the previously defined damage states (e.g. very light, light, etc) expressed as a function of the associated structural and nonstructural building performance. Moreover, the nonstructural components are drift-sensitive (e.g. partition walls, cladding, ceiling, etc.) and acceleration-sensitive (e.g. mechanical equipment, piping, electrical system, etc.). Additionally, the physical structural and nonstructural losses were

determined based on the methodology given in HAZUS. According to the results, losses computed for the 6-story building are relatively large compared to the 3-storey building. Such a result is expected because higher buildings are normally more vulnerable to earthquakes than lower buildings. On the other hand, resilience is a non-dimensional parameter that measures the remaining functionality of the building after an earthquake. In this study, an exponential recovery function was selected for the retrofitted 3- and 6-storey office buildings located in Quebec City. Due to the increased retrofit level for both 3- and 6-storey buildings, the N-S direction shows a larger resilience when compared to the E-W direction. In addition, the resilience attributes were also discussed in this Chapter.

CHAPTER 6. CONCLUSIONS AND RECOMMENDATIONS

6.1. Conclusions

This study was conducted to evaluate the seismic resilience of existing low- and middle-rise CBF office buildings designed in agreement with NBCC 1980 and CSA/S16.1-M78. The following findings are reported:

- To assess the vulnerability of office buildings designed in 1980 and their post-retrofit performance, as well as their seismic resilience, a specifically developed methodology that employs the performance-based method (ASCE/SEI 41-13) and the general framework developed by Cimellaro et al. (2006, 2009), was proposed. In this light, damage levels were defined as function of performance levels associated to earthquake intensity. Further, fragility curves were derived from IDA curves obtained from time-history analyses and both aleatoric and epistemic uncertainties were considered. Seismic resilience was calculated by combining system fragility with loss estimation and recovery model. Only structural and nonstructural losses were considered. The required Rehabilitation Objective Class for office buildings was selected to be *Basic Safety*.
- To quantify the seismic vulnerability of the studied buildings, two identical 3- and 6-storey fictitious office buildings located in Quebec City (Qc.) and Vancouver (B.C.) were selected for investigation. In addition, two seismic force resisting systems consisting of CBFs with chevron braces and CBFs with tension-compression diagonal braces were studied in order to identify possible seismic deficiencies. Therefore, the assessment process was based on the equivalent static force procedure followed by nonlinear time-history analysis by means of IDA. However, because the percentage of steel CBF buildings in B.C. is low, the 3- and 6-storey buildings located in Vancouver were considered for comparison purposes and were assessed only according to the equivalent static force procedure.
- Important to note that Quebec City and Vancouver were in the same seismic zone 3 according to the first probabilistic seismic map released in NBCC 1970. Under these circumstances, the design lateral seismic force for Quebec buildings is slightly larger than the buildings located in Vancouver; the only difference consisted in the snow load at the roof level and implicitly on the seismic weight. As a consequence, all members and the brace-to-frame connections of the 3V and the 6V buildings were selected to be the same as for the 3Q and 6Q buildings, respectively. Additionally, the existing building stock, designed and built prior to the 1970 was

proportioned to carry gravity and wind load only, while that constructed between 1970 and 1985 was designed to withstand lower seismic forces in comparison with those required by the current code.

- According to the results from the equivalent static force procedure, both the 3- and the 6- storey buildings located in Quebec City and Vancouver showed deficiencies at the level of structural members, especially the buildings located in Vancouver. It is noted that the CSA/S16.1-M78 standard did not include any special provisions for ductile structures. Therefore, brace-to-frame gusset plate connections were designed to factored loads resulted from load combinations and were verified to carry 50% of the factored tension or compression brace member resistance, depending on which one governs the brace member design. Thus, under large demands, the brace-to-frame connections cannot sustain the development of braces tensile capacity and are prone to failure due to shearing of the welds causing the storey mechanism formation. Besides, the brace-to-frame connections, do not have the $2t_g$ clearance necessary for the plastic hinge formation when braces buckle out-of-plane.
- A numerical 3D model was developed through OpenSees framework which is capable of simulating: yielding, buckling and fracture of braces, also hinging of beams and columns. The model was subjected to a suit of 10 ground motions incremented up to collapse. In the model, nonlinear beam-column elements with distributed plasticity and fiber cross-section formulation were assigned to braces, beams and columns. Additionally, a fatigue model calibrated based on experimental test results was assigned to braces in order to capture the fracture due to low-cycle fatigue, while the brace-to-frame connections properties were modeled as rotational springs.
- The IDA methodology proposed by Vamvatsikos and Cornell (2002) was performed only on buildings located in Quebec City using OpenSees framework. As reported from IDA curves, all studied buildings experienced collapse when subjected to ground motion intensities in agreement with the current code demand, whereas under 50% in 50 years hazard level, which was the seismic demand according to NBCC 1980, all buildings show adequate strength having the response in the elastic range. In addition, the studied office buildings have a collapse safety bellow *1.0*, especially for the N-S direction of the 3Q building. It is noted that the results from the equivalent static force procedure were consistent with the results from nonlinear time-history analysis. Thus, the retrofit action was required.

- A typical Rehabilitation Objective Class for the office buildings is *Basic Safety*. To reach the *Basic Safety* objective, the retrofitted building should sustain light damage from *10%/50 years* earthquakes and severe damage from *2%/50 years* hazard level. In this study, the selected retrofit strategy consisted of local replacement and strengthening of structural components (e.g. replacement of brace-to-frame connections, columns and beam strengthening by adding cover plates, etc.). Thus, after increasing the gusset plate capacity, braces were able to dissipate energy through yielding and buckling. In addition, brace fracture failure due to low-cycle fatigue which is a desirable failure mode, was observed only at the 6-storey CBF in the E-W direction. However, brace failure is strongly dependent on the effective length and width of the member. It can be summarized that the retrofit action was efficient and the *CMR* was larger than *1.0* for both 3- and 6-storey buildings located in Quebec City.
- Conversely, for the Vancouver buildings, besides the retrofit action, it is suggested to double the number of CBFs in order to pass the current code requirements.
- Using collapse data obtained from IDA results, a collapse fragility function was defined through a cumulative distribution function (CDF), relating the ground motion intensity to the probability of collapse, incorporating two sources of uncertainties. Thus, the performance levels were defined such as: Immediate Occupancy at the end of the elastic segment when the first brace experienced buckling, Life Safety when the maximum residual interstorey drift reached $0.5\%h_s$ and Collapse Prevention when the slope of the IDA curve approaches zero. Three damage levels were associated to each performance level such as: *light (LD)*, *moderate* (*MD*) and *severe (SD)* damage. The results clearly show that existing pre-retrofitted buildings are at high risk to earthquakes while the vulnerability significantly decreased after the retrofit action. As expected, the probabilites for *LD* for the retrofitted buildings complying with the current code demand (NBCC 2010) are relatively larger compared with those for *MD* and *SD*. In addition, the probability for all retrofitted buildings to develop *SD* is bellow 10%, except for the retrofitted 6-storey building (E-W direction) wich has a probability of exceedance of *33%*.
- Resilience was characterized by performance metrics such as: fragility, loss and recovery functions developed for structural systems designed to withstand the corresponding seismic hazard level. Thus, the physical structural and nonstructural losses were determined based on the methodology given in HAZUS. According to the results, losses computed for the 6-storey building are relatively large compared to the 3-storey building. Such a result is expected because

higher buildings are normally more vulnerable to earthquakes than lower buildings. In this study, an exponential recovery function was selected for the retrofitted 3- and 6-storey office buildings located in Quebec City. Due to the increased retrofit level of 3- and 6-storey CBFs, the CBFs in the N-S direction showed larger resilience when compared to CBFs in the E-W direction.

- Regarding the resilience attributes, the retrofitted 3-storey building (E-W) located in Quebec City showed a slightly larger average recovery rate for a hazard of *2%/50 years* when compared with 3-storey building (N-S) direction. On the other hand, for *10%/50 years* hazard level, the rapidity is larger for CBF building (N-S direction). Conversely, the 6-storey building in N-S direction showed a higher recovery rate when subjected to *2% /50 years* earthquake intensity. However, for *10% /50 years* hazard level, the rapidity was larger when loading was applied in the E-W direction. Referring to system's robustness, the N-S direction of CBF building shows a larger robustness when compared with the E-W direction for both 3- and 6-storey buildings.

Summarizing, improving the seismic resilience of office buildings helps community to limit the impact of business disruption in the aftermath of earthquake and to recover immediately after the event. By identifying the level of structural deficiency and the hierarchy of potential failure modes, this study is an effective tool that may be used by decision makers to reduce the cost of a potential seismic disaster.

6.2. Recommendations and Future Work

Many assumptions have been made in the proposed methodology for quantification of seismic resilience of CBF office buildings, designed and built prior to modern code provisions in Canada. The following are specific recommendations for further research regarding the topic:

- More comprehensive and precise investigations of braced frames would lead further to better understanding of systems behaviour, especially for the seismically deficient brace-to-frame connections. Experimental tests conducted on existing brace-to-frame connections are required in order to better calibrate the numerical model and to validate the failure hierarchy.
- Various building heights and different seismic zones should be considered. In addition, other types of seismic force resisting systems and different brace configurations (X-bracing, split X, etc.) are also suggested.
- Different retrofit strategies can be proposed and further investigated. It is suggested the use of passive energy dissipation devices. These devices added in-line with diagonal braces of CBF

buildings, are able to reduce the demand of the primary frame system and the intersorey drift, as well as, possess the property of controlling the exposure to damage of nonstructural components including the building envelope.

- Further research can be addressed on the validation of the model with real cases, since this study evaluates the behaviour of fictitious buildings. Performing an assessment and a retrofit study for an existing steel building structure would be very useful to account for possible limitations and other un-predicted situations, which have not been considered in this study.
- It was found that IDA is very sensitive to the applied incremental step. Thus, a smaller step would capture more accurately the seismic response of structure. When subjected to different ground motions, the model behaviour is very difficult to predict, thus "softening" and "hardening" are very common behaviours of structure due to changing in global stiffness. However, a smaller incremental step would lead to an increase in the computational time.
- Additional improvements can be made on the OpenSees braced frame model used in this study. For example, it is suggested that the non-convergence of the time-integration scheme is the safest numerical equivalent of the actual dynamic collapse, but this in turn can suffer from the quality of the numerical code, stepping or even round-off error of the integration process. Further research should be carried out in order to revise these assumptions and to develop a more robust model. The interaction between SFRS and the gravity system should be carefully investigated and considered in future studies.
- Uncertainties are inherent in any loss estimation methodology. This methodology evaluates only building risk assessment without any evaluation of the recovery plan and only a gross estimation of the recovery time. Many assumptions and interpretations had to be made in this study. However, the formulations presented in this study include the physical structural and nonstructural damage using a simple probabilistic model, combined in a single resilience measure for pre- and post-retrofit office buildings. Further research should be carried out in order to verify or revise these assumptions. A more complex damage estimation model which incorporates: casualties due to structural damage including fatalities, losses due to business interruption and relocation expenses, other economic and social impacts are suggested in order to have an accurate resilience quantification model.
- Extending this framework to other public facilities such as: hospitals, schools, military buildings, bridges, dams, utility lifelines it is also suggested.

REFERENCES

Adams, J., and Atkinson, G.M. (2003). "Development of seismic hazard maps for the proposed 2005 edition of the National Building Code of Canada." *Can. J. Civ. Eng.*, 30, 255-271.

Aguero, A., Izvernari, C., Tremblay, R. (2006). "Modelling of the seismic response of concentrically braced steel frames using the opensees analysis environment." *International journal of Advanced Steel Construction*, 2(3), 242-274.

American Institute of Steel Construction (AISC). (2005). "Specification for structural steel buildings." *ANSI/AISC 360-05*, AISC, Chicago.

American Society of Civil Engineers (ASCE). (2013). "Seismic rehabilitation of existing buildings." *ASCE/SEI Standard 41-13*, Reston, VA, in press.

Applied Technology Council (ATC). (1985). "Earthquake damage evaluation data for California." *Report ATC-13*, Redwood City, CA.

Atkinson, G. (2009). "Earthquake time histories compatible with the 2005 National Building Code of Canada uniform hazard spectrum." *Can. Journal of Civil Eng.*, 36(6), 991-1000.

Baker, J. W., and Cornell, C. A. (2005). "A vector-valued ground motion intensity measure consisting of spectral acceleration and epsilon." *Earthquake Engineering & Structural Dynamics*, 34(10), 1193–1217.

Bankoff, G., Frerks, G., and Hilhorst, D., eds. (2004). "Mapping vulnerability: disasters, development and people." Earthscan, London, UK.

Bruneau, M., and Reinhorn, A. M. (2004). "Seismic resilience of communities conceptualization and operationalization*." Proc., Int. Workshop on Performance-Based Seismic Design Concepts and Implementation*, P. Fajfar and H. Krawinkler, eds., Bled, Slovenia, 161–172.

Bruneau, M., and Reinhorn, A. M. (2007). "Exploring the concept of seismic resilience for acute care facilities." *Earthquake Spectra*, 28(1), 41–62.

Bruneau, M., Chang, S., Eguchi, R. T., Lee, G. C., O'Rourke, T., Reinhorn, A. M., Shinozuka, M., Tierney, K., Wallace, W. A., and von Winterfeldt, D. (2003). "A framework to quantitatively assess and enhance the seismic resilience of communities." *EERI Spectra Journal*, 19(4), 733-752.

Canadian Standards Association (CSA). (1978). "Limit states design of steel structures." *S16.1-M78 Standard*, CSA, Toronto, ON.

Canadian Standards Association (CSA). (2009). "Design of steel structures." *S16-09 Standard*, CSA, Toronto, ON.

Canadian Standards Association (CSA). (2014). "Design of Steel Structures", *S16.1-14 Standard*, CSA, Mississauga, ON.

Computers and Structures, Inc., (CSI). (2011). "ETABS Nonlinear- extended 3d analysis of building systems, version 9.7.4 (computer program)." CSI, Berkeley, CA.

Cassidy, J.F., Rogers, G.C., Lamontagne, M., Halchuk, S., and Adams, J. (2010). "Canada's earthquakes: 'The Good, the Bad, and the Ugly'." *J. Geo. Assoc. of Canada*, 37(1).

Chang, S., and Shinozuka, M. (2004). "Measuring improvements in the disaster resilience of communities." *Earthquake Spectra*, 20 (3), 739–755.

Cimellaro, G. P., Fumo, C., Reinhorn, A. M., and Bruneau, M. (2009). "Quantification of disaster resilience for health care facilities." *MCEER Technical Report*, the State University of New York, Buffalo, NY.

Cimellaro, G. P., Reinhorn, A. M., and Bruneau, M. (2006). "Quantification of seismic resilience." *Proc., 8th Nat. Conf. of Earthquake Eng.*, paper No. 1094, San Francisco, CA.

Cimellaro, G. P., Reinhorn, A. M., and Bruneau, M. (2010). "Seismic resilience of a hospital system." *Structure and Infrastructure Eng.*, 6(1–2), 127–144.

Coburn, A. and Spence, R. (2002). "Earthquake protection." J. Wiley & Sons, Chichester, UK.

Ellingwood, B., Celik, O.C., Kinali, K. (2007). "Fragility assessment of building structural systems in Mid-America." *Earthquake Engineering & Structural Dynamics*, 36, 1935-1952.

Federal Emergency Management Agency (FEMA). (2000). "Recommended seismic design criteria for new steel moment-frame buildings." *FEMA 350*, prepared by the SAC Joint Venture, Washington, D. C.

Federal Emergency Management Agency (FEMA). (2003). "Multi-hazard loss estimation methodology: Earthquake model, *HAZUS-MR4."* Technical manual, *FEMA*, Washington, D.C.

Federal Emergency Management Agency (FEMA). (2006). "Techniques for the seismic rehabilitation of existing buildings." *FEMA 547*, prepared by Rutheford & Chekene Consulting Engineers under contract with National Institute of Standards and Technology (NIST), Washington, D. C.

Federal Emergency Management Agency (FEMA). (2009). "Quantification of building seismic performance factors." *FEMA P695*, prepared by Applied Technology Council (ATC), Washington, D.C.

Haddad, M., and Tremblay, R. (2006). "Influence of connection design on the inelastic seismic response of HSS steel bracing members", *Proc., 11th Int. Symp and IIW Int. Conf. on Tubular Struct.*, Quebec City , Qc, 639-649.

Hsiao, P.C., Lehman, D., Roeder, C. (2013). "A model to simulate special concentrically braced frames beyond brace fracture." *J. of Earthquake Eng. and Struct. Dynamics*, 42, 182-200.

Heidebrecht, A. C. (1999). "Concerning the seismic level of protection for the next edition of NBCC." Canadian National Committee of Earthquake Engineering (CANCEE), *NRCC*, Ottawa, ON.

Heidebrecht, A. C. (2003). "Overview of seismic provisions of the proposed 2005 edition of NBC." Can. J. Civ. Eng., 30, 241-254.

Ibarra, L., Medina, R., and Krawinkler, H. (2002). "Collapse assessment of deteriorating SDOF systems." *Conf. Proc., 12th European Conference on Earthquake Engineering*, London, Elsevier Science Ltd, paper no. 665.

Jiang, Y., Balazadeh-Minouei, Y., Tremblay, R., Koboevic, S., Tirca, L. (2012). "Seismic assessment of existing steel braced frames designed in accordance with the 1980 Canadian code provisions." *Proc., STESSA 2012*, Santiago, Chile.

Jiang, Y. (2013). "Numerical and experimental seismic assessment and retrofit of steel tension-only double angle braced frames designed before the implementation of detailing provisions for ductile seismic response." *M.Sc. thesis*, Ecole Polytechnique de Montreal, Montreal, QC.

Kafali, C., and Grigoriu, M. (2005). "Rehabilitation decision analysis." *Proc., 9th Int. Conf. on Structural Safety and Reliability*, *ICOSSAR'05*, Rome, Italy.

Lamarche, C.P., and Tremblay, R. (2008). "Accounting for residual stresses in the seismic stability of nonlinear beam-column elements with cross-section fiber discretization", *Annual Stability Conference*, 59-78.

Lamontagne, M., Halchuk, S., Cassidy, J.F., and Rogers, G.C. (2008). "Significant Canadian earthquakes of the period 1600-2006." *Seismological Research Letters*, 79(2), 211-223.

Liu, J., and Astaneh-Asl, A. (2004). "Moment-rotation parameters for composite shear tab connections." *J. of Struct. Engineering*, ASCE, 130(9), 1371-1380.

Luco, N., and Cornell, C. A. (2007). "Structure-specific scalar intensity measures for near source and ordinary earthquake ground motions." *Earthquake Spectra*, 23(2), 357-392.

Martinez-Saucedo, G. and Packer, J.A. (2009). "Static design recommendations for slotted end HSS connections in tension." *Journal of Structural Engineering*, ASCE, 135(7), 797-805.

Mazzoni, S., McKenna, F., Scott, M., Fenves, G.L. et al., (2013). "Open system for earthquake engineering simulation." *OpenSees software*, Pacific Earthquake Engineering Research Center (PEER), University of California, Berkeley.

Milne, W.G., and Davenport, A.G. (1969). "Distribution of earthquake risk in Canada." *Seismological Soc. of America*, 59, 729-754.

Mitchell, D., Paultre, P., Tinawi, R., Saatcioglu, M., Tremblay, R., Elwood, K., Adams, J., and DeVall, R. (2010). "Evolution of seismic design provisions in the National Building Code of Canada." *Can. J. Civ. Eng.*, 37(9), 1157-1170.

National Earthquake Hazard Reduction Program (NEHRP). (1997). "Recommended provisions for seismic regulations for new buildings and other structures." *NEHRP*, Building Seismic Safety Council, Washington, D.C.

National Research Council of Canada (NRCC). (1941). (1953). (1960). (1965). (1970). (1975). (1980). (1985). (2005). (2010). "National Building Code of Canada." Associate Committee on the National Building Code, *NRCC*, Ottawa, ON.

Natural Resources Canada (NRC). (2012). "Survey of commercial and institutional energy used buildings." *Detailed statistical report*, Canada.

Packer, J.A. (2014). "Shear lag in slotted-end HSS welded connections." *Technical note*, Steel Tube Institute.

Pillai, S. (1974). "Beam-columns of hollow structural sections" *Can. J. Civ. Eng.*, 1(2), 194-198.

Reyes, J.C., and Kalkan, E. (2011). "How many records should be used in an ASCE/SEI-7 ground motion scaling procedure?." *Earthquake Spectra*, 28(3), 1223-1242.

RS Means Co. (2014). "Yardsticks for costing 2014: Canadian construction cost data". RS Means Co., Kingston, MA, 158-163.

Thornton, W.A. (1984). "Bracing connections for heavy constructions" *Eng. J. AISC*, 21(3), 139-148.

Tirca, L., Chen, L. (2014). "Numerical simulation of inelastic cyclic response of HSS braces upon fracture." *Int. Journal of Advanced Steel Construction*, 10(4), 442-462.

Tirca, L., Chen, L. (2013). "Simulating the seismic response of concentrically braced frames using physical theory brace models." *Open Journal of Civil Engineering*, 3(2), 69-81.

Tirca, L., Serban, O., Wang, M. Z., and Di Modica, D. (2013). "Incremental dynamic analysis of existing steel braced frame buildings in moderate seismic zones." *Proc., Structures Congress*, ASCE, Reston, VA, 2298-2309.

Tirca, L., Serban, O. M., Lin L., Wang, M., Lin, N. (2015). "Improving the seismic resilience of existing braced frame office buildings." *Journal of Structural Engineering* (ASCE), Special issue: Resilience-based design of structures and infra-structures, Guest editors: Cimellaro, G.P., Duenas-Osarios, L., and Reinhorn, A., in press.

Tremblay, R., Bruneau, M., Driver, R., Metten, A., Montgomery, C.J., and Rogers, C. (2010). "Seismic design of steel structures in accordance with CSA-S16-09." *Proc., 9th US Nat. and 10th Can. Conf. on Earthquake Eng.,* Toronto, ON, Paper No. 1768.

Tremblay, R. (2011). "Evolution of the Canadian seismic design provisions for steel structures since 1989." *Proc. CSCE Annual Conf.,* Ottawa, ON.

Vamvatsikos, D., and Cornell, C. A. (2002). “Incremental dynamic analysis”. *Earthq. Eng. Struct. Dynamics*, 31(3), 491-514.

Viti, S., Cimellaro, G. P., and Reinhorn, A. M. (2006). “Retrofit of a hospital through strength reduction and enhanced damping.” *Smart Structures and Systems*, 2(4), 339-355.

Wang, M. (2014). “Seismic fragility assessment of pre- and post-retrofit 1980s concentrically braced frame office buildings in moderate seismic zones.” *MASc thesis*, Building Civil and Environmental Engineering, Concordia University, Montreal.

Wen, Y.K., Ellingwood, B., and Bracci, J. (2004). “Vulnerability function framework for consequence-based engineering.” *MAE Center Project DS-4 Report*.

Whitmore, R.E. (1952). “Experimental investigation of stresses in gusset plates.” Bulletin No.16, *Engineering Experiment Station*, University of Tennessee.

APPENDIX I.

Gravity column design of 3-storey CBF building located in Quebec City

Table I.1 Live load reduction for interior column S4 (A_t= *56.25 m²*)

St	A_t	DL	LL	O	DL_{floor}	ΣDL_{floor}	ΣA_t	f	ΣLL/occ.		LL_{tot}	C_{fmax}
	m²	*kPa*	*kPa*	-	*kN*	*kN*	*m²*	-	*(0)*	*(1)*	*kN*	*kN*
3	56.25	3.0	2.24	0	168.8	168.8	56.25	1.00	126	-	126	400
2	56.25	3.4	2.40	1	191.3	360	56.25	0.72	126	97	223	784
1	56.25	3.4	2.40	1	191.3	551.3	112.5	0.60	126	161	287	1119

Occupancy type (O): 0-snow, 1-office.

Table I.2 Live load reduction for edge column S5 (A_t= *28.13 m²*)

St	A_t	DL	LL	O	DL_{floor}	ΣDL_{floor}	ΣA_t	f	ΣLL/occ.		LL_{tot}	C_{fmax}
	m²	*kPa*	*kPa*	-	*kN*	*kN*	*m²*	-	*(0)*	*(1)*	*kN*	*kN*
3	28.13	3.0	2.24	0	84.4	84.4	28.13	1.00	63	-	63	200
2	28.13	3.4	2.40	1	95.7	180	28.13	0.89	63	60	123	410
1	28.13	3.4	2.40	1	95.7	275.6	56.25	0.72	63	97	160	584

Occupancy type (O): 0-snow, 1-office.

The design live load due to use and occupancy, excluding snow, is reduced with the live load reduction factor *f*, given below. For tributary areas smaller than *20 m²* no live load reduction is applied.

$$f = 0.3 + \sqrt{9.8/A_t} \qquad 20\ m^2 \leq A_t < 80\ m^2$$

$$f = 0.5 + \sqrt{20/A_t} \qquad 80\ m^2 \leq A_t$$

The total axial compressive force in the column, C_{fmax} is determined from the most unfavorable load combination: 1.25DL + 1.5LL. For example in **Table I.1** for storey 3: C_{fmax} *=1.25*168.8 + 1.5*126 =400 kN.*

Table I.3 and **Table I.4** summarize the gravity column design for the building located in Quebec City. As illustrated the factored axial compressive resistance C_r, has been computed for effective lengths (*KL)* with respect to the least radius of gyration using **Eq. (2.17)** depending on the non-

dimensional slenderness ratio, $\lambda=KL/r\ (F_y/\pi^2E)^{0.5}$. The class of section verification depends on the maximum width-to-thickness ratios of the elements subjected to compression as described below:

Class 1 flanges : $\frac{b}{tf} \leq \frac{145}{\sqrt{F_y}} = 8.37$

Class 1 webs in axial compression: $\frac{h}{w} \leq \frac{670}{\sqrt{F_y}} = 38.7$

Class 2 flanges : $\frac{b}{tf} \leq \frac{170}{\sqrt{F_y}} = 9.81$

Class 2 webs in axial compression: $\frac{h}{w} \leq \frac{670}{\sqrt{F_y}} = 38.7$

Where b, t_f represent the flange width and thickness respectively, while h is the web clear depth between flanges and w is the web thickness.

Table I.3 Design Summary for gravity interior column S4 (A_t= *56.25 m²*)

St	C_{fmax}	Section	A	r_x	r_y	KL/r	λ	C_r	$b/2t_f$	h/w	Class
	kN	*S4*	*mm²*	*mm*	*mm*	-	-	*kN*	-	-	-
3	400	W200x31	4000	88.60	32.00	107.81	1.33	450	6.57	29.6	1
2	784	W200x42	5310	87.70	41.20	83.74	1.03	841	7.03	25.2	1
1	1119	W250x58	7420	108.00	50.40	86.31	1.06	1129	7.52	28.1	1

F_y=300MPa

Table I.4 Design Summary for gravity edge and corner column S5 and S6 (A_t= *28.13 m²*)

St	C_{fmax}	Section	A	r_x	r_y	KL/r	λ	C_r	$b/2t_f$	h/w	Class
	kN	*S5/S6*	*mm²*	*mm*	*mm*	-	-	*kN*	-	-	-
3	200	W150x24	3060	66.30	24.40	141.4	1.74	233	4.95	21.1	1
2	410	W200x31	4000	88.60	32.00	107.81	1.33	450	6.57	29.6	1
1	584	W200x42	5310	87.70	41.20	105.60	1.30	615	7.03	25.2	1

F_y=300MPa

APPENDIX II.

Brace connection design of 3-storey CBF building located in Quebec City according to CSA/S16.1-M78 standard

In this study, the gusset plate transfers the force from the HSS brace to the frame. Welding connections were selected for the studied building. The angle made by the brace and the horizontal line is 50.2° and 31° for braces at the ground floor in the E-W and N-S direction respectively, while for typical floor the angle is 44° for the E-W direction and 26° for the braces in N-S direction. The corner connection detail of the ground floor brace of the 3–storey building located in Quebec City is given in **Figure II.1** and **Figure II.2** for E-W and N-S direction respectively while the middle connection detail for the chevron braces is illustrated in **Figure II.3** and for the tension-compression braces (N-S direction) is shown in **Figure II.4**.

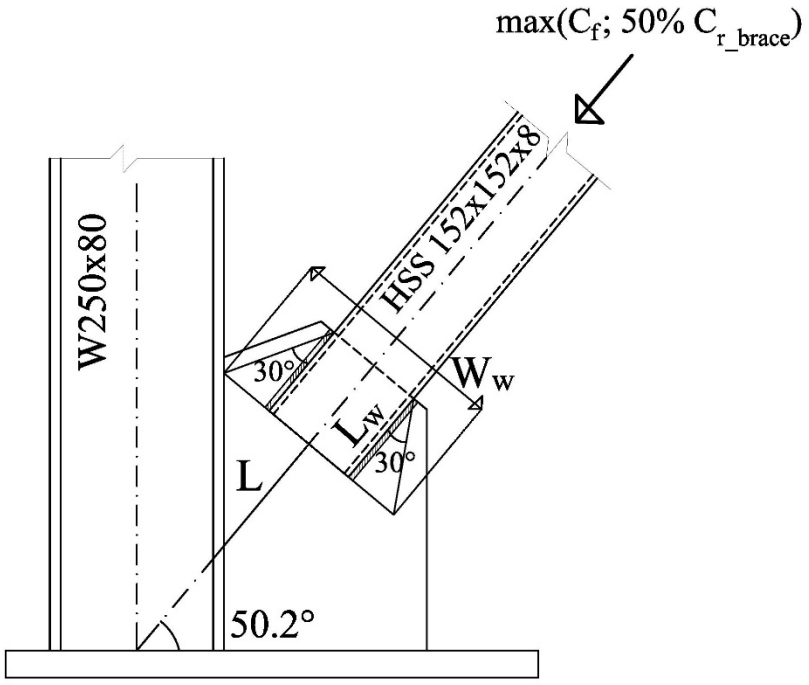

Figure II.1 Corner connection detail at ground floor in E-W direction (pre-retrofit connection of 3-storey CBF, Quebec City)

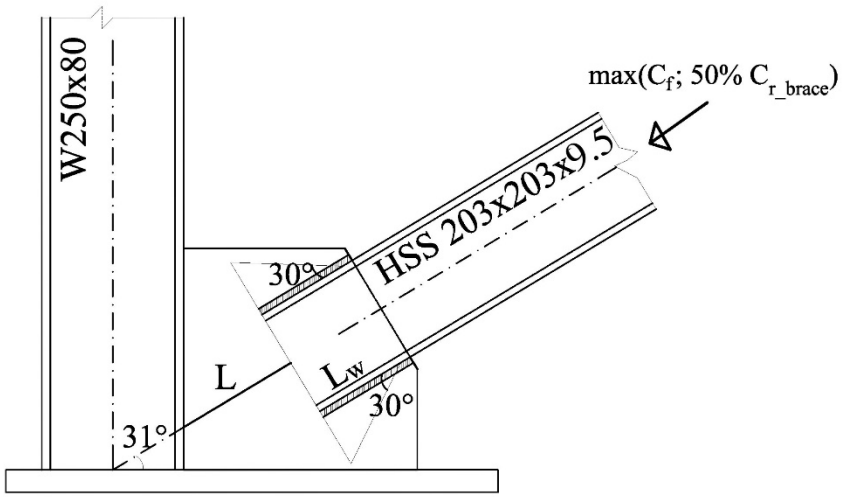

Figure II.2 Corner connection detail at ground floor in N-S direction (pre-retrofit connection of 3-storey CBF, Quebec City)

A design example is further presented. Namely, the connection of the ground floor brace of the 3-storey CBF (E-W direction) to the column and base plate is considered. All the gusset plates were assumed to be made of steel having the yielding strength *Fy = 300 MPa.* The electrode type used for welding is *E480 XX*, having the ultimate strength X_u = 480 MPa and the weld leg width, D_w was taken as *8.0 mm*. The required welding length of the HSS 152x152x8 brace to gusset plate is the maximum value between:

$$L_w = \frac{\frac{\max(C_f\ ;50\%C_{rbrace})}{4}}{0.66\phi D_w F_y} = \frac{\frac{625}{4}}{0.66*0.9*8.0*300/1000} \cong 110mm$$

$$L_w = \frac{\frac{\max(C_f\ ;50\%C_{rbrace})}{4}}{0.50\ \phi\ 0.707 D_w X_u} = \frac{\frac{625}{4}}{0.50*0.9*0.707*8.0*480/1000} \cong 128mm$$

The required fillet weld length is rounded to *150 mm* for construction convenience (including *20mm* HSS interior welding). After calculating the welding length, the factored shear resistance of the fillet weld can be verified. Thus, the shear resistance of the welds consists in verifying the fracture of the weld metal through the weld throat and yielding at the weld-to-base metal interface whichever happens first. The respective equations are: *i)* $V_r = 0.50\Phi A_w X_u$ and *ii)* $V_r = 0.66\Phi A_m F_y$. The shear area is $A_w = 0.707 D_w L_w$ and the interface area is $A_m = D_w L_w$.

- Shear resistance of the welds:

$$Vr = 0.50\ \phi\ A_w X_u = 0.50 * 0.9 * 130 * 0.707 * 8.0 * \frac{480}{1000} = 159\ kN$$

$$Vr = 0.66\ \phi\ A_m F_y = 0.66 * 0.9 * 130 * 8.0 * 300 = 185\ kN$$

$$Vr = \min(159\ kN; 185\ kN) > \frac{\max(C_f; 50\%C_{rbrace})}{4} = \frac{625}{4} kN \text{ OK}$$

- The Whitmore width (W_w) can be then calculated using the following equation:

$$W_w = 2 * L_w (tan30°) + b_{brace} = 2 * 150 * tan30° + 152.4 = 326\ mm$$

- Next a preliminary gusset plate thickness can be determined based on yielding of the Whitmore width cross section:

$$t_{gp} = \frac{\max(C_f\ ; 50\%C_{rbrace})}{0.85\phi W_w F_y} = 8.4\ mm$$

Consider t_{gp}=*9.53 mm* .

- The tensile resistance of metal base (gusset plate) is equal to:

$$\phi\, t_{gp}\, L_w F_y = 0.9 * 2(9.53 * 150) * \frac{300}{1000} = 772\ kN > \max(T_f\ ; 50\%T_{rbrace}) = 619\ kN$$

Then the compression resistance of gusset plate is calculated. In this light, the slenderness is given below, where *r*, is the radius of gyration of Whitmore cross-section and it corresponds to out of plane buckling and *L* represents the critical length calculated from the gusset plate geometry. (See **Figure II.1**).

$$\lambda = \frac{KL}{r}\sqrt{\frac{F_y}{\pi^2 E}} = 0.67 * \frac{220.6}{2.75} * \sqrt{\frac{300}{\pi^2 E}} = 1.26$$

- The compressive gusset plate resistance $C_{rgp,}$ is then calculated based on **Eq. (2.17)**:

$$C_{rgp} = 0.9 * 326 * 15.875 * \frac{300(-0.111 + 0.636 * 1.26^{-1} + 0.087 * 1.26^{-2})}{1000} = 672\ kN$$

$$> \max(C_f\ ; 50\%C_{rbrace}) = 625\ kN\ \ OK.$$

- The tensile resistance of the gusset plate T_{rgp} is calculated as:

$$T_{rgp} = 0.9 * W_w * t_{gp} * F_y = 0.9 * 326 * 9.53 * \frac{300}{1000} = 836\ kN$$

$$> \max(T_f\ ; 50\%T_{rbrace}) = 619\ kN\ \ OK.$$

- Net rupture of brace due to the reduction of cross section area for the gusset plate slot is also checked:

i) $T_r = \varphi A_n F_y$ When $\frac{A_n}{A_g} \geq \frac{F_y}{F_u}$

$$= 0.9 * (0.9 * A_g) * F_y = 0.9 * 0.9 * 4430 * \frac{345}{1000} = 1238\ kN$$

ii) $T_r = 0.85\varphi A_n F_u = 0.85 * 0.9 * (0.9 * Ag) * \frac{448}{1000} = 1366\ kN$

$T_{r.br\text{-}net} = \min(1238\ kN; 1366\ kN) > \max(T_f\ ; 50\%T_{rbrace}) = 619 \quad Ok$

Table II.1 Design summary for the corner connection at ground floor in E-W direction (3-storey Quebec City) according to CSA/S16.1-M78 standard

Failure Mode	Equation	Capacity	Demand/Capacity
1. Shear resistance of welding	V_r=min($0.66\phi A_m F_y$; $0.5\phi A_w X_u$)	635 kN	0.98
2.Tensile resistance of metal base	$T_r=\phi\, t_{gp}\, L_w\, F_y$	772 kN	0.80
3.Yielding of gusset	$T_r=\phi\, A_{gp}\, F_y$	836 kN	0.74
4. Buckling of gusset	$Cr=\phi\, A_{gp}\, F_y\, (-0.111+0.636\lambda^{-1}+0.087\lambda^{-2})$	672 kN	0.93
5. Net fracture of brace	$T_r=min(\phi\, A_n\, F_y\, ;\, 0.85\phi\, A_n\, F_u)$	1238 kN	0.50

$A_{gp}=W_w * t_{gp}$

The middle gusset plate design shown in **Figure II.3** for E-W direction and **Figure II.4** for N-S direction is similar to that of the corner gusset plate, however for the E-W direction, one or two stiffeners are required to sustain the braces if the buckling occurs.

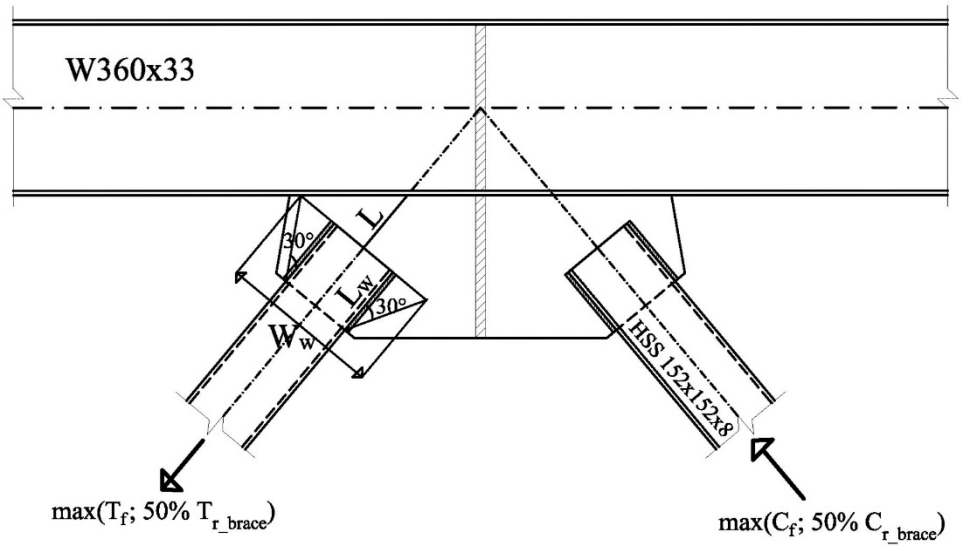

Figure II.3 Middle connection detail at ground floor in E-W direction (pre-retrofit connection of 3-storey CBF, Quebec City)

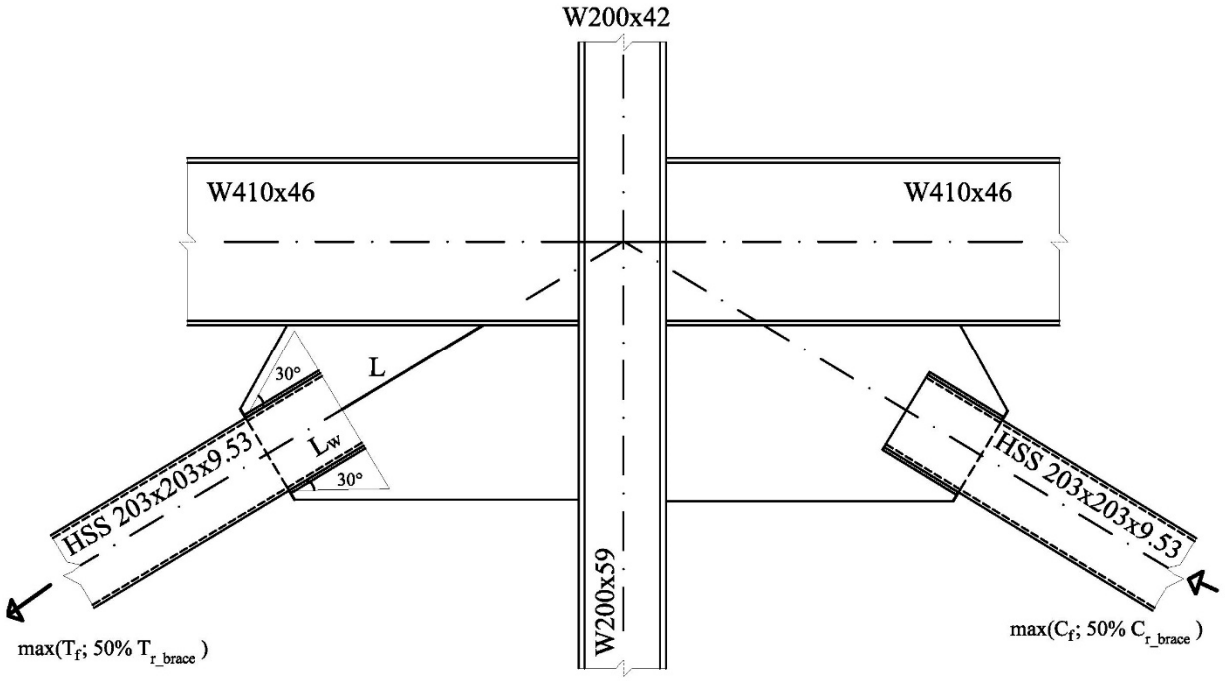

Figure II.4 Middle connection detail at ground floor in N-S direction (pre-retrofit connection of 3-storey CBF, Quebec City)

APPENDIX III.

Brace-to-frame connection design of 3-storey CBF building located in Quebec City according to CSA/S16-09 standard

In this design example, the connection of the ground floor brace of the 3-storey CBF (E-W direction) to the column and base plate is considered. The design process is similar with the 1980's approach; however changes have been implemented in the CSA/S16-09 standard. It is noted that besides the typical verifications presented in **Appendix II**, block shear failure and the shear lag effect were introduced as new verifications. The corner connection detail of the ground floor brace of the 3–storey building located in Quebec City is given in **Figure III.1(a)** and **Figure III.1(b)** for the E-W and N-S direction respectively, while the middle connection detail for the chevron braces is illustrated in **Figure III.2(a)** and for the tension-compression braces (N-S direction) is shown in **Figure III.2(b).**

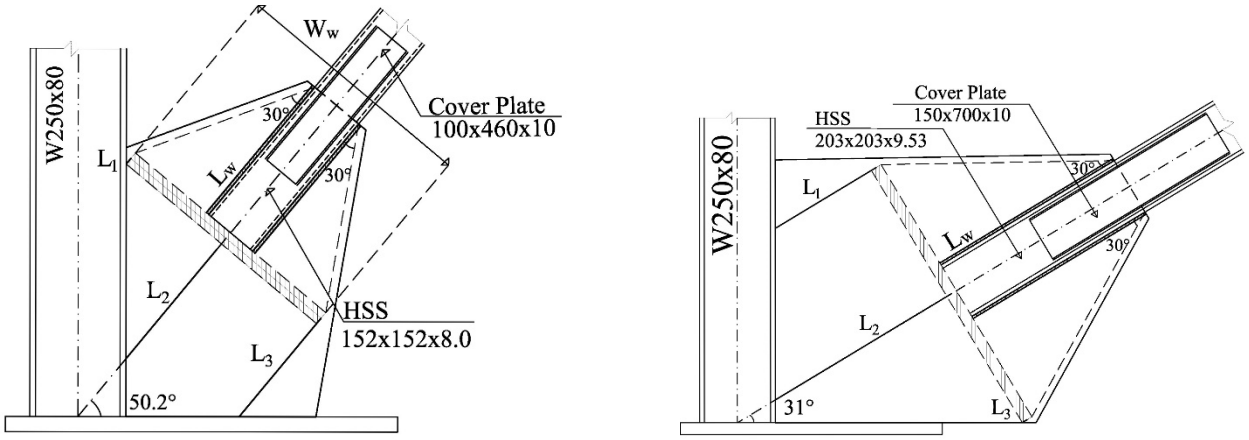

(a) (b)

Figure III.1 Corner connection detail at ground floor according to CSA/S16-09 (post-retrofit connection of 3-storey CBF, Quebec City): a) E-W direction; b) N-S direction.

Similar with the 1980's design all the gusset plates were assumed to be made of steel having the yielding strength $F_y = 300\ MPa$. The electrode type used for welding is *E49 XX*, having the ultimate strength X_u = 490 MPa and the weld leg width, D_w was taken as *8.0 mm*. In addition the coefficient Φ_w can be considered *0.67*. Thus, the required welding length of the HSS 152x152x8 brace to gusset plate is the maximum value between:

$$L_w = \frac{\frac{Tu}{4}}{0.67\phi w\, D_w\, F_u} = \frac{\frac{2038}{4}}{0.67*0.67*8.0*450/1000} \cong 315mm$$

$$L_w = \frac{\frac{Tu}{4}}{0.67\ \phi w\ \ 0.707 D_w X_u} = \frac{\frac{2038}{4}}{0.67*0.67*0.707*8.0*490/1000} \cong 409.5mm$$

The required fillet weld length is rounded to *440 mm* for construction convenience (including *20mm* HSS interior welding). After calculating the welding length, the factored shear resistance of the fillet weld can be verified. Thus, the shear resistance of the welds consists in verifying the fracture of the weld metal through the weld throat and yielding at the weld-to-base metal interface whichever happens first. The respective equations are: *i)* $V_r = 0.67 \Phi_w A_w X_u$ and *ii)* $V_r = 0.67 \Phi_w A_m F_u$. The shear area is $A_w = 0.707 D_w L_w$ and the interface area is $A_m = D_w L_w$.

- Shear resistance of the welds:

$$Vr = 0.67\ \phi w\ \ A_w\, X_u = 0.67 * 0.67 * 440 * 0.707 * 8.0 * \frac{490}{1000} = 548\ kN$$

$$Vr = 0.67\ \phi w\ \ A_m\, F_y = 0.67 * 0.67 * 440 * 8.0 * 450 = 711\ kN$$

$$Vr = \min(548\ kN; 711\ kN) > \frac{\mathrm{Tu}}{4} = \frac{2038}{4} kN \ \text{OK}$$

- The Whitmore width (W_w) can be then calculated using the following equation:

$$W_w = 2 * L_w (tan30°) + b_{brace} = 2 * 440 * tan30° + 152.4 = 660\ mm$$

- Next a preliminary gusset plate thickness can be determined based on yielding of the Whitmore width cross section:

$$t_{gp} = \frac{Tu}{0.9 \phi W_w F_y} = 11.44\ mm$$

Consider $t_{gp} = 19.05\ mm$.

- The tensile resistance of metal base (gusset plate) is equal to:

$$\phi\, t_{gp}\, L_w\, F_y = 0.9 * 2(19.05 * 440) * \frac{300}{1000} = 4526\ kN > \ T_u = 2038\ kN$$

Then the compression resistance of gusset plate is calculated. In this light, the slenderness is given below, where *r*, is the radius of gyration of Whitmore cross-section and it corresponds to out of plane buckling and L_{ave} represents the critical length calculated as the average value between the three lines L_1, L_2, L_3 illustrated in **Figure III.1(a)** from the gusset plate geometry.

$$\lambda = \frac{KL_{\text{ave}}}{r} \sqrt{\frac{F_y}{\pi^2 E}} = 0.67 * \frac{258.4}{5.50} * \sqrt{\frac{300}{\pi^2 E}} = 0.39$$

- The compressive gusset plate resistance $C_{rgp,}$ is then calculated according to **Eq. (2.19)** based on the gusset plate area taken as $A_{gp}=W_w*t_{gp}$=12574 mm^2:

$$C_{rgp} = 0.9 * 12574 * 300 * \frac{(1 + 0.39^{\,2.68})^{-1/1.34}}{1000} = 3207\ kN$$

$$> Cu = 1198\ kN \quad OK.$$

- The tensile resistance of the gusset plate T_{rgp} is calculated as:

$$T_{rgp} = 0.9 * W_w * t_{gp} * F_y = 0.9 * 660 * 19.05 * \frac{300}{1000} = 3395\ kN$$

$$> Tu = 2038\ kN \quad OK.$$

The tensile resistance of HSS brace due to block shear failure is checked according to the current code demand as per **Eq. (2.20)**, where Φ_u is a factor taken as *0.75* for steel, U_t represents the efficiency factor taken as *1.0* for symmetrical blocks, which is the case for this study; while A_n and A_{gv} represent the net area in tension and the gross area along the shear failure plane, respectively. It is noted that the gusset plate is not welded to the brace at the end, thus $A_n = 0$ mm^2 while A_{gv} = *4x440x8.0= 14080* mm^2.

$$T_{r-BS} = \Phi_u \left[U_t A_n F_u + 0.6 A_{gv} \frac{(F_y + F_u)}{2} \right]$$

$$= 0.75 \left[(1.0)(0)(345) + (0.60)(4 * 440 * 8.0) \frac{(345 + 448)}{2} \right] / 1000 = 2376\ kN$$

$$> Tu = 2038\ kN \quad OK.$$

- The calculation of nominal capacity for tensile rupture in the net section of HSS brace with shear lag effect is calculated bellow where A_{ne} is the effective net area given in **Eq. (4.8).** It is noted that, the effective net area it is reduced with the shear lag factor *U* if it is affected by the shear lag effect.

$$T_{NR} = 0.85 \Phi A_{ne} F_u$$

L_w = 440 mm > 2b_{brace} = 2x152.4 = 304.8 mm

Thus, the net area is given by **Eq. (4.8.(i))** : A_{n2} = 4x152.4 x 8.0 = 4877 mm^2

Next the shear lag factor *U* is calculated as: $U = 1.1 - \frac{\overline{x'}}{L_w}$, $but \geq 0.8\ when\ \ 0.1 < \frac{\overline{x'}}{L_w} \leq 0.3$ or

$$U = 1.0\ , when\ \frac{\overline{x'}}{L_w} \leq 0.1$$

Based on the calculations, the center of gravity (centroid) for the top half of the HSS brace from the face of the gusset plate as illustrated in **Figure 2.5(a)** is: $\bar{x'} = 34.83 - \frac{19.05}{2} = 25.3\ mm$.

Thus the ratio: $\frac{\bar{x'}}{L_w} = \frac{25.3}{440} = 0.06 \leq 0.1$ thus $U = 1.0$

Then the effective net area is modified as $A_{ne} = A_{n2}U$ = 4877 x1.0=4877 mm^2 and nominal capacity for tensile rupture in the net section of HSS brace is:

$T_u = 0.85\Phi A_{ne} F_u = 0.85 \times 0.9 \times 4877 \times 448/1000 = 1672\ kN$

$< Tu = 2038\ kN$ *NOT GOOD.*

The middle gusset plate design shown in **Figure III.2(a)** for E-W direction and **Figure III.2(b)** for N-S direction is similar to that of the corner gusset plate, however for the E-W direction, one or two stiffeners are required to sustain the braces if the buckling occurs.

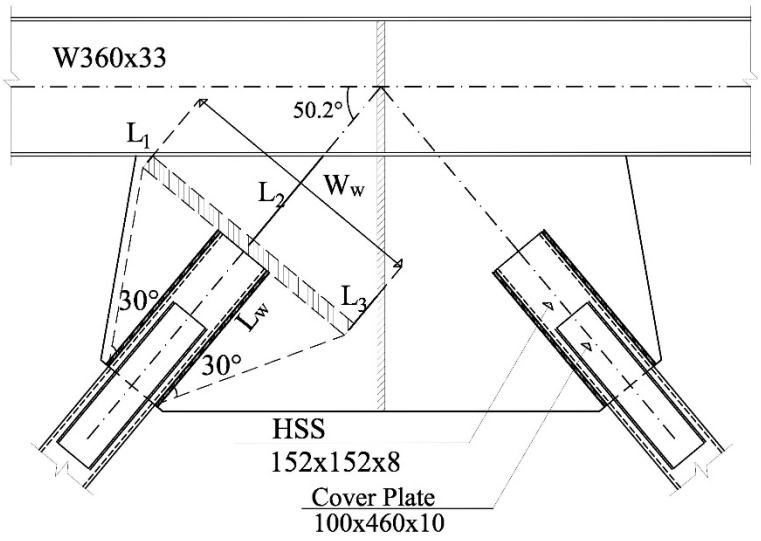

(a)

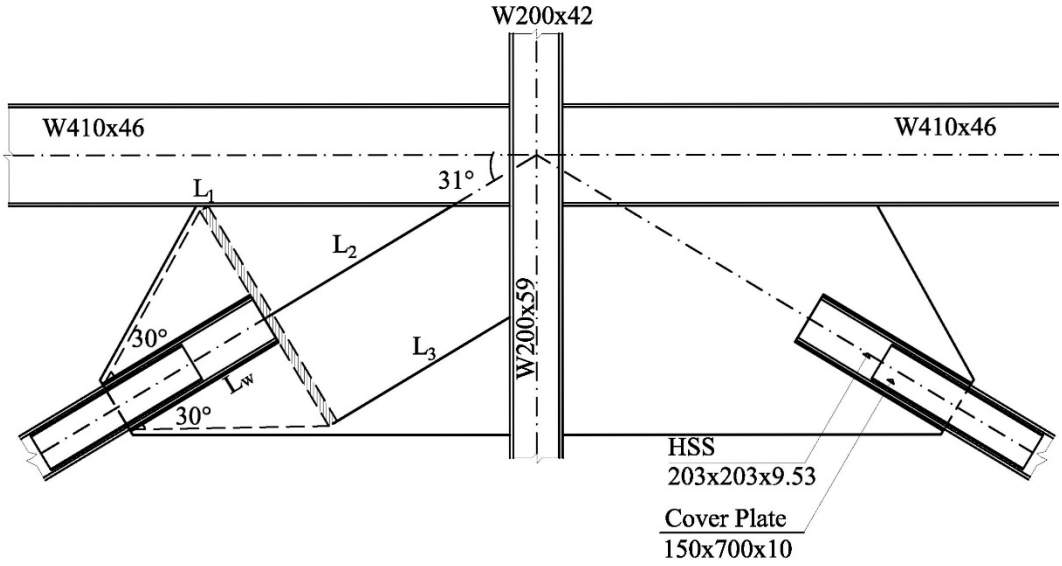

(b)

Figure III.2 Middle brace-to-frame connection detail at ground floor according to CSA/S16-09 (post-retrofit connection of 3-storey CBF, Quebec City): a) E-W direction; b) N-S direction

Cover Plate design

As shown above, after retrofitting the connections the brace is prone to net rupture, due to the reduction of the cross-sectional area at the gusset plate slot. Therefore, in order to strengthen the net section of the brace, a cover plate is necessary as illustrated in **Figure III.3**.

All the cover plates were selected G40.21-300W type, with F_y= *300 MPa*. Although the process of determining the cover plate thickness is iterative and time consuming because the center of gravity ($\bar{X}$), depends on the cover plate thickness, this process can be conducted using a spreadsheet. The same ground floor brace: *HSS 152 x 152 x 8.0* from the CBF in the E-W direction is taken for the exemplification.

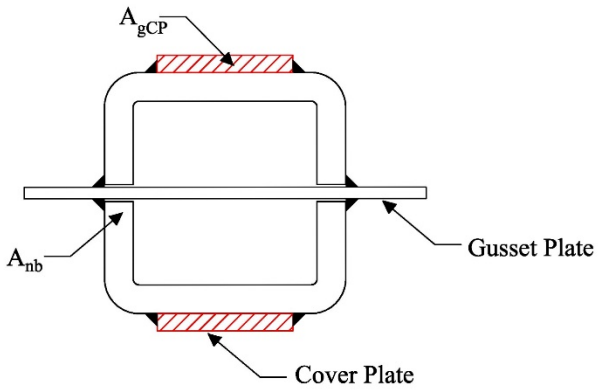

Figure III.3 Cross-section view of HSS brace connection with cover plate

After going through several iterations, a plate thickness of *10 mm* and *100 mm* width was selected. Thus, the selected plate width of *100 mm* allows enough room for the plate to be set on the flat part of the brace with additional space for the fillet welds on both sides. The final step is to ensure that the net section capacity of the brace reinforced with the cover plate is larger than the probable tensile resistance of the brace (T_u). To do so, **Eq. (5.1)** can be employed to calculate the connection resistance:

$$T_{rb} = U(\Phi_r R_t A_{nb} F_{u,b} + \Phi A_{gCP} F_{u,CP})$$

A_{nb} represents the cross-sectional area of the brace with the consideration of the gusset plate slot. In addition, a *1.5 mm* cutting spacing between brace and gusset plate at the slot was also considered. Thus, $A_{nb} = 4430 - 2(8.0)(19.05 + 2 * 1.5) = 4077\ mm^2$

A_{gCP} is the gross cross-sectional area of the added cover plate: $A_{gCP} = 2(10)(100) = 2000\ mm^2$

The centre of gravity ($\bar{X}$) was determined to be 65 mm, therefore the shear lag factor can be calculated as: $U = 1.1 - \frac{\overline{X'}}{L_W} = 1.1 - \frac{65-19.05/2}{440} = 0.974$

Therefore: $T_{rb} = (0.974)[(0.75)(1.1)(4077)(448) + (1.0)(2000)(450)]/1000$

$= 2342\ kN > T_u = 2038\ \text{kN}$ OK

In the above equation R_t was taken as *1.1*, while the coefficients Φ_r and Φ were taken as *0.75* and *1.0* respectively.

The length of the cover plate was set at 460 mm, in order to match the brace splice length. Therefore an: *10-mm* x *100-mm* x *460-mm* net section cover plate is adequate to develop the expected tensile yield capacity of the brace.

The longitudinal fillet welds used to connect the cover plates to the brace were designed conservatively so that they can develop the full plastic capacity of the plate. Thus the selected electrode type was *E49XX* having the ultimate strength X_u = 490 *MPa* and the required weld leg D_w is:

$$D_W = \frac{R_y F_{y,CP} A_{g,CP}}{0.67 \Phi_W L_{W,CP} X_u} = \frac{1.1(300)(10)(100)}{0.67(0.67)(460)(490)(2)(0.707)} = 2.3\ mm$$

However, the minimum value of D_w is *5 mm*.

END of Thesis.